A “two birds with one stone” approach to the targeted treatment and imaging of tumors: vitamin B_{12}-functionalized metallotheranostic agents

Eirini Fotopoulou, M.Chem.

School of Chemistry

Presented to

The National University of Ireland, Galway

For the degree of

Doctor of Philosophy

Supervisor: Dr. Luca Ronconi

Head of School: Prof. Olivier Thomas

April 2021

Declaration

This thesis has not been submitted before, in whole or in part, to this or any other university for any degree, and is, except where otherwise stated, the original work of the author.

Signature:

Eirini Fotopoulou

This thesis is based on the collaborative research work of various groups. The contribution of the candidate represents the majority of the work (> 90%) although, where otherwise stated, the contribution of other groups is described.

Signature:

Eirini Fotopoulou

Abstract

Vitamin B_{12} (aka cyanocobalamin) is a vital nutrient characterized by very low bioavailability. Owing to their extremely high proliferation rates, tumor cells show increased demand for nutrients compared with healthy ones, including the greater uptake of vitamin B_{12}. Such avidity of cyanocobalamin can thus be exploited for the site-specific delivery of drugs directly into the tumor by conjugating vitamin B_{12} (carrier) to either anticancer (chemotherapeutics) or imaging (fluorophores) agents. Accordingly, this research project includes the rational design and synthesis of vitamin B_{12}-based metallotheranostics of the type [{B_{12}–Co–C≡C–Ph–Inp–dtc–M}] and [{FLUO-B_{12}–Co–C≡C–Ph–Inp–dtc–M}]. As such, cyanocobalamin is functionalized at the 5'-hydroxo group of the ribose unit with a fluorophore (FLUO), whereas the cyano (CN) group is replaced with phenylacetylide-containing metal-dithiocarbamato complexes ({M(dtc)}; M = Au(III)/Pt(II), dtc = various dithiocarbamates). The rationale behind the proposed designing approach is based on the evidence that vitamin B_{12} converted into its cofactors (methylcobalamin or adenosylcobalamin) inside the cell through the reduction of Co(III) to Co(II) and the subsequent release of the cyano group. Therefore, by binding metal-containing scaffolds to the cyanocobalamin Co(III)-CN moiety, should the overall bioconjugate accumulate preferentially in the tumor cells, the cytotoxic metal complexes are expected to be released directly into the diseased site where it can exert its anticancer activity without affecting healthy tissues. At the same time, the fluorophore attached at the 5'-ribose moiety would allow the transport and biodistribution to be followed and assessed by fluorescence spectroscopy. Therefore, the goal is to take advantage of the increased demand of cyanocobalamin in tumor cells by exploiting its carrier properties to design selective "Trojan Horse"-type theranostics in which the structural features of vitamin B_{12} conceal both the attached imaging agent and the metallodrug, to achieve a better therapeutic outcome and reduce side-effects. Additionally, considering the role of amino acids in tumor metabolism as nutrients, inhibitors, and epigenetic regulators, we designed four novel naturally fluorescent metal-dithiocarbamato *L*-tyrosine ester complexes. Furthermore, four new platinum(II) glycomimetic analogs were synthesized and fully characterized. Notably, all of the novel platinum(II)-glycoconjugates proved cytotoxic against the A2780 ovarian

cancer cell line, and three of them against the resistant cell line A2780cis, with GI_{50} values lower than 20μM.

Table of Contents

Declaration 2
Abstract 3
Table of Contents 5
Contributions 8
Symbols and abbreviations 11
Acknowledgements 13
Chapter 1: Introduction 14
1. Cancer 15
1.1 Detection, Diagnosis and Treatment 16
1.1.1 Treatment Regimes 19
1.1.2 Theranostics: An All-In-One Strategy 22
1.1.3 Trojan Horse approach 24
1.2 Vitamin B_{12} 24
1.2.1 Vitamins 24
1.2.3 Structural Characteristics 27
1.2.4 Recommended Intake of Vitamin B_{12} 30
1.2.5 Deficiency of Vitamin B_{12} 31
1.2.6 Uptake, Transport and Metabolism of Vitamin B_{12} 31
1.3 Vitamin B_{12} in drug design and delivery 35
1.3.1 Diagnostic Vitamin B_{12} Metal Bioconjugates 38
1.3.1.1 Radiolabeled Vitamin B_{12} Scaffolds 38
1.3.1.2 Fluorescent Vitamin B_{12} Metal Complex Conjugates 42
1.3.2 Therapeutic Vitamin B_{12} Metal Complex Bioconjugates 45
1.4 Rationale Behind the research work: the “two birds with one stone” strategy…... 51
1.5 Research Objectives and Thesis Outline 53
1.6 References 54
Chapter 2 63
2. Synthesis, Purification and Characterization of Two Novel Fluorescent Vitamin B_{12} Scaffolds 64
2.1 Background 64
2.2 Synthetic Strategy 68
2.3 Preparation of FLUO-1, FLUO-2 and their active derivatives 70
2.3.1 Synthesis and activation of FLUO-1 71
2.3.2 Synthesis and activation of FLUO-2 74

2.6 Conclusions 85
2.7 Literature 85
Chapter 3 89
3. Platinum(II)- and Gold(I)-Dithiocarbamato Precursors: The Initial Approach 90
3.1 Background and Rationale 90
3.1.1 Platinum(II)-based chemotherapeutics 90
3.1.2 Dithiocarbamates 91
3.1.3 Gold(I)-based chemotherapeutics 92
3.2 Initial Designing Strategy 93
3.3 Syntheses and characterizations 95
3.3.1 Preparation of K[Pt(am)Cl_3] precursors 95
3.3.2 Preparation of the dithiocarbamate ligands 100
3.3.3 Attempted synthesis of the platinum(II)-dithiocarbamato precursors. 104
3.3.4 Synthesis of the zinc(II)-dithiocarbamato precursors 109
3.3.5 Metal conjugation to vitamin B_{12}: initial attempt 112
3.4 Conclusions 115
3.5 References 115
Chapter 4 120
4. Vitamin B_{12} Conjugation Strategies 121
4.1 Rationale 121
4.2 Synthesis 124
4.2.1 Preparation of the model B_{12}-1 scaffold 124
4.2.2 Preparation of the zinc(II)-dithiocarbamato complexes 127
4.2.3 Preparation of the gold(III)-dithiocarbamato complexes 131
4.2.4 Preparation of the platinum(II)-dithiocarbamato complexes 137
4.3 Vitamin B_{12}-metal conjugated: preliminary results 139
4.4 Conclusions 142
4.5 References 143
Chapter 5 146
5. Design, Synthesis and Characterization of Novel Fluorescent Pt(II)- and Au(III)-based Dithiocarbamato *L*-tyrosyl Ester Derivatives as Potent Anticancer Agents 147
5.1 Background 147
5.1.1 Briefly the role of amino acids in tumors 149
5.1.2 Platinum(II)- and gold(I/III)-based complexes incorporating amino acids 149

5.2 Strategy 153
5.3 Synthesis 154
5.3.1 Preparation of the zinc(II)-dithiocarbamato *L*-tyrosyl ester derivatives 155
5.3.2 Synthesis and characterization of the novel platinum(II)-dithiocarbamato *L*-tyrosyl ester complexes 157
5.3.3 Synthesis and characterization of the novel gold(III)-dithiocarbamato *L*-tyrosyl ester derivatives 162
5.4 Conclusions 168
5.6 References 169
Chapter 6 172
6. Design, Synthesis and Biological Evaluation of Novel Platinum(II)-glycoconjugates 173
6.1 Background 173
6.1.1 Tumor glycolysis: a brief overview 173
6.1.2 GLUTs: glucose transporters 174
6.1.3 Targeting glucose transporters 175
6.1.4 Metal-based glycoconjugates 176
6.2 Strategy 180
6.3 Synthesis 182
6.3.1 Carbohydrate precursors 183
6.3.2 Synthesis of the zinc(II)-dithiocarbamato glycoconjugates 183
6.3.3 Synthesis of the novel platinum(II)-glycoconjugates 186
6.4.1 Materials and methods 193
6.4.2 Study of the antiproliferative activity 194
6.5 Conclusions 196
6.6 References 196
General Conclusions 201
Chapter 7 203
7. Experimental 204
7.1 Materials 206
7.2 Instrumentation 206
7.3 Chapter 2 – Experimental 208
7.4 Chapter 3 – Experimental 216
7.5 Chapter 4 – Experimental 224
7.6 Chapter 5 – Experimental 235
7.7 Chapter 6 – Experimental 239

Contributions

Scholarships/awards

Hardiman Research Scholarship granted by the National University of Ireland Galway, September 2016

IRC Government of Ireland Postgraduate Scholarship granted by the Irish Research Council, October 2017

Erasmus^{+} Traineeship award granted by the National University of Ireland Galway, November 2019

Publications

E. Fotopoulou, L. Ronconi, "Application of heteronuclear NMR spectroscopy to bioinorganic and medicinal chemistry – 1st Currency Review", in: Elsevier Reference Module in Chemistry, Molecular Sciences and Chemical Engineering; Reedijk, J., Ed.; Elsevier: Waltham (MA), 2018, 10.1016/B978-0-12-409547-2.10947-3 (e-book).

A. Pettenuzzo, K. Vezzù, M.L. Di Paolo, E. Fotopoulou, L. Marchiò, L. Dalla Via, L. Ronconi, "Design, physico-chemical characterization and in vitro biological activity of organogold(III) glycoconjugates", Dalton Trans. 2021, submitted.

E. Fotopoulou, I. Titilas, L. Ronconi, "Metallodrugs as anticancer chemotherapeutics and diagnostic agents: a critical patent review (2010 - 2020)", Recent Pat. Anticancer Drug Discov. 2021, submitted.

Conference Proceedings

Eirini Fotopoulou, Luca Ronconi, A “two birds with one stone” approach to the targeted treatment and imaging of tumors: vitamin B_{12}-functionalized metallotheranostic agents, 46th International Symposium on Metal Complexes - ISMEC 2019 Debrecen/Hajdúszoboszló (Hungary), June 2019 (poster presentation)

Eirini Fotopoulou, Luca Ronconi, 'Vitamin B_{12}-functionalized metallotheranostic agents for the targeted treatment and imaging of tumors', 14th European Biological Inorganic Chemistry Conference (EuroBIC 14), University of Birmingham (UK), August 2018 (poster presentation)

Eirini Fotopoulou, Luca Ronconi, A "two birds with one stone" approach to the targeted treatment and imaging of tumors: vitamin B_{12}-functionalized metallotheranostic agents, Irish Biological Inorganic Chemistry Society-IBICS-2 Symposium, NUI Galway (Ireland), November 2018 (poster presentation)

Eirini Fotopoulou, Luca Ronconi, A "two birds with one stone" approach to the targeted treatment and imaging of tumors: vitamin B_{12}-functionalized metallotheranostic agents, 1st Irish Biological Inorganic Chemistry Society Symposium-IBICS-1 Maynooth (Ireland), November 2017 (poster presentation)

Eirini Fotopoulou, Luca Ronconi, A "two birds with one stone" approach to the targeted treatment and imaging of tumors: vitamin B_{12}-functionalized metallotheranostic agents, 69th Irish Universities Chemistry Research Colloquium Dublin (Ireland), June 2017 (poster presentation)

Contribution as Teaching Assistant

- 1st Year Chemistry Practicals (2016-2017)
- 2rd Year Inorganic Chemistry Practicals (2017-2018)
- 3rd Year Inorganic Chemistry Practicals (2018-2019)
- Instructor of the 1st year course "Environmental Science for Chemistry and Physics" (2018)
- Supervising the 4th year students Levent Faracli and Ellen Keyes in their final year projects (2017-2019)

Summary of outreach activities

Volunteer demonstrator / teaching assistant in events organized by NUIG :

- Spectroscopy in a Suitcase Group and Kitchen Chemistry Group (2016-2019)

- Galway Science and Technology Festival (November 2016)
- Scientist for a Day Festival (February 2017)
- Cell Explorer and Eco Explorer Summer Camp (July 2017)
- Galway Science and Technology Festival (November 2017)
- Scientist for a Day Festival (February 2018)

Social Media Manager of An Cumann Ceimice (ChemSoc) (2017-2018)

Modules Attended (for Structured PhD Program)

Core Skills for Chemical Research

Process Development and Scale-Up in the Pharmaceutical Industry

Innovation, Enterprise and Entrepreneurship

Communications and Outreach

Seminar Program

Teaching and Learning

Symbols and abbreviations

δ	Bending (IR)
δ	Chemical shift (NMR)
ε	Molar extinction coefficient
μM	Micromolar, μmol L^{-1}
ν	Stretching (IR)
ν_{as}	Anti-symmetric stretching
ν_s	Symmetric stretching
A2780	Human ovarian carcinoma (wild type)
A2780cis	Human ovarian carcinoma (cisplatin resistant variant)
CD_3OD	Methanol-d_4
$CDCl_3$	Chloroform-d_3
CH_2Cl_2	Dichloromethane
CH_3OH	Methanol
cm^{-1}	Centimeter^{-1} (wavenumber)
CORM	CO-releasing molecule
CS_2	Carbon disulfide
CsI	Cesium iodide
DIPEA	N,N-diisopropylethylamine
DMF	N,N-dimethylformamide
DMSO	Dimethyl sulfoxide
dtc	Dithiocarbamate
ESDT	Ethyl sarcosine dithiocarbamate
Et_3N	Triethylamine (TEA)

FDA	Food and Drug Administration
FT-IR	Fourier transform infrared
GLUT	Glucose transporter
IC_{50}	Inhibitory concentration (at 50%)
Inp	Isonipecotic
KOH	Potassium hydroxide
KPF_6	Potassium hexafluorophosphate
m	Medium (IR)
MS	Mass spectrometry
NaOH	Sodium hydroxide
nm	Nanometers
NMR	Nuclear magnetic resonance (spectroscopy)
oop	Out-of-plane
OSu	O-succinimide
P_2O_5	Phosphorous pentoxide
PET	Positron emission tomography
PPh_3	Triphenylphosphine
ppm	Parts per million
q	Quartet
s	Strong (IR)
Sar	Sarcosine (N-methyl glycine)
SNAP	S-nitroso-N-acetylpenicillamine
UV-Vis	Ultraviolet-visible (spectroscopy)
w	Weak

Acknowledgements

I would like to sincerely thank my supervisor Dr. Luca Ronconi, for his guidance and constant support. During these four years, I had the opportunity to collaborate with people who were always willing to help me. As such, I would like to thank Seamus Collier and Dr. Roisin Doohan for the NMR assistance. Thanks to the establishment of a collaboration network, crucial aspects of the present Ph.D. project were achieved. Therefore, I would like to kindly thank the research groups of Prof. Olivier Thomas for HPLC/UPLS measurements, Prof. Lisa Dalla Via for the opportunity she gave me to perform preliminary biological studies of my platinum(II) complexes in her lab in Padova, Prof. Fabio Zobi for the B_{12} conjugation studies and Prof. Orla Howe for the ongoing biological studies on the platinum(II)/gold(III) compounds. Special thanks go to Dr. Wenming Tong and Dr. Pau Farras for all the help and guidance with fluorescence spectroscopy measurements. Moreover, I want to express my gratitude to my family for their constant support, the strength they gave me to go through this Ph.D., all their love and understanding. Finally, a big THANK YOU goes to my colleagues, lab mates, and true friends Andrea, Gianni, and Rosy for everything they did for me inside and outside the lab, I will really miss working with you guys!!!!!!!!! I would like to thank also my students Levent and Ellen. I also want to thank some great people I had the chance to meet during these years, whom I can now call friends, Camila, Roberta, Deborah, Isabel, Carla, Sean, Nora, Amelie, Adele, Francesco, Styliana, Leila, Marta, Maria, Shauna, Ana, Augusto, Sarah, Psemek, Niall, Carlos, Lina and Maria Francesca. Thank you guys!

Chapter 1: Introduction

1. Cancer

Overview and Impact

Cancer is a widely used term, generally referring to a large class of diseases that can originate from almost any organ or tissue of the body. Over time, other names have been given to portray this genetic condition, such as neoplasm or (malignant) tumor. A common feature of all types of cancer is the uncontrolled growth of cancerous cells beyond their usual boundaries. An abnormal spread of these cells in adjacent parts of the body and/or other organs leads to uncontrolled metastasis, which is a major cause of death from cancer.[1]

According to the World Health Organization (WHO),[2] cancer is the second leading cause of death globally and is estimated to account for 8.1 M new cancer cases and 9.6 M deaths worldwide in 2018 (**Figure 1.1**). By 2040, the overall cancer intake is expected to grow to 9.4 M new cases and 16.3 M deaths per year simply owe to the growth and aging of the population. In addition to the human toll of cancer, as well as the social, emotional, and mental issues expected by patients, the associated economic costs are substantial. Direct costs include expenditures for treatment, care, and rehabilitation. Indirect costs include the loss of economic output due to missed productivity (morbidity costs) and premature death (mortality costs). The exact global cost of cancer is unknown, but it is estimated to be $ 1.2 Tn per year and is expected to grow due to increases in the number of new cancer cases, together with the increasing costs of cancer therapies.

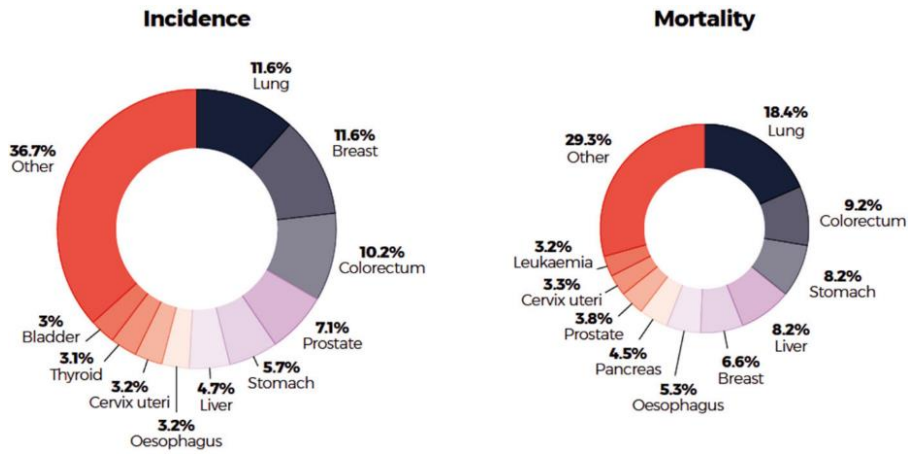

Figure 1.1: Distribution of cases and deaths by the leading cancer types in 2018 for both sexes (adapted from ref.2)

In this scenario, it is not surprising that the global health agenda is focusing on making an impact on cancer through the development and implementation of strategies to provide more effective prevention and treatment plans. In addition to cancers caused by genetic changes within the human body which control essential cell functions, several external cancer-inducing agents have been identified, such as physical carcinogens (e.g., UV and ionizing radiation), chemical mutagens (e.g., asbestos, aflatoxins, and arsenic), and biological factors (e.g., some bacterial, viral and parasitic infections).[3–5]

Epidemiological analyses showed that aging influences carcinogenesis, most likely due to perilous habits increasingly acquired with age such as smoking, alcohol, unhealthy diet, and physical inactivity. Insights into the pathophysiology of cancer also suggest that gender plays a crucial role in the incidence and mortality of a variety of cancers.[6,7] It is possible, therefore, that this is a result of gene polymorphism, altered enzymes, and hormonal differences between males and females. Collectively, lung, prostate, colorectal, stomach, and liver cancer are the most common types of cancer in men, while lung, breast, colorectal, cervical, and thyroid malignancies are the most prevalent among women.

Although the way to ultimately defeat cancer remains an enigma, substantial progress has been made in terms of effective prevention regimes, early detection, and diagnosis.[8,9] Moreover, data generated from multiple sources, such as cancer genetics, biology, and drug discovery, have led to favorable methods for innovative and effective treatments of tumors and have inspired the development of potential molecularly targeted therapeutics.[10,11]

1.1 Detection, Diagnosis and Treatment

The challenge posed by an early and prompt cancer diagnosis to tackle the disease and, eventually, improve survival rates, has been taken up since the beginning of the Twentieth Century. Before the discovery of "X-rays" by Wilhelm Conrad Roentgen, physicians were not able to know what was happening inside the patient's body, due to the lack of an accurate representation of the inner physiology. This significant scientific breakthrough became the principal tool in medical diagnosis, promoted the development of medical imaging, and triggered the generation of new imaging tools.[12]

Neoplasms in humans display characteristic structural, physiologic, and molecular features which can be 'imageable' (although exceptions have been reported).[13] Thus, making use of imaging techniques proved advantageous for the detection of malignancies, characterization of tissue damages, estimation of locoregional and systemic staging and provision of prognostic information.[14] Nowadays, medical imaging instruments are available at all levels of public and private hospital care, to detect, cure, palliate and follow-up malignancies previously diagnosed and/or treated.

The types of medical imaging modalities currently in use allow unprecedented accuracy in tumor detection by producing three-dimensional multimodal images at high resolution, and can be classified as follows: a) computed tomography (CT) using X-ray beams projected into the body from different angles to produce cross-sectional (i.e. tomographic) images, such as mammography, interventional radiology, computed and digital radiography; b) nuclear medical technology, including positron emission tomography (PET) and single-photon emission computed tomography (SPECT); c) optical imaging using light in the visible-infrared frequency range to obtain images from inside the body, tissues or cells, such as endoscopy, optical coherence tomography (OCT) and diffused optical tomography (DOT) d) other non-radioactive imaging techniques, such as ultrasonography (US, using high-frequency sound waves) and magnetic resonance imaging (MRI, exploiting the magnetic properties of specific nuclei); e) theranostic imaging, in which therapy and diagnosis are combined in one single (i.e. theranostic) tool. Each of the aforementioned imaging modalities allows high-resolution non-invasive detection of tumors and have their strengths and weaknesses (**Table 1.1**).[15]

Modality	Spatial Res.	Sensitivity	Advantages	Disadvantages	Phys. Principle	Depth
Nuclear CT	50-200 μm	10^{-6}	High sensitivity; excellent penetration depth; fast and cross-sectional images	Low contrast; radiation risk	X-rays	Limitless
Radionuclide PET	1-2 mm	10^{-11} -10^{-12}	High sensitivity;	High cost of cyclotron	γ-rays	Limitless

			excellent penetration depth; whole-body imaging	needed; radiation risk		
SPECT	1-2 mm	10^{-10} -10^{-11}	High sensitivity; no tissue penetrating limit; no need for cyclotron	Low spatial resolution; radiation risk; hard to quantify	γ-rays	Limitless
MRI	25-100 μm	10^{-9} -10^{-6}	High spatial resolution; no tissue penetrating limit; no radiation	Relatively low sensitivity and low contrast; high cost; long scanning time	R-waves	Limitless
Optical OFI	2-3 mm	10^{-9} -10^{-17}	High sensitivity; inexpensive; activable; no radiation	Low spatial resolution; poor penetration depth	Vis or Near IR	<1 cm
OBI	3-5 mm	10^{-15}-10^{-12}	High sensitivity; inexpensive; non-damaging imaging; no radiation	Low spatial resolution; poor penetration depth	Vis	1-2 cm
Ultrasound	25-100 μm	Excellent	High sensitivity; high temporal resolution; no radiation	High spatial resolution; poor penetration depth; low contrast and strong boundary effect	High frequency sound wave	mm - cm

Table 1.1: Main features of the various molecular imaging modalities.[15]

According to experts, the healing of cancer starts with finding. Therefore three crucial parameters should be identified to apply the appropriate imaging technique: (i) the part of the body to be examined; (ii) how quickly the images can be produced (relevant in emergency cases); and (iii) certain patient's conditions that prevent the use of a specific scanning technique (e.g. pregnancy).[16] Although there are no

ultimate tools to image certain types of malignancies, numerous cases have been reported where specific modalities are favorable, such as magnetic resonance imaging of brain cancers, ultrasound for kidneys, bladder, pelvis, and computed tomography scanning for chest and abdomen.[17]

Data gathered from multiple sources over the last decades depict the idea of combining current imaging methods, notably, PET-CT, SPECT-CT, and PET-MRI, to provide multimodal scans which are beneficial from a diagnostic point of view owing to increased accuracy, faster results and improved patient safety owing to reduced radiation exposure. Also, the aforementioned concept facilitates real-time image-guided interventions and the effective treatment planning of the subsequent treatment regime.

Prospects of medical imaging emphasize the need for a sharper and more focused visualization of tumors.[18] For this reason, research efforts in the field include the development of new minimally invasive methodologies such as imaging biomarkers, radiomics/radiogenomics, multiparametric analysis, artificial intelligence systems, and bifunctional methods where a radionuclide-based probe and an optical probe may guide diagnosis and surgery through CT, ultrasonography, fluoroscopy and innovative MRI systems.

1.1.1 Treatment Regimes

Over the last two centuries, several approaches have been developed to manage and cure the complex phenomena of cancer (**Figure 1.2**).[19–21] The choice of an efficient therapeutic method depends highly on the type of cancer, localization of the malignancy, and stage of progression. There are cases where patients with this multifactorial disorder would receive only one type of treatment, but most undergo a combination of the existing therapeutic techniques nowadays.

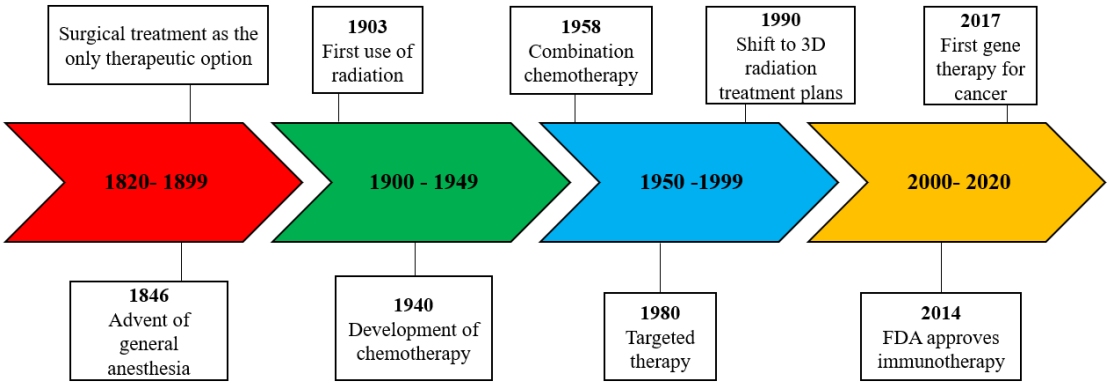

Figure 1.2: Progress of cancer treatment methods over the last two centuries. (Source: American Society of Clinical Oncology, www.asco.org)

Until the early 1900s, the invasive practice of surgery was the first and only applicable method to treat solid tumors. This operational procedure can be effective when the disease is in the early stages. However, in cases where metastasis is observed, the malignancy cannot be cured solely by resection.[4,19] For this reason, several methods were subsequently established, such as radiation therapy and chemotherapy, to achieve better therapeutic outcomes.

After the discovery of radium by Marie Curie at the beginning of the Twentieth Century, the adoption of radiation therapy for skin tumors proved successful while led to its extensive use for decades to cure several other types of cancers, such as cervical, prostate, and breast tumors. The aforementioned technique is used to target localized tumors through high-energy radiations (e.g., electrons, protons, and various ions) to eliminate the malignant cells by damaging directly the cellular DNA or triggering the generation of toxic free radicals within the cells. Gradually, advanced techniques were developed, including fractionation, three-dimension conformal radiotherapy (3D-CRT), intensity-modulated radiation therapy (IMRT), and image-guided radiotherapy (IGRT). As a result, this type of treatment became one of the most distinguished therapeutic tools in oncology.[22]

Over the years, pioneering strategies emerged, where a small area of the body is exposed to a very high dose of radiation to damage and destruct only selected parts within an organ or tissue.[23] The so-called radiation-based surgical knives (e.g., stereotactic radiosurgery (SRS), gamma knife systems, linear accelerator (LINAC) systems, and proton beam therapy) include no actual cutting or blade during the entire

process. However, it is still referred to as surgery because the results of this treatment are quite similar to ordinary surgery.[24]

A few years after the successful application of radiation therapy, the German biochemist Paul Ehrlich envisaged the possibility of preparing chemical substances which would be able to target specific diseases in the human body (the so-called "magic bullets").[25] Remarkably, the cure of syphilis by administrating the organoarsenic compound arsphenamine (Salvarsan) represented a major success supporting the "magic bullet" concept at the time. Thus, the term chemotherapy was first introduced to describe this pioneering chemical approach for the treatment of several diseases. A few decades later, the golden age of cancer chemotherapy began and despite the various drawbacks, even nowadays it is one of the most significant therapeutic modalities. In contrast with surgery and radiation therapy, chemotherapy is mainly systemic, traveling through the body to reach cancer cells.[1,26]

Initially, partial remission of pediatric leukemia was achieved by treatment with the chemical compound 4-aminopteroic acid (Aminopterin). The Food and Drug Administration (FDA) approved in 1949 the first chemotherapeutic drug specifically addressing cancer, namely, the alkylating agent nitrogen mustard, to treat Hodgkin's lymphoma.[27] Currently there are 132 FDA-approved chemotherapeutics, which can be administered alone or in combination with other therapies.[28] These drugs present a variety of compositional and structural characteristics, and modes of action, and are designed in such a way to specifically target and terminate tumor cells. Depending on their features, these anticancer agents can be categorized as alkylating agents, antimetabolites, anthracyclines, antitumor antibiotics, topoisomerase inhibitors, mitotic inhibitors, and miscellaneous drugs.[28]

A major drawback of chemotherapy is the lack of selectivity, meaning that drugs can affect also healthy cells and, consequently many side-effects may arise upon treatment such as hair loss, nausea, fatigue, vomiting and organ toxicity (among others). For this reason, the concept of combination chemotherapy was developed, in which multiple drugs are administered together to achieve an effective therapeutic outcome and at the same time, minimize side effects. In 1997, advances in targeted cancer therapies led to the FDA approved drug Rituxan, which belongs to a new class of therapeutic agents known as monoclonal antibodies.[29]

The successful decoding of the human genome in 2003, allowed the identification of the genetic flaws that can lead to tumor genesis and opened up new perspectives to

the development of alternative cancer therapies which can be applied to patients with advanced tumors, that cannot be surgically removed or do not respond to other treatments. Characteristic examples of these immunotherapies are the FDA approved pharmaceuticals, PD-1 inhibitors pembrolizumab (Keytruda),[30] and nivolumab (Opdivo),[31–33] alongside with the gene therapy's chimeric antigen receptor-modified T cell (CAR-T) tisagenlecleucel (Kymriah, also known as the 'living therapy').[34]

In parallel, advances in the field of molecular biology have indicated hormone therapy as an effective way to manage malignancies since almost 25% of tumors in men and 40% in women are known to have a hormonal basis. Additionally, utilization of stem cells can be considered as a promising strategy for the treatment of cancer (although still at an early clinical trial stage) due to their ability to differentiate into any type of cells in the body, thus advocating for their use in the regeneration of damaged tissues including heart, liver, bones, skin, and cornea.[34]

Current research efforts in the field are advocating for fit-for-purpose therapeutic strategies as potential substitutes for more invasive practices, which can selectively target tumor sites with no or limited impact on the surrounding environment. More precisely, nanomedicine, thermal ablation and magnetic hyperthermia, radiomics and pathomics, antioxidant molecules, and theranostics have been proposed to provide a broader perspective in diagnosis and therapy, overcome limitations and drawbacks of conventional therapies and improve the therapeutic outcome.[10,35]

1.1.2 Theranostics: An All-In-One Strategy

Theranostics is one of the most important fields within medicine denoted to cancer management and treatment. This approach relies on one single agent which combines diagnostic and therapeutic modalities, thus allowing diagnosis but also drug delivery and treatment response monitoring. After the discovery of the radionuclide ^{131}I in 1938,[36] observations from application in animal models, shortly led to its utilization as the first theranostic agent for thyroid dysfunctions. Once easy accessibility to the ^{123}I isotope was achieved, the pair of radiotracers ^{123}I/^{131}I found general recognition in nuclear medicine practice due to its application in both diagnosis and therapy.

Interestingly, the term 'theranostics' was first proposed in 2002 by Funkhouser, to describe such bimodal agents and emphasize their capability to monitor pharmacokinetics and pharmacodynamics of the drug injected into the human body.[37]

Progressively, new therapeutic radionuclides have been developed and approved by the FDA. Theranostics with highly specific radiopharmaceutical activity such as the ^{177}Lu-DOTATATE (Lutathera) and ^{131}I-MIBG (Azedra), demonstrate feasible applications far beyond the thyroid diseases such as treatment of neuroendocrine tumors. Also, more recent agents like ^{177}Lu-PSMA, currently in Phase II Clinical Trials, may become an integral therapy in the treatment of patients with advanced prostate cancer.[37]

Considering the potentials and advances in the field of nanotechnology, including i) improved delivery of poorly water-soluble drugs; ii) targeted delivery of drugs in a cell- or tissue-specific manner; iii) transcytosis of drugs across tight epithelial and endothelial barriers; iv) delivery of large macromolecule drugs to intracellular sites of action; v) co-delivery of two or more drugs or therapeutic modalities for combination therapy; vi) visualization of sites of drug delivery by combining therapeutic agents with imaging modalities and real-time read on the in vivo efficacy of a therapeutic agent, the development of various multifunctional nanomaterials as theranostic agents is currently a hot topic.[37]

The rationale behind the design of potential nanotheranostics, which would carry or act as both a therapeutic and an imaging agent, is based on the specific delivery of the therapeutic moiety directly to the site of interest and, simultaneously, the monitoring of the progress of treatment by MRI, CT, PET or fluorescence imaging. In this regard, several inorganic materials (e.g., Superparamagnetic Iron Oxide Nanoparticles (SPIONs) and gold nanoparticles), carbon-based (Graphene Oxide (GO), Carbon Nanotube (CNT)), and polymeric nanomaterials (biodegradable polymers and polymeric micelle nanoparticles) have been developed. Studies have shown potential as carrier/delivery or imaging agents.[38]

However, the aforementioned nanomaterial-based systems present characteristics that may limit their use in pre-clinical trials, such as poor biostability, biocompatibility and non-specific recognition. To overcome these issues, research efforts have been made to design and develop a range of intelligent mono- and/or multi-functional systems as cancer theranostics. Typical examples are novel nanomaterials such as DNA nanostructures as “Trojan Horse”-type theranostics which aim to exclusively target the tumor’s microenvironment.[39]

1.1.3 Trojan Horse approach

Inspired by Greek mythology and the ancient legend of the 'Trojan Horse' which was the key to success against the walled city of Troy, scientists have been proposing strategies to target the hallmarks of tumor cells. The idea of anticancer drug delivery systems which are imitating the delivery process of the Trojan Horse, led to the development of several molecules with tunable size, different structures, and morphology which are aiming at efficient treatment regimes.[40]

Advances in the understanding of the molecular biology of cancer allowed the identification of suitable targets in biological pathways and the development of several alternative "smart" strategies to create a drug and/or imaging agent carriers that can specifically target biomolecules playing key roles in tumor cell metabolism.[41]

The targeted therapy termed as "Trojan Horse approach" can achieve effective delivery of therapeutic macromolecules (e.g., proteins, DNA, siRNAs, and organic or inorganic anticancer drugs), through carriers with favorable pharmacological profiles, to attack specific processes that control tumor cell growth, division, metastasis, and signaling. In 1992, the discovery of the Antennapedia prompted research towards the Antp-mediated transduction of heterologous proteins into cells,[42] and other 'Trojan Horse'-type peptides followed. Such as, genetically engineered proteins that cross the blood-brain barrier via endogenous receptor-mediated transport processes, drug-containing nanostructures, nucleoside analogs which can be integrated into DNA strands, and extracellular microvesicles like exosomes.[43]

Despite the medical advantages of nanotechnology for diagnosis, treatment, prevention, and cure of cancer disease. The disadvantages reported for colloidal carriers such as liposomes, polymeric micro-, and nanoparticles,[44] would turn research efforts towards alternative drug or imaging agents delivery systems for pharmaceutical applications, including vital nutrients such as vitamins.[45]

1.2 Vitamin B_{12}

1.2.1 Vitamins

Undoubtedly, energy, vitality, growth, development, and healthy maintenance of the human body are primary pursuits of nutrition and medical sciences. These aspects are mainly associated with the essential vitamins which constitute necessary dietary

micronutrients due to their diverse roles in fundamental cellular metabolic pathways. In particular, their involvement in energy-yielding metabolism, DNA synthesis, oxygen transport, and neuronal activities makes them critical for the efficient function of cells, tissues, and organs.[46]

The term 'vitamins' was first proposed in the early 1900s by the biochemist Casimir Funk following the extraction and isolation of a mixture of compounds from rice husks, assuming that all of them were 'vital amines' to all living organisms. Although in a later stage it was proved that not all of these substances were amine, the 'vitamin concept' triggered the scientific interest to investigate the structure and activity of these naturally occurring entities, and over the following century studies from multiple disciplines revealed the morphology and the biological behavior of such products. In-depth studies suggested that the vast majority of those compounds were not necessary elements for a balanced and healthy organism since they are biologically inactive, toxic, or with unclassified effects. However, thirteen of these vitamins are proved of vital importance for living organisms and could be classified into the fat-soluble retinol (vitamin A), calciferol (D), tocopherol (E) and phylloquinone (vitamin K) (**Figure 1.3**), and the water-soluble ascorbic acid (vitamin C) and B complex nutrients, including thiamine (B_1), riboflavin (B_2), niacin (B_3), pantothenic acid (B_5), pyroxidine (B_6), biotin (B_7), folate (B_9) and cobalamin (B_{12}) (**Figure 1.4**).[47]

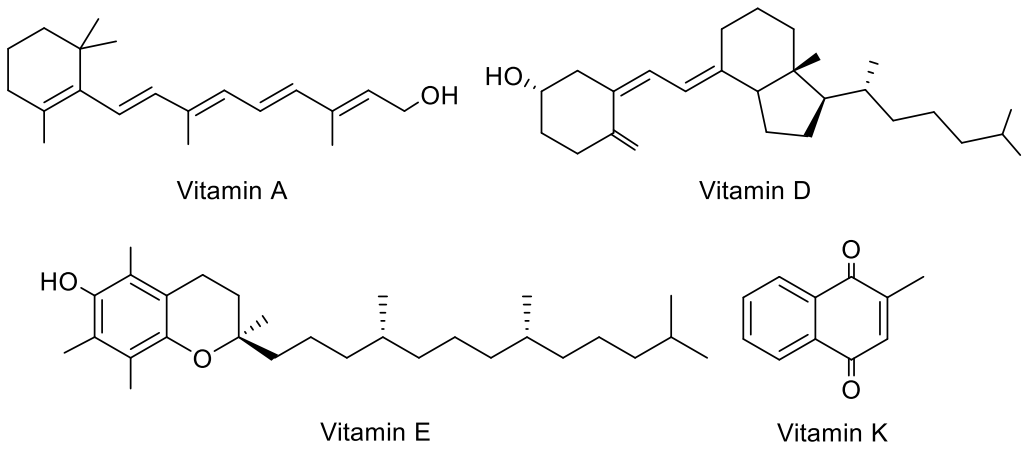

Figure 1.3: Chemical structures of the fat-soluble vitamins.

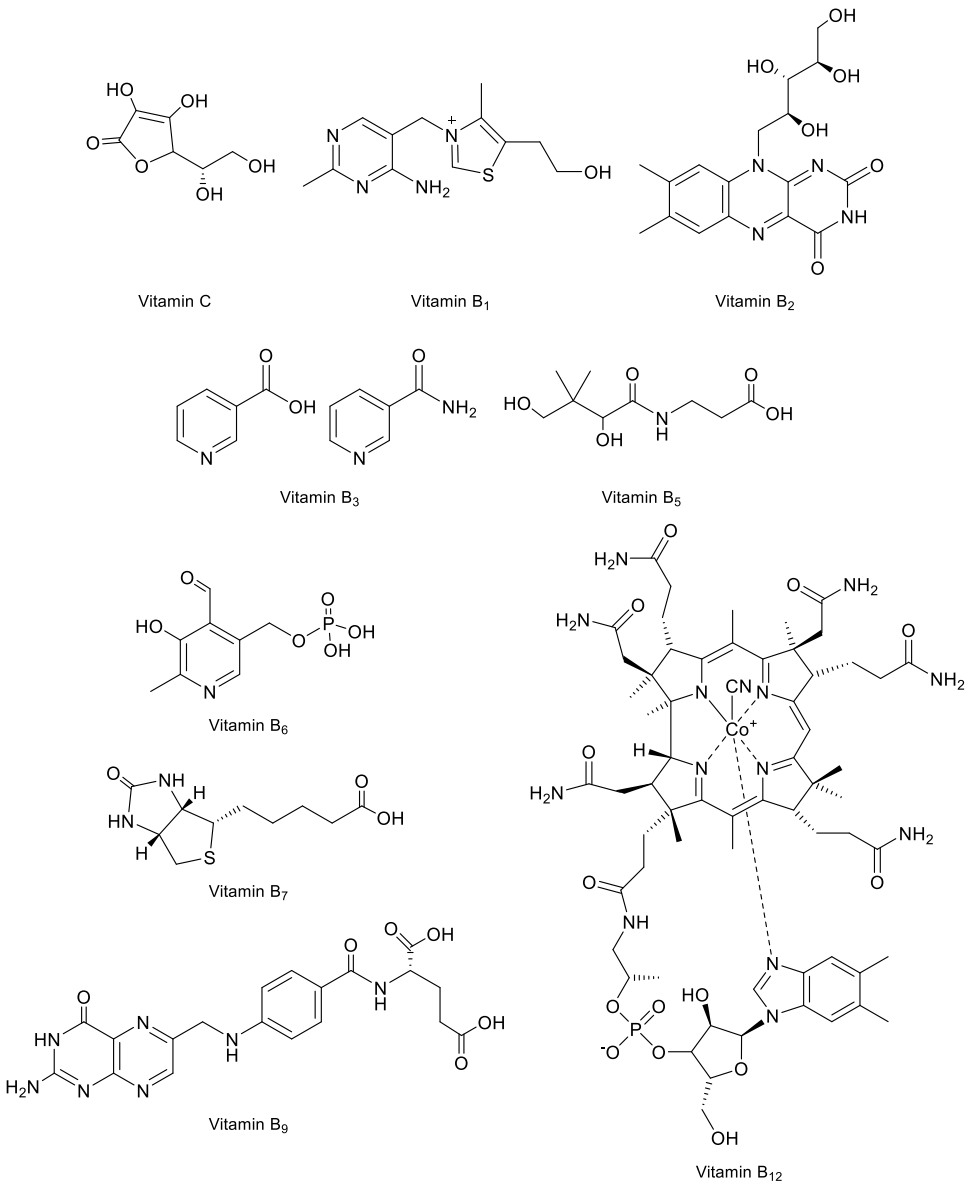

Figure 1.4: Chemical structures of the water-soluble vitamins.

Interestingly, the majority of these bioactive compounds are organic molecules of different chemical nature (e.g., alcohols, aldehydes, nucleotide derivatives, carboxylic acids, and amines), the only exception being the organometallic derivative vitamin B_{12} (aka cyanocobalamin, CNCbl) which contains a transition metal ion (Co^{III}).[48] It is worth pointing out that the term 'vitamin B_{12}' from a chemical point of view, only applies to cyanocobalamin, whereas in the field of nutrition and pharmacology, it generally refers to all cobalamin analogs exerting biological activity in humans (that is, those in which the cyano group is replaced by other moieties such as CH_3, H_2O, etc.).[49]

1.2.2 Annals of Vitamin B_{12}

In 1849, Thomas Addison laid the foundation for the discovery of vitamin B_{12} in an attempt to find a possible treatment for pernicious anemia.[50] Although several treatments were investigated to cure the disease, outcomes proved minimal until the late 1920s. At the time, supplementing the patient's diet with large amounts of the slightly cooked liver in the patient's diet showed to somewhat minimize the symptoms of anemia and prevent death. This observation attracted the interest of the physicians George Minot and William Murphy to identify the actual therapeutic agent.[51] Eventually, in 1948 Folkers and co-workers managed to isolate the new vitamin which was purified and recrystallized from the liver.[52,53] Due to the complexity of the deep pink colored molecule, its chemical structure was determined only a decade later by the crystallographer Dorothy Hodgkin,[54] who was awarded the Nobel Prize in Chemistry in 1964 for her achievement (**Figure 1.5**). The extensive studies carried out by the research groups of Woodward[55] and Eschenmoser[56] resulted in the chemical synthesis of vitamin B_{12} in 1971. Particular interest was exhibited by the 30-step biosynthetic pathway of the vitamin from certain prokaryotes such as Propionibacterium freudenreichii and Lactobacillus lechmanii, which was completely elucidated in the late 1990s.[57] Due to lack of specific dedicated enzymes mammals are unable to synthesize vitamin B_{12}, hence they call for the vitally necessary amount of the vitamin from dietary sources.

Figure 1.5: Dorothy Crowfoot Hodgkin (1910-1924) (Source: The Nobel Price Foundation, The Nobel Prize in Chemistry 1964, www. nobelprize.org/prizes/chemistry/1964/summary/).

1.2.3 Structural Characteristics

Vitamin B_{12} ($C_{63}H_{88}CoN_{14}O_{14}P$, 1355.39 g/mol) is the largest of all vitamins and is regarded as one of the most visually appealing biomolecules due to its shining dark

pink crystals.[58] Like the other cobalamin analogs, it belongs to the family of the natural products name corrinoids, which includes also cobamides and cobinamides.[50] Numerous theoretical calculations, spectroscopic measurements, and refinements of the crystal structure determined its general configuration (**Figure 1.6**), consisting of a central corrin ring where a cobalt(III) ion is coordinated by four equatorial nitrogen atoms, an α-axial benzimidazole moiety, and a sixth ligand (the cyano group specifically in vitamin B_{12}), whose variations account for the different cobalamin isoforms.[57,59]

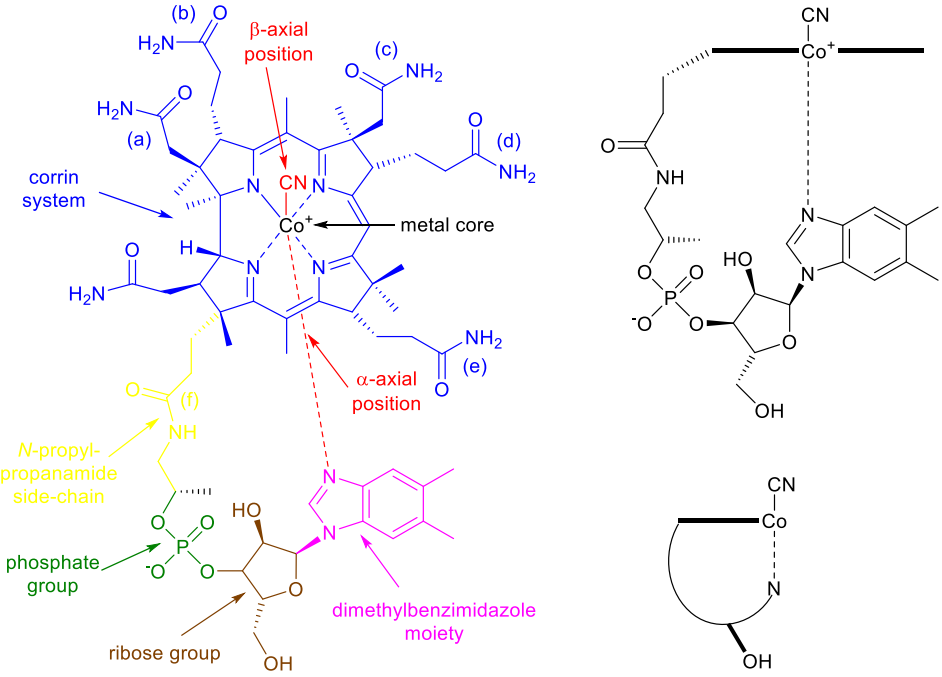

Figure 1.6: Structure (left) and simplified schematic representations (right) of vitamin B_{12}.

In-depth analysis of the crystallographic data unveiled the complexity of the finely structured organometallic compound. The core of the molecule is the planar macrocyclic corrin system resulting from the linkage of four reduced pyrrole rings, which also pose various peripheral side groups. The Co(III) ion is located in the center of the corrin ring, adopting an octahedral geometry through the formation of six coordination bonds with atoms from the surrounding environment. Four of which provided by the nitrogen atoms of the corrin pyrrole subunits, occupying the four equatorial positions. The fifth coordination site (α-axial position) extends below the plane of the corrin frame and is occupied by one of the nitrogen atoms of a 5,6-dimethylbenzimidazole moiety, whilst the other nitrogen atom is linked to a ribose

sugar. The latter is connected to a phosphate group, and thence back onto the periphery of the corrin ring via an N-propyl-propionamide linker. The metal ion completes its coordination sphere with a cyano group (β-axial position), which expands above the plane of the corrin system. Replacement of the cyano group with other moieties would determine the name and physiological properties of the resulting cobalamin analogue.[59] Cyanocobalamin (CNCbl) is the synthetic form of vitamin B_{12} which is commercially available for multiple purposes such as medical applications, food fortification, and nutrient supplements. This framework appears to be the most stable and replacement of the cyano group in mammals mainly leads to the bioactive isoforms hydroxocobalamin, methylcobalamin, adenosylcobalamin, and glutathionylcobalamin.[60,61] Hydroxocobalamin (OH-Cbl) is commonly used as a dietary supplement, while methylcobalamin (Met-Cbl) and adenosylcobalamin (Ado-Cbl) constitute the bioactive coenzymes of vitamin B_{12} in cells.[62] Earlier studies indicate glutathionylcobalamin (GS-Cbl) as an intermediate in cobalamin metabolism, which is likely to play a key role in anti-oxidative and anti-inflammatory processes, as well as in the regulation of NO syntheses. Additionally, aquocobalamin (B_{12a}) can act as an intermediate in metabolic pathways, and some other vitamers show unspecified activity profiles such as nitritocobalamin (B_{12c}), nitrosocobalamin, and sulfitocobalamin (**Table 1.2**).[63]

Vitamers	Abbreviation	Description
Adenosylcobalamin	Ado-Cbl	Biologically active coenzyme
Aquocobalamin	B_{12a}	Intermediate product
Cyanocobalamin	CN-Cbl	Synthetic cobalamin
Glutathionylcobalamin	GS-Cbl	Transient precursor of coenzyme
Hydroxocobalamin	OH-Cbl	Produced by microorganisms
Methylcobalamin	Met-Cbl	Biologically active coenzyme
Nitritocobalamin	B_{12c}	B_{12} and nitrogen dioxide (NO_2)
Nitrosocobalamin	N/A	B_{12} and nitrogen monoxide (NO)
Sulfitocobalamin	N/A	B_{12} and sulfur trioxide (SO_3)

Table 1.2: Vitamers of vitamin B_{12} and their general description.

1.2.4 Recommended Intake of Vitamin B_{12}

Considering the bioformulation of vitamin B_{12} from specific bacteria, several studies attempted to estimate the ability of mammalian intestinal flora to synthesize and subsequently supply the host organism with the nutrient. Interestingly, the bacterial activity in animals' gastrointestinal region, turned out to be the exclusive biosynthetic pathway to vitamin B_{12}, which is then made available in the organism's tissues. In humans, although living microorganisms were able to synthesize the vitamin, the amount generated is negligible and unlikely to be absorbed since it is produced in the colon. As a result, the nutrient can be assimilated only from food of animal origin, supplements, or fortified nutriments.[64] Taking into account the above observations and given the vital involvement of vitamin B_{12} in life-threatening diseases like anemia and neurological dysfunctions, health organizations introduced the Recommended Dietary Intake (RDI in μg/d) for individuals, to maintain adequate Cbl levels. The suggested daily intake of vitamin B_{12} depends on specific criteria such as gender, age, and specified health conditions (**Table 1.3**).[50]

Life stage	RDA/AI USA/CA	RDI WHO	RDA AU/NZL	RNI UK	AI EU	RI NNR	IRDA
Infants							
0 – 6 m	0.4	0.4	0.4	0.3	-	-	
7 – 12 m	0.5	0.5	0.5	0.4	1.5	0.5	0.2
Children							
1 – 3 y	0.9	0.9	0.9	0.5	1.5		0.2 -1.0
4 – 8 y	1.2	1.2	1.2	0.8	1.5	1.3	0.2 -1.0
Males							
9 – 13 y	1.8	1.8	1.8	1.0	3.5	2.0	0.2 -1.0
≥ 14 y	2.4	2.4	2.4	1.5	4.0	2.0	1.0
Females							
9 – 13 y	1.8	1.8	1.8	1.0	3.5	2.0	0.2 -1.0
≥ 14 y	2.4	2.4	2.4	1.5	4.0	2.0	1.0
Pregnancy	2.6	2.6	2.6	1.5	4.5	2.0	1.2
Lactation	2.8	2.8	2.8	2.0	5.0	2.6	1.5

Table 1.3: Recommended Dietary Intake (in μg/d) around the globe. (Abbreviations: RDA, Recommended Dietary Allowance; AI, Adequate Intake; RDI, Recommended Dietary Intake; WHO, World Health Organization; RNI, Recommended Nutrient Intake; RI, Recommended Intake; NNR, Nordic Nutrition Recommendations; IRDA, Indian Recommended Dietary Allowances).[50]

Comprehensive guidelines indicate an RDI of 1-5 μg, although there are cases that may require a higher intake of vitamin B_{12} due to individual gastrointestinal absorption capacity. These variations often arise from intestine malfunctions such as atrophic gastritis and can progressively lead to vitamin B_{12} deficiency.[50,64]

1.2.5 Deficiency of Vitamin B_{12}

Cyanocobalamin is an essential nutrient involved in a variety of biochemical processes in the human body. Interestingly, the micronutrient retains a key role in several functions, including the formation of DNA bases and red blood cells, appropriate neurologic signaling, methyl group transportation, as well as the metabolism of branched-chain amino acids and fatty acids with an odd number of carbon atoms. Consequently, its deficiency can lead to metabolic anomalies and several mild health conditions, including weakness, fatigue, constipation, and more serious illnesses such as hematopoietic disorders and spinal cord-related neuropathies.[50,64] In the past, it was assumed that vitamin B_{12} deficiency developed mainly in patients affected by pernicious anemia, however, more recent studies reported cases of other types of anemia such as the malignant Addison Biermer and megaloblastic anemia, as well as various neurological complications, which are associated with the lack of the vitamin. Additionally, individuals with chronic atrophic gastritis, celiac disease, tropical sprue, Crohn's disease, and blind loop syndrome show an extensive vitamin B_{12} deficiency. In all of the pathologies conditions mentioned above, administration of the injectable form of the nutriment is deemed crucial to their successful treatment.[65]

1.2.6 Uptake, Transport and Metabolism of Vitamin B_{12}

The considerable number of health conditions caused by vitamin B_{12} deficiency led to extensive research to elucidate the complex pathway to nutrient absorption and to clarify its cellular trafficking and metabolism. In an attempt to estimate the absorbed

vitamin B_{12} within the human body, various methods have been employed such as serum gastrin, pepsinogen levels, and castle factor antibodies estimation. Other approaches include the Schilling test and MMA, tHcy markers. Additionally, alternative techniques had been adapted including whole-body counting of radiolabeled cyanocobalamin, metabolic balance studies, and controlled feeding studies in individuals with insufficient Cbl levels.[50]

The form in which vitamin B_{12} is ingested into the human body can influence the absorption pathway (**Figure 1.7**). The nutriment is taken in either bound to food proteins or in its free form. In the first case, the protein-Cbl complex must undergo an early proteolytic cleavage in the stomach or duodenum before it can be absorbed in the ileum of the small intestine in its free form; on the other hand, vitamin B_{12} isoforms found in supplements are not subject of the same process, as they are available as is. Absorption, transport, and eventual distribution of the nutriment in the body follow a complex but well-defined pathway which includes a sequence of homologous carrier proteins with similar peptidic molecular weights of about 45 kDa, different specificities, and high affinity for Cbl. Namely, following the stepwise aggregation of transport protein-Cbl, these are the haptocorrin (HC, also known as R-protein or transcobalamin I), intrinsic factor (IF or castle factor), and transcobalamin (TC or transcobalamin II).[57,58]

The non-protein bound form of Cbl is initially linked with salivary HC, which is secreted by both the salivary glands in the oropharynx and the gastric mucosal cells within the stomach, to form the complex HC-Cbl. The cluster is gradually transported to the second segment of the duodenum in the small intestine, where the enzymatic activity of pancreatic proteases promotes degradation and subsequent release of vitamin B_{12}. When the vitamin is ingested in its protein-bound form, it can be transported to the stomach. At this point, the acidic environment provided by the parietal cells is necessary to convert the pepsinogen to pepsin, whose functional activity is responsible for the proteolytic cleavage of the protein-Cbl complex. Following this protein degradation, the free vitamin B_{12} will then proceed as discussed previously.

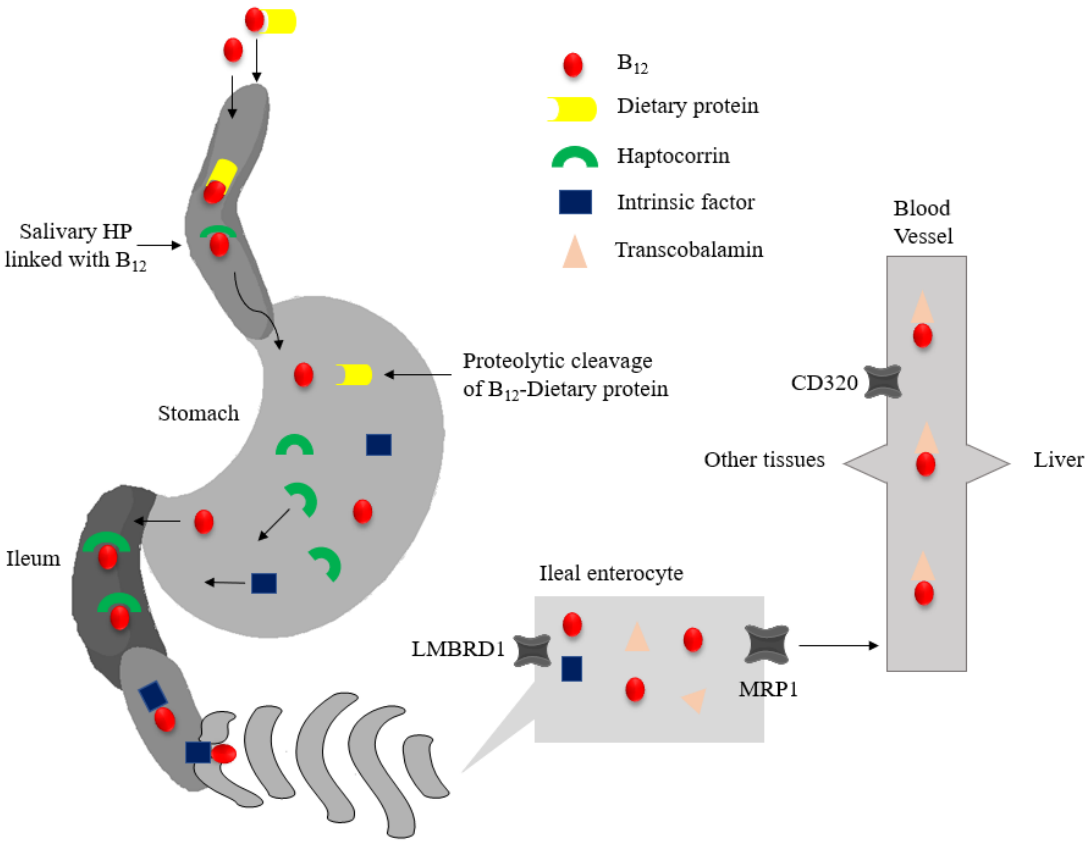

Figure 1.7: General representation of the absorption pathway of Cbl.

The vitamin in its free form can now be tightly bonded to the intrinsic factor, to form the IF-Cbl adduct and proceeds toward the ileum of the small intestine for absorption. The aforementioned polypeptide protects vitamin B_{12} from enzymatic digestion due to the presence of various glycosylation sites on its surface. Once the aggregate reaches the terminal ileum, can be internalized through a receptor-mediated endocytosis process inside the enterocytes, where the complex is degraded in the lysosomes. After the dissociation of the IF-Cbl, the nutriment through the transmembrane protein LMBRD1 crosses the intracellular lysosomal membrane to the cytoplasm either for cellular utilization or release from the basolateral side of the enterocyte to the bloodstream. The presence of the transporter TCII leads to the formation of the circulating bioavailable form of the vitamin TCII-Cbl, which can then be transported to other tissues of the human body. Following the internalization and metabolism within the ileal enterocyte, vitamin B_{12} can be processed for release into the portal circulation through the MRP1 protein to reach other sites after receptor-mediated endocytosis. It is known that serum B_{12} is bound to the active transport protein transcobalamin II (TCII), which delivers about 20% of the nutriment in other organs

and tissues. Interestingly, Cbl mainly accumulates in hepatic cells, where it is stored until needed by the body. The subsequent release of the TCII-Cbl complex into the cellular plasma of the tissues is operated by the transmembrane protein CD320 (also known as TCb1R) through a TCII receptor-mediated endocytosis process. In the cell, the TCII-Cbl aggregate can be internalized into the lysosomes and dissociated by lysosomal proteases. Whereas the carrier protein is recycled to the membrane and the free cobalamin can then follow the cellular trafficking and be converted into its biologically active forms, adenosylcobalamin, which serves as a cofactor for the mitochondrial enzyme methylmalonyl CoA mutase and methylcobalamin. Which functions as a cofactor in folate-dependent conversion of homocysteine to methionine by the enzyme methionine synthase in the mitochondria and cytosol, respectively. In the mitochondrion, the catalytic effect of reductase enzymes results in the reduction of cob(III)alamin to cob(II)alamin. The former after the attachment on MMAB (methylmalonic aciduria type B), an ATP-dependent adenosyltransferase, undergoes an additional reduction by reductases to form cob(I)alamin that is adenosylated in presence of ATP to form adenosylcob(III)alamin (AdoCbl). Then, MMAB transfers the coenzyme AdoCbl to methylmalonyl-CoA mutase (MCM), an enzyme that is involved in metabolic degradation pathways of odd-chain fatty acids, branched-chain amino acids, and cholesterol. It has been postulated that AdoCbl-MCM complex catalyzes the conversion of methylmalonyl-CoA into succinyl-CoA, which can enter the Krebs cycle for catabolic utilization. In the cytosol, the provitamin form of cob(II)alamin (without the β-axial ligand) is reduced directly to cob(I)alamin upon exceptional organometallic enzymatic reactions with a sequence of proteins, to acquire a methyl group. Initially, the polypeptide MMADHC (methylmalonic aciduria type D and homocystinuria) escorts the provitamin to methionine synthase reductase (MSR), the enzyme responsible for MetCbl formation and transformation of N5-methyltetrahydrofolate to tetrahydrofolate. Subsequent interaction with the cytoplasmatic methionine synthase (MS) leads to the catalytic transfer of a methyl group from N5-methyltetrahydrofolate to homocysteine (HCY) molecule, to yield methionine. The aforementioned amino acid plays a crucial role in the synthesis of S-adenosylmethionine, a methyl group donor used in numerous biochemical reactions, including the methylation of many sites within DNA, RNA, proteins and polyamines.

1.3 Vitamin B_{12} in drug design and delivery

Considering the metabolic pathway of vitamin B_{12}, where reduction of Co(III) to Co(II) and subsequent release of the β-axial ligand occurs preferentially in the cell, derivatization of vitamin B_{12} with a cytotoxic (chemotherapeutics) or imaging (fluorophores or radionuclides) agent has been envisaged. The well-known high demand for methionine and energy from rapidly dividing tumor cells (greater than in healthy cells), rationally draws attention to the vitamin as a potential smart carrier for pharmacologically active agents specifically on tumor sites. Thus, a tailored design of vitamin B_{12}-based bioconjugates, meticulously modified on available sites to preserve recognition by the transport proteins, would be regarded as a Trojan Horse-type approach for targeted chemotherapy and diagnosis, in which the inherent structural characteristics of cobalamin can release the substance of interest attached to it only once internalized in cancer cells.[66–68] Conventional anticancer chemotherapy generally aims at interfering with DNA synthesis and mitosis, ultimately leading to the elimination of uncontrollably growing and dividing cancer cells. Although successful to some extent, these strategies are non-selective and can also damage healthy tissues and organs, thus causing a lot of undesirable side-effects possibly increasing the mortality rate of cancer patients. In this context, research focus has turned toward the development of targeted chemotherapies able to enhance the specificity of the pharmacological treatment by designing drug delivery systems capable to deliver the chosen chemotherapeutics directly into the target site. Considering the essential features of a potential drug (or imaging agent) carrier, research in the field of drug design and delivery identified (among others) cyanocobalamin as a suitable candidate.[69] This molecule presents a considerable number of favorable characteristics that may increase the therapeutic outcome, such as low bioavailability, water-solubility, stability under physiological conditions, lack of toxicity, and preferential accumulation in fast proliferating malignant cells.[70] So far, studies have shown that the incorporation of Cbl successfully enhanced the oral bioavailability of tethered peptides, proteins and drugs with poor solubility / low intestinal absorption.[60,71] Additionally, recent advances in the field have achieved the delivery of erythropoietin, hormones, and insulin on the target site.[72] Consequently, taking into account the chemical features of vitamin B_{12} and the aforementioned encouraging results, the rational design of fit-for-purpose functionalized vitamin B_{12}-

based bioconjugates can be regarded as a 'Trojan Horse' strategy for the effective delivery of antitumor drugs or diagnostic agents into cancer cells. The first step of this elegant approach would be to identify the proper attachment site of the molecule of interest to vitamin B_{12}, which can be either coupled directly or through a 'spacer' in a way that creates distance between Cbl and the cargo moiety. From a chemical point of view, there are several functional groups readily available for modification on vitamin B_{12} to link the therapeutic or diagnostic agent, including the propionamides, acetamides, hydroxyl groups, the cobalt(III) center, and the phosphate moiety.[73–76] However, from a biological perspective there are some limitations since these modifications may affect the recognition by, or reduce the affinity towards proteins included in vitamin B_{12} uptake and metabolic pathway.[77] In general, conjugation of the desired drug to vitamin B_{12} may be achieved (at least in principle) in multiple positions (**Figure 1.8**).[78–81] Starting from the β-axial position of vitamin B_{12}, reductive alkylation of the Co(III) center or coordination to the N atom of the cyano (CN) group in CNCbl could lead to the formation of the desired bioconjugate. Conjugation may be also achieved by functionalized the peripheral carbonyl groups of the corrin framework (following the hydrolysis of the amide moieties), as well as through esterification of the 2'-/5'-OH sites of the ribose unit. Research reports have identified the 5'-OH ribosyl group and the β-axial Co(III) position as the most suitable conjugation sites to prevent or limit disruption of recognition of vitamin B_{12} by transport proteins involved in the vitamin trafficking and metabolic processing.[69,71,82] Hence, linkage of a cytotoxic or diagnostic agent at the aforementioned locations conduces successful cellular uptake and delivery and protects the complex from dissociation before its release into the cancer cell.

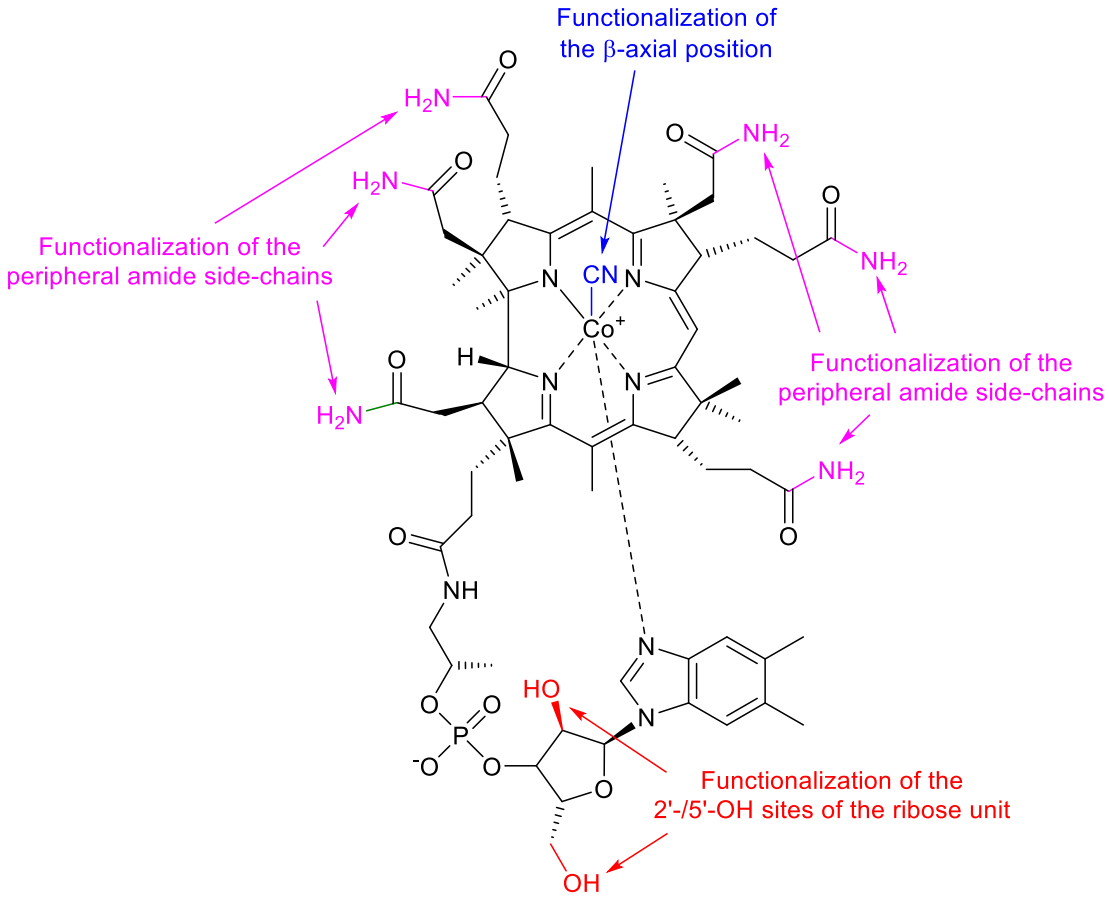

Figure 1.8: Potential functionalization sites of vitamin B_{12}.

During the last few decades, an impressive number of metal-based derivatives have shown promising antitumor activity. However, these compounds are often accompanied by major drawbacks, such as low water solubility and stability under physiological conditions, side effects and lack of tumor selectivity. As a result, their application in targeted anticancer treatment, clinical approval, and global marketing has been limited.[83–87] In an attempt to overcome these challenges, alternative approaches have been sought, including the functionalization of the pharmacologically active metal derivatives with a carrier biomolecule for tumor-targeting delivery and accumulation. Taking into account the main features of vitamin B_{12}, along with its higher demand in tumor cells compared with healthy ones, the generation of cyanocobalamin-metallodrugs bioconjugates turns out to be a promising strategy that is expected to mitigate drawbacks by generating more efficient, selective, and less toxic metal-based conjugates for diagnostic or therapeutic purposes.

1.3.1 Diagnostic Vitamin B_{12} Metal Bioconjugates

1.3.1.1 Radiolabeled Vitamin B_{12} Scaffolds

A milestone in the history of nuclear hematology was set in 1953, when Robert F. Schilling developed a radiolabeled vitamin B_{12} test, to determine the intestinal absorption capacity in patients with vitamin B_{12} deficiency.[64] This procedure included multiple stages and the most commonly used radioisotopes, at the time, were ^{57}Co and ^{58}Co. In the late 1990s, attempts to evaluate the accumulation of the vitamin in transplanted tumors with ^{57}Co-labeled occurred.[88,89] Then, the research interest directed towards the development of vitamin B_{12} derivatives functionalized with other radiodiagnostics for medicinal imaging. Over the last two decades, various cobalamin-based radioisotope scaffolds have been reported, aiming at providing diagnostic and follow-up information of cancer patients. In particular, the gamma-emitting ^{99m}Tc, ^{111}In, and ^{131}I isotopes and the positron-emitting ^{68}Ga, ^{64}Cu, and ^{89}Zr radionuclides have been considered for application in SPEC and PET, respectively.[70]
Technetium-99m ($t_{½}$ = 6.0 h) was discovered in 1938 by Emilio Segre and Glenn Seaborg. Due to its beneficial use for in vivo applications, radionuclide became popular in diagnostic nuclear medicine. Notably, in 1970 Eckelman and Richards developed the first commercially available ^{99m}Tc "instant kit" radiopharmaceuticals containing the complex Techneplex (^{99m}Tc-DTPA, DTPA = diethylenetriamine-N,N,N′,N″,N″-pentaacetic acid), which was approved for renal, brain and lung imaging.[90,91] In 1997, the first ^{99m}Tc-labelled cobalamins were reported by Collins and Hogenkamp. The study describes the successful preparation of a family of ^{99m}Tc-DTPA conjugates of cyano-, methyl-, and adenosylcobalamin via derivatization of the b-, d- and e-propionamide sidechains on the periphery of the corrin ring with a butylene diamine spacer and subsequent attachment of the radioactive scaffold. Despite the impressive synthetic results and effectiveness in animal models, the desired tumor visualization was prevented due to the accumulation of the bioconjugate in the kidneys, liver, and spleen.[89] A few years later, Alberto and co-workers proposed a novel strategy for the preparation of vitamin B_{12}-labeled radiopharmaceuticals.[92–94] This approach relies on the functionalization of the corrin ring with tridentate ligands like *N*ε-derivatized histidines,[95,96] S-derivatized cysteines,[97] or picolylamine-monoacetic acid (PAMA)[98] and the subsequent

attachment of the organometallic {fac-$^{99m}Tc^{I}(CO)_3$} scaffold. Interestingly, studies on mice revealed that the [B_{12}-$(CH_2)_4$-PAMA-(fac-$^{99m}Tc^{I}(CO)_3$)] derivative (**Figure 1.9**) accumulates preferentially in tumors, while there is limited uptake in the liver and kidneys.[99,100] Results from preliminary clinical trials unveiled the feasibility of selective tumor imaging in a variety of different metastatic tumors with reduced renal uptake.

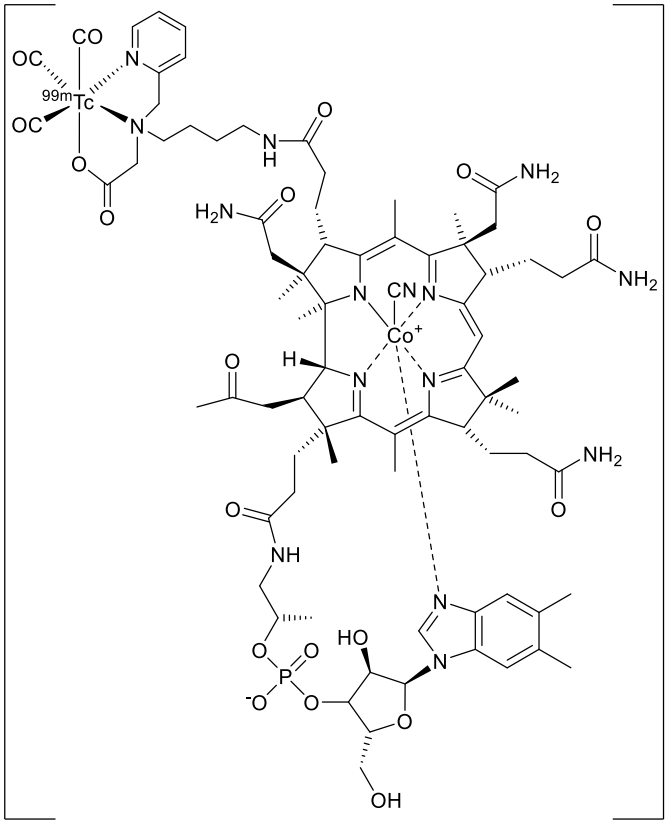

Figure 1.9: Chemical structure of the [B_{12}-$(CH_2)_4$-PAMA-fac-$^{99m}Tc^{I}(CO)_3$]) conjugate.

Indium-111 ($t_{½}$ = 67.9 h) is the most stable radioisotope of the element and one of the most widely used radionuclides in routine clinical diagnosis. In 1990, its successful use by Alan Fischman on chemotactic peptides for the detection of infections triggered research into the generation of ^{111}In complexes for the potential radiolabeling of biomolecules. In this regard, several such species had been obtained bearing multifunctional chelating agents.[101,102] Among all, the ^{111}In-DTPA derivative exhibited great potential for imaging studies in patients affected by different types of cancer.[103] Derivatization of cobalamins with the aforementioned radiocomplex, drew the attention of the scientific community due to the successful visualization of a wide

range of human tumors.[104] However, selective accumulation in tumor sites was not achieved due to high uptake of the bioconjugate from other tissues and organs.[105]

Soon after the discovery of iodine-131 ($t_{½}$ = 8.02 d) in 1938 by John Livingood, the researcher's Joseph Gilbert Hamilton, Mayo Soley and Robley Evans suggested its use for diagnostic purposes. At the beginning of the 1950s, the radioisotopic drug ($Na^{131}I$) was approved by FDA for use in patients affected by thyroid dysfunction. In 2007, Alberto and co-workers reported the first examples of ^{131}I-B_{12} derivatives obtained by a ligand exchange reaction from the chlorinated B_{12}-platinum(II) analogs (**Figure 1.10**). To date, monitoring of in vivo distribution and migration of the radio-iodinated bioconjugates has not been reported.[106,107]

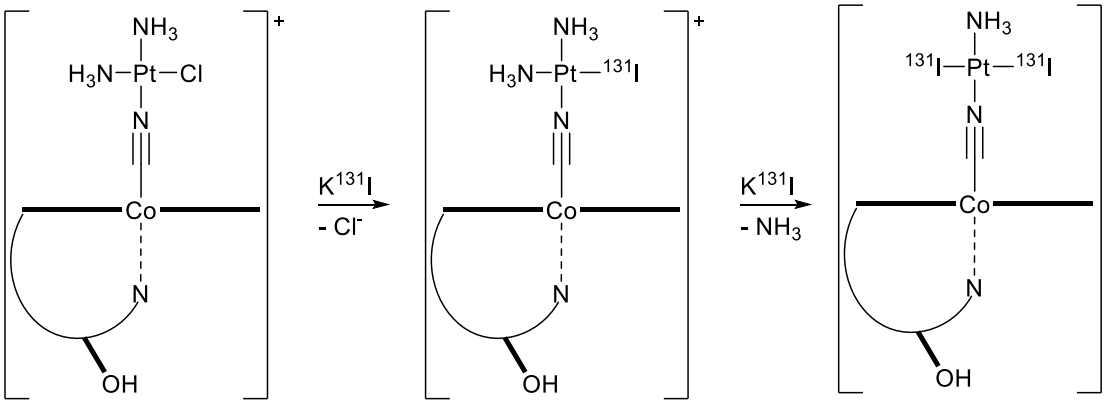

Figure 1.10: ^{131}I-labeled B_{12}-platinum(II) conjugates.

Gadolinium, like most of the rare earth elements, tends to form trivalent Gd^{3+} ions which present paramagnetic properties. Chelated gadolinium(III) compounds have various applications especially as contrast agents to improve the resolution of the scan images. In 2009, Siega and co-workers generated two gadolinium(III)-containing vitamin B_{12} conjugates upon esterification of the 5'-site of the ribose with the chelating ligands diethylenetriamine-N,N,N′,N″,N″- pentaacetic acid (DTPA) and triethylenetetramine- N,N,N′,N″,N‴,N‴-hexaacetic acid (TTHA).[108] Results from in vitro cytotoxicity studies in human immortalized myelogenous leukemia K562 cells showed decreased cell viability for the gadolinium(III)-DTPA-B_{12} conjugate due to the release of Gd^{3+} ions, whilst for the more stable gadolinium(III)-TTHA-B_{12} no significant change on cell viability was detected.

Due to its positron-emitting and chemical properties, copper-64 ($t_{½}$ = 12.6 h) has been used in diagnostic imaging as a PET tracer, and as a radiopharmaceutical by labeling biological molecules for targeted tumor visualization. After the successful probing of monoclonal antibodies and proteins,[109] a ^{64}Cu-vitamin B_{12} PET imaging agent was reported.[110] The radiolabeled bioconjugate was prepared via derivatization at the 5′-OH site of the ribose with the ethylendiaminebenzyl-1,4,7-triazacyclononane-N,N′,N″-triacetic acid ligand and subsequent inclusion of the copper-64 isotope. Biological studies in allograft melanoma and xenograft models of pancreatic, ovarian and colorectal cancer implanted in mice showed a high accumulation of copper-64. However, a major issue once again was renal accumulation, most likely due to the over-expression of the Holo-TCII binding receptor megalin.[111]

Over the last twenty years, extensive research in the development of molecular imaging cancer biomarkers indicated ^{89}Zr ($t_{½}$ = 78.4 h) as a radiometal with nearly ideal physical and chemical properties for antibody-based positron emission tomography (immuno-PET).[112] In a view to visualize and characterize tumor sites, various ^{89}Zr-labeled antibodies have been synthesized via well-established chelating and transmetallation procedures.[113] Recent studies in the field are suggesting the exploitation of the vitamin B_{12} uptake pathway components, such as the IF-B_{12} receptor cubilin, as potential targets of novel radiolabeled cobalamin derivatives. In this regard, Doyle and co-workers investigated the effects of systemic administration of ^{89}Zr-B_{12} conjugates (**Figure 1.11**) pre-bound to human gastric IF (IF-[^{89}Zr]-B_{12}).[114] In vivo PET imaging studies carried out in mice showed the absence of effects on IF uptake by endogenous Cbl, thus suggesting the potential use of IF on B_{12} conjugates for imaging or therapeutic purposes. Since the IF factor used in this study originates from plants, the high accumulation of the IF-[^{89}Zr]-B_{12} complex in the liver was attributed to the most likely recognition by the mannose CD206 receptor present in liver epithelial cells and macrophages, and not the cubilin receptor which is the only known receptor for holo-IF in humans.

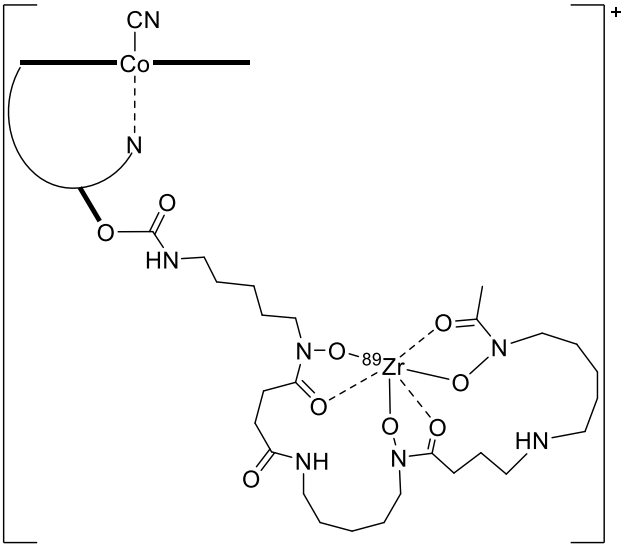

Figure 1.11: Chemical structure of the ^{89}Zr-B_{12} conjugate.

1.3.1.2 Fluorescent Vitamin B_{12} Metal Complex Conjugates

Alongside the radiolabeled vitamin B_{12} metallodrugs, some examples of luminescent probes containing Cbl have been reported. While vitamin B_{12} is a poor light-emitting molecule (maximum fluorescence emission at 305 nm upon excitation at 275 nm at pH 7),[114] its presence can affect the fluorescence efficiency of other conjugated fluorophores such as organic dyes, fluorescent metal complexes, CdTe quantum dots, graphene oxide layers and thermally reduced carbon dots.[115] The latter three examples have been shown to experience fluorescence quenching in presence of vitamin B_{12}, while modified Cbl analogs with both the organic and inorganic chromophores constitute suitable candidates as markers for in vitro investigations of biological processes.

As discussed in **Section 1.3**, theoretically, there are multiple sites in vitamin B_{12} that may be derivatized with a fluorophore. However, in practice, only three (namely, the 5ˈ-OH site of the ribose unit and the b-/ c- propionamide side chains of the corrin ring) allowed conjugation of fluorophores without affecting their luminescent properties. In particular, functionalization at the cobalt(III) center, has been discussed since it resulted in quenching of fluorescence due to overlapping amongst the orbitals of Cbl and those of the excited state of the fluorophores.[116] On the contrary fluorescent vitamin B_{12} conjugates have been successfully generated by attaching the ribose unit to a fluorescent probe through a rigid linker, to minimize through-space

intramolecular interactions between the two substances and thus increase the overall fluorescence emission quantum yield.[117] To date, fluorescent rhenium(II) and ruthenium(II) complexes, as well as various organic dyes, have been successfully attached to vitamin B_{12} to target cancer cells for clinical imaging purposes. Considering the $\{Re^{I}(CO)_3\}$ scaffold, the completion of the metal's coordination sphere may be achieved by using suitable multidentate chelating ligands, leading to the formation of fluorescent rhenium-based potential imaging agents.[118] Doyle and co-workers, in an attempt to demonstrate this potential of cubilin as a new target of anticancer drug candidates, reported on two fluorescent IF-B_{12}-$\{Re^{I}(CO)_3\}$ conjugates, via attachment of the luminescent probe to the 5'-OH group of the ribose unit through an alkyl linker (**Figure 1.12**) which proved, capable of probing cancer cells.[119,120] Although the adduct **ReI-a** exhibited poor water solubility and weak fluorescence, it was successfully delivered and internalized in the nuclear and cytosolic region of the cubilin over-expressing human placental choriocarcinoma BeWo cells. On the contrary, the bioconjugate **ReI-b** demonstrated a 15-fold increase in fluorescence intensity upon addition of the IF factor and was preferentially internalized inside cells through the IF-cubilin transport mechanism in the human lung carcinoma A549 cells.

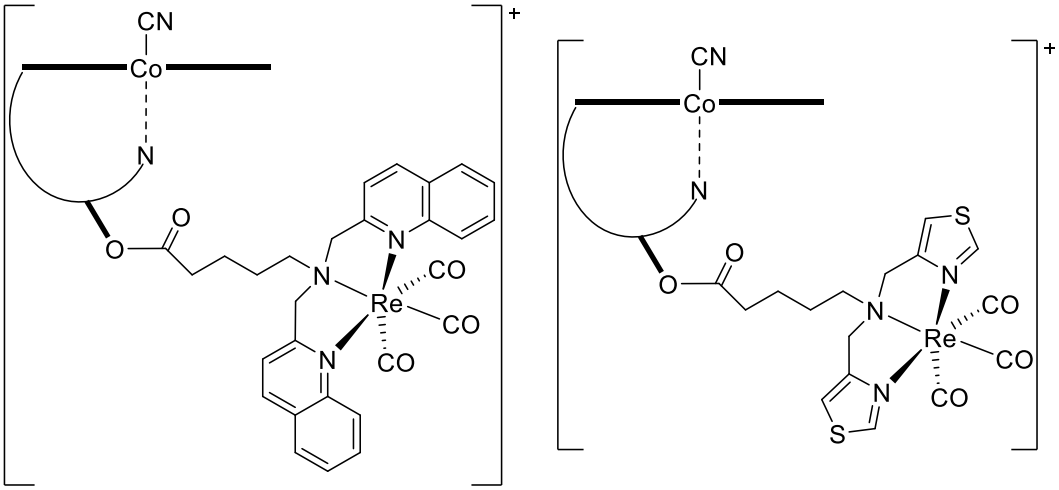

Figure 1.12: Chemical structures of the vitamin B_{12} conjugates **Re^{I}-a** (left) and **Re^{I}-b** (right).

On the same line, Alberto and co-workers reported on the conjugate [B_{12}-$(CH_2)_3$-PAMA-(fac-$Re^{I}(CO)^3$)]. Interestingly, these moieties (**Figure 1.13**) obtained by

derivatization of the b- or e- propionamide side-chain of the corrin framework either through direct reaction with the precursor $[Re^{I}(CO)_3(H_2O)_3]^+$ (post-labeling) or via conjugation of the pre-generated metal intermediate with the b- or e-hydrolyzed cyanocobalamins (pre-labeling).[98] So far, no clinical imaging studies of the aforementioned complexes have been reported.

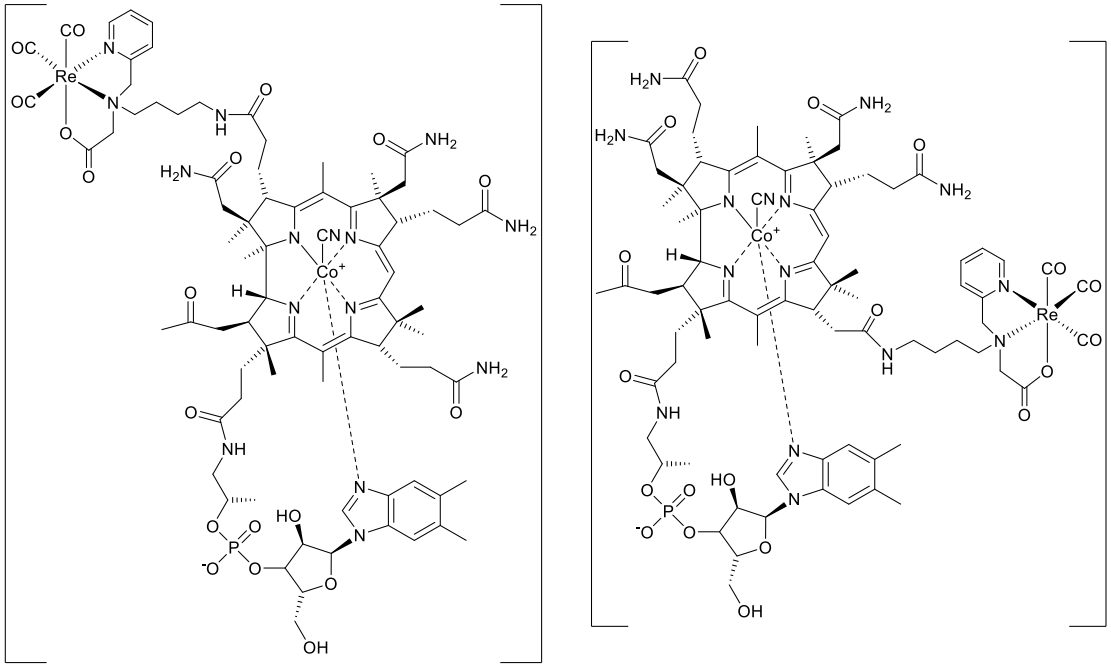

Figure 1.13: Chemical structures of the $[B_{12}\text{-}(CH_2)_3\text{-PAMA-}(fac\text{-}Re^{I}(CO)_3)]$ conjugates.

More recently, Zobi and co-workers reported on the dual luminescent ruthenium(II) compound shown in **Figure 1.14**.[121] This compound was obtained by first functionalizing the 5′-OH site of the ribose unit of cyanocobalamin with a rhodamine label through a linker, followed by the orthogonal attachment of the $[(HCCbpy)Ru(bpy)_2]^{2+}$ complex to the cobalt(III) center which replaced the cyano group.

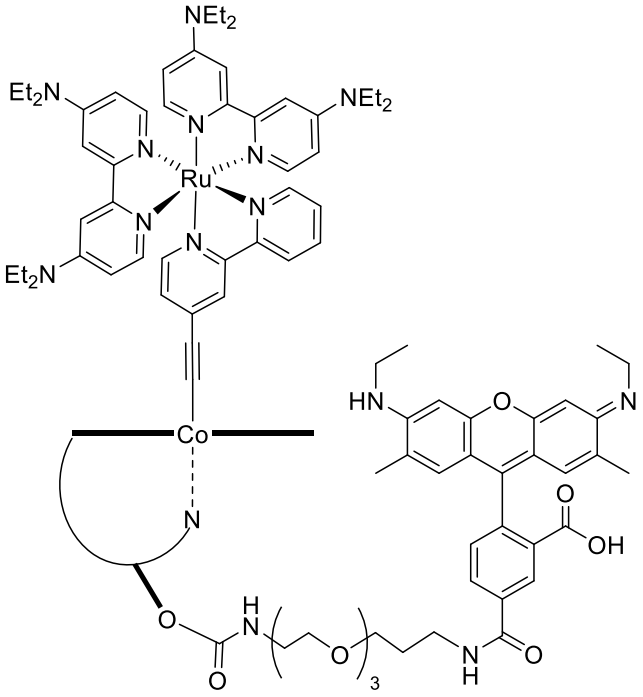

Figure 1.14: Chemical structure of the ruthenium-containing dual luminescent vitamin B_{12} conjugate.

1.3.2 Therapeutic Vitamin B_{12} Metal Complex Bioconjugates

Soon after its discovery in the 1960s, the widely known platinum anticancer drug cisplatin,[122,123] entered clinical trials and has been marketed for the treatment of diverse types of malignancies, including testicular and ovarian cancer, medulloblastoma and osteogenic sarcoma.[124,125] Thereupon, research efforts yielded a variety of platinum derivatives and other metal-based (e.g. rhenium, ruthenium, manganese, vanadium, and gold) anticancer agents. Over the last decades, vitamin B_{12} has been progressively recognized as a suitable carrier for the targeted delivery of metal-based anticancer drugs directly into tumor sites. Nevertheless, regardless of the encouraging results reported to date, none has progressed beyond preliminary biological and pre-clinical studies so far.

Considering the higher demand of vitamin B_{12} by fast proliferating cancer cells, compared with healthy cells, its consequent enhanced accumulation in tumor sites and the expected intracellular reduction of Co(III) to Co(II) with subsequent release of the attached β-axial group, Alberto and co-workers introduced a rational methodology to the conjugation of metal-based bioactive molecules (such as cisplatin and its analogs) to the β-upper site of the molecule, which would lead to the subsequent release of the metallodrug selectively into the tumor cell.[126–128] Specifically, they reported on the

generation of heterodinuclear complexes of the type {B_{12}-Co^{III}-CN-Pt^{II}} (**Figure 1.15**) via direct conjugation of the metal-containing scaffolds to the cyano group of Cbl.

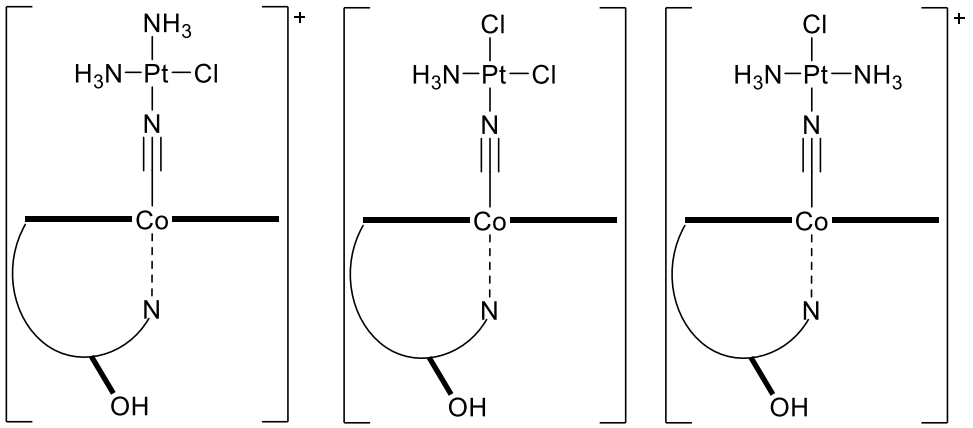

Figure 1.15: Chemical structure of the heterodinuclear complexes of the type {B_{12}-Co^{III}-CN-Pt^{II}}.

Following their intracellular adenosylation, all conjugates underwent the release of the cytotoxic Pt(II)-cyano species only inside the cell and showed some anticancer activity towards both human breast adenocarcinoma MCF7 cells and human ovarian adenocarcinoma A2780 cells. Although such conjugates proved less cytotoxic than cisplatin, the successful release of the β-upper platinum(II)-containing scaffold provided a promising proof-of-concept to the generation of pro-drugs which can exert their cytotoxicity selectively in the intracellular environment. Another interesting example relates to the preparation of the dual cytotoxic species incorporating both an organic drug and transplatin-like moiety. In this approach, the initial conjugation of well-known organic chemotherapeutics like cytarabine, dacarbazine, or anastrozole to the {trans-$Pt^{II}(NH_3)_2$} moiety was followed by attachment on vitamin B_{12} (**Figure 1.16**).[129] Biological studies showed that the B_{12}-metal containing moiety [(cytarabine)-(trans-$Pt^{II}(NH_3)_2$)(NC-Co^{III}-B_{12})]$^{2+}$ was less cytotoxic (IC_{50} = 230 nM) compared to the [$Pt^{II}(NH_3)_2$(NC)(cytarabine)]$^{+}$ scaffold (IC_{50} = 30 nM) toward human chronic myelogenous leukemia K562 cells.

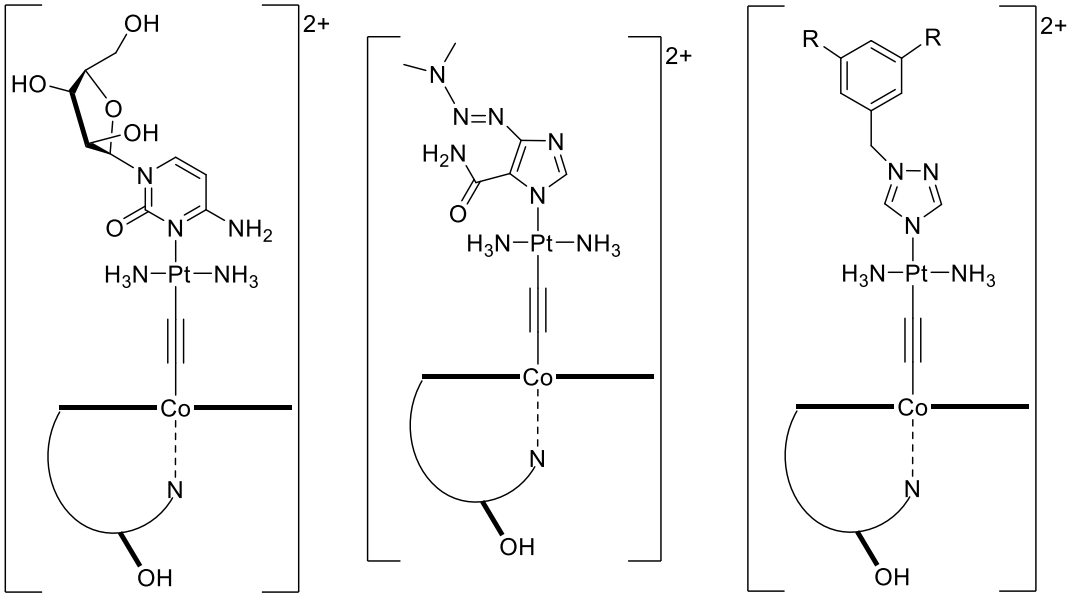

Figure 1.16: Chemical structure of the dual cytotoxic species of the type [(organic drug)-(trans-$Pt(NH_3)_2$)(NC-Co-B_{12})]$^{2+}$ (organic drug: cytarabine (left), dacarbazine (middle) and anastrozole (right)).

The most recent advancement in the field relates to the preparation of a new water-soluble vitamin B_{12} pro-drug bearing a platinum(II) bipyridyl complex with a terminal alkyne conjugated to the β-upper site of the cobalt(III) center (**Figure 1.17**).[121] The pro-drug was successfully recognized by transcobalamin and taken up by cells via receptor-mediated endocytosis. Cytotoxicity assays against MCF-7 breast cancer cells for both the free bipyridyl platinum(II) complex and the corresponding vitamin B_{12} conjugate, demonstrated IC_{50} values of 5μM and 29μM respectively, most likely due to different uptake mechanisms. Again, notwithstanding the decreased cytotoxic activity, contrary to the parent-free metallodrug, the platinum(II) bioconjugate was shown to specifically target the vitamin B_{12} transport pathway.

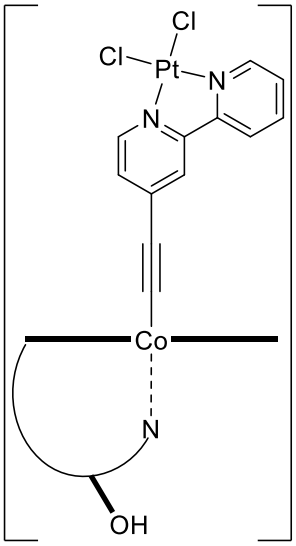

Figure 1.17: Chemical structure of the B_{12}-bioconjugate with the general motif {Co–C≡C-bpy–M}.

Administration of tiny amounts of carbon monoxide has shown several beneficial therapeutic effects, including relief of inflammations, protective effects for cardiovascular diseases, and organ preservation and transplantation.[130–135] However, when in a gaseous state, safe handling and site-specific delivery of the substance proved challenging. Thus, the development of biocompatible transition metal CO-releasing molecules (CORMs) has been proposed as an alternative approach, due to the promising results in the protection of cardiomyocytes against ischemia-reperfusion injury. The careful design of CORMs would allow the pH-dependent controlled delivery of small doses of CO inside the cells, of the affected tissues.[136] Examples of {cis-$Re^{II}(CO)_2$} CORMs bearing various multidentate ligands conjugated on the axial position of Co(III), to either the β- or the 5'-OH site of the ribose unit of vitamin B_{12} have been reported by Zobi and co-workers (**Figure 1.18**).[137,138] Conjugate **Re^{II}-a** was shown to protect heart tissue from ischemia-reperfusion injury, although, atomic absorption spectroscopy measurements confirmed that it was not internalized by the cells. In contrast, the analogs **Re^{II}-b** and **Re^{II}-c** were both internalized, and proved cytotoxic against human prostate carcinoma PC3 cells, with IC_{50} values in the low micromolar range.

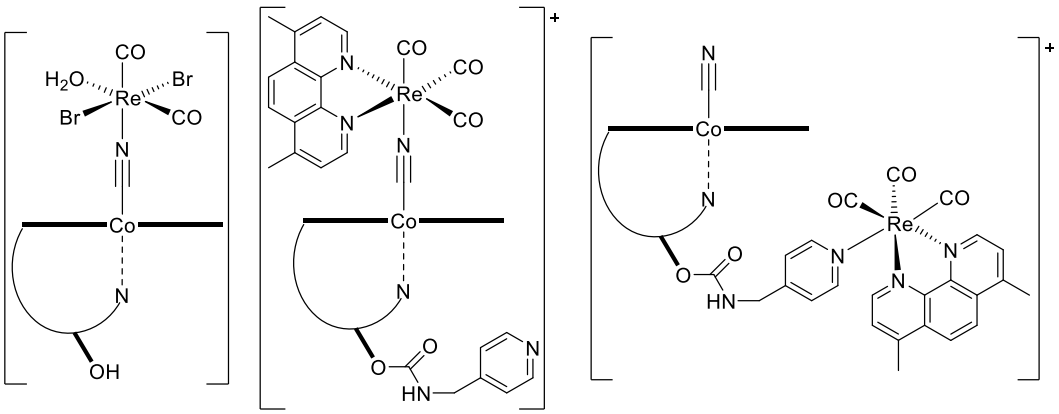

Figure 1.18: Chemical structures of the B_{12}-CORMs, **Re^{II}-a** (left), **Re^{II}-b** (middle) and **Re^{II}-c** (right).

At the same time, the rhenium-B_{12} derivative **Re^{II}-d** (**Figure 1.19**) was also developed, in which the CORM scaffold is linked to the cobalt(III) center through an organometallic bond (and not via the cyano group). The biological evaluation demonstrated that such bioconjugate was successfully taken up by the cells and proved cytotoxic against MCF-7 breast cancer cells, with an IC_{50} value of 6.3μM.

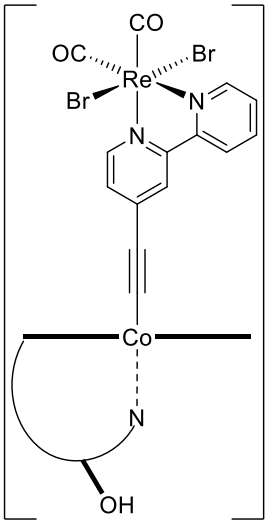

Figure 1.19: Chemical structure of the B_{12}-CORM **Re^{II}-d**.

In 2013, Zobi and co-workers reported on a photoactivatable Cbl-manganese CORM conjugate, in which the fac-$[Mn^{I}(CO)_3(TACD)]^+$ unit (TACD = 1,4,8,11-tetraazacyclotetradecane) is appended to the 5'-site of the ribose unit (**Figure 1.20**).[139] Biological studies demonstrated its actual transport and accumulation into the 3T3 fibroblasts and upon light activation, CO was slowly released, protecting in that way fibroblasts from death under conditions of hypoxia and metabolic depletion.

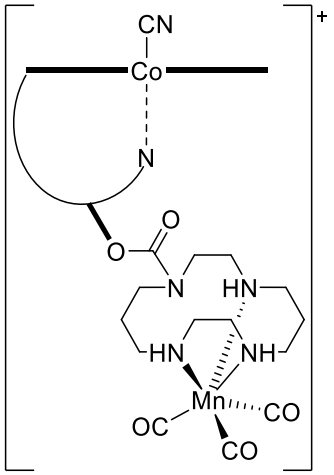

Figure 1.20: Chemical structure of the photoactivatable vitamin B_{12}-manganese CORM conjugate.

Along with the bioconjugate **Re^{II}-d**, the Zobi group also reported on the analogous ruthenium(II)-based analogs.[121] Its recognition by the TCII carrier protein and active transport was confirmed by fluorescent imaging experiments in live cells. The overall derivative proved cytotoxic against MCF-7 breast cancer cells, with an IC_{50} value of 10 μM. Considering the promising results, this strategy could be a major option for the generation of cytotoxic vitamin B_{12}-metallodrug conjugates.

Vanadium-containing scaffolds have been long evaluated as potential agents for the treatment of Type 1 and Type 2 diabetes mellitus. The latest results suggested that vanadium complexes bearing selected organic ligands did not cause gastrointestinal discomfort and hepatic or renal toxicity.[140–144] Within this framework, the idea of vanadium-containing antidiabetic agents attached to vitamin B_{12} may lead to the desired site-specific delivery of the vanadium scaffolds. In 2008, Brasch and co-workers reported on two vanadium-Cbl conjugates as potential antidiabetics (**Figure 1.21**),[144] which were obtained by alkylation of the cobalt(III) center of vitamin B_{12} with the reagent 1-(3- chloropropyl)-3-hydroxy-DMPP (DMPP = 2-methyl-1H-pyridin-4-one), and subsequent reaction with $Na[V^{V}O_3]$. Upon administration of the vanadium-Cbl conjugate toward the streptozotocin (STZ) rat model for Type 1 diabetes, a significant reduction of glucose (down to 230 mg dL^{-1}) was observed, compared with the 300 mg dL^{-1} recorded upon administration of $Na[V^{V}O_3]$ only under the same conditions.

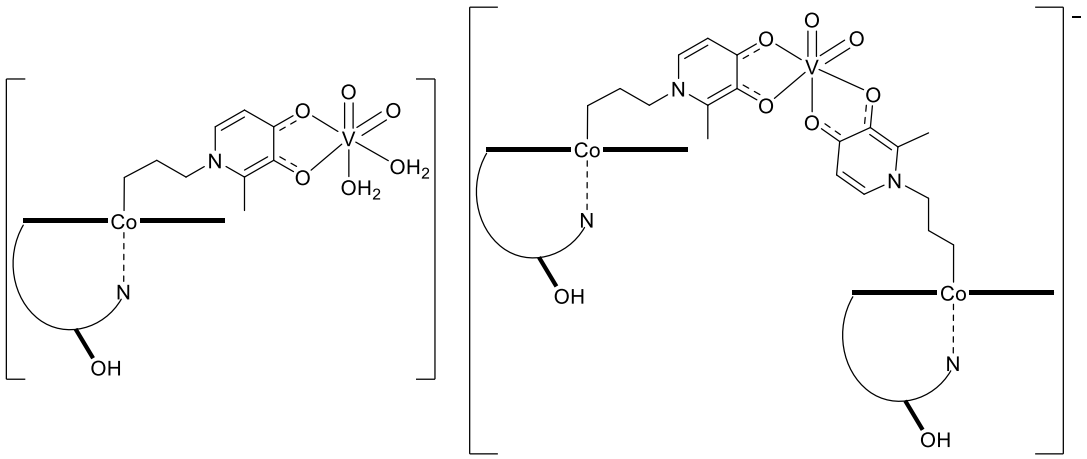

Figure 1.21: Chemical structures of the monomeric (left) and dimeric (right) potential antidiabetic vanadium-containing Cbl scaffolds.

1.4 Rationale Behind the research work: the "two birds with one stone" strategy

As previously mentioned, vitamin B_{12} is a vital nutrient characterized by very low bioavailability. After its uptake from the cell, it is converted into the biologically active cofactors methylcobalamin (used to produce methionine) and adenosylcobalamin (used as a coenzyme to enter the tricarboxylic acid cycle) through the reduction of Co(III) to Co(II) and the subsequent release of the cyano group. Remarkably, tumor cells show an increased demand for vitamin B_{12} compared with healthy ones, given that the faster metabolism of the nutriment can amplify the intracellular energy levels to sustain their extremely high proliferation rates.

Based on the aforementioned considerations, cyanocobalamin may be exploited as a carrier to either anticancer or imaging agents for the site-specific delivery of drugs directly into the cancer cell. Over the last decades, positive outcomes have been for some metal-based vitamin B_{12} conjugates in which the cytotoxic species is bound to the β-axial cyano group. Remarkably, the coordinated cyanocobalamin proved to undergo Co(III)/Co(II) reductive adenosylation, leading to the release of the actual metallodrug directly inside the tumor cell. Besides, Cbl has been successfully modified on either the corrin ring or the ribose group to act as a carrier of imaging agents, such as radionuclides or fluorophores for diagnostic purposes.

Accordingly, the goal of the present work is to take advantage of the higher demand of the nutrient in tumors by designing bimodal fluorescent metallotheranostic

derivatives of vitamin B_{12} in which both an imaging agent attached on the 5'-site of the ribose moiety via a rigid ligand and a cytotoxic metal-containing scaffold (bound to the cobalt(III) center through an organometallic linker) are incorporated. It is worth pointing out that the use of vitamin B_{12} for such a bifunctional strategy to the targeted treatment and imaging of tumors has been rarely reported to date. This original and innovative strategy provides a two-fold advantage. Firstly, the cytotoxic species are expected to be released directly into the site of interest and to exert their anticancer activity without affecting healthy tissues. At the same time, the attached fluorophore would allow the transport and biodistribution of the bioconjugate to be followed and assessed by fluorescence spectroscopy, epifluorescence microscopy, flow cytometry, and intraoperative visualization. This elegant approach requires specific modifications on specific sites of vitamin B_{12} for the preparation of such novel metal-based fluorescent vitamin B_{12} bioconjugates as 'Trojan Horse'-type theranostics (**Figure 1.22**).

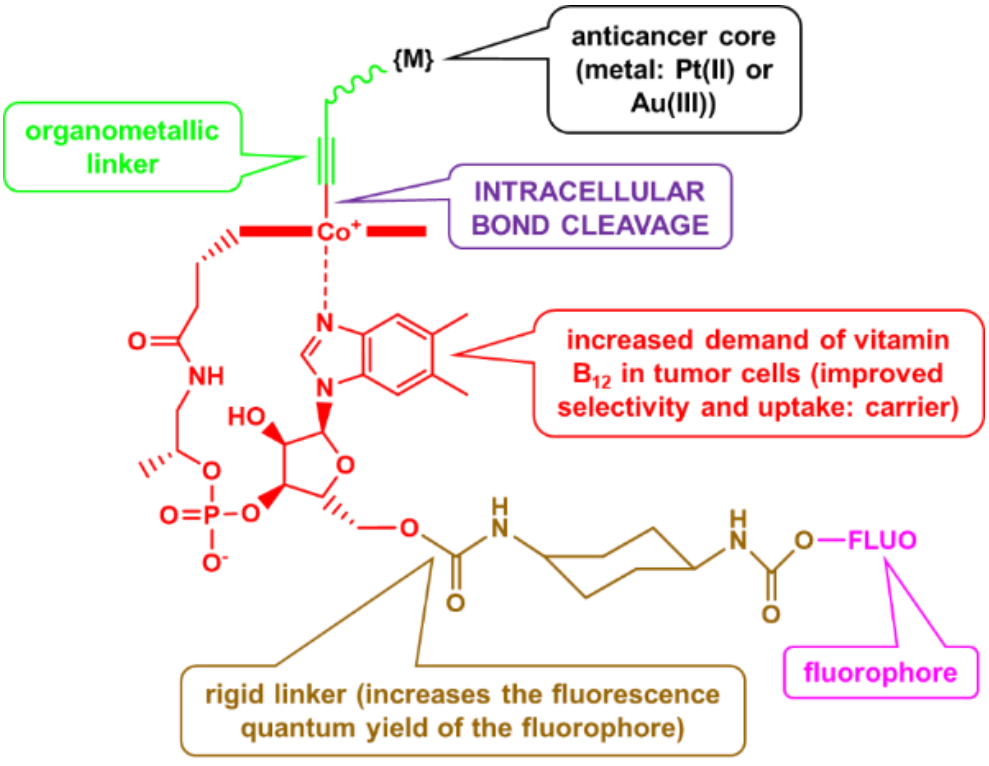

Figure 1.22: General schematic representation of the novel fluorescent metal-based vitamin B_{12} bioconjugates (FLUO: fluorophore, M: Pt(II), Au(III) scaffolds).

1.5 Research Objectives and Thesis Outline

The research work here described focused on the rational design, synthesis and characterization of 'Trojan Horse'-type potential theranostic agents of the type shown in **Figure 1.23**.

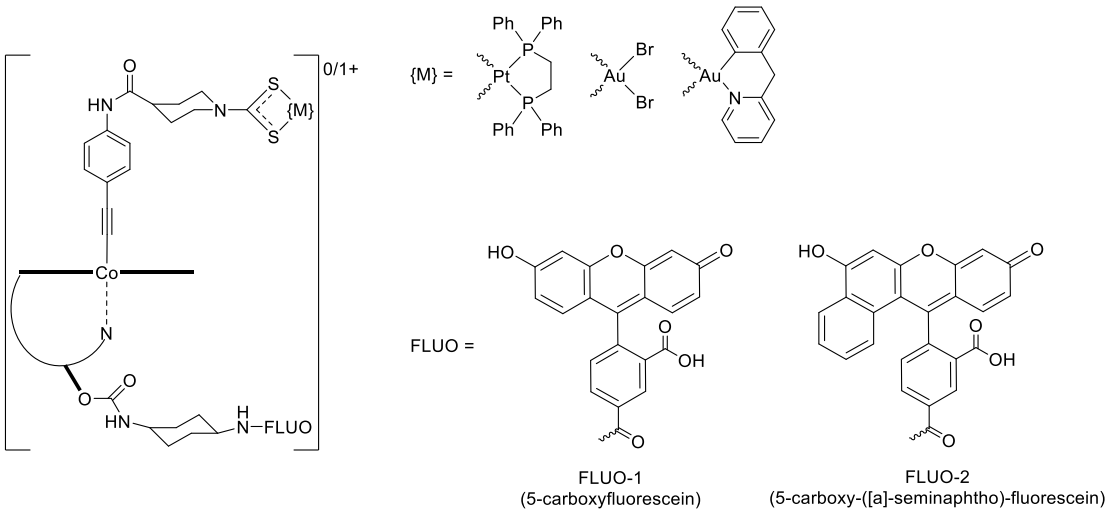

Figure 1.23: General chemical structure of the target metal-cobalamin bioconjugates here reported.

The generation of the target metal-cobalamin bioconjugates required the implementation and optimization of complex multistep syntheses and subsequent purifications. The first stage of the synthetic route dealt with the generation of the fluorophores (FLUO-1 and FLUO-2) and then subsequent attachment to the 5'-site of the ribose unit of cyanocobalamin through one rigid linker derived from trans-1,4-diaminocyclohexane (**Chapter 2**). The original plan was expected to involve the direct coordination of the cyano group of vitamin B_{12} to the metal scaffolds. Therefore, several platinum(II) and gold(I) precursors have been synthesized and fully characterized. Although attachment of such metal precursors to the axial β-site of vitamin B_{12} proved unsuccessful, **Chapter 3** describes in detail the various synthetic attempts in this regard. An alternative approach was then designed, based on a straightforward ligand exchange reaction. The new plan involved the pre-generation of suitable platinum(II) and gold(III) precursors bearing an alkyne moiety which form a new organometallic bond with the cobalt(III) center of the cobalamin by replacing the original cyano group. This approach is discussed in **Chapter 4**. During the four-year Ph.D. program, two side-projects were also carried out, which are within the field of metal-based anticancer agents. **Chapter 5** deals with the generation of novel

platinum(II)- and gold(III)-dithiocarbamato derivatives of tyrosine esters. The rationale behind this project is to combine the well-known anticancer activity of the metal dithiocarbamato scaffold with the intrinsic fluorescent properties of the naturally occurring a-amino acid L-tyrosine.[145] This would allow not only to generate novel metallodrugs but also to monitor their biodistribution through non-invasive luminescent spectroscopic techniques. As previously discussed, fast proliferating tumor cells require more nutrients and energy than healthy cells. Together with vitamin B_{12}, another nutrient in high demand by cancer cells is glucose. With this in mind, **Chapter 6** reports on the synthesis characterization and preliminary biological evaluation of some novel platinum(II)-based glycoconjugates. Similarly, to the main objective of the present research work, once again the idea is to exploit the greater demand of glucose by tumor cells to achieve the tumor site-specific delivery of cytotoxic metallodrugs. Finally, the experimental section is reported in **Chapter 7**, which includes details on the various synthetic routes, characterization data of both the starting materials and final products, and techniques used.

1.6 References

1. Zaigham, A., Sakina, R., *Neoplasm*, **6**, 140-157, (2018).
2. WHO report on cancer, ISBN 978-92-4-000129-9, **1**, 23-32, (2020).
3. Prescott, D., Flexer, A., The Misguided Cell, Chapter 1, (1986).
4. Cooper, M., Elements of Human Cancer, Chapter 1, (1992).
5. Fu, L., Kettner, N., *Prog. Mol. Biol. Transl. Sci*., **119**, 221–282, (2013).
6. Dorak, M., Karpuzoglu, E., *Front. Genet.,* **3**, 1–11, (2012).
7. Kim, I., Lim, H., Moon, A., *Biomol. Ther,* **26**, 335–342, (2018).
8. Takahashi, H., Terad, K., Morita, T., *Cortex.*, **58**, 289-300, (2014).
9. Vincent, A., Herman, J., Schulick, R., Hruban, R., Goggins, M., *The Lanset*, **378**, 607-620, (2011).
10. Pucci, C., Martinelli, C., Ciofani, G., *Can.Med.Science,* **13**, 1–26, (2019).
11. Chang, H., Bioengineering Innovative Solutions for Cancer, Chapter 1-3,

(2020).

12. Bercovich, E., Javitt, M., *Rambam Maimonides Med. J.*, **9**, e0034, (2018).

13. García-Figueiras, R., Baleato-González, S., Padhani, R., Luna-Alcalá, A., Vallejo-Casas, A., et al. *Insights into Imaging*, **10**, 28, (2019).

14. Fass, L., *Mol. Oncol.*, **2**, 115–152, (2008).

15. Wallyn, J., Anton, N., Akton, S., Vondamme, T., *Pharm. Res*., **36**, 78, (2019).

16. Frangioni, J., *J Clin Oncol.*, **20**, 4012–4021, (2008).

17. Ganguly, D., Chakraborty, S., Balitanas, M., Kim, T. *Medical Imaging*, **78**, 63, (2010).

18. Alexander,A., McGill, M., Tarasova, A., Ferreira, C., Zurkiya, D., *J. Am. Coll. Radiol.*, **16**, 501–507, (2019).

19. Mattsson, W., Gynning, I., Carlsson, B., Mouritzon, S., *Acta Radiol Oncol*., **18**, 509-513, (1979).

20. Halperin, E., Wazer, D., Perez, C., Brady, L., Principles and Practices of Radiation Oncology, Chapter 1, (1987).

21. Brueggemeier, R., *J. Med. Chem.*, **3**, 807–808, (1996).

22. Meeks, L., Pukala, J., Ramakrishna, N., *J. of radiosurgery*, **1**, 21–29, (2011).

23. Chen, C., Girvigian, R., *The Permanente journal*, **9**, 23–26, (2005).

24. Diao, K., Bian, X., Routman, M., et al., *J Neurooncol.*, **139**, 421, (2018)

25. Vasir, K., Labhasetwar, V., *Cancer Research & Treatment*, 363-374, 2005.

26. Ruddon, R., Ensminger, W., *The Anticancer drugs*, Chapter 1,(1994).

27. Goodman, S., Wintrobe, M., *J Am Med Assoc.*, **132,** 126-132, (1946).

28. a) Scott, B., *Med. J.* **4**, 259–265, (1970); b) Piccolo, T., Menale, C., Crispi, S., *Med Chem*., **15**, 408-22 (2015); c) Jiang, N., Wang, X., Yang, Y., Dai, W., *Mini Rev Med Chem*., **8**, 885-95, (2006).

29. McLaughlin, P., Grillo-López, J., Link, K., Levy, R., *J Clin Oncol.*, **16**, 2825-33, (1998); b) Lu, M., Hwang, C., *J Biomed Sci*., **27**, 1 (2020).

30. Robert, C., *Lancet*, **384**, 1109–1117, (2014).

31. Weber, J., *Lancet Oncol*, **16**, 375–384, (2015).

32. Topalian, L., *J. Clin. Oncol*, **32**, 1020–1030, (2014).

33. Robert, C., *J. Med*, **372**, 320–330, (2015).

34. a) Buechner, J., *Clin. Lymphoma, Myeloma Leuk.*, **17**, S263–S264, (2017); b) Zakrzewski, W., Dobrzyński, M., *Stem Cell Res Ther*, **10**, 68 (2019).

35. Arruebo, M., *Cancers*, **3**, 3279–3330, (2011).

36. Solnes, B., *J. Nucl. Med*, **61**, 311–318, (2020).

37. a) Mukherjee, S., Chowdhury, D., Kotcherlakota, R., Patra, S., Bhadra, P., *Theranostics*, **4**, 316-335, (2014). b) Hehakaya, C., Moors, M., Verkooijen, M., *Eur J Nucl Med Mol Imaging*, (2020).

38. Senapati, S., Mahanta, K., Kumar, S., *Sig Transduct Target Ther.*, **3**, 7, (2018).

39. Yuan, L., Sheng, Y., Jing, Z., Zhen Z., Ronghua Y., *Langmuir*, **34**, 15028-15044, (2018).

40. Quanbing, M., Yuan, M., Gaifang, P., Bai, X., Deyue, Y., *Angew. Chemie*, **129**, 12702–12706, (2017).

41. Luengo A, Gui, Y., Vander Heiden, G., *Cell Chem Biol.*, **24**, 1161-1180, (2017).

42. Dietz, P., Bähr, M., *Mol Cell Neurosci*., **27**, 85-131, (2004).

43. Qiao, L., Hu, S., Huang, K., *Theranostics*, **10**, 3474-3487, (2020).

44. Genç, L., Kutlu, M., Güney, G., *Pharm Dev Technol*., **20**, 337-44, (2015).

45. Smeltzer, C., Cannon, J., Pinson, R., *Org Lett.*, **3**, 799-801, (2001).

46. Tardy, L., Pouteau, E., Marquez, D., Yilmaz, C., Scholey, A., *Nutrients.*, **12**, 228. (2020).

47. a) Sieniawska, E., Pharmacognosy: Fundamentals, Applications and Strategy, Chapter 1, (2017); b) Blumberg, B., Bailey, L., Sesso, D., Ulrich, M., *Nutrients*, **10**, 248, (2018).

48. Brown, L., *Chem. Rev.*, **105**, 2075–2149, (2005).

49. Driskell, A., Cobalamins-Properties and Determination, Chapter 1., (2003).

50. Allen, H., Miller, W., De Groot, L., Rosenberg, H., Smith, D., *J Nutr.*, **148**, 1995S-2027S, (2018).

51. Murphy, P., *Bost. Med. Surg. J.*, **195**, 410–411, (1926).

52. Folkers, K., *Science*, **107**, *80*, (1948).

53. West, R., *Science*, **107**, 398, (1948).

54. Hodgkin, C., *Science*, **150**, 979, (1965).

55. Woodward, B., Synthetic vitamin B_{12}, 37-88, (2019).

56. Eschenmoser, A., Vitamin B_{12}, Chapter 1, (1979).

57. Rizzo, G., Laganà, A., *Mol. Nutr. Vitam.*, 105–129, (2019).

58. Nielsen, J., Rasmussen, R., Andersen, B., Nexø, E., Moestrup, K., *Biochem. Soc. Trans.*, **33**, 806–810, (2005).

60. Randaccio, L., Geremia, S., Demitri, N., Wuerges, J., *Molecules*, **15**, 3228–3259, (2010).

61. Siega, P., Wuerges, J., Arena, F., Gianolio, E., Sergey, N., *Chem. Eur. J.*, **15**, 7980–7989, (2009).

62. Baxter, N., Norris, F., Fernandes Baker, J., Jacob, E., Rajan, K., *Medical Journal*, **5293**, 1658-661, (1962).

63. Jacobsen, W., *Biochem. Biophys. Res. Commun.*, **169**, 443–450, (1990).

64. O'Leary, F., Samman S., *Nutrients* **2**, 299–316, (2010).

65. Pannérec, A., *J. Cachexia. Sarcopenia Muscle*, **9**, 41–52, (2018).

66. Russell-Jones, G., McTavish, K., McEwan, J., Rice, J., Nowotnik, D., *J. Inorg. Biochem.* **98**, 1625–1633, (2004).

67. Thorson, M., *Mayo Clin. Proc.*, **75**, 568–580, (2000).

68. Sawyers, C., *Nature*, **294** (2004).

69. Clardy, M., Allis, G., Fairchild, J., Doyle, P., *Expert Opin. Drug Deliv.,* **8**, 127–140, (2011).

70. Pettenuzzo, A., Pigot, R., Ronconi, L., *Eur. J. Inorg. Chem.*, 1625–1638, (2017).

71. Petrus, K., Fairchild, J., Doyle, P., *Angew. Chemie,* **48**, 1022–1028, (2009).

72. Petrus, K., Allis, G., Smith, P., Fairchild, J., Doyle, P., *ChemMedChem*, **4**, 421–426, (2009).

73. Ruiz-Sánchez, P., Mundwiler, S., Spingler, B., Buan, R., Escalante- Alberto, R., *J. of Biol. Inorg. Chem.*, **13**, 335-347, (2008)

74. Alsenz, J., Russell-Jones, G.J., Westwood, S. et al., *Pharm. Res.,* **17**, 825–832, (2000).

75. Doyle, P., *ChemMedChem*, **2**, 717–1721, (2007).

76. Kotra, P., *Bioorg. Med. Chem*, **15**, 1780–1787, (2007).

77. Ostermann, S., The Porphyrin Handbook, Chapter 1, (2003).

78. Giedyk, M., Goliszewska, K., Gryko, D., *Chem. Soc. Rev.,* **44**, 3391–3404, (2015).

79. Proinsias, K., Giedyka, M., Gryko, D., *Chem. Soc. Rev.,* **42**, 6605–6619, (2013).

80. Chromiński, M., Lewalska, A., Karczewski, M., Gryko, D., *J. Org. Chem.,* **79**, 7532–7542, (2014).

81. Wierzba, A., Hassan, S., Geremia, G., Fedosov, S., Petersen, T., et al., *Proc. Natl. Acad. Sci.,* **103**, 4386–4391, (2006).

83. Medici, S., Peana, M., Nurchi, V.M., Lachowicz, J.I., Crisponi, G., et al., *Coord. Chem. Rev.,* **284**, 329–350, (2015).

84. Mjos, K., Orvig, C., *Chem. Rev.,* **114**, 4540–4563, (2014).

85. Boulikas, T., Pantos, A., Bellis, E., Christofis, P., *Cancer Ther.* **5**, 537–583, (2007).

86. Jakupec, A., Galanski,M., Arion, V., Hartingera, C., Keppler, B., *Dalt. Trans.*, **2**, 183–194, (2008).

87. Kelland, L., *Nat. Rev. Cancer*, **7**, 573–584, (2007).

88. Bose, S., Komorowski, R., Seetharam, S., Gilfix, B., Rosenblatt, D., *J. Biol. Chem.*, **271**, 4195–4200, (1996).

89. Collins, D., *J. Nucl. Med.* **38**, 717–723, (1997).

90. Eckelman, W., Meinken, G., *J. Nucl. Med.*, **13**, 577–581, (1972).

91. Alberto, R., *Compr. Coord. Chem. II* , **5**, 127–270, (2003).

92. Alberto, R., Ortner, K., Wheatley, N., Schibli, R., Schubiger, A., *J. Am. Chem. Soc.*, **123**, 3135–3136, (2001).

93. Alberto, R., *Eur. J. Nucl. Med. Mol. Imaging*, **30**, 1299–1302, (2003).

94. Alberto, R., Pak, K., Van Staveren, R., Mundwiler, S., Benny, P., *Biopolymers*, **76**, 324–333, (2004).

95. Alberto, R., Waibel, R., Mundwilera, P., Schubiger, A., *J. Organomet. Chem.*, **689**, 4803–4810, (2004).

96. Nolte, A., *Org. Biomol. Chem.*, **2**, 259–2603, (2004).

97. Van Staveren, D., Benny, P., Waibel. R., Kurz, P., Alberto, R., *Helv. Chim. Acta*, **88**, 447–460, (2005).

98. Spingler, B., Mundwiler, S., Ruiz-Sánchez, P., Van Staveren, D., Alberto, R., *Eur. J. Inorg. Chem.*, **18**, 2641–2647, (2007).

99. Arendt, J., Nexø, E., *PLoS One* **7**, e45979 (2012).

100. Schibli, R., *Cancer Res.*, **68**, 2904–2911, (2008).

101. Meares, C., Moi, K., Diril, H., Kukis, L., McCall, J., *Br. J. Cancer Suppl.*, **10**, 21–26, (1990).

102. Psimadas, D., Georgoulias, P., Valotassiou, V., Loudos, G., *J. Pharm. Sci.*, **101**, 2271–2280, (2012).

103. Nakamoto, Y., *Nucl. Med. Biol.*, **25**, 95–99, (1998).

104. Collins, D., Hogenkamp, H., Gebhard, M., *Mayo Clin. Proc.*, **74**, 687–691, (1999).

105. Collins, D., Hogenkamp, H., O'Connor, M., Benson, L., Hardyman, T., *Mayo Clin. Proc.*, **75**, 568–580, (2000).

106. Daniels, H., Durski, J., Brito, J., Bhagra, S., Thapa, P., Bahn, R., *Thyroid*, **23**, 253–258, (2013).

107. Ruiz-Sánchez, P., *J. Organomet. Chem.*, **692**, 1358–1362, (2007).

108. Siega, P., *Chem. Eur. J.*, **15**, 7980–7989, (2009).

109. Anderson, C., Ferdani, R., *Cancer Biother. Radiopharm.*, **24**, 379–393, (2009).

110. Ikotun, F., Marquez, B., Fazen, C., Kahkoska, A., *ChemMedChem*, **9**, 1244–1251, (2014).

111. Moestrup, S., Birn, H., Fischer, B., Petersen, M., Verroust, J., et al., *Natl. Acad. Sci.*, **93**, 8612–8617, (1996).

112. Severin, W., Engle, W., Barnhart, E., Nickles, J., *Med. Chem.*,**7**, 389–394, (2011).

113. Van De Watering, J., Rijpkema, M., Perk, L., Brinkmann, U., Oyen, W. J., *BioMed res int.*, 203601, (2014).

114. a) Workinger, L., *Sci. Rep.*, **9**, 1–8, (2019); b) Wallyn, J., Anton, N., Akram, S., Vandamme, F., *Pharm Res.*, **36**, 78, (2019).

115. Tsiminis, G., Schartner, E., Brooks, J., Hutchinson, M., *Appl. Spectrosc. Rev.*, **52**, 439–455, (2017).

116. Smeltzer, C., Cannon, M., Pinson, P., Munger, J., West, F., et al., *Org. Lett.*, **3**, 799–801, (2001).

117. Lee, M., Grissom, B., *Org. Lett.*, **11**, 2499–2502, (2009).

118. Coogan, M., Doyle, R., Valliant, J., Babich, J., Zubieta, J., *J.Labelled Compd. Radiopharm.*, **57**, 255–261, (2014).

119. Viola-Villegas, N., *J. Med. Chem.*, **52**, 5253–5261, (2009).

120. Vortherms, A., *Chem. Commun.*, **47**, 9792–9794, (2011).

121. Rossier, J., Hauser,D., Kottelat,E., Rothen-Rutishauser, B., Zobi, F., *Dalt. Trans.*, **46**, 2159–2164, (2017).

122. Rosenberg, B., Van Camp, L., Krigas, T., *Nature*, **205**, 698–699, (1965).

123. Rosenberg, B., Van Camp, L., Trosko, J., *Nature*, **222**, 385–386, (1969).

124. Berek, S., Bertelsen, K., Du Bois, A., Brady, F., Carmichael, et al., J., *Ann. Oncol.*, **10**, 87–92, (1999).

125. Saeter, G., Wiebe, T., Böhling, T., Brosjö, O., Jonsso, K., et al., *Acta Orthop. Scand.*, **70**, 74–82, (1999).

126. Mundwiler, S., *Chem. Eur. J.*, **11**, 4089–4095, (2005).

127. Kunze, S., *Angew. Chem. Int. Ed.*, **43**, 5025–5029, (2004).

128. Ruiz-Sánchez, P., König, C., Ferrari, S., Alberto, R., *J. Biol. Inorg. Chem.*, **16**, 33–44, (2011).

129. Tran, M., *Org. Biomol. Chem.*, **11**, 3247–3254, (2013).

130. Clark, J., Naughton, P., Shurey, S., Green, J., Johnson, R., *Circ. Res.*, **93**, E2–E8, (2003).

131. Motterlini, R., *Circ. Res.*, **90**, E17–E24, (2002).

132. Alberto, R., Motterlini, R., *Dalt. Trans.*, **17**, 1651–1660, (2007).

133. Romao, C., Blättler, W., Seixasab, J., Bernardes, G., *Chem. Soc. Rev.*, **41**, 3571–3583, (2012).

134. Motterlini, R., Foresti, R., Sarathchandra, P., Mann, B., Green, C., *Nat. Rev. Drug Discov.*, **9**, 742–743, (2010).

135. Mann, B., *Top. Organomet. Chem.*, **32**, 247–285, (2010).

136. Schatzschneider, U., *Inorg. Chim. Acta*, **374**, 19–23, (2011).

137. Zobi, F., Degonda, A., Schaub, M., Yu, A., *Inorg. Chem.*, **49**, 7313–7322, (2010).

138. Zobi, F., Kromer, L., Spingler, B., Alberto, R., *Inorg. Chem.*, **48**, 8965–8970,

(2009).

139. Zobi, F., Quaroni, L., Santoro, G., Zlateva,T., Blacque, O., *J. Med. Chem.*, **56**, 6719–6731, (2013).

140. Srivastava, A., *Mol. Cell. Biochem.*, **206**, 177–182, (2000).

141. Gorodetskii, K., Tochilkin, I., Belayeva, F., *J. Inorg. Biochem.*, **103**, 554–558, (2009).

142. Karmaker, S., Saha, T., Sakurai, H., *J. Biomater. Appl.*, **22**, 449–464, (2008).

143. Saha, T., *Bull. Chem. Soc. Jpn.*, **79**, 1191–1200, (2006).

144. Mukherjee, R., Mukherjee, R., Donnay, E., Radomski, M., Miller, C., et al, *Chem. Commun.*, **7**, 3783–3785, (2008).

145. Cheruku, P., Huang, H., Yen, J., Iyer, S., Rector, D., et al., *Chemical science*, **6**, 1150–1158, (2015).

Chapter 2

2. Synthesis, Purification and Characterization of Two Novel Fluorescent Vitamin B_{12} Scaffolds

2.1 Background

In 1852, Stokes introduced the term "fluorescence" to describe the "remarkable phenomena of light"[1] observed in some materials (such as fluorophores, fluorescent dyes, luminescent probes, imaging agents, or chromophores) which were emitting photons at lower energy compared to the absorbed light. This type of energy emission often detected for gaseous, liquid, or solid aromatic compounds is the result of allowed electronic transitions from the first excited electronic state to the electronic ground state of the molecule. More precisely, when the compound of interest is irradiated with (usually) UV light, absorption of specific wavelengths of this radiation occurs and instantaneous electronic transitions to the singlet excited state (S_1) from the singlet ground state (S_0) lead to the emission of some of the absorbed energy as fluorescence. Typically, the emission rates of fluorescence are 10^8 s^{-1} and the widely used schematic representation of this process is known as the Jablonski energy diagram (**Figure 2.1**),[2] named after the acknowledged father of fluorescence spectroscopy, Alexander Jablonski, as a tribute to his remarkable achievements in the field.[3,4]

It should be noted that fluorescence spectroscopy is an elegant and sensitive analytical tool capable of detecting concentrations as low as 10^{-8} to 10^{-10} g/ml. Soon after its discovery, this technique found application in many disciplines, including chemistry, biology, biochemistry, medicine for analytical measurements, DNA sequencing and cellular imaging. Nowadays, the use of luminescent probes is a promising procedure in numerous scientific areas, such as modern optics, in vitro diagnostics and prognostics, in vivo molecular imaging, image-guided therapy, biosensors, system biology, molecular and personalized medicine, and theranostics.[5–8]

Remarkably within the field of drug design and delivery, incorporation of a fluorescent moiety into a therapeutic entity (directly attached or through a spacer), may be exploited for imaging purposes.[9] One crucial aspect of this strategy is the selection of the appropriate fluorophores with specific chemical (stability, solubility, reactivity toward conjugation) and photophysical (maximum absorption and emission wavelengths, Stokes shift, quantum yield) profiles. An equally important parameter is

the identification of the site of conjugation to the therapeutics (see **Section 1.3**), whose pharmacological activity should not be affected (in case of direct attachment), as well as not to prevent its recognition by specific biomolecules (in case a carrier/spacer molecule is involved). At least in principle, this strategy may allow monitoring of the transport and biodistribution of the fluorescent conjugate via fluorescence spectroscopy.

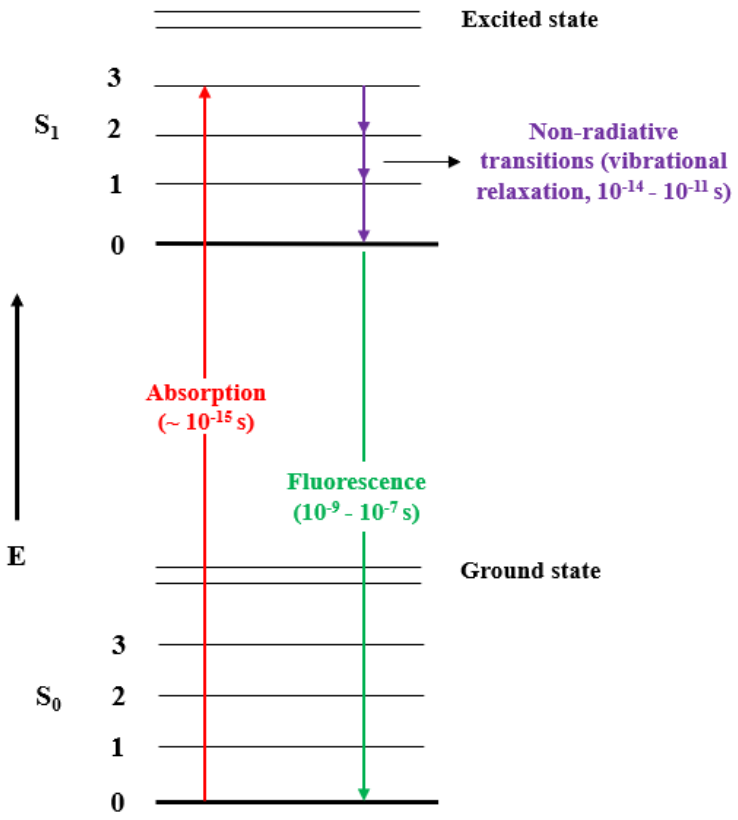

Figure 2.1: General schematic illustration of the Jablonski energy diagram of absorption and fluorescence procedures.

In nature, there are numerous examples of biologically relevant compounds containing aromatic or conjugated double bond systems, which are potentially or actually fluorescent. In general, fluorophores are divided into two categories,[2,10] intrinsic (those in which fluorescence occurs naturally) and extrinsic (those synthetically modified to fluoresce). Aromatic amino acids, certain proteins, carotenoids, purines, indoles, phenols, estrogens, hormones, co-enzymes, some vitamins, porphyrins, and corrinoids are recognized as intrinsic fluorophores. Interestingly, the biologically active forms of species belonging to the latter two families contain metal ions (e.g., Fe, Co, Cu) and are non or weakly fluorescent.[11]

One typical example of a poorly fluorescent biomolecule is vitamin B_{12} (**Figure 2.2**), which shows low-intensity emission in the long-wavelength region. Several methods have been reported to date to identify, quantify and track cyanocobalamin, including optical spectroscopy, chemiluminescence, surface plasmon resonance, Raman spectroscopy, as well as absorption and fluorescence spectroscopy. Although vitamin B_{12} is an inadequate luminescent species, its presence in the solution can be detected indirectly through interaction with light-emitting molecules, such as aridine orange (AO), rhodamine 6G and 4-N,N-di(2-hydroxyethyl) imino-7-nitrobenzo-2-oxa-1,3-diazole (HINBD).[12–14] In all cases, vitamin B_{12} has been shown to quench the fluorescence of the object luminescent species, thus allowing its detection by fluorescence-based analytical techniques.

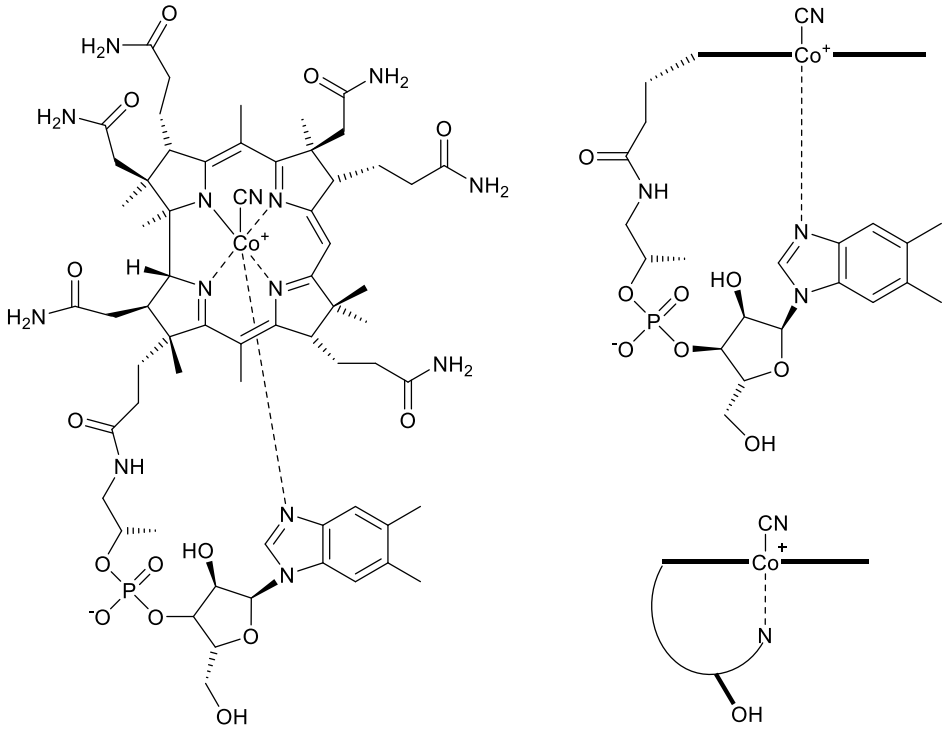

Figure 2.2: Structure (left) and simplified schematic representations (right) of vitamin B_{12}.

As a starting point, both the excitation and emission spectra of vitamin B_{12} were recorded (**Figure 2.3**). Usually, the energy differences in the absorption and emission spectra are similar, thus the Gaussian bands are approximate mirror images of each other. Since the vitamin B_{12} sample was irradiated with a wide range of wavelengths, several allowed transitions between the various vibrational energy levels of the excited states emerged. In particular, the absorption spectrum returned multiple peaks

at 279, 304, 338, and 388 (maximum intensity) nm. The wavelength of maximum absorption relates to the most probable electronic transition to the highest excited state. Upon excitation of the sample at 388 nm, scanning of the region from 400 to 700 nm revealed its weak emission spectral profile. Although the same transitions are most favorable for both absorption and emission processes, the fluorescence spectrum of the vitamin does not adhere to the mirror image rule, which appears as broadband with a maximum at 433 nm and overlapped peaks at around 468 nm. The difference between the maximum wavelengths in the emission (λ_{em}) and excitation (λ_{ex}) spectra is known as Stokes shift ($\Delta\lambda = \lambda_{em} - \lambda_{ex}$), which in this case is 45 nm.

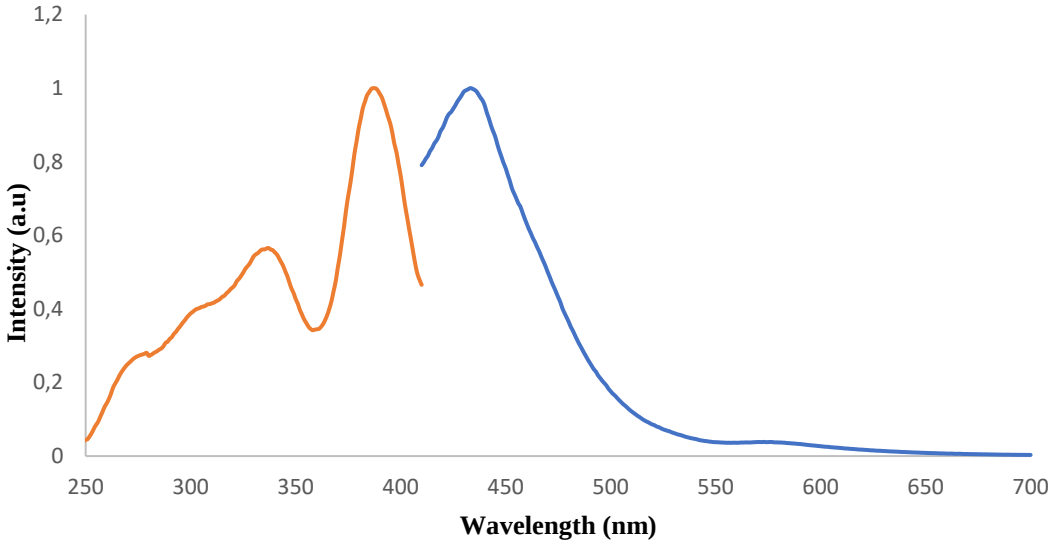

Figure 2.3: Absorption (orange) and emission (blue) spectra of vitamin B_{12} 1mg/ml in DMSO. Intensity has been normalized to the maxima.

Fluorophores with small $\Delta\lambda$ (< 70 nm)[15] are subject to self-quenching via energy transfer and result in poor signal-to-noise ratio,[16] thus limiting their bioimaging applications due to lack of scattering from biological samples.[17,18] The lifetime of the excited state (τ) may range from 0.1 to over 100 ns, and it is an important parameter for time-resolved measurements and fluorescence polarization applications.[19,20] Another critical property of a fluorophore is the quantum yield (Φ), defined as the ratio of the number of photons emitted to the number of photons absorbed, and compounds showing $\Phi \geq 0.1$ are generally regarded as fluorescent.[21] Given the whole range of biological applications, including the labeling of biomolecules, the suitability of a specific fluorophore is dictated by its chemical and photophysical properties. A

simple but yet useful parameter is the product of molar excitation coefficient (ε, also indicated as molar absorptivity) and the quantum yield: the greater the ε × Φ value, the greater the "brightness" of the fluorophore and, thus, the fluorescence detection and resolution.[22] Although vitamin B_{12} itself has poor photophysical properties (small Stoke shift, low quantum yield, tendency to self-quenching),[23] its essential biological role and involvement in diseases such as cancer, have been triggering a major interest in the development of analytical approaches aimed at probing its trafficking. In particular, fluorescent cobalamin analogs have been designed, in which suitable fluorophores are attached to vitamin B_{12}.[24]

Based on the aforementioned considerations, in this chapter, the rational design and improved synthetic strategies for the generation of two fluorescent vitamin B_{12}-based conjugates are reported. Two highly conjugated polycyclic aromatic fluorophores (namely, 5-carboxyfluorescein/**FLUO-1** and 5-carboxy-([a]-seminaphtho)-fluorescein/**FLUO-2**) were prepared and subsequently appended to the ribose 5'- site of vitamin B_{12} through a rigid linker (1,4-diaminocyclohexane), yielding the corresponding fluorescent cyanocobalamin derivatives. Although the synthetic route to the generation of both the fluorophores and the corresponding vitamin B_{12} conjugates were already reported in the literature, substantial modifications have been implemented to optimize the reaction times and improve purity and yield. In particular, a major effort was made to establish a more efficient purification protocol.

To sum up, the present Chapter is organized as follows:

- Description of the rationale behind the synthetic plan.
- Description of the methodology employed to generate the fluorophores and the corresponding vitamin B_{12} analogs, focusing on the optimization of the synthetic routes and purification protocols implemented.
- Full characterization of all the chemical species obtained.

2.2 Synthetic Strategy

The synthetic approach was built upon the encouraging results previously reported on visual indicators containing vitamin B_{12} in murine xenografts of human tumors.[25] Earlier attempts in the synthesis of cobalamin analogs bearing a fluorophore directly

attached to either the β-axial position of cobalt(III) or the 5'- site of the ribose moiety proved successful. Nevertheless, all such fluorescent vitamin B_{12} conjugates suffered from severe fluorescence quenching due to the overlap of the electronic orbitals of cyanocobalamin and the excited state of the fluorophores.[26] Consequently, an alternative approach was proposed by Grissom *et. al*,[27] where the introduction of a rigid linker between vitamin B_{12} and the luminescent probe could veer the two entities apart in a way that an orthogonal alignment of their electronic dipoles can be easily achieved.[14,28] Interestingly, this approach increased the photochemical stability and improved fundamental parameters of fluorescence, such as the extinction coefficient, fluorescence lifetime, and quantum yield of the final conjugates.[29]

Remarkably, one of the dyes used by Grissom was a mixture of constitutional isomers of 5(6)-carboxyfluorescein,[30,31] which was successfully attached to the ribose ring of vitamin B_{12}, yielding photostable fluorescent cobalamin analogs which would be useful in medicine (but not limited to) as intraoperative tumor markers for optimal results in cancer resections or as vehicles for potential therapeutic agents. On the other hand, there is increasing evidence suggesting that, from a pharmacological point of view, isomerism (in therapeutics and/or in their framework) can affect processes such as absorption, distribution and metabolism of drugs due to possible differences in pharmacokinetic profiles.[32,33] Thus, the complete severance of the isomers is crucial, to achieve accurate and optimal therapeutic results. Taking that into consideration, a rational stepwise methodology was planned for the preparation of fluorescent vitamin B_{12} scaffolds, as carriers of antitumor metal-containing complexes. To avoid the formation of isomeric carboxyfluorescein mixtures, an optimized experimental procedure was designed using 5-benzophenone as a key intermediate for the subsequent synthesis of the isomerically pure **FLUO-1** and **FLUO-2** (**Figure 2.4**).[34]

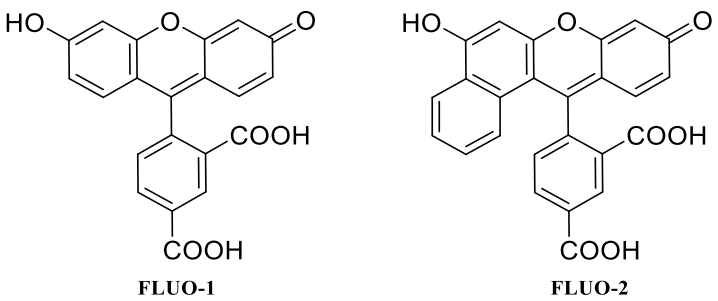

FLUO-1 **FLUO-2**

Figure 2.4: Chemical structures of the fluorescent labeling agents **FLUO-1** and **FLUO-2**.

Implementation of coupling and subsequently, amide formation procedures resulted in the preparation of the fluorescent vitamin B_{12}-based derivatives [B_{12}-5'-(FLUO)] (FLUO = **FLUO-1 (Figure 2.5 left)** or **FLUO-2 (Figure 2.5 right)**).[35] All reactions were carried out in the dark to reduce the adventitious photobleaching of the fluorophore. Additionally, an efficient purification protocol for the isolation of the desired conjugates was established.

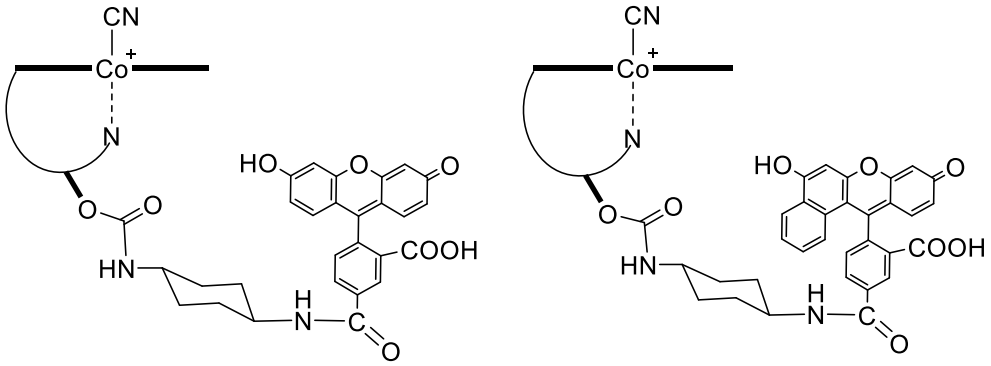

Figure 2.5: Schematic representation of [B_{12}-5'-(FLUO)] (FLUO = FLUO-1 (**left**); FLUO-2 (**right**)).

2.3 Preparation of FLUO-1, FLUO-2 and their active derivatives

For detailed experimental conditions, structure numbering and full characterization see **Chapter 7**.

Esterification of isomeric fluoresceins could result in a substantial reduction of their fluorescence emission intensity. Therefore, the early separation of the isomers would be desirable.[36–38] The Burgess[39] and Clausen[34] research groups have successfully differentiated isomeric mixtures by fractional crystallization.[40] Isolation of the crucial intermediate 5-benzophenone from a combination of the 5- and 6-benzophenone isomers (**Figure 2.6**) resulted in the preparation of **FLUO-1** and **FLUO-2**.

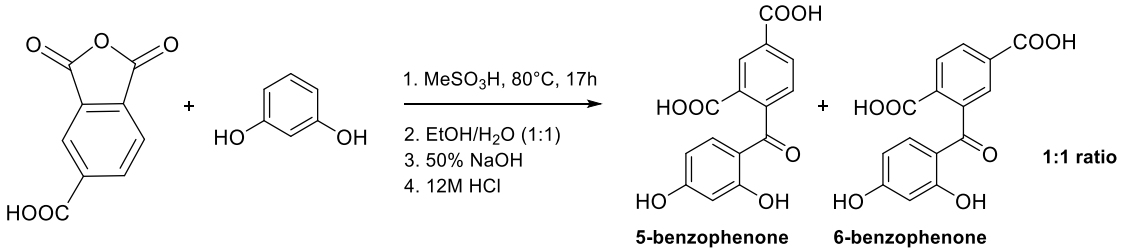

Figure 2.6: Synthetic route to the preparation of the regioisomers 5- and 6-benzophenones.

The object 5- and 6-benzophenone were obtained by refluxing trimellitic anhydride and resorcinol in methanesulfonic acid. Subsequently, the crude mixture was precipitated upon addition to a 1:1 boiling mixture of EtOH/H_2O.[41] Separation of the isomers was then achieved by fractional crystallization in MeOH/H_2O. The desired intermediate 5-benzophenone was isolated as small off-white crystals in high yield and 100% regioisomeric purity. Spectroscopic characterizations were fully consistent with those reported in the literature.

2.3.1 Synthesis and activation of FLUO-1

The target fluorophore **FLUO-1** (**Figure 2.7**) was synthesized by reacting 5-benzophenone and resorcinol in methanesulfonic acid at room temperature for 17 hours. The desired compound was obtained at a 97% yield as a bright orange solid and was used without further purification in the subsequent activation stage.

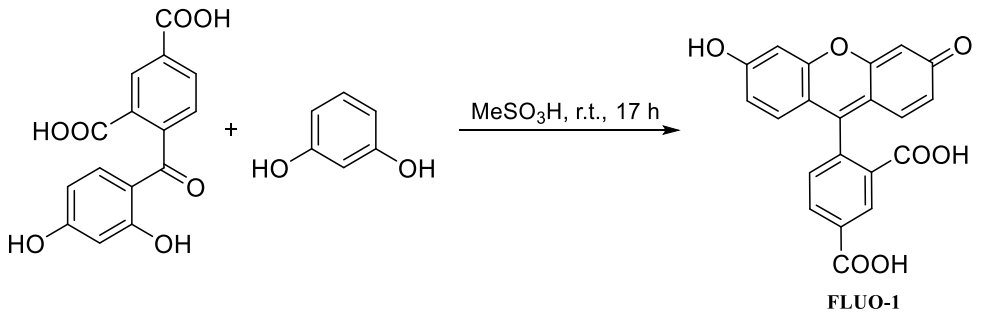

Figure 2.7: Synthetic route to the preparation of **FLUO-1**.

Characterization of **FLUO-1** was carried out by FTIR, NMR, UPLC-MS/MS, and fluorescence spectroscopy. Analysis of the FTIR spectrum revealed the diagnostic stretching modes of both the carboxylic acid and alcohol moieties of the fluorescent dye **FLUO-1**. Additionally, data from mono- and multidimensional NMR spectroscopy were in agreement with the literature (**Figure 2.8**).

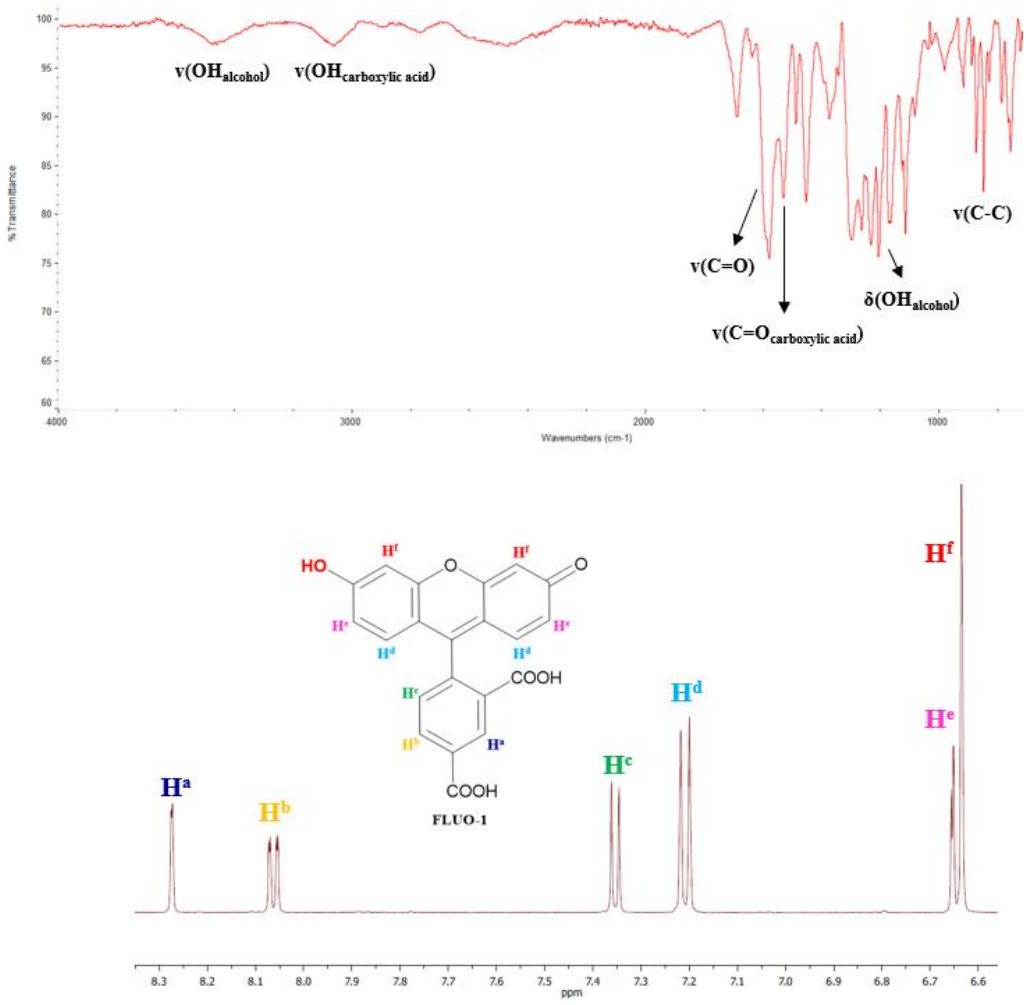

Figure 2.8: Top: Mid-IR spectrum (CsI disk, wavenumber in cm^{-1}) of **FLUO-1**. Bottom: ^{1}H NMR spectrum in DMSO-d_6 of **FLUO-1**.

Furthermore, the characteristic $[M+H]^+$ (calcd. 376.1 and found 377.1) fraction was identified in the positive mode of UPLC-MS/MS (**Figure 2.9**).

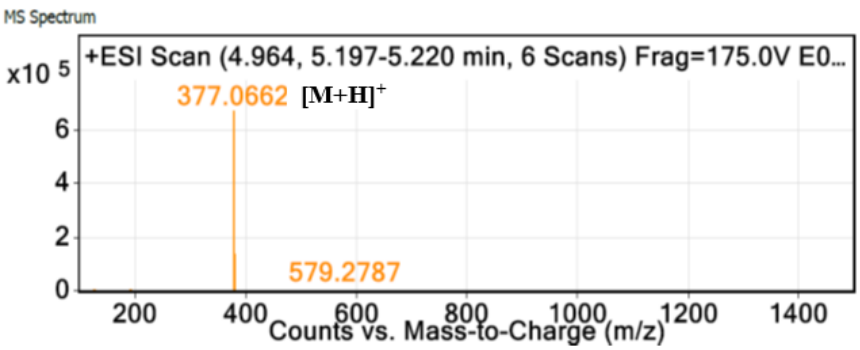

Figure 2.9: Mass spectrometric profile of **FLUO-1**.

Fluorescence measurements were performed in the region 440 to 670 nm. The graph below illustrates the spectral overlap of excitation and emission bands with the intensity normalized to the highest value (**Figure 2.10**). Absorption maxima were recorded at 521, 531, 535, and 543 nm, due to multiple allowed electronic transitions to energetically higher excited states. Intense energy emission in the form of fluorescence was recorded as a broadband with a maximum at 578 nm, the Stokes Shift being equal to 43 nm.

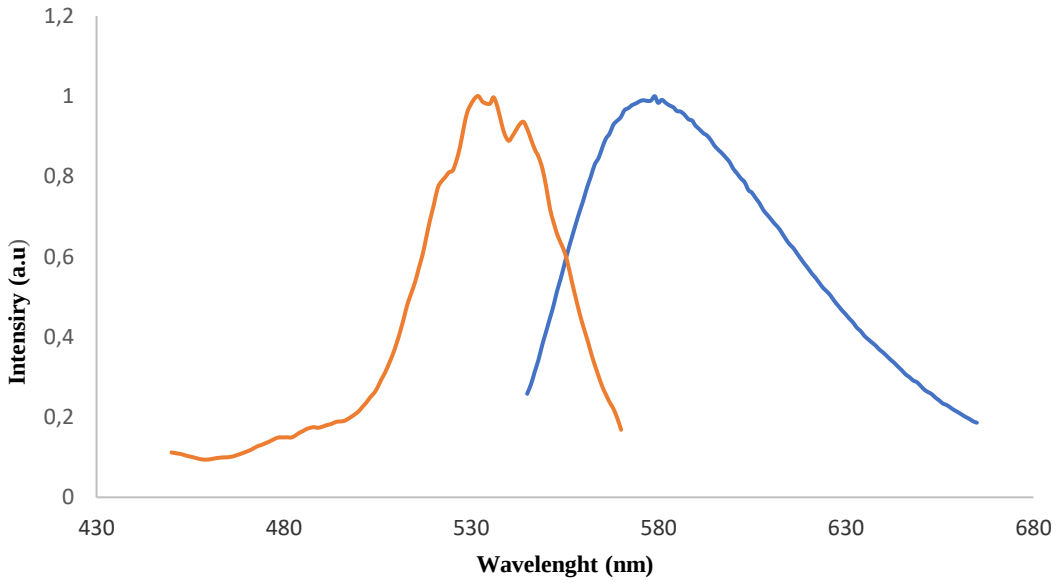

Figure 2.10: Graphic illustration of absorption (orange) and emission (blue) gaussian bands of **FLUO-1** 1 mg/ml in DMSO.

Subsequently, activation of the 5-site of **FLUO-1** was achieved by reacting with N-hydroxysuccinimide (NHS) and N-(3-dimethylaminopropyl)-N′-ethyl carbodiimide hydrochloride (EDAC) (**Figure 2.11**).[42] The crude product was dissolved with dry DMF, acetone, and 0.05 M sodium phosphate buffer and then extracted with EtOAc/EtO_2. The organic phase was washed with H_2O and brine and dried with sodium sulfate. Purification by column chromatography afforded the bright orange solid in 65% yield. Spectroscopic characterizations confirmed the successful generation of **FLUO-1a** (**Figure 2.21, Figure 2.23**).

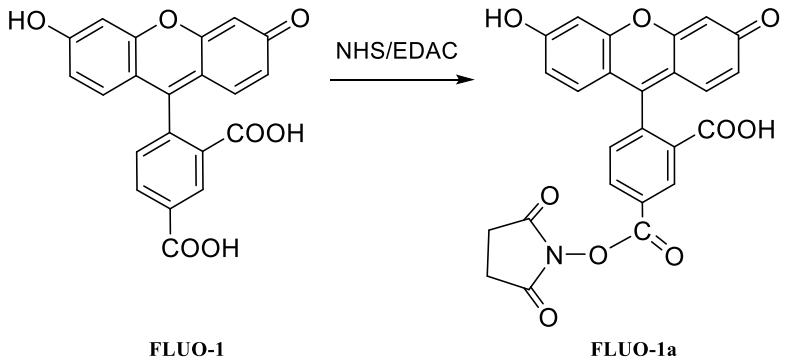

Figure 2.11: Synthetic route to the preparation of **FLUO-1a**.

2.3.2 Synthesis and activation of FLUO-2

Similarly, **FLUO-2** was prepared upon reacting 5-benzophenone and naphthalene-1,3-diol (**Figure 2.12**). The bright red solid was isolated by precipitation in 72% yield and used in the next step without further purification.

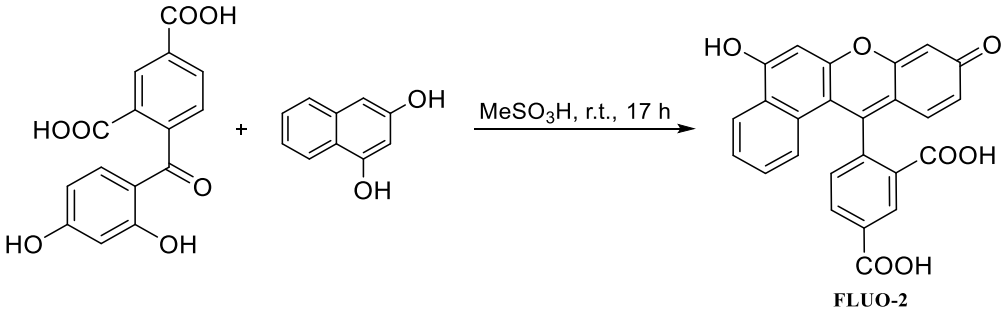

Figure 2.12: Synthetic route to the preparation of **FLUO-2**.

Analysis of the FTIR spectrum revealed the diagnostic stretching modes of both the carboxylic acid and alcohol moieties of the fluorescent dye **FLUO-2**. Additionally, data from mono- and multidimensional NMR spectroscopy were in agreement with the literature (**Figure 2.13**).

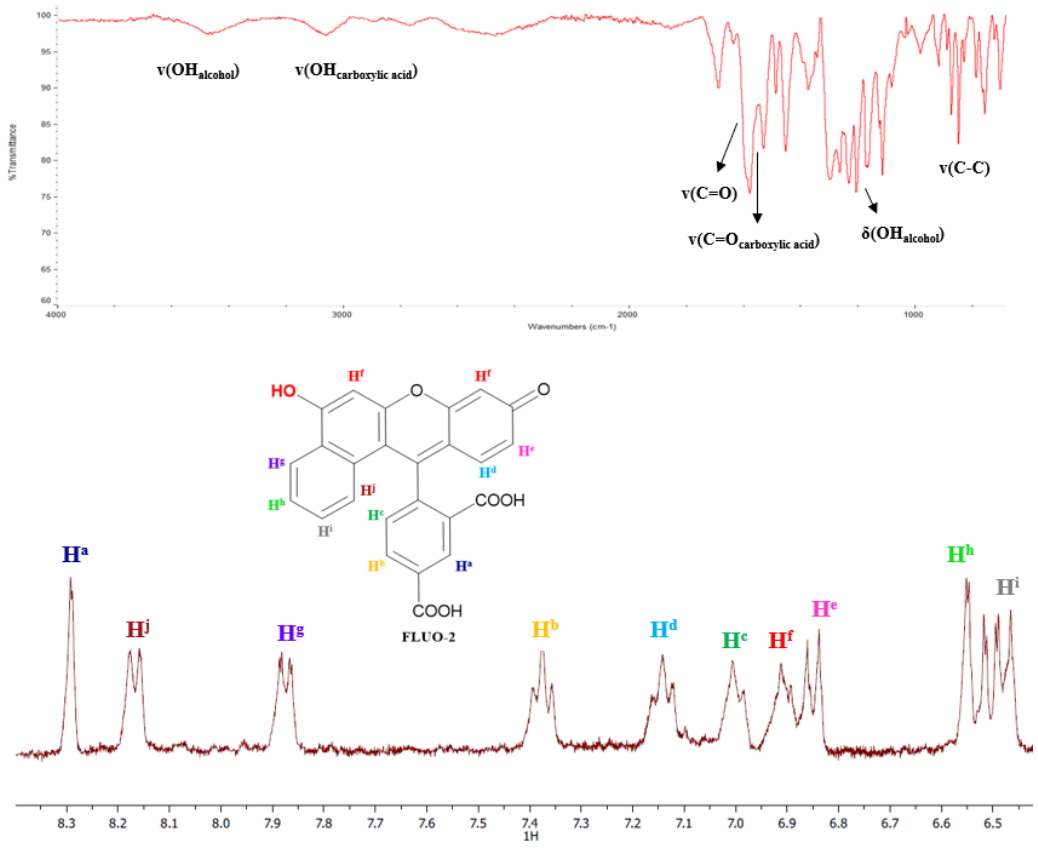

Figure 2.13: Top: Mid-IR spectrum (CsI disk, wavenumber in cm^{-1}) of **FLUO-1**. Bottom: ^{1}H NMR spectrum in DMSO-d_6 of **FLUO-1**.

UPLC-MS/MS displayed the $[M+H]^+$ (calcd. 426.38 and found 427.1) (**Figure 2.14**).

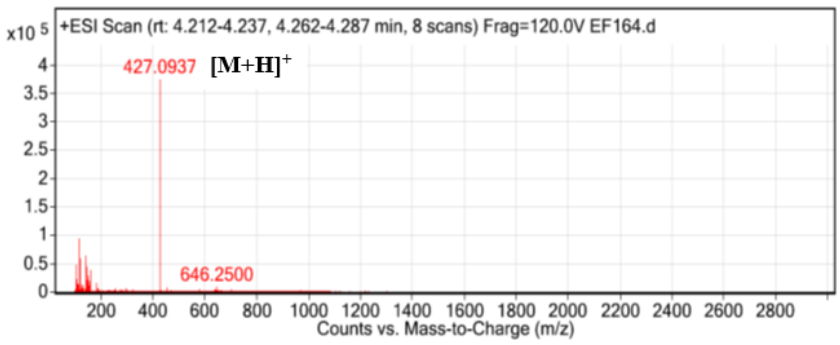

Figure 2.14: Mass spectrum of **FLUO-2**.

For **FLUO-2** the absorption maximum was observed at 512 nm, along with two overlapped peaks at 480 and 520 nm. Emission occurred in the form of a broadband giving an intense peak maximum at 558 nm. The shape of the band at around 592 nm indicates a possible peak overlapping. In this case, the difference between the absorption and emission maxima is equal to 46 nm (**Figure 2.15**).

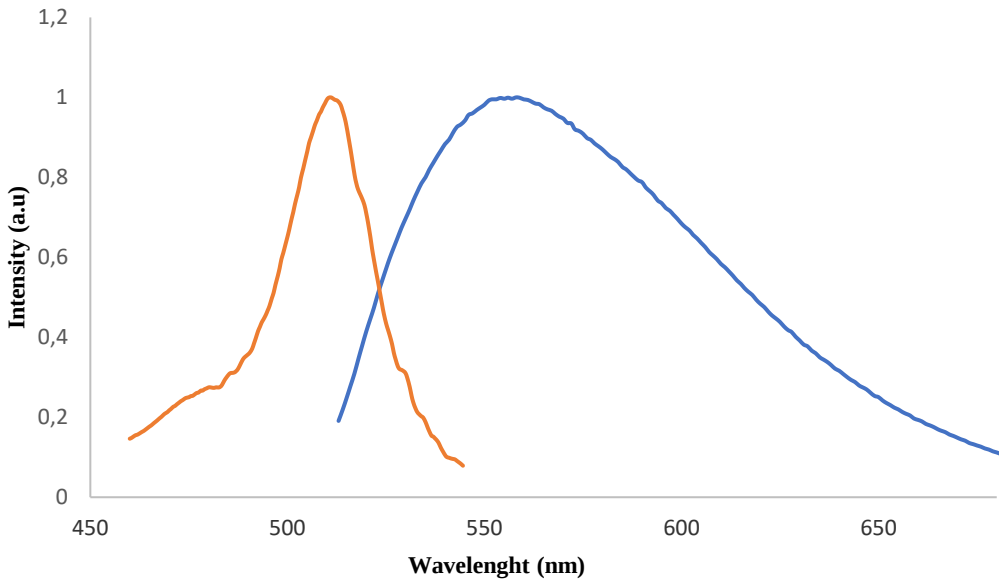

Figure 2.15: Absorption (orange) and emission (blue) bands overlapping of **FLUO-2**, 1 mg/ml in DMSO. Intensity has been normalized to the maxima.

Conversion of **FLUO-2** into the corresponding activated ester was performed under the same experimental conditions reported for **FLUO-1a**. Purification by column chromatography yielded 79.8% of the activated derivative **FLUO-2a** (**Figure 2.16**). FTIR (**Table 2.1**) and NMR data (**Table 2.2**) were in agreement with the literature.

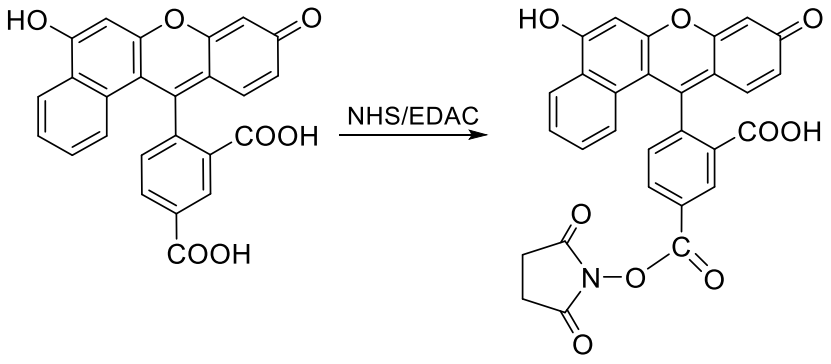

FLUO-2 **FLUO-2a**

Figure 2.16: Synthetic route to the preparation of **FLUO-2a**.

2.4 Functionalization of Vitamin B_{12} with a rigid linker

For detailed experimental conditions, structure numbering and full characterization see **Chapter 7**.

To obtain the target vitamin B_{12}-fluorophore conjugates,[27,35] preliminary activation of the 5'-OH site of the ribose unit was required, followed by attachment of a rigid linker. The initial approach involved the use of CDT as a coupling reagent and the trans-1,4-diaminocyclohexane as a linker, which proved time-consuming with yields lower than 30%. An alternative methodology was then explored, using a different coupling reagent (CDI) and attaching the rigid linker in a one-pot reaction (**Figure 2.17**). Numerous attempts aimed at the separation of the pure desired compound by employing protocols already reported in the literature proved unsuccessful. Therefore, an alternative efficient eluting protocol capable of separating the individual components of the mixture from each other in high purity and yields was designed. Initially, removal of the unreacted reagents and side-products was achieved on silica gel with the eluent system MeOH/MeCN/H_2O 1/0.225/0.025. Derivative **2** was then collected with MeOH in the form of fine pink crystalline powder and used in the next step for the subsequent attachment of the fluorescent dyes.

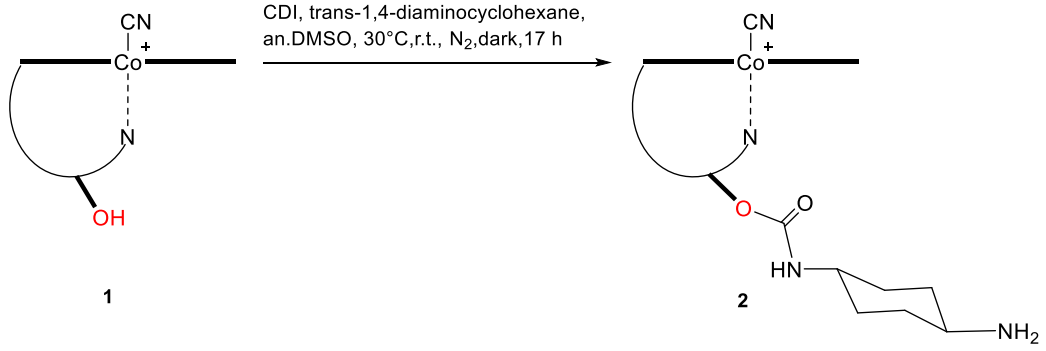

Figure 2.17: One-pot synthesis to the vitamin B_{12} rigid linker intermediate.

In the mid-IR spectrum, bands at 1674 and 2139 cm^{-1} were assigned to the (CNH) and (C≡N) stretching modes. Broadbands at around 3400 cm^{-1} were attributed to overlapped stretching modes of N-H and O-H present in the vitamin B_{12} scaffold. Moreover, a medium intensity band at 1082 cm^{-1} was recorded, consistent with the stretching vibration of the phosphate group (**Table 2.1**). Although the ^1H NMR spectrum of the pure product proved challenging to be interpreted, four characteristic changes in the pattern of the peaks (compared with native vitamin B_{12}) confirmed the successful formation of **2** (**Figure 2.18**): (i) a 0.04 ppm downfield shifting of the methyl group $C^{20}H_3$, (ii) disappearance of the R5-OH signal at 6.40 ppm, (iii)

appearance of a new peak at 8.31 ppm assigned to the amide NH group and (iv) the overlapped signals of the rigid linker in the region 1.0 to 2.4 ppm.

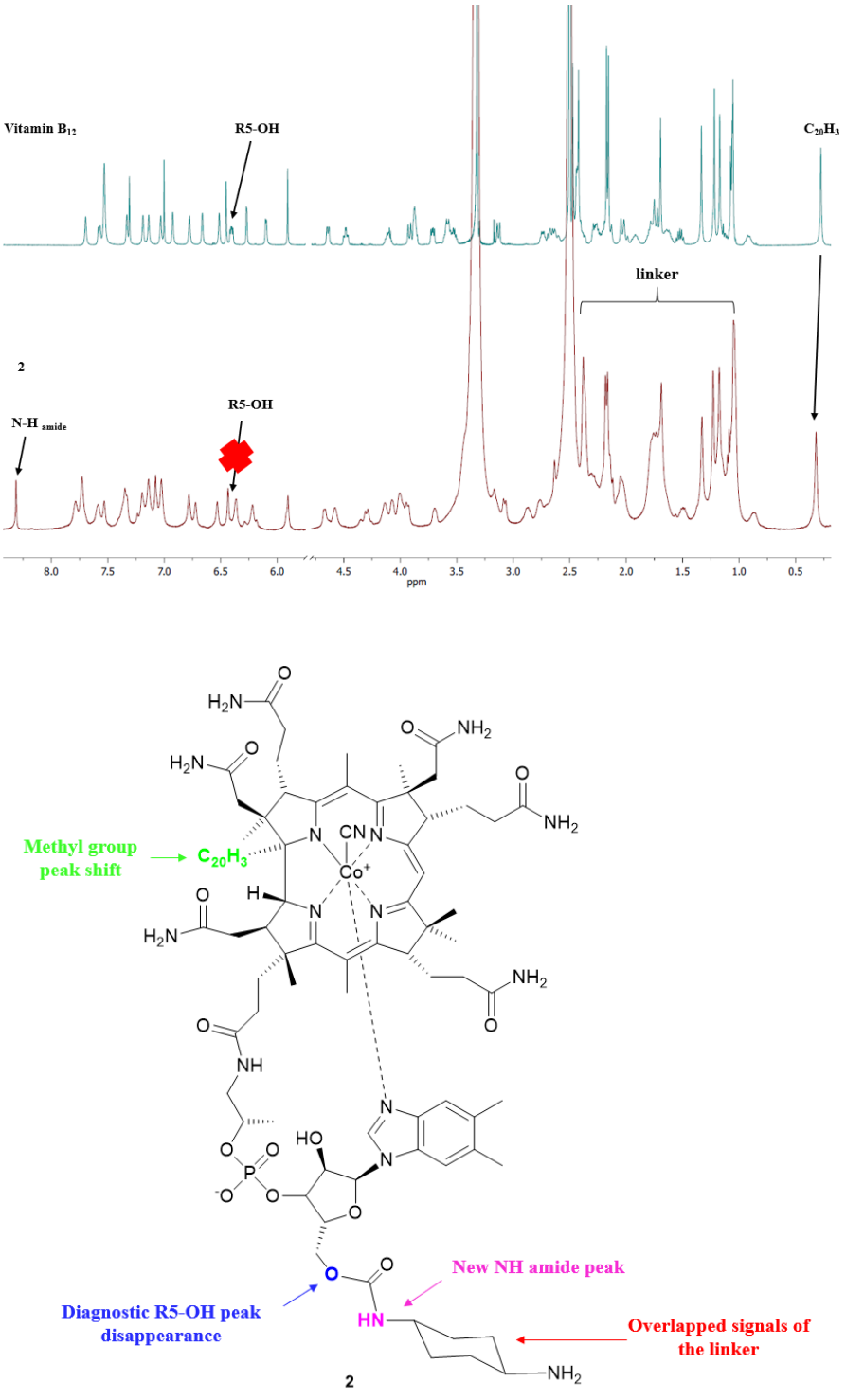

Figure 2.18: Top: Comparative ^{1}H NMR spectrum in DMSO-d_6 of vitamin B_{12} and intermediate **2**. Bottom: Indicative spectral changes confirming the successful conversion of vitamin B_{12} into intermediate **2**.

Additionally, MS analysis returned an intense peak of the double charged $[M+2H]^{2+}$ (calcd. 746.4 and found 748.3) while also the $[M+H+2Na]^{3+}$ (calcd. 511.4 and found 511.9) and $[M+H]^{+}$ (calcd. 1494.4 and found 1495.7) fragments were detected (**Figure 2.19**).

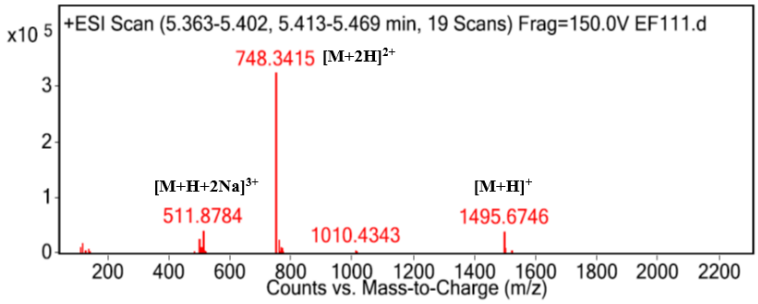

Figure 2.19: Mass spectrum of compound **2**.

2.5 Preparation of the luminescent Vitamin B_{12}-based derivatives

For detailed experimental conditions, structure numbering and full characterization see **Chapter 7**.

The target derivatives **3** ([B_{12}-5'-(FLUO-1)]) and **4** ([B_{12}-5'-(FLUO-2)]) were generated by following a modified literature procedure (**Figure 2.20**). A mixture of compound **2**, the appropriate fluorescent dye, and DIPEA was stirred in anhydrous DMSO at room temperature in the dark for 24 h. The reactions carried out with both the activated dyes resulted in a dark red solution which upon addition under stirring of a 1:1 mixture of DCM/Et_2O, led to the precipitation of a red solid, which was subsequently collected by filtration. Purification by column chromatography (see **Section 2.5)** afforded the desired products as fine bright red crystalline solids in 57% (**3**) and 48% (**4**) yield.

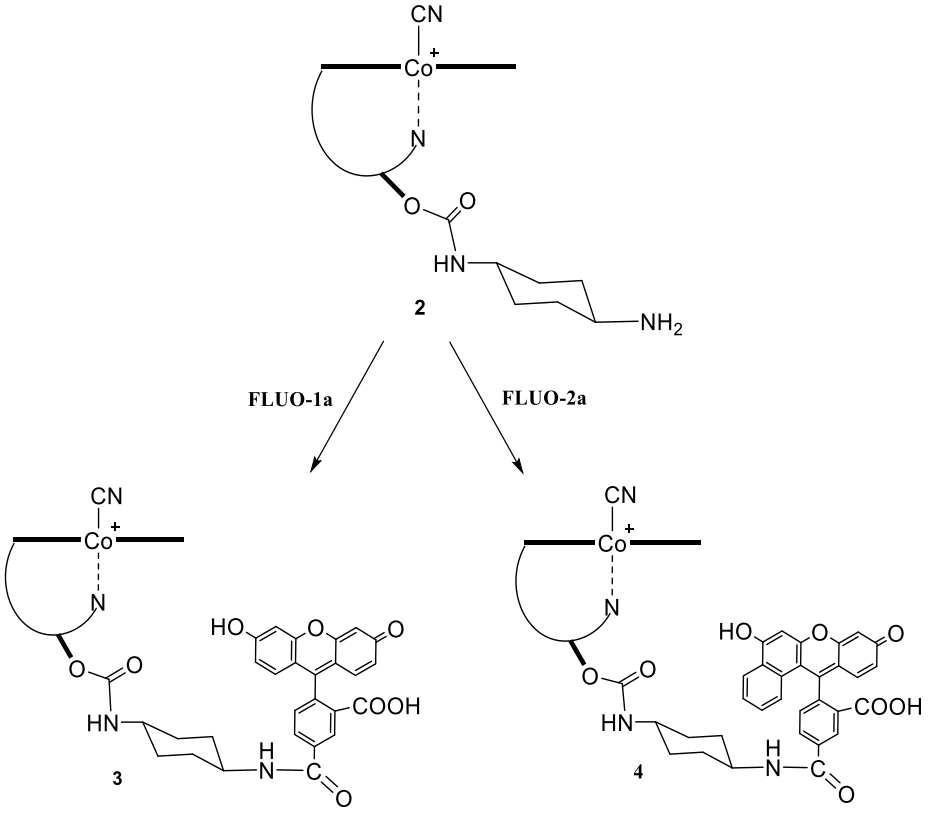

Figure 2.20: Synthetic route to the generation of the fluorescent vitamin B_{12}-based derivatives **3** and **4**.

The mid-IR spectra of **3** and **4** showed the characteristic vibrations at around 1100 and 2100 cm^{-1} for the phosphate and the cyano groups, respectively. The broadband at 3400 cm^{-1} was attributed to overlapped stretching modes of N-H and O-H groups. Additional vibration at around 1650 cm^{-1} was assigned to the overlapped $\nu(C{=}O_{amide})$ and $\delta(N\text{-}H_{amide})$ while the stretching modes of $\nu_{oop}(PO_2^-)$ and $\nu(P{=}O)$ were present at around 1170 and 1105 cm^{-1}, respectively (**Figure 2.21**, **Table 2.1**). Both ligands displayed almost identical spectral patterns due to similar chemical structures. For this reason, only the comparative mid-IR spectrum of derivatives **FLUO-1a**, **2**, and **3** presented.

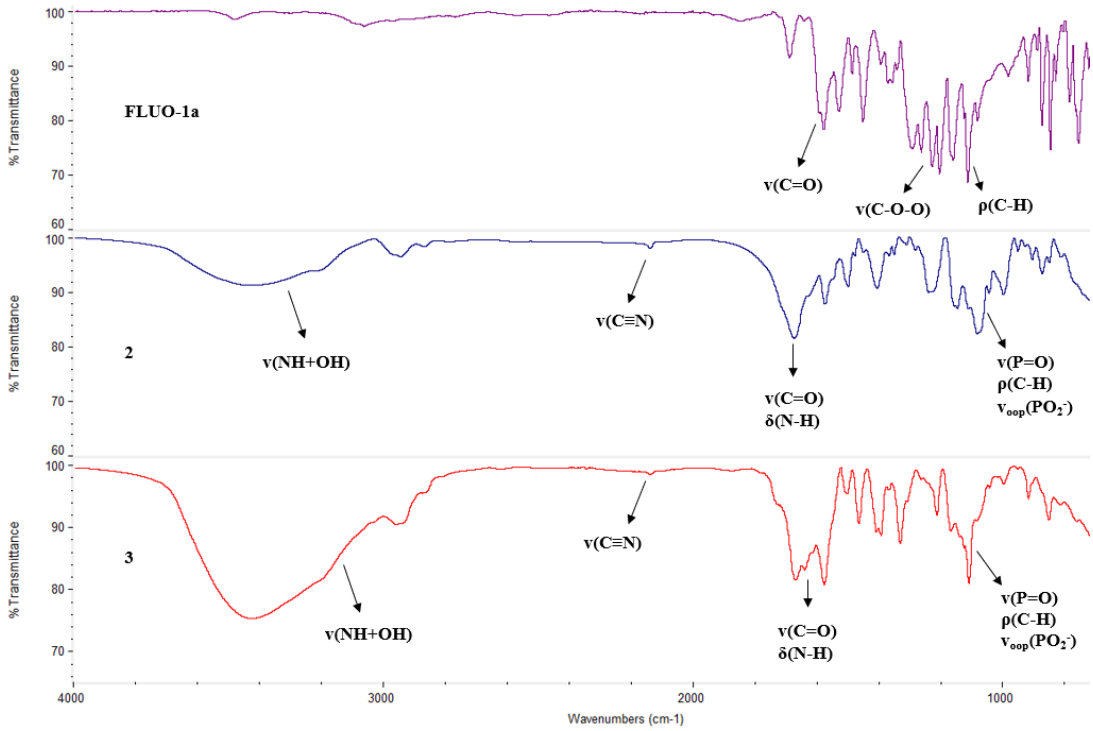

Figure 2.21: Comparative Mid-IR spectrum (CsI disk, wavenumber in cm^{-1}) of **FLUO-1a**, **2** and **3**.

Compound	ν(C=O)[43]	ν_{ca}(C=O)[43]	ν(NH)[44]	ν(C≡N)[44]	ν(P=O)[44]	ρ(C-H)[43]
FLUO-1	1691	1580	-	-	-	1112
FLUO-1a	1745	1594	-	-	-	1115
FLUO-2	1685	1580	-	-	-	1119
FLUO-2a	1732	1589	-	-	-	1111
2	-	-	1638	2137	1009	-
3	1666	1594	1573	2138	1103	1117
4	1578	1561	1570	2159	1005	1011

Table 2.1: Selected FT-IR absorptions (CsI disk, wavenumber in cm^{-1}) of **FLUO-1, FLUO-1a**, **FLUO-2, FLUO-2a**, **2**, **3** and **4**.

Despite the complexity of **3** and **4**, NMR spectroscopy provided insights into their chemical structure. As expected, the spectral pattern of vitamin B_{12} was substantially retained, while the newly formed amide bond in **3** and **4** returned a peak at 8.3 and 8.6 ppm, respectively. The peak of the methyl group $C^{20}H_3$ was shifted downfield of about 0.1 ppm. High-intensity peaks in the region 6.5-8.5 ppm were assigned to the aromatic protons of the dyes. More precisely, protons H^a, H^b, and H^c (**Figure 2.22**) showed an upfield trend due to proximity to the newly formed amide bond. Further

evidence of successful conjugation was the appearance of broad peaks between 10 and 10.3 ppm arising from the alcoholic OH groups. The characteristic peaks of all the newly formed species are summarized in **Table 2.2**.

Compound	$C^{20}H_3$ (Cbl)	H^a (FLUO)	H^b (FLUO)	H^c (FLUO)	NH (Cbl)	OH (FLUO)
FLUO-1	-	8.39	8.30	7.40	-	10.16
FLUO-1a	-	8.54	8.42	7.55	-	10.19
FLUO-2	-	8.18	7.26	7.02	-	10.02
FLUO-2a	-	8.70	7.49	7.19	-	10.06
2	0.32	-	-	-	8.31	-
3	0.33	8.47	8.23	7.09	8.62	10.23
4	0.32	8.32	7.23	6.80	8.55	10.08

Table 2.2: Selected ^{1}H NMR signals of **FLUO-1, FLUO-1a**, **FLUO-2, FLUO-2a**, **2**, **3** and **4**.

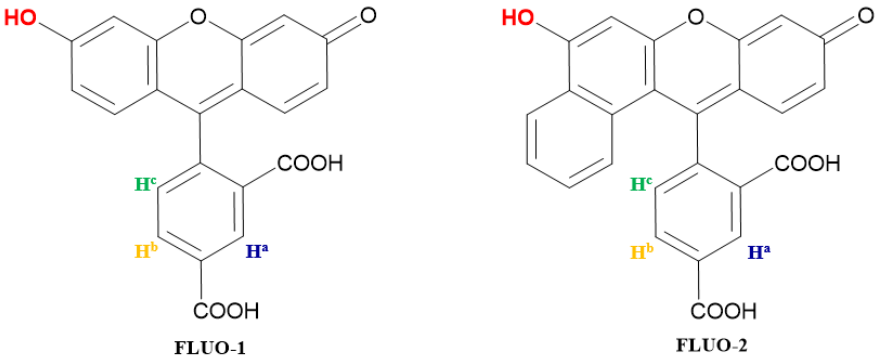

Figure 2.22: Hydrogen atoms of the fluorescent dyes showing an upfield shifting upon conjugation to the modified derivative **2**.

The comparative ^{1}H NMR spectra of derivative **3** are reported in **Figure 2.23** as an example.

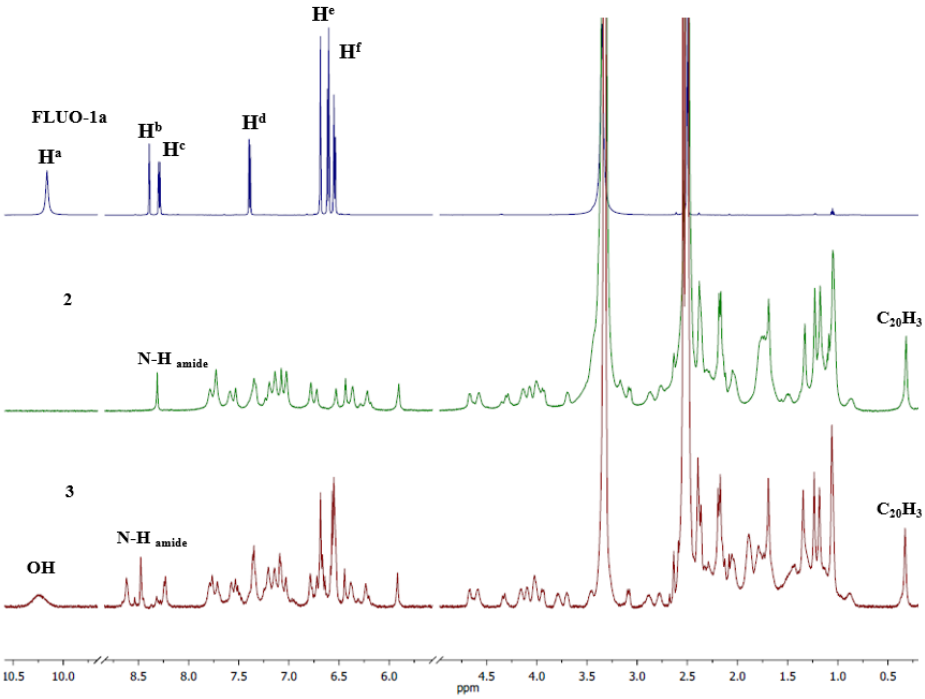

Figure 2.23: Comparative ^{1}H NMR spectra of **FLUO-1a**, **2** and **3** in DMSO-d_6.

The mass spectrums included the indicative $[M+2H+Na]^{3+}$ (calcd. 616.7 and found 618.9) and $[M+H+Na]^{2+}$ (calcd. 925.2 and found 927.9) segments of derivative **3** (**Figure 2.24 top**) and the corresponding $[M+3H]^{3+}$ (calcd. 625.2 and found 628.5) fragment of **4** (**Figure 2.24 bottom**).

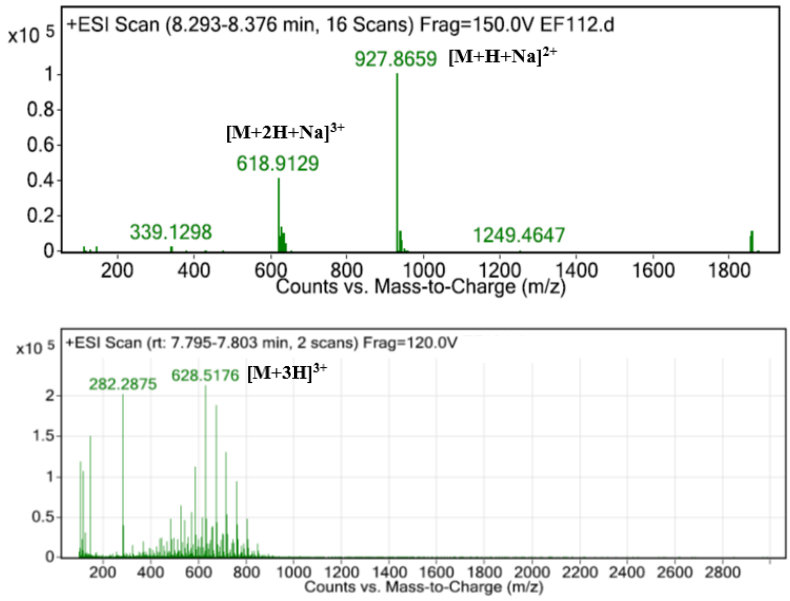

Figure 2.24: UPLC-MS/MS mass spectrum of compound **3** (top) and **4** (bottom).

Additionally, fluorescence spectroscopy revealed the enhanced luminescent properties of **3** with an excitation maximum at 555 nm and strong emission at 571 nm (**Figure 2.25**).

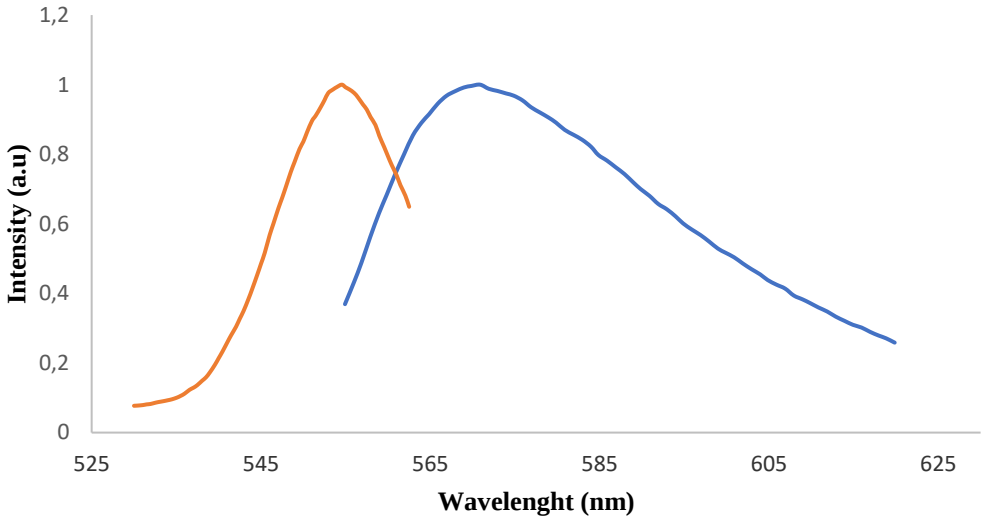

Figure 2.25: Excitation (orange) and emission (blue) bands overlapping of **3** 1 mg/ml in DMSO. Intensity has been normalized to the maxima.

Interestingly, analog **4** demonstrated two absorption maxima at 488 and 566 nm, most likely due to multiple allowed electronic transitions. The fluorescence emission maximum was observed at 590 nm. In the case of **4**, the resulting bands do not adhere to the mirror image rule (**Figure 2.26**).

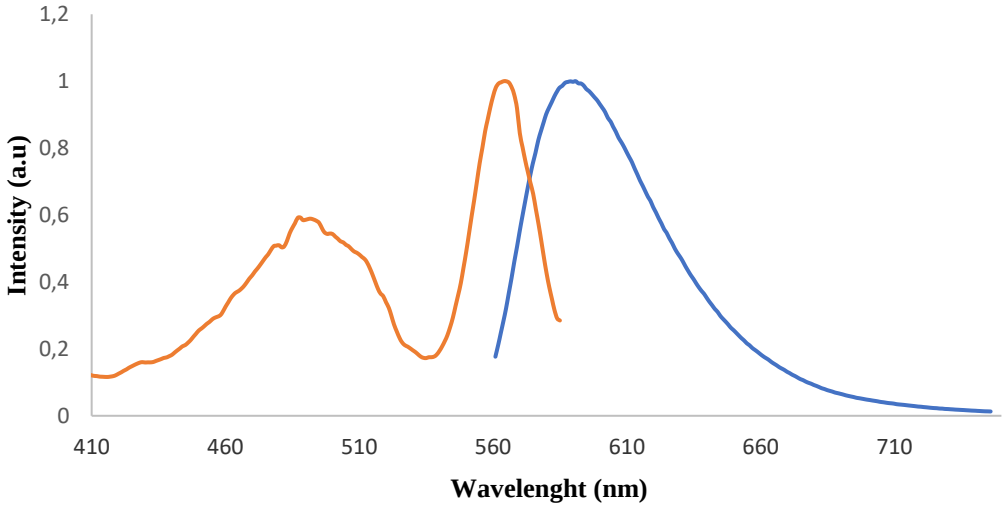

Figure 2.26: Excitation (orange) and emission (bleu) bands overlapping of **4** 1 mg/ml in DMSO. Intensity has been normalized to the maxima.

Both fluorescent vitamin B_{12}-based derivatives **3** and **4** demonstrated a good response to visible light with absorption maxima at 555 and 566 nm and emission maxima at 571 and 590 nm, respectively. As a result, each compound exhibits green light absorption and yellow light emission.

2.6 Conclusions

Due to its high sensitivity and straightforward apparatus, fluorescence spectroscopy is an analytical tool widely exploited in many disciplines, including biotechnology, DNA sequencing, forensics, genetic analysis, medical diagnostics, cellular and molecular imaging. Furthermore, this technique could offer several advantages in the field of anticancer research. To name a few, it can detect diseased areas and assess the transport and biodistribution of therapeutics within the human body. **Chapter 2** reports an optimized synthetic methodology for the preparation of two novel luminescent vitamin B_{12}-based carriers of potential anticancer drugs. To obtain the vitamin B_{12}-based scaffolds, we followed a stepwise experimental procedure to generate the fluorophores **FLUO-1**, **FLUO-2**, and their corresponding activated esters **FLUO-1a** and **FLUO-2a**. The synthetic approach subsequently involved the functionalization of vitamin B_{12} at the 5'-OH site of the ribose unit with the rigid linker *trans*-1,4-diaminocyclohexane. Indeed, intermediate compound **2** was isolated by modifying already reported experimental conditions and optimizing purification procedures. Combination of the active fluorophores and **2** under mild conditions in the dark resulted in the target derivatives **3** and **4**. Techniques such as FTIR, NMR, UPLC-MS/MS, and fluorescence measurements were used to confirm the generation of all the newly synthesized species.

2.7 Literature

1. Datta, R., Heaster, M., Sharick, T., Gillette, A., Skala, C., *J. Biomed. Opt.*, **25**, 1, (2020).
2. Lakowicz, J., *Principles of Fluorescence Spectroscopy,* Chapter 1-4, (2010).
3. Szudy. J., *Born 100 years ago: Aleksander Jablonski (1898–1980),* Wydawnictwo Uniwersytet Mikołaja Kopernika, Chapter 1, (1998).

4. Chrostowski, J., Krasiński, J., Phys. Lett., **A65**, 326, (1978).

5. James, L., Gambhir, S., *Physiol. Rev.,* **92**, 897–965, (2012).

6. Boro, P., Kishore, J., *Int J Preven Curati Comm Med*, **2**, 1–3, (2016).

7. Mehrotra, P., *J. Oral Biol. Craniofacial Res.,* **6**, 153–159, (2016).

8. Li, C., Chen, G., Zhang, Y., Wu, F., Wang, Q., et al., *J. Am. Chem. Soc.* **142**, 14789–14804, (2020).

9. Wang, Z. Yanping Z., Deqiang, Z., Ziwei, Z., Lixin, L., *et. al., J. Innov. Opt. Health Sci.,* **11**, 1–17, (2018).

10. Lichtman, J., Conchello, J., *Nat. Method*, **2**, 910–919, (2005).

11. Williams, T., Bridges, W., *J. Clin. Pathol.,* **17**, 371–394, (1964).

12. Liu, S., Gao, J., Yang, L., *Spect.Spectral Anal,* **25**, 1080–1082, (2005).

13. Shang, B., Wen, Y., Yan, X., Sun, H., Wang, Y., et al., *Luminescence,* **29**, 598–602, (2014).

14. Tsiminis, G., Schartner, P., Brooks, L., Hutchinson, R. *Appl. Spectrosc. Rev.*, **52**, 439–455, (2017).

15. Gao, Z., Hao, Y., Zheng, M., Chen, Y., *RSC Adv.*, **7**, 7604–7609, (2017).

16. Ren, B., Tian, B., Xu, W., Zhang, W., Zhang, X., et al., *J. Am. Chem. Soc.*, **140**, 7716–7722, (2018).

17. Xue, X. Shubin, J., Zhipeng, L., Chunqiu, Z., Weisheng, G., et al., *Adv. Sci.,* **4**, 1–7, (2017).

18. Liu, C., Xiaojie, J., Qing, W., Kun H., Song H., et al., *Chem. Commun.*, **53**, 10727–10730, (2017).

19. Bright,V., Munson, A., *Anal. Chim. Acta,* **500**, 71–104, (2003).

20. Owicki, C., *J. Biomol. Screen.,* **5**, 297–306, (2000).

21. Rubin, B., Braslavsky, E., *Photochem. Photobiol. Sci.*, **9**, 670–674, (2010).

22. Li, H., Vaughan, C., *Chem. Rev.,* **118**, 9412–9454, (2018).

23. Jones, R., *Photochem. Photobiol. Sci.*, **16**, 820–834, (2017).

24. Lawrence, D., Nemoto-Smith, E., Deery, E., Baker, J., Schroeder, S., et al., *Cell Chem. Biol.*, **25**, 941-951, (2018).

25. Cannon, M., Ph. D. Thesis, University of Utah, Salt Lake City, UT, (2001).

26. Smeltzer, C., Cannon, M., Pinson, P., Munger, J., West, F., *et al.*, *Org. Lett.*, **3**, 799–801, (2001).

27. Lee, M., Grissom, C., *Org. Lett.*, **11**, 2499–2502, (2009).

28. Horton, R., Ph. D. Thesis, University of Utah, Salt Lake City, UT, (2004).

29. Martin, B., Finke, R., *J. Am. Chem. Soc*., **114**, 585, (1992).

30. Orndorff, R., Hemmer, J., *J. Am. Chem. Soc.*, **49**, 1272–1280, (1927).

31. Sun, C., Gee, R., Klaubert, H., Haugland, P., *J. Org. Chem.*, **62**, 6469–6475, (1997).

32. Hammami, R., Nouira, I., Frein, Y., *Decis. Sci.*, **49**, 1116–1155, (2018).

33. Chhabra, N., Aseri, M., Padmanabhan, D., *Int. J. Appl. Basic Med. Res.*, **3**, 16, (2013).

34. Hammershøj, P., Kumar, P., Harris, P., Andresen, L., Clausen, M., *European J. Org. Chem.*, **33**, 7301–7309, (2015).

35. McEwan, F., Veitch, S., Russell-Jones, J., *Bioconjug. Chem.*, **10**, 1131–1136, (1999).

36. Urano, Y., Kamiya, M., Kanda, K., Ueno, T, Hirose, K., et al., *J. Am. Chem. Soc.*, **127**, 4888–4894, (2005).

37. Ueno, T., Urano, Y., Setsukinai, K., Takakusa, H., Kikuchi, et al., *J. Am.Chem. Soc.*, **126**, 14079–14085, (2004).

38. Mineno, T., Ueno, T., Urano, Y., Kojima, H., *Org.Lett.*, **8**, 5963–5966, (2006).

39. Ueno, Y., Jiao, G., Burgess, K., *Synthesis*, **15**, 2591–2593, (2004).

40. Skinner, B., US2891099A, (1959)

41. Woodroofe, C., Lim, H., Bu, W., Lippard, S., *Tetrahedron*, **61**, 3097–3105,

(2005).

42. Adamczyk, M., Fishpaugh, J., Heuser, K., *Bioconjug. Chem.*, **8**, 253–255, (1997).

43. Wang, L., Roitberg, A., Meuse, C., Gaigalas, K., *Spectrochim. Acta - Part A Mol. Biomol. Spectrosc.*, **57**, 1781–1791, (2001).

44. Russell, H., Ph. D. Thesis, The University of Manchester, UK, (2013).

Chapter 3

3. Platinum(II)- and Gold(I)-Dithiocarbamato Precursors: The Initial Approach

3.1 Background and Rationale

3.1.1 Platinum(II)-based chemotherapeutics

In 1844 Peyrone successfully synthesized the square-planar platinum(II) complex cisplatin (cis-diamminedichloroplatinum(II), cis-$[PtCl_2(NH_3)_2]$ or cis-DDP).[1] A century later, Rosenberg observed that cisplatin can cause inhibition of cell growth and division of E.Coli.[2,3] Soon after this discovery, cisplatin showed unquestionable clinical success and became the first metal-based anticancer drug approved by the Food and Drug Administration (FDA).[4,5] As previously mentioned (**Section 1.3.2**), cisplatin is typically administered to treat various types of cancers and its commonly acknowledged biological target is cellular DNA. Unfortunately, during the treatment, the drug displayed several side effects, including nephrotoxicity, neurotoxicity, ototoxicity, nausea, alopecia, and vomiting.[6] To overcome these issues, extensive research in the field has led to numerous analogs of cisplatin, to name a few, the second-and third-generation derivatives carboplatin, oxaliplatin, satraplatin, aroplatin, enloplatin, zeniplatin, sebriplatin, miboplatin, nedaplatin, heptaplatin, and lobaplatin (**Figure 3.1**).[7–9] In general, platinum(II) presents a strong binding affinity to S-donor ligands.[10,11] Thus, sulfur-containing biomolecules (such as glutathione, metallothionines, albumins, cysteine, and methionine residues of enzymes) could interact with platinum-based drugs,[12–14] resulting in their mechanism of action and therapeutic potential being negatively affected. To date, many sulfur-based compounds have been developed and investigated as coadministrative chemoprotectants (e.g., glutathione and sodium thiosulfate).[12–15] Also, several potential anticancer agents are incorporating sulfur donor ligands as intrinsic chemoprotectants (e.g., dithiocarbamates).[16–24]

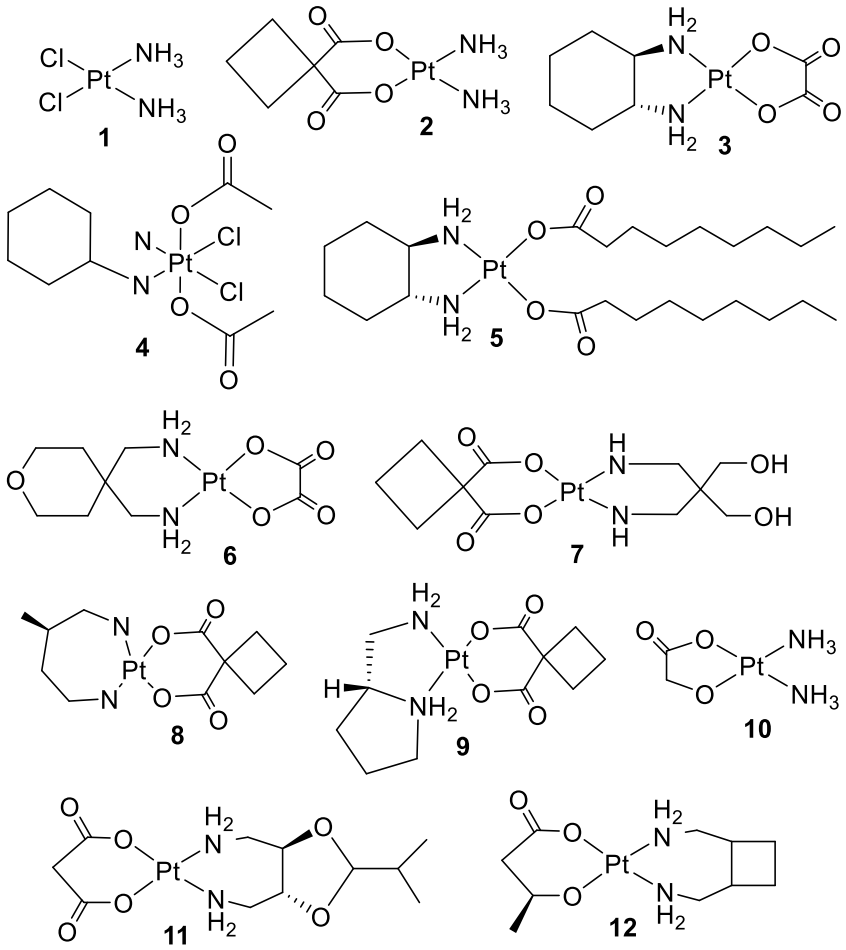

Figure 3.1: Chemical drawing of platinum-based anticancer complexes in clinical use or preclinical development: (**1**) cisplatin, (**2**) carboplatin, (**3**) oxaliplatin, (**4**) satraplatin, (**5**) aroplatin, (**6**) enloplatin , (**7**) zeniplatin , (**8**) sebriplatin, (**9**) miboplatin, (**10**) nedaplatin, (**11**) heptaplatin, and (**12**) lobaplatin.

3.1.2 Dithiocarbamates

Dithiocarbamates (dtcs) were first reported in 1850 by Debus.[25] These organosulfur scaffolds (containing the -NCSS functional group) demonstrate various pharmacological activities, such as anticancer, antiparasitic, antiviral, and antifungal.[26,27] Dithiocarbamates have applications in several fields, such as agriculture, biology, materials science, medicine and chemistry. They may act as strong monodentate chelating agents (or either bidentate or anisobidentate type of bonding) to give stable coordination compounds to metal centers in different oxidation states.[25,28] Their chelating potential is due to the two donor sulfur atoms,

acting as either 'soft' or 'hard' Lewis bases depending on the major contribution of their resonance forms (**Figure 3.2**), as well as to the small bite angle of the dithiocarbamate moiety.[29–31]

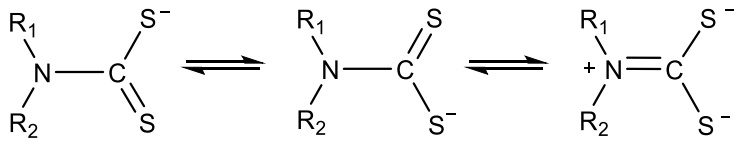

Figure 3.2: Resonance forms of dithiocarbamates.

Considering the above, the formation of square-planar metal complexes with dithiocarbamato scaffolds should, at least in principle, act as intrinsic chemoprotectants against the toxicity of metal-based drugs, prevent further coordination of S-containing biomolecules (e.g., thiol-containing renal enzymes) and, thus, reduce the nephrotoxic side-effects. Several dithiocarbamato-containing complexes of Pt(II), Pd(II), Au(I/III), Ni(II), Zn(II), Cu(II), Ru(II/III) metal ions have been reported as alternative anticancer drugs.[32–35]

3.1.3 Gold(I)-based chemotherapeutics

Gold(I)-based compounds could offer several advantages in many diseases.[36] Interestingly, complexes such as aurothiomalate, aurothioglucose, and auranofin were used for tuberculosis or rheumatoid arthritis. Additionally, solganal, myocrisin, sanocrysin, allocrysin, and auranofin are well-known anti-inflammatory drugs (**Figure 3.3**).[37-40]

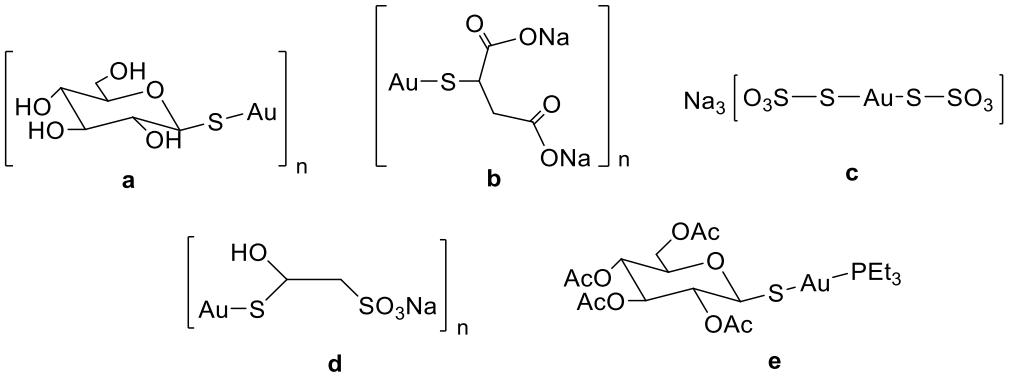

a **b** **c** **d** **e**

Figure 3.3: Clinically-established gold(I) antiarthritic drugs: (**a**) solganal, (**b**) myocrisin, (**c**) sanocrysin, (**d**) allocrysin, and (**e**) auranofin.

To date, there are several gold(I)-derivatives of carbenes, phosphines, alkynes, N-donor ligands, and thiolates exhibiting anticancer, antimalarial, anti-HIV, and antibacterial properties.[41–44] In particular, gold(I) complexes incorporating the structural feature S–Au–P, such as auranofin, showed promises as antiarthritic and anticancer agents, although acute toxicity proved a major drawback. Nonetheless, it was shown that trimethyl-, ethyl-, and tert-butyl-phosphine gold(I) scaffolds with various dithiocarbamato ligands exhibited remarkable anticancer activity against HeLa, MCF7, A549, and HepG2 cell lines. [45,46]

3.2 Initial Designing Strategy

On account of the aforementioned considerations, the initial idea was to prepare a series of platinum(II)-dithiocarbamato precursors of the general formula [Pt(dtc)(am)Cl] and [Pt(dtc)Cl_2] (dtc = various dithiocarbamates, am = various amines), in a view to subsequently conjugating them to the β-upper site of vitamin B_{12} by coordinating the cyano group to the platinum(II) center (i.e., by replacing one chloride ligand).[47-49] To generate the desired complexes, the initial synthetic plan included the synthesis of the symmetric cis-bis(amine)diiodidooplatinum complexes cis-[Pt(am)$_2$$I_2$], which would be then converted into the analogous iodido-bridged platinum dimers [Pt(am)I_2]$_2$. The iodo-bridged dimers would then be cleaved by several types of reagents to give the desired monoamine platinum derivatives K[Pt(am)Cl_3] (**Figure 3.4**).[50-54]

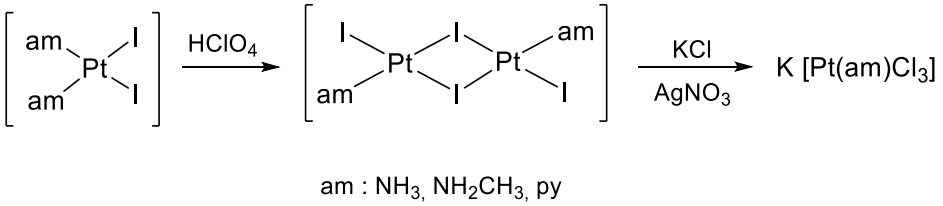

Figure 3.4: General synthetic scheme for the preparation of K[Pt(am)Cl_3] .

As far as the dithiocarbamato ligands are concerned (PPh_4)(dtc-Sar-OEt) **(PPh_4) ESDT**, Me-dtc-Sar-OEt, **ESDTM** and Me-dtc-Me_2, **DMDTM** were prepared (**Figure 3.5**) according to the literature.[52-55]

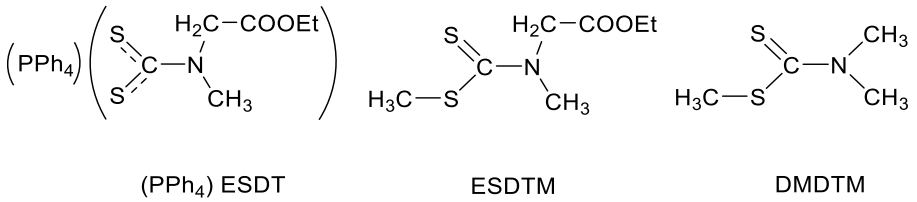

Figure 3.5: Chemical drawing of the ligands **(PPh4) ESDT**, **ESDTM** and **DMDTM**.

To verify the capability of the dithiocarbamato ligands to bind to platinum(II), the dithiocarbamates **(PPh4) ESDT**, **ESDTM** and **DMDTM** were reacted directly with $PtCl_2$ leading to the successful generation of the platinum(II)-dithiocarbamato derivatives [Pt(ESDTM)Cl_2] (**Pt10)** and [Pt(DMDTM)Cl_2] (**Pt11**). Unfortunately, the direct reaction of K[Pt(am)Cl_3] with the dithiocarbamato ligands **(PPh4) ESDT**, **ESDTM**, and **DMDTM** proved unsuccessful, always resulting in the generation of the bis-dithiocarbamato species [Pt(dtc)$_2$]. (**Figure 3.6**).

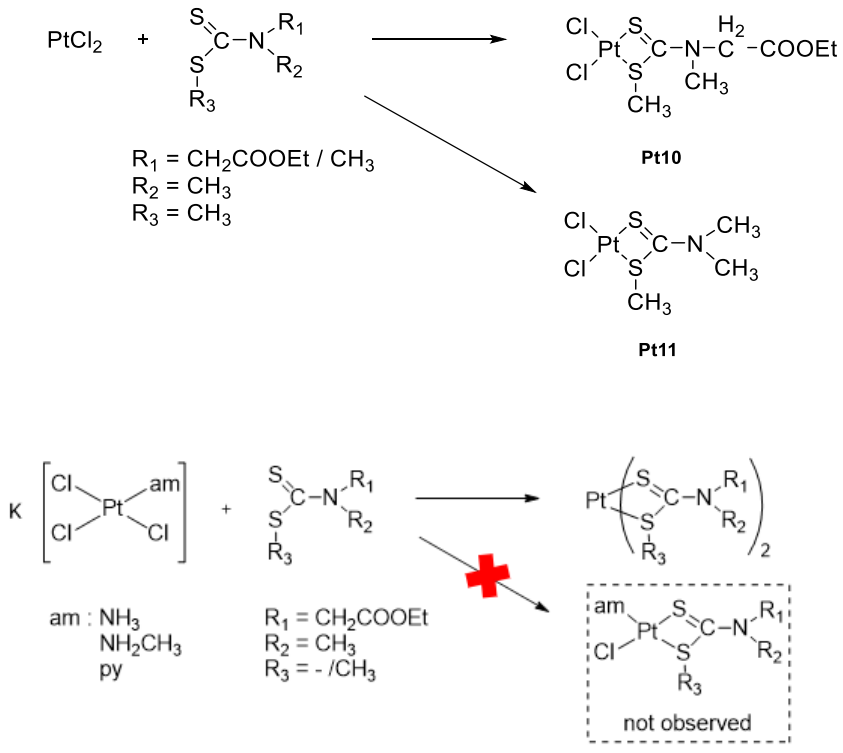

Figure 3.6: Initial synthetic route to the generation of platinum(II)-dithiocarbamato precursors.

Therefore, the synthetic approach was reconsidered, and the transmetallation reaction from selected [Zn(dtc)$_2$] intermediates to platinum(II) substrates was attempted (**Figure 3.7**).[56] Once more, the only products obtained were bis-dithiocarbamato species.

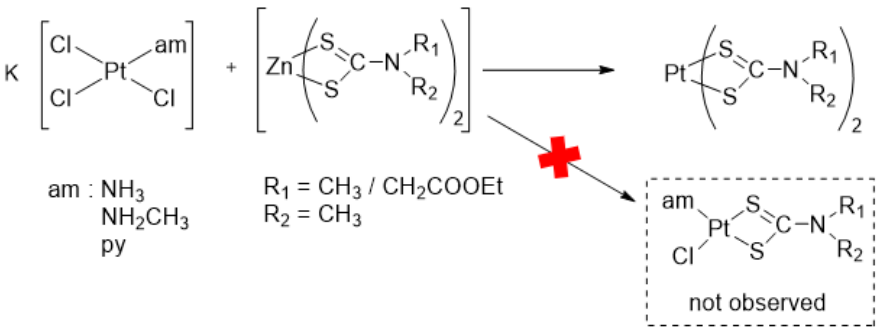

Figure 3.7: Reaction scheme for the zinc(II)-platinum(II) transmetallation reaction.

Given that only the platinum(II)-dithiocarbamato complexes **Pt10** and **Pt11** were successfully obtained, their conjugation to the cyano group of vitamin B_{12} was attempted.[57-59] Moreover, the commercially available gold(I) complex [(Ph_3P)AuCl] (**Figure 3.8**) seemed promising considering the well-known anticancer activity of auranofin. For this reason, attempts to attach the gold(I) complex to the β-upper site of vitamin B_{12} were also carried out.

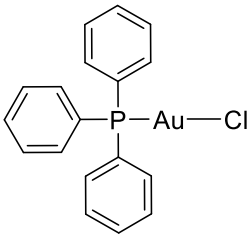

Figure 3.8: Chemical drawing of the [(Ph_3P)AuCl].

In the following sections, the experimental results here anticipated are summarized and critically discussed in detail.

3.3 Syntheses and characterizations

For detailed experimental conditions and full characterizations see **Chapter 7**.

3.3.1 Preparation of K[Pt(am)Cl_3] precursors

The platinum complex K[Pt(NH_3)Cl_3] was synthesized according to Dhara's method.[60] Initially, the reaction of NH_4Cl, $K_2[PtCl_4]$, and KI in water resulted in the

formation of cis-[Pt(NH$_3$)$_2$I$_2$] (**Pt1**) in almost quantitative yield. Then the diiodo derivative was treated with AgNO$_3$ and NaCl in water to yield cisplatin **Pt2**, which was then reacted with (PPh$_4$)Cl and (Et$_4$N)Cl to give the object compound **Pt3** (**Figure 3.9**).

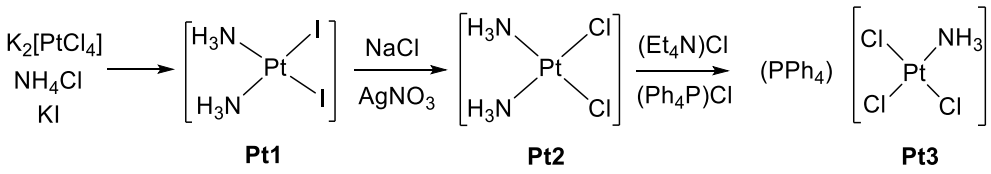

Figure 3.9: Stepwise synthesis of **Pt3**.

Characteristic IR bands at 488, 479, and 243 cm^{-1} assigned to ν_a(Pt-N), ν_s(Pt-N), and δ(N-Pt-N), respectively for **Pt1**. The new broad band recorded for **Pt2** at 323 cm^{-1} ($\nu_{a/s}$(Pt-Cl)) supported the generation of the dichloro derivative. Finally, vibrations at 527 and 325 cm^{-1} ($\nu_{a/s}$(Pt-Cl) and δ_{oop}(PPh$_4$), respectively) confirmed the successful preparation of **Pt3** (**Figure 3.10**).[61,62]

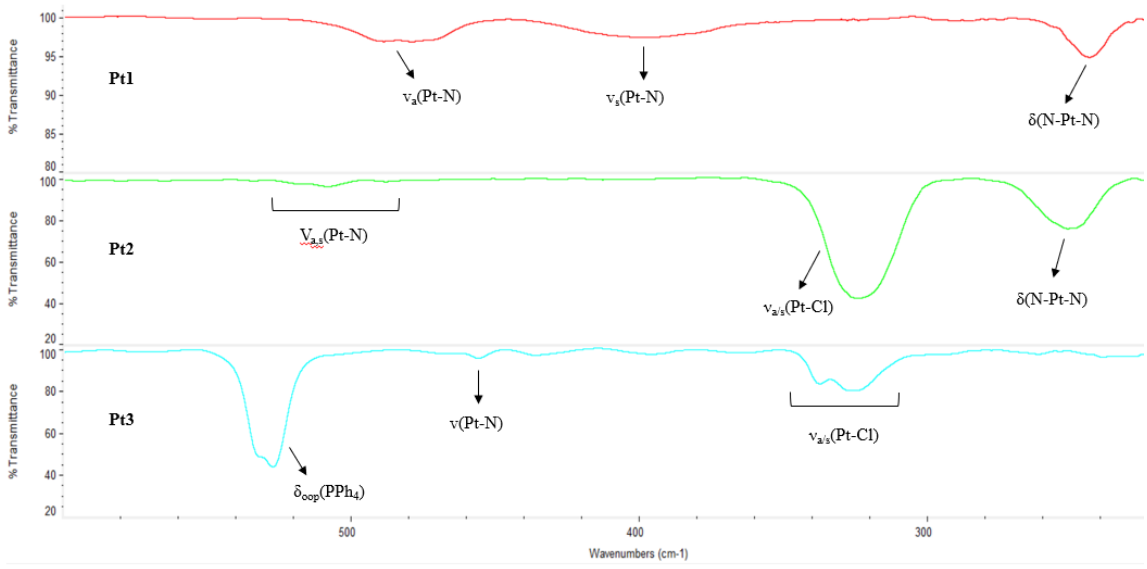

Figure 3.10: Far-IR (600-200 cm^{-1}) spectra (CsI disk, wavenumber in cm^{-1}) of the platinum (II) complexes **Pt1, Pt2** and **Pt3**.

In the NMR spectrum of **Pt1**, a broad signal at 4.42 ppm was recorded (associated with the NH_3 groups), which shifted upfield at 3.95 ppm for **Pt2**. Finally, multiplets at around 7.75 ppm were observed for **Pt3**, consistent with the presence of $(PPh_4)^+$ counterion (**Figure 3.11**).[63,64]

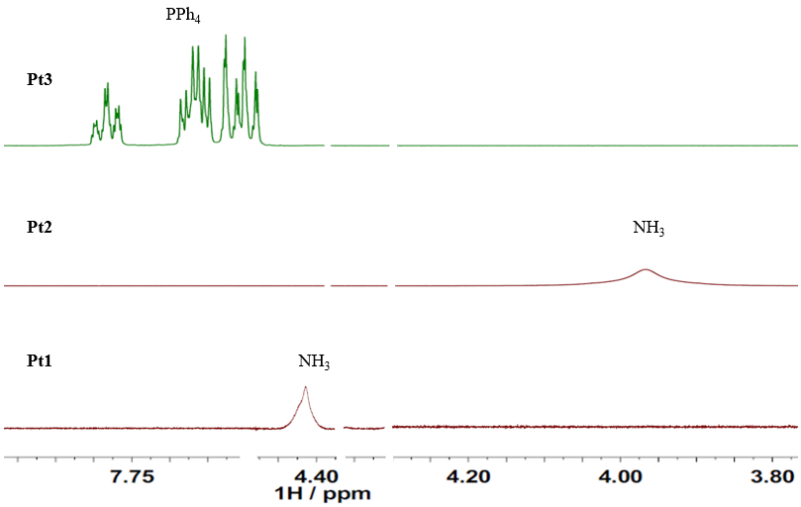

Figure 3.11: ^{1}H NMR spectra in DMSO-d_6 of **Pt1, Pt2** and **Pt3**.

The K[Pt(am)Cl_3] derivatives (am = $MeNH_2$, py) were prepared as reported in the literature. Cis-[Pt(am)$_2I_2$] (**Pt4**) was obtained upon the reaction of methylamine with $K_2[PtCl_4]$ and KI in water. Conversion into the iodido-bridged dimeric species [Pt($MeNH_2$)I_2]$_2$ (**Pt5**) was obtained upon treatment with perchloric acid. The subsequent treatment with silver nitrate and potassium chloride gave the corresponding monoamine precursor K[Pt($MeNH_2$)Cl_3] (**Pt6**) (**Figure 3.12**).[65]

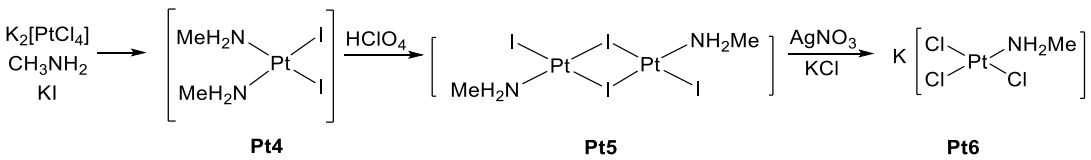

Pt4 **Pt5** **Pt6**

Figure 3.12: Stepwise synthesis of **Pt6**.

The IR spectrum of **Pt4** showed a broad band at 475 cm^{-1}, which was assigned to the $\nu_{a,s}$(Pt-N). For **Pt5**, bands at 486 and 475 cm^{-1} (ν(Pt-N)) were in agreement with literature data.[65] Additionally, characteristic bands at 333 and 314 cm^{-1} (ν_a(Pt-Cl) and ν_s(Pt-Cl), respectively) confirmed the successful preparation of **Pt6** (**Figure 3.13**).

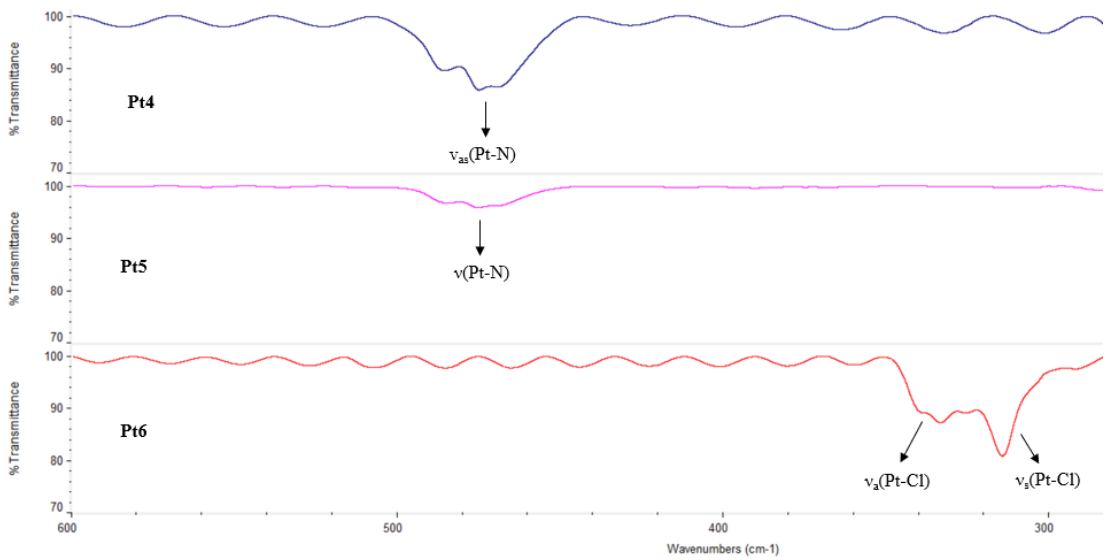

Figure 3.13: Far-IR (600-200 cm^{-1}) spectra (CsI disk, wavenumber in cm^{-1}) of the platinum(II) complexes **Pt4, Pt5** and **Pt6** derivatives.

The ^1H NMR spectrum of **Pt4** returned signals at 4.99 and 2.65 ppm of the NH_2 and CH_3 groups, respectively. The iodo-bridged dimer **Pt5** revealed shifted signals at 4.43 and 2.53 ppm. Then, downfield shifting at 5.74 and 4.33 ppm (NH_2 and CH_3, respectively) indicated the preparation of **Pt6** (**Figure 3.14**).

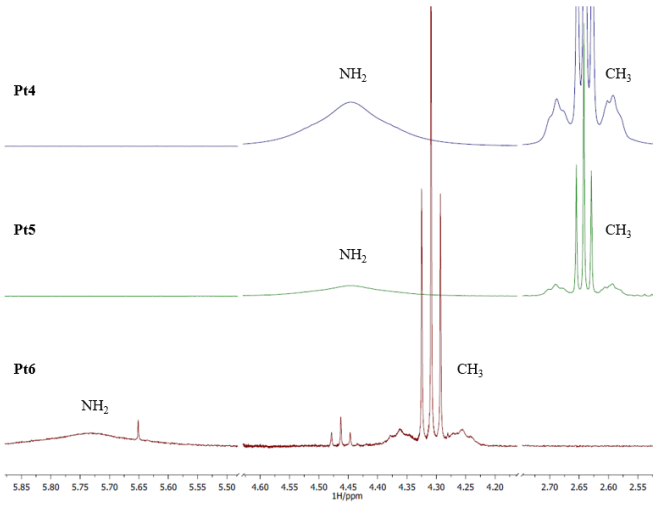

Figure 3.14: ^1H NMR spectra in DMSO-d_6 of the platinum(II) complexes **Pt4, Pt5** and **Pt6**.

Complexes **Pt7** - **Pt9** were synthesized in a similar way (**Figure 3.15**).[65]

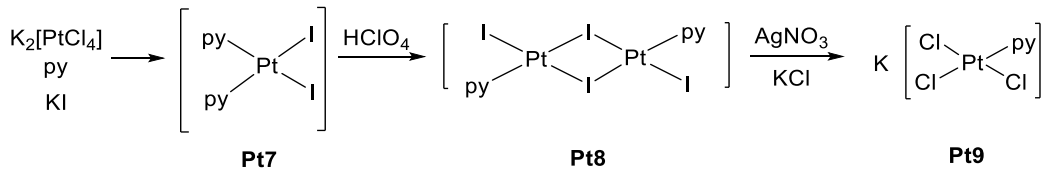

Figure 3.15: Stepwise synthesis of **Pt9**.

Complex **Pt7** presented bands at 461, 447, and 244 cm^{-1} (ν_a(Pt-N), ν_s(Pt-N), and δ(N-Pt-N), respectively). Then, **Pt8** revealed the characteristic band ν(Pt-N) at 455 cm^{-1}. For **Pt9**, the vibration ν(Pt-Cl) was recorded at 326 cm^{-1} (**Figure 3.16**).

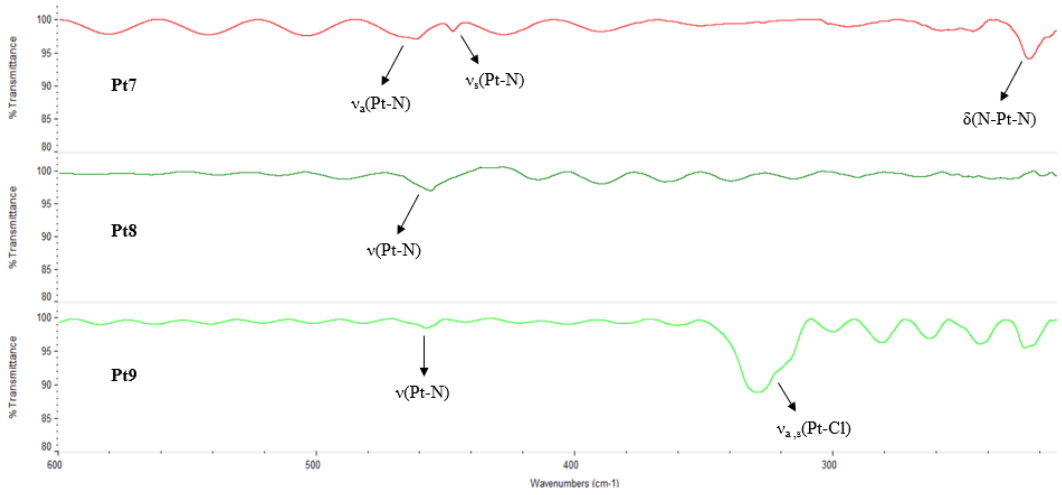

Figure 3.16: Far-IR (600-200 cm^{-1}) spectra (CsI disk, wavenumber in cm^{-1}) of the platinum(II) complexes **Pt7, Pt8** and **Pt9** derivatives.

Peaks recorded in the ^{1}H NMR spectra confirmed the generation of the three platinum(II) complexes **Pt7-Pt9**, which was proved not only by the shifting of proton signals but also by the appearance of satellites at the sides of the ortho-CH protons due to the ^{195}Pt - ^{1}H coupling (**Figure 3.17**).

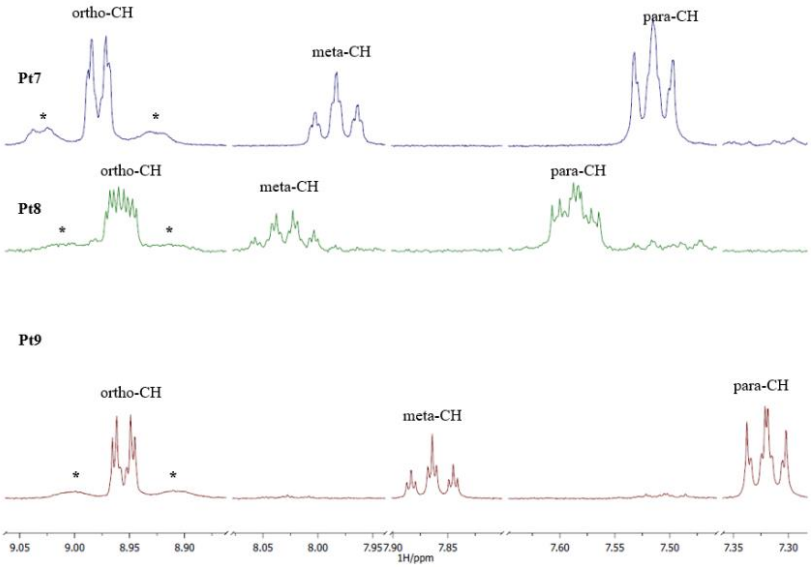

Figure 3.17: ^{1}H NMR spectra in DMSO-d_6 of the platinum(II) complexes **Pt7, Pt8** and **Pt9**. (*) indicates the ^{195}Pt - ^{1}H couplings.

3.3.2 Preparation of the dithiocarbamate ligands

The synthesis of dithiocarbamates typically occurs upon reacting a primary or secondary amine with carbon disulfide under alkaline conditions at low temperature. However, it is common for dithiocarbamates to decompose back to the starting amine and CS_2 at room temperature. Thus, unstable dithiocarbamates should be immediately reacted with the chosen metal precursor in the appropriate stoichiometry to obtain the corresponding metal-dithiocarbamato derivative. The dithiocarbamato ligands **(PPh_4) ESDT**, **ESDTM**, and **DMDTM** were obtained as follows.[66-71]

The ethylsarcosinedithiocarbamato ligand **(PPh_4) ESDT** was obtained by reacting aqueous solutions of ethyl sarcosine hydrochloride, NaOH, CS_2, and PPh_4Cl in a one-pot synthesis (**Figure 3.18**).

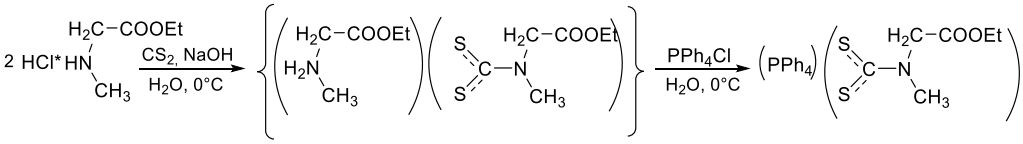

Figure 3.18: Synthesis of the ligand **(PPh_4) ESDT**.

Diagnostic IR bands were recorded at 2980, 1732, 1434, 1268, 1193 and 1029 cm^{-1}(ν(C-H), ν(C=O), ν(N-CSS), ν_a(CSS) + ρ(CSS) + ν_a(C-N-C), ν_a(CSS) and ν(N-CH_3), respectively). Additionally, bands at 1109 and 730 cm^{-1} were assigned to the $\nu_{q\text{-}vib}$(P-Ph) and $\nu_{r\text{-}vib}$(P-Ph), respectively (**Figure 3.19**).

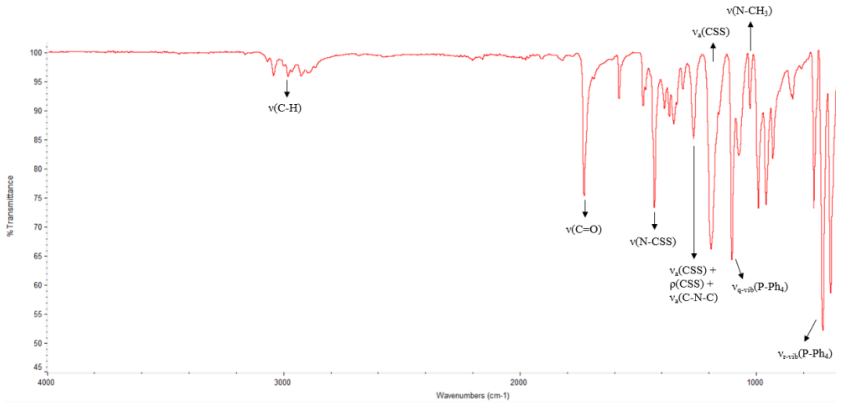

Figure 3.19: Mid-IR (4000-600 cm^{-1}) spectrum (CsI disk, wavenumber in cm^{-1}) of **(PPh_4) ESDT**.

Additionally, the ^1H NMR spectrum showed all the expected signals at 7.97 (para-CH), 7.81 (meta-CH), 7.77 (ortho-CH), 4.95 (N-CH_2), 4.07 (O-CH_2), 3.39 (N-CH_3), and 1.18 (CH_3) ppm (**Figure 3.20**), confirming the generation of the dithiocarbamato ligand **(PPh_4) ESDT**.

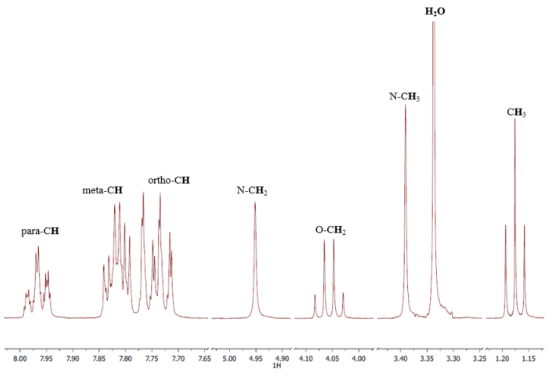

Figure 3.20: ^1H NMR spectrum in DMSO-d_6 of **(PPh_4) ESDT**.

Preparation of the ligand **ESDTM** was carried out by reacting ethyl sarcosine, hydrochloride, CS_2, NaOH, and MeI (**Figure 3.21**). Initially, an ethanol solution of ethyl sarcosine hydrochloride was treated with carbon disulfide and sodium hydroxide, followed by the addition of methyl iodide and then H_2O to yield a white flocculent solid.

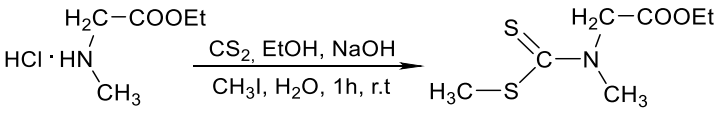

Figure 3.21: Synthesis of the ligand **ESDTM**.

In the mid-IR spectrum of **ESDTM**, two strong absorptions at 1728 cm^{-1} (ν(C=O)) and 1469 cm^{-1} ν(N-CSS) were recorded. The overlapped bands assigned to ν_a(CSS), ρ(CSS) and ν_a(C-N-C) were observed at 1201 cm^{-1}, as well as the ν_a(CSS) at around 998 cm^{-1} (**Figure 3.22**).

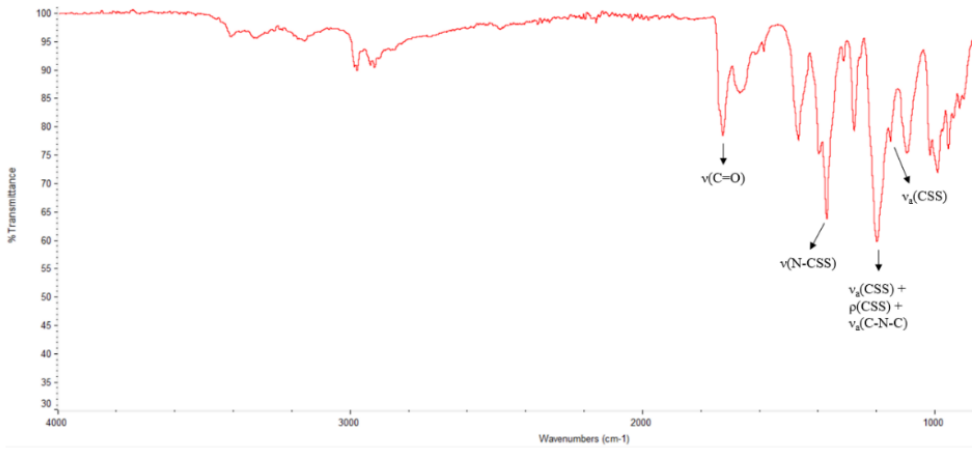

Figure 3.22: Mid-IR (4000-600 cm^{-1}) spectrum (CsI disk, wavenumber in cm^{-1}) of **ESDTM**.

The ^{1}H NMR spectrum of **ESDTM** showed the CH_3 and CH_2 peaks at 1.29 and 4.22 ppm, respectively. Additionally, the SCH_3 signal was recorded at 2.64 ppm, while the NCH_3 and NCH_2 peaks were recorded at 4.80 and 3.43 ppm, respectively (**Figure 3.23**).

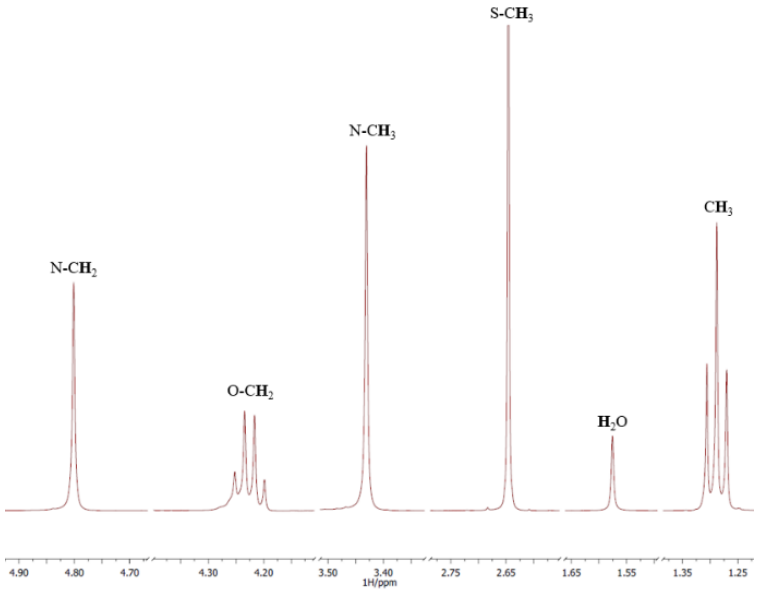

Figure 3.23: ^{1}H NMR spectrum in DMSO-d_6 of **ESDTM**.

The ligand **DMDTM** was prepared by reacting the corresponding commercially available sodium dithiocarbamato N,N-dimethyldithiocarbamate with NaOH, and MeI (**Figure 3.24**).

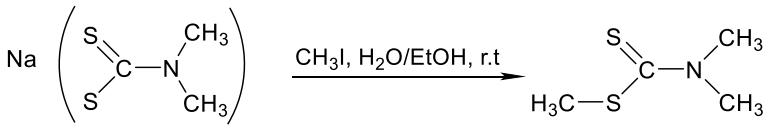

Figure 3.24: Synthesis of the ligand **DMDTM**.

The IR spectrum of the **DMDTM** showed the expected diagnostic vibrations (**Figure 3.25**).

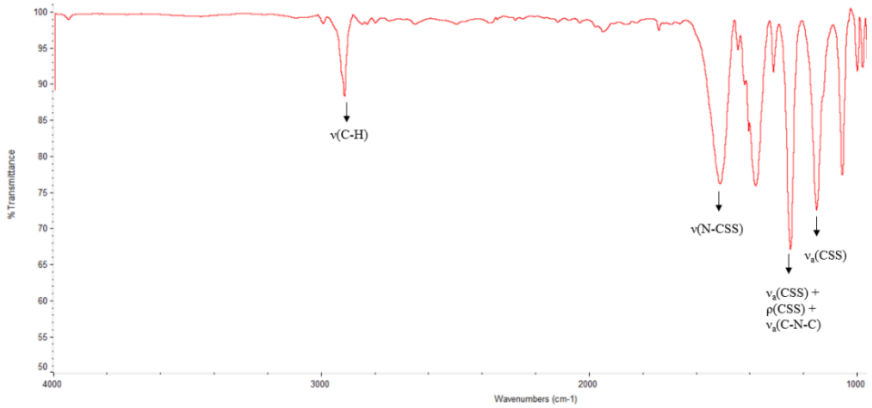

Figure 3.25: Mid-IR (4000-600 cm^{-1}) spectrum (CsI disk, wavenumber in cm^{-1}) of **DMDTM**.

Strong evidence of the successful synthesis was given by the ^{1}H NMR spectrum showing the characteristic peaks of the methyl groups (-SCH_3) at 1.23 and (-NCH_3) at 3.34 ppm (**Figure 3.26**).

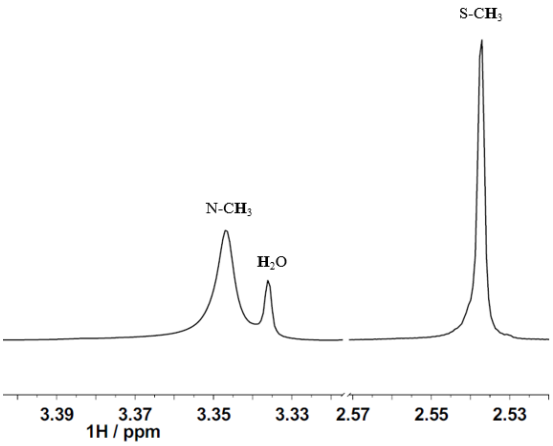

Figure 3.26: ^{1}H NMR spectra in DMSO-d_6 of **DMDTM**.

3.3.3 Attempted synthesis of the platinum(II)-dithiocarbamato precursors.

Platinum(II)-dithiocarbamato derivatives have shown promising anticancer activity.[55-58] Interestingly, coordinated dithiocarbamato moieties may provide intrinsic chemoprotection against further metal binding by other sulfur-containing biomolecules, thereby potentially preventing inactivation of the drug and avoidance of undesirable toxic side effects.[59,72-74] Amongst others, complex [Pt(ESDT)(py)Cl] proved the most effective with IC_{50} values of 2.94 and 6.95 μM against HL-60 and HeLa cells, respectively.

Accordingly, numerous synthetic strategies were investigated to prepare complexes of the type [Pt(dtc)Cl_2] and [Pt(dtc)(am)Cl]. Initially, reaction between $PtCl_2$ and **ESDTM** or **DMDTM** led to the generation of the complexes [Pt(ESDTM)Cl_2] (**Pt10**) and [Pt(DMDTM)Cl_2] (**Pt11**) respectively. On the other hand, reaction with **(PPh$_4$) ESDT** yielded the bis-dithiocarbamato adduct [Pt(dtc)$_2$] (**Pt12**) regardless of the experimental conditions (**Figure 3.27**).

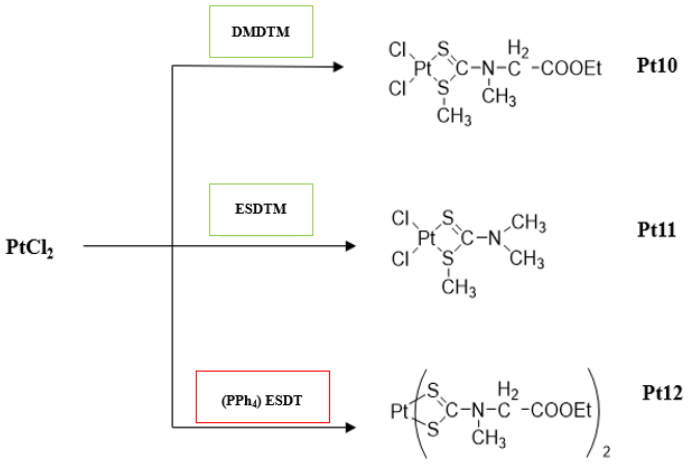

Figure 3.27: General reaction scheme to the generation of the platinum(II) complexes **Pt10**, **Pt11** and **Pt12**.

Complex **Pt10** was prepared in anhydrous benzene by reacting $PtCl_2$ and **ESDTM** in a 1:1 ratio. The reaction was performed in the dark because light might induce S-methylation, and eventually afforded the object compound as a yellow powder in 70% yield. In the far-IR spectrum, the diagnostic bands $\nu_{a/s}$(Pt-S) and $\nu_{a/s}$(Pt-Cl) were observed in agreement with literature data (**Figure 3.28**).[73]

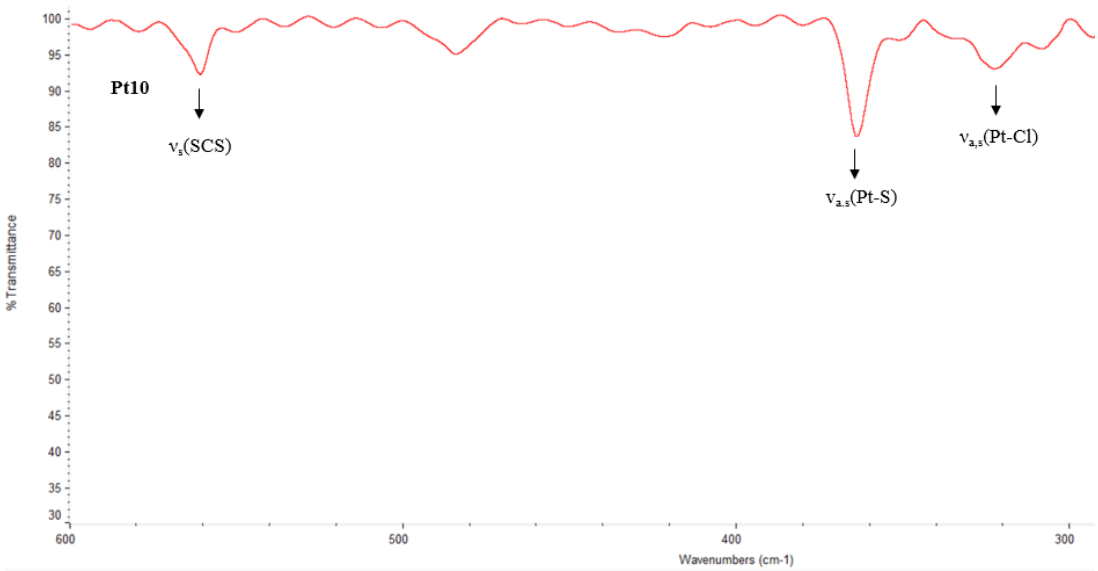

Figure 3.28: Far-IR (4000-600 cm^{-1}) spectrum (CsI disk, wavenumber in cm^{-1}) of **Pt10**.

The ^{1}H-NMR analysis confirmed the proposed structure showing the expected signals at 1.30 (CH_3), 3.26 (SCH_3), 3.28 (NCH_3), 4.25 (NCH_2), and 4.29 (OCH_2) ppm (**Figure 3.29**).[73] Remarkably, the peak originated by the SCH_3 group showed the side bands arising from the coupling with ^{195}Pt - ^{1}H.

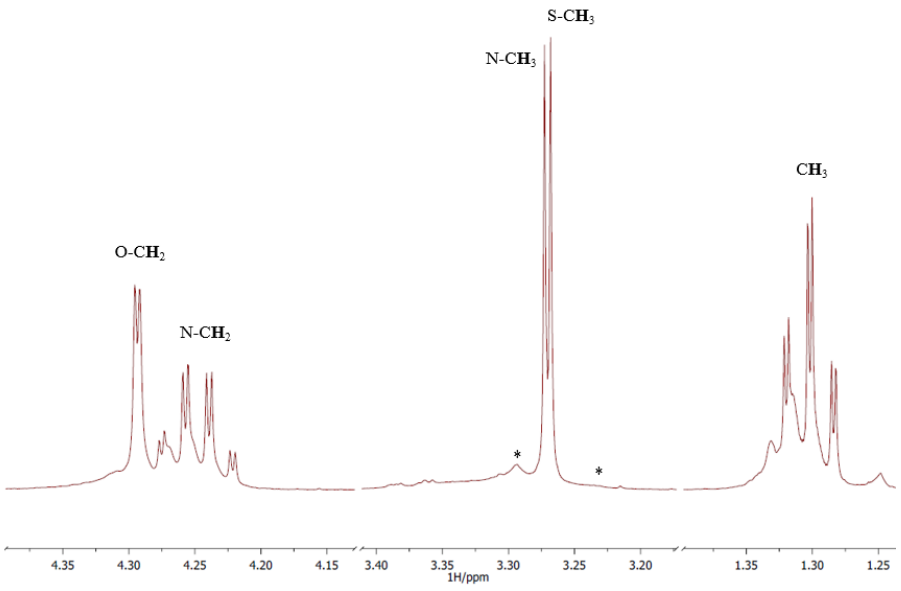

Figure 3.29: ^{1}H NMR spectrum in DMSO-d_6 of **Pt10**. (*) indicates the ^{195}Pt - ^{1}H coupling.

Complex **Pt11** was prepared in DCM by reacting $PtCl_2$ and **DMDTM** in a 1:1 ratio. The reaction was performed in the dark because light might induce S-methylation, and eventually afforded the object compound as a yellow powder in 70% yield. In the

far-IR spectrum, the diagnostic bands $\nu_{a/s}$(Pt-S) and $\nu_{a/s}$(Pt-Cl) were observed in agreement with literature data (**Figure 3.30**).[56]

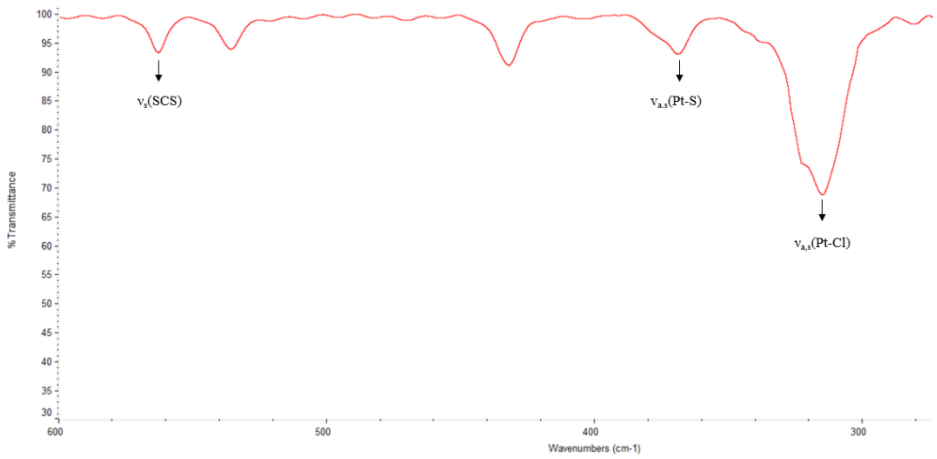

Figure 3.30: Far-IR (4000-600 cm^{-1}) spectrum (CsI disk, wavenumber in cm^{-1}) of **Pt11**.

^{1}H-NMR analysis confirmed the proposed structure showing the expected signals at 2.53 (SCH_3), 3.34 (NCH_3), and 3.46 (NCH_3) ppm (**Figure 3.31**).

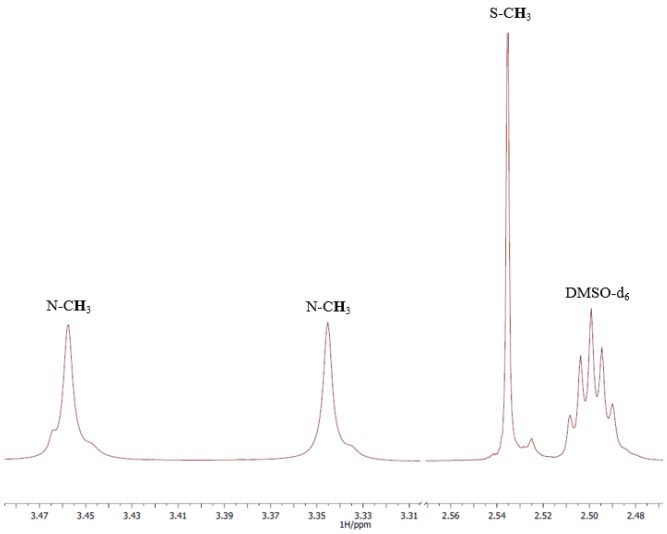

Figure 3.31: ^{1}H NMR spectrum in DMSO-d_6 of **Pt11**.

As previously anticipated, several attempts were made to synthesize complexes of the type [Pt(ESDT)Cl_2]. Unfortunately, all failed and invariably led to the bis-dithiocarbamato derivative [Pt(ESDT)$_2$] (**Pt12**)[72] regardless of the experimental conditions analyzed (**Table 3.1**). In all cases, the generated compounds returned identical spectroscopic data. For example, in the far-IR spectra, no band consisted of ν(Pt-Cl) was recorded in the expected range (300-350 cm^{-1}) (**Figure 3.32**).

Pt complex	Experimental conditions	Final Product
$PtCl_2$	1.5 - 20h, r.t, DCM 24h, r.t, dark, an.benzene 24h, r.t, dark, MeCN 10d, r.t, dark, an.benzene 10d, r.t, dark, MeCN 10d, r.t, dark, MeOH 10d, r.t, dark, DCM 10d, r.t, dark, Acetone	**$[Pt(ESDT)_2]$**

Table 3.1: Experimental conditions for the reaction between $PtCl_2$ with **(PPh_4) ESDT**.

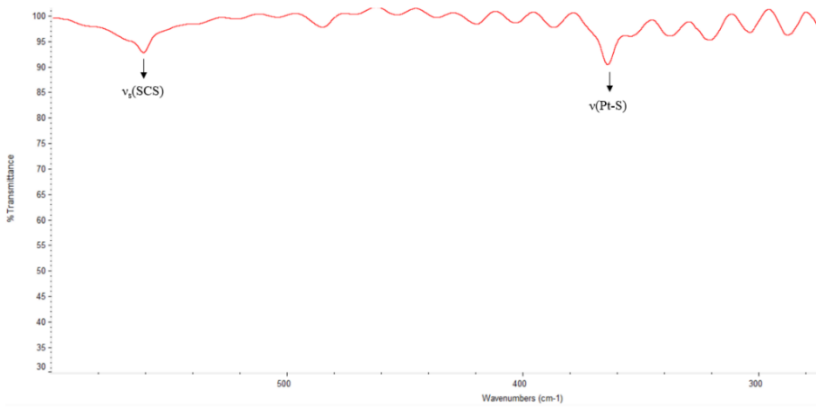

Figure 3.32: Far-IR (4000-600 cm^{-1}) spectrum (CsI disk, wavenumber in cm^{-1}) of **Pt12**.

Moreover, the ^{1}H-NMR spectrum of **Pt12** were fully consistent with that reported for $[Pt(ESDT)_2]$ in the literature (**Figure 3.33**).[72]

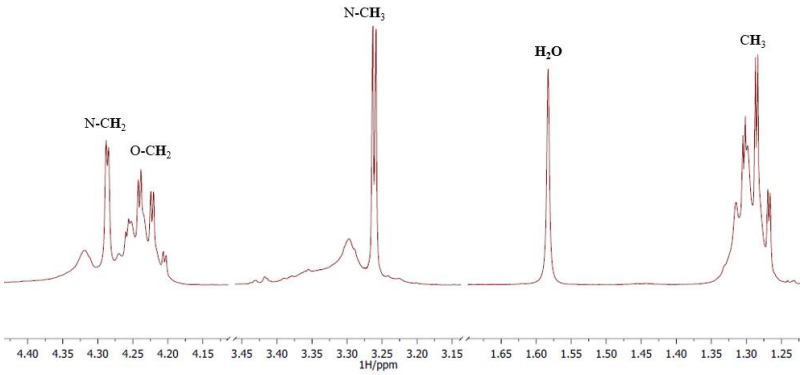

Figure 3.33: ^{1}H NMR spectrum in DMSO-d_6 of **Pt12**.

To overcome the aforementioned issues, an alternative synthetic approach was designed, involving the reaction of that platinum(II) precursor previously obtained, namely (PPh_4)[$PtCl_3(NH_3)$] (**Pt3**) and K[Pt(am)Cl_3] (am = $MeNH_2$) (**Pt9**) with the dithiocarbamato ligands **(PPh_4) ESDT**, **ESDTM**, and **DMDTM**. However, despite the numerous different experimental conditions employed (**Table 3.2**), the expected mono-dithiocarbamato derivatives of the type [Pt(dtc)(am)Cl)] were not obtained. In all attempts, inconclusive spectroscopic data were recorded, which did not allow a clear identification of the final products. The only exception occurred with the ligand **(PPh_4) ESDT** was used. In fact, in all cases always the same product was generated, that is, again the bis-dithiocarbamato derivative [Pt(ESDT)$_2$] (**Pt12**). This confirmed the strong affinity of the ESDT ligand towards the platinum(II) canter, which proved highly effective in replacing any amine and chloride ligands to afford the bis-dithiocarbamato adduct. On the contrary, reaction with the ligands **ESDTM** and **DMDTM**, a mixture of products was obtained whose nature was hardly identified. This agrees with previous reports demonstrating that, when reacted with platinum(II), dithiocarbamato thioesters may give rise to several compounds, including polymers, S-demethylated derivatives, bis-adducts, and mixed ligand complexes, even upon careful control of the stoichiometric ratios, temperature, conditions, solvent, and reaction times.[57,58,72-74]

Pt complex	Experimental conditions	dtc	Final Product
(PPh_4)[$PtCl_3(NH_3)$] (Pt3)	0.5 - 2h, r.t, dark, DCM	**(PPh_4) ESDT**	**Pt12**
		ESDTM	mixture
		DMDTM	mixture
	0.5 - 2h, r.t, dark, $CHCl_3$	**(PPh_4) ESDT**	mixture
		ESDTM	mixture
		DMDTM	mixture
	17 – 48h, r.t, dark, MeOH	**(PPh_4) ESDT**	mixture
		ESDTM	mixture
		DMDTM	mixture
K[Pt(am)Cl_3]	0.5 - 2h, r.t, dark, DCM	**(PPh_4) ESDT**	mixture
		ESDTM	mixture
		DMDTM	mixture
	0.5 - 2h, r.t, dark, $CHCl_3$	**(PPh_4) ESDT**	mixture
		ESDTM	mixture

(am = $MeNH_2$, py) **(Pt6, Pt9)**		**DMDTM**	mixture
	17 – 48h, r.t, dark, MeOH	**(PPh_4) ESDT**	mixture
		ESDTM	mixture
		DMDTM	mixture

Table 3.2: Experimental conditions of the reaction between **Pt3**, **Pt6** and **Pt9** with the ligands **(PPh_4) ESDT**, **ESDTM** and **DMDTM**.

3.3.4 Synthesis of the zinc(II)-dithiocarbamato precursors

In a view to finally generating the target platinum(II) derivatives [Pt(ESDT)Cl_2], the exploitation of the transmetallation reaction was also attempted. In several studies, this method proved efficient to obtain the desired metal-dithiocarbamato complexes through the straightforward transmetallation reaction from the corresponding zinc(II) derivatives (**Figure 3.34**).[75-77] This experimental design involves the use of a pre-generated zinc(II)-dithiocarbamato complex of the type [Zn(dtc)$_2$] which would then transfer the dithiocarbamato ligand to another metal center via transmetallation. Zinc(II) is selected due to its borderline Lewis acid nature and allowing the formation of stable covalent adducts with the soft dithiocarbamato ligands. Interestingly, zinc(II) (d^{10}) is recognized for its ability to transfer such ligands through a ligand exchange reaction to a "softer" metal, such as platinum(II).[78,79]

Figure 3.34: General scheme of the ligand exchange (transmetallation) reaction.

The feasibility of such a synthetic approach was first evaluated by reacting the commercially available zinc(II)-dithiocarbamato complex [Zn(TMDT)$_2$] **Zn0** with (PPh_4)[$PtCl_3(NH_3)$] and K[Pt(am)Cl_3] (am = $MeNH_2$, py), to obtain [Pt(TMDT)(am)Cl] as proof-of-concept (**Figure 3.35**). Interestingly, several reactions under different experimental conditions and lengthy work-ups confirmed that the transmetallation reaction was successful. However, analysis and spectroscopic characterization of the final products confirmed once again the formation of the bis-

dithiocarbamato derivative **Pt14,** notwithstanding the different experimental conditions were employed (**Table 3.3**).

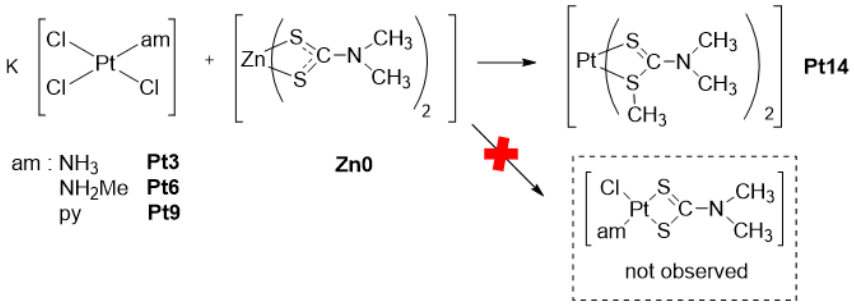

Figure 3.35: Reaction scheme of the ligand exchange reaction of **Pt3**, **Pt6** and **Pt9** with **Zn0**.

In the far-IR region the ν_s(SCS) at 565 cm^{-1} and $\nu_a(ZnS_4)$ at 381 cm^{-1} were recorded for **Zn0**,[80-82] Whereas the formation of **Pt14** was confirmed by the characteristic ν_s(SCS) at 561 cm^{-1} and the ν(Pt-S) at 364 cm^{-1} but no bands assignable to ν(Pt-Cl) and ν(Pt-N). NMR analysis also supported the generation of [Pt(TMDT)$_2$] (**Figure 3.36**).

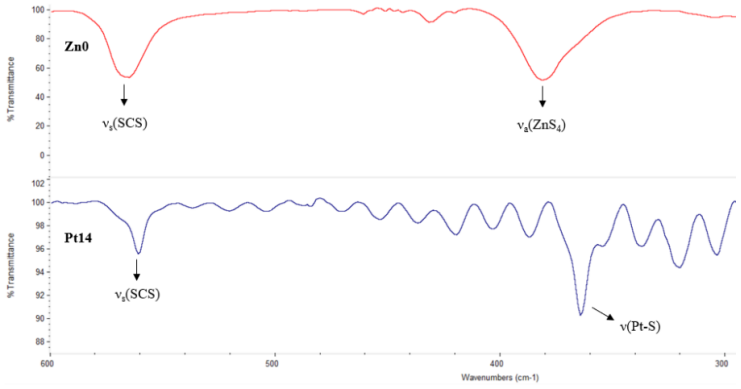

Figure 3.36: Comparative far-IR (4000-600 cm^{-1}) spectra (CsI disk, wavenumber in cm^{-1}) of **Zn0** and **Pt14**.

Following a well-established procedure previously developed in our research group, another zinc(II)-dithiocarbamato intermediate [Zn(ESDT)$_2$] (**Zn1**) was synthesized (**Figure 3.37**). The IR (**Figure 3.38**) and NMR (**Figure 3.39**) analysis confirmed the successful generation of **Zn1**.[82,83]

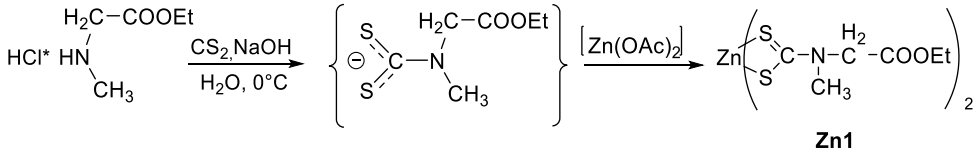

Zn1

Figure 3.37: Synthetic procedure to the synthesis of **Zn1**.

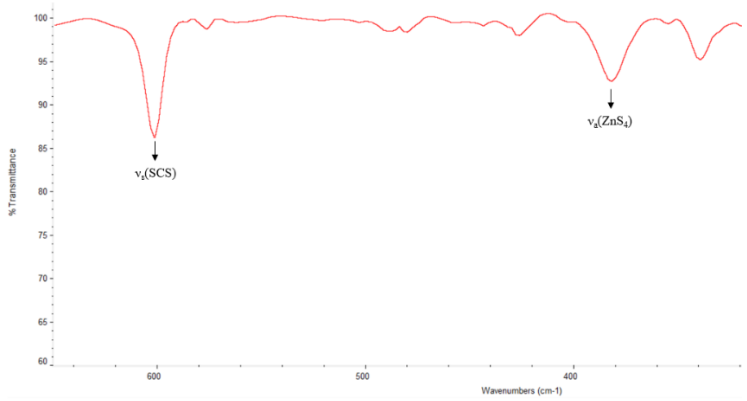

Figure 3.38: Far-IR (4000-600 cm^{-1}) spectrum (CsI disk, wavenumber in cm^{-1}) of **Zn1**.

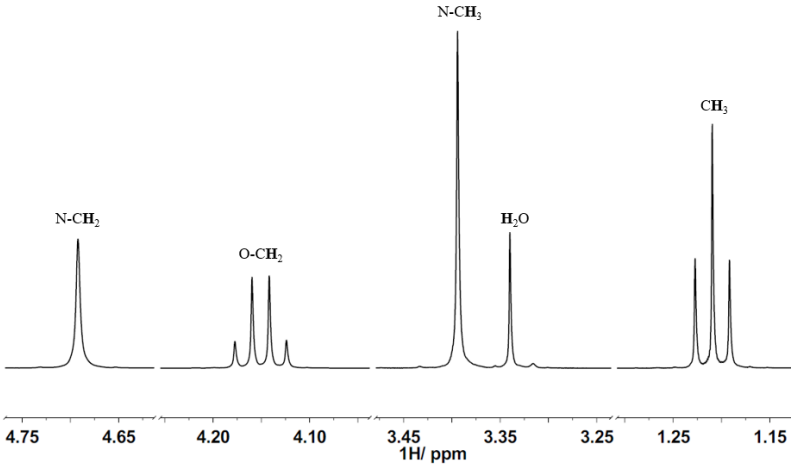

Figure 3.39: ^{1}H NMR spectrum in DMSO-d_6 of **Zn1**.

Next, the transmetallation reaction was attempted by reacting **Zn1** with complexes **Pt3**, **Pt6**, and **Pt9** to obtain the platinum(II) complexes of the type [Pt(ESDT)(am)Cl] (**Figure 3.40**).

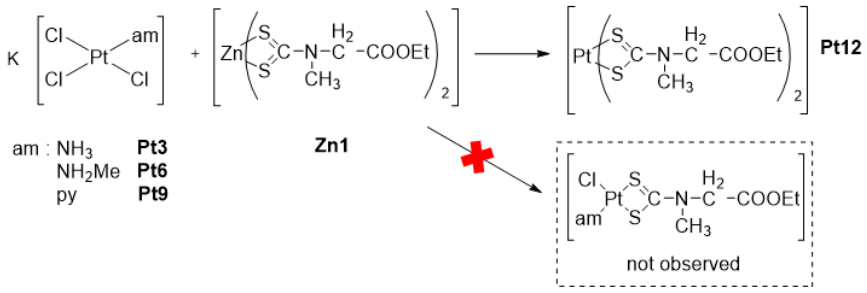

Figure 3.40: Reaction scheme for the transmetallation reaction of **Pt3**, **Pt6** and **Pt9** with **Zn1**.

Regardless of the various attempts and the exploitation of different experimental conditions (**Table 3.3**), the target metal complexes were not obtained, even when using an excess of the starting platinum(II) reagent, the final product being once again always the bis-dithiocarbamato adduct [Pt(ESDT)$_2$] (**Pt12**).

Pt complex	Experimental conditions	[Zn(dtc)$_2$]	Final Product
(PPh$_4$)[PtCl$_3$(NH$_3$)] **(Pt3)**	17 h, r.t, dark, MeOH	[Zn(DMDT)$_2$]	**Pt14**
	17 h, r.t, dark, DMF	[Zn(ESDT)$_2$]	**Pt12**
	17 h, r.t, dark, MeOH	[Zn(DMDT)$_2$]	**Pt14**
	17 h, r.t, dark, DMF	[Zn(ESDT)$_2$]	**Pt12**
K[Pt(am)Cl$_3$] **(am = MeNH$_2$, py)** **(Pt6, Pt9)**	17 h, r.t, dark, MeOH	[Zn(DMDT)$_2$]	**Pt14**
	17 h, r.t, dark, DMF	[Zn(ESDT)$_2$]	**Pt12**
	17 h, r.t, dark, MeOH	[Zn(DMDT)$_2$]	**Pt14**
	17 h, r.t, dark, DMF	[Zn(ESDT)$_2$]	**Pt12**

Table 3.3: Experimental conditions for the transmetallation reaction of **Pt3**, **Pt6** and **Pt9** and **Zn1**.

3.3.5 Metal conjugation to vitamin B$_{12}$: initial attempt

As previously mentioned vitamin B$_{12}$ can be a potential carrier of metal-containing species into cancer cells. Should suitable metal complexes be appended on the β-upper side of vitamin B$_{12}$, their intracellular release would be achieved upon reduction of Co(III) to Co(I) through three district biochemical steps. Specifically, cob(III)alamin is initially reduced nonenzymatically to cob(II)alamin in the cytosol, then cob(II)alamin converts into cob(I)alamin by flavodoxin and adenosyltransferase CobA (see **Section 1.2.6**). Given that the β-upper metal complex can be released

preferentially in the cell, the vitamin B_{12}-metal conjugates are regarded as prodrugs, where the structural features of vitamin B_{12} conceal the active drug attached to it.[48, 83-87]

Therefore, a series of synthetic procedures were designed to conjugate to the cyano group of vitamin B_{12} to either the two platinum(II)-dithiocarbamato derivatives previously synthesized [Pt(ESDTM)Cl_2] (**Pt10**) and [Pt(DMDTM)Cl_2] (**Pt11**) or the commercially available gold(I) derivative [(Ph_3P)AuCl]. Taking into account the above considerations, a series of experiments planned for the preparation of [B_{12}-Co(III)-CN-M-L] (M = Pt(II) / Au(I), L = various dtc / PPh_3). Numerous syntheses under various experimental conditions were carried out (**Table 3.4**), all were followed by lengthy purification attempts and several spectroscopic characterizations.

Metal Complex	Experimental Conditions	Solvent	Purification Method
[Pt(ESDTM)Cl_2] (Pt10)	10d, r.t, dark	MeOH	0.1% TFA in H_2O/ MeOH
			MeOH/MeCN/H_2O
			H_2O/ MeOH
		H_2O	0.1% TFA in H_2O/ MeOH
			MeOH/MeCN/H_2O
			H_2O/ MeOH
		MeCN	0.1% TFA in H_2O/ MeOH
			MeOH/MeCN/H_2O
			H_2O/ MeOH
	17h, r.t, dark	MeOH	0.1% TFA in H_2O/ MeOH
			MeOH/MeCN/H_2O
			H_2O/ MeOH
		H_2O	0.1% TFA in H_2O/ MeOH
			MeOH/MeCN/H_2O
			H_2O/ MeOH
		MeCN	0.1% TFA in H_2O/ MeOH
			MeOH/MeCN/H_2O
			H_2O/ MeOH
	17h, 45°C, dark	MeOH	0.1% TFA in H_2O/ MeOH
			MeOH/MeCN/H_2O
			H_2O/ MeOH
		H_2O	0.1% TFA in H_2O/ MeOH
			MeOH/MeCN/H_2O
			H_2O/ MeOH

		MeCN	0.1% TFA in H_2O/ MeOH
			MeOH/MeCN/H_2O
			H_2O/ MeOH
[Pt(DMDTM)Cl_2] (Pt11)	10d, r.t, dark	MeOH	0.1% TFA in H_2O/ MeOH
			MeOH/MeCN/H_2O
			H_2O/ MeOH
		H_2O	0.1% TFA in H_2O/ MeOH
			MeOH/MeCN/H_2O
			H_2O/ MeOH
		MeCN	0.1% TFA in H_2O/ MeOH
			MeOH/MeCN/H_2O
			H_2O/ MeOH
	17h, r.t, dark	MeOH	0.1% TFA in H_2O/ MeOH
			MeOH/MeCN/H_2O
			H_2O/ MeOH
		H_2O	0.1% TFA in H_2O/ MeOH
			MeOH/MeCN/H_2O
			H_2O/ MeOH
		MeCN	0.1% TFA in H_2O/ MeOH
			MeOH/MeCN/H_2O
			H_2O/ MeOH
	17h, 45°C, dark	MeOH	0.1% TFA in H_2O/ MeOH
			MeOH/MeCN/H_2O
			H_2O/ MeOH
		H_2O	0.1% TFA in H_2O/ MeOH
			MeOH/MeCN/H_2O
			H_2O/ MeOH
		MeCN	0.1% TFA in H_2O/ MeOH
			MeOH/MeCN/H_2O
			H_2O/ MeOH
[(Ph_3P)AuCl]	17h, r.t, dark	MeOH	MeOH/MeCN/H_2O
	17h, 45°C, dark	MeOH	MeOH/MeCN/H_2O
	10d, r.t, dark	MeOH	MeOH/MeCN/H_2O
	$AgNO_3$, 15min, r.t, dark	MeOH/DCM	H_2O/ MeOH

Table 3.4: Experimental conditions for the attempted reactions between **Pt10**, **Pt11** and [(Ph_3P)AuCl] with vitamin B_{12}.

Unfortunately, results proved always inconclusive, and no clear evidence of a successful vitamin B_{12}-metal conjugation was obtained.

3.4 Conclusions

A major part of the original research plan should have involved the generation of metal-dithiocarbamato scaffolds (especially platinum (II)-based) containing (at least) one metal-coordinated chloride which could have been replaced by the cyano group of vitamin B_{12}, to obtain the desired vitamin B_{12}-metal conjugates. The present chapter summarizes all the synthetic attempts that have been carried out in this regard, most of which unfortunately failed. Only two suitable platinum(II)-dithiocarbamato derivatives were obtained (that is, [Pt(ESDTM)Cl_2] (**Pt10**) and [Pt(DMDTM)Cl_2] (**Pt11**)), whereas in most cases the bis-dithiocarbamato adducts [Pt$(dtc)_2$] formed, despite of all the different experimental conditions tested. This disappointing outcome seems to confirm the strong affinity of dithiocarbamates for the platinum(II) center, which can replace other ligands (such as chlorides and amines) to form stable square planar metal-bis adducts. Moreover, contrary to what was reported in the literature for other platinum(II) substrates, conjugation of **Pt10**, **Pt11**, and even [(Ph_3P)AuCl] to the cyano group of vitamin B_{12} proved unexpectedly challenging and returned inconclusive results. Consequently, to the unpredictable failure of the designing strategy initially designed, the overall research program had a screening halt, and we were forced to identify suitable alternative options, including a complete change of course (see **Chapter 4**).

3.5 References

1. Peyrone, M., *Ann. Chim.Phys.* **3**, 193, (1884).
2. Rosenberg, B., Van Camp, L., *Nature*, **205**, 698–699, (1965).
3. Rosenberg, B. Van camp, L., Trosko, E., *Nature,* **222**, 385–386, (1969).
4. Kelland, L., *Nat. Rev. Cancer*, **7**, 573–584 (2007).
5. Johnstone, T., Suntharalingam, K., *Chem. Rev.,* **116**, 3436–3486, (2016).

6. Rabbab, O., Moussa, Y., *Dalton Trans.*, **47**, 6645–6653, (2018).

7. Tylkowski, B., Jastrza, R., Odani, *Physical Sciences Reviews*, **3**, 91, (2019).

8. Christopher, M., *Physiology & behavior*, **176**, 100–106, (2016).

9. Cersosimo, R., *Cancer Treat. Rev.*, **16**, 195–211, (1989).

10. Shahraki, S., Shiri, F., Mansouri, H., *J. Iran. Chem. Soc.*, **13**, 723–731, (2016).

11. Patel, N., Patel, R., *Appl. Biochem. Biotechnol.*, **172**, 1846–1858, (2014).

12. Berners-Price, S., *J. Inorg. Biochem.*, **38**, 305–326, (1990).

13. Dabrowiak, J., *Drug Metab. Dispos.*, **30**, 1378–1384, (2002).

14. Sadowitz, P., Hubbard, B., *Drug. Metab. Dispos.*, **30**, 183-190, (2002).

15. Wang, X., Guo, Z., *Anti-Cancer Agents Med. Chem*, **7**, 19–34, (2008).

16. Milacic, V., *et al.*, *Cancer Research*, **66**, 10478–10486, (2006).

17. Dou, H., *Phosphorus Sulfur Silicon Relat. Elem.*, **192**, 1219–1223, (2017).

18. Altaf, M., *et al.*, *New Journal of Chemistry*, **39**, 377–385, (2015).

19. Irfandi, R., Raya, I., *Annals of Medicine and Surgery*, **60**, 396–402, (2020).

20. Buac, D., Schmitt, S., *et al.*, *Mini-Rev. Med. Chem*, **12**, 1193–1201, (2012).

21. Reis, A., Stern, A., Monteiro, P., *Redox Biology*, **27**, 101190, (2019).

22. Amtmann, E., Zöller, M., *Cancer Chemother. Pharmacol.*, **47**, 461–466, (2001).

23. Gabbiani, C., Casini, A., Messori, L., *Coord. Chem. Rev.*, **253**, 1692–1707, (2009).

24. Ronconi, L., Fregona, D., Bindoli, A., *Chem. Biol.*, **14**, 1128–1139, (2007).

25. Odularu, T., Ajibade, A., *Bioinorg Chem Appl.*, **2019**, 15, (2019).

26. Hogarth, G., *Mini-Rev. Med. Chem*, **12**, 1202–1215, (2012).

27. Oliveira, W., Rocha, O., Medeiros,. Q., Silva, S., *Molecules*, **24**, 2806, (2019).

28. Sharma, K., *Thermochimica Acta*, **104**, 339–372, (1986).

29. Awang, N., Nordin, A., Rashid, N., *Orient J. chem.*, **31**, 333–339, (2015).

30. Adeyemi, O., Onwudiwe, C., *Molecules*, **23**, 1–27, (2018).

31. Adeyemi, O. Onwudiwe, C., *Molecules*, **25**, 1–22, (2020).

32. Ronconi, L., *Dalton Trans.*, 10670–10680, (2009).

33. Cvek, B., Milacic, V., Taraba, J., *J. Med. Chem*, **51**, 6256–6258, (2008).

34. Altaf, M., *et al.*, *Oncotarget*, **8**, 490–505, (2017).

35. Ostrowski, D., Ford, C., *Dalton Trans.*, 10660–10669, (2009)

36. Fricker, P., *Gold Bull*, **29**, 53–60, (1996).

37. Madeira, M., Gibson, L., Kean, F., *Inflammopharmacology*, **20**, 297–306, (2012).

38. Chaffman, M., Brogden, N., Heel, C., Speight, M., *Drugs*, **27**, 378–424, (1984).

39. Lee, S., *et al.*, *Front. Pharmacol.*, **10**, 1–10, (2019).

40. Eisler, R., *Inflamm. Res*, **52**, 487–501, (2003).

41. Yue, S., Luo, M., Liu, H., Wei, S., *Front. Pharmacol*., **8**, 11, (2020).

42. Kim, H., Reeder, E., Parkin, S., *Scientific Reports*, **9**, 1–18, (2019).

43. Fernández-Moreira, V., Herrera, P., *J Pure Appl. Chem.*, **91**, 247–269, (2019).

44. Yeo, I., Ooi, K., Tiekink, T., *Molecules*, **23**, 14–23, (2018).

45. Altaf, M., *Eur. J. Med. Chem.*, **95**, 464–472, (2015).

46. Ostrowski, D., Ford, C., *Dalton Trans.*, 10660–10669, (2009).

47. Tran, Q., Furger, E., Alberto, R., *Org. Biomol. Chem*, **11**, 3247–3254, (2013).

48. Tran, Q., *et al.*, *Metallomics*, **8**, 298–304, (2016).

49. Proinsias, K., Giedyk, M., Gryko, D., *Chem. Soc. Rev.*, **42**, 6605–6619, (2013).

50. Hu, J., *Bioorg. Med. Chem. Lett.*, **27**, 3591–3594, (2017).

51. Messori, L., *Inorganic Chemistry*, **51**, 1717–1726, (2012).

52. Chalovich, M., Eisenberg, E., *Chemical reviews*, **114**, 4470–4495, (2014).

53. Matysiak, W., Gustaw-Rothenberg, K., *J. Clin. Res.*, **3**, 20–23, (2009).

54. Rochon, D., Kong, C., *Can. J. Chem.*, **64**, 1894–1896, (1986).

55. Faraglia, G., Sindellari, L., Trincia, L., *Inorg. Chim. Acta*, **106**, 31–35, (1985).

56. Mansouri-Torshizi, H., *J. Biomol. Struct. Dyn.*, **26**, 575–586, (2009).

57. Faraglia, G., *J. Inorg. Biochem.*, **83**, 31–40, (2001).

58. Faraglia, G., Sindellari, L., **161**, 63–73, (1990).

59. Rasmussen, C., *ChemTexts*, **7**, 1–8, (2021).

60. Dhara, S., *Indian J. Chem.*, **8**, 193–194, (1970).

61. Torres, M., *J. Phys. Chem. A*, **122**, 6934–6952, (2018).

62. Wang, Y., *Spectrochim. Acta A Mol. Biomol. Spectrosc.*, **150**, 902–908, (2015).

63. Vinje, J., Sletten, E., *Anti-Cancer Agents Med. Chem.*, **7**, 35–54, (2008).

64. Haddad, B., *J. Mol. Struct.*, **1146**, 203–212, (2017).

65. Rochon, D., Kong, C., *Can. J. Chem.*, **64**, 1894–1896, (1986).

66. Messori, L., Abbate, F., Marcon, G., *J. Med. Chem.*, **43**, 3541–3548, (2000).

67. Ronconi, L., Marzano, C., Zanello, P., *J. Med. Chem.* **49**, 1648–1657, (2006).

68. Cantuaria, G., Magalhaes, A., Angioli, R., *Cancer*, **88**, 381–388, (2000).

69. Calamai, P., Guerri, A., Messori, L., *Inorg. Chim. Acta*, **285**, 309– 312, (1999).

70. Sun, L., Zeng, X., Yan, C., Sun, X., *Nature*, **490**, 361–366, (2012).

71. Deng, D., Xu, C., Sun, P., Wu, J., *Nature*, **510**, 121–125, (2014).

72. Fregona, D., Tenconi, S., Sitran, S., *Polyhedron*, **16**, 3795-3805, (1997).

73. Faraglia, G., Sindellari, L., Sitran, S., *Transit. Met. Chem*, **19**, 248–252, (1994).

74. Faraglia, G., Longo, G., Cherchi, V., *Polyhedron*, **14**, 1905-1914, (1995).

75. Wong, W., Cookson, J., Evans, L., *Chem. Commun.*, **17**, 2214–2216, (2005).

76. Lutsenko, I., Ivanov, A., Kiskin, M., *Russ. J. Inorg. Chem.*, **60**, 92– 99, (2015).

77. Fox, O., Cookson, J., Wilkinson, E., *J. Am. Chem. Soc.*, **128**, 6990–7002, (2006).

78. Pearson. R., *J. Am. Chem. Soc.*, **85**, 3533–3539, (1963).

79. Sokolov, M., Imoto, H., Saito, T., *Inorg. Chem. Commun.*, **2**, 422–423, (1999).

80. Kellner, R., *J. Inorg. Nucl. Chem.*, **43**, 1183–1188, (1981).

81. Nakamoto, K., Theory and Applications in Inorganic Chemistry, Part A, (2008).

82. Bonati, F., Ugo, R., *J. Organomet. Chem.*, **10**, 257–268, (1967).

83. Ruiz-Sánchez, P., König, C., Ferrari, S., *J. Biol. Inorg. Chem.*, **16**, 33–44, (2011).

84. Ruiz-Sánchez, P., *J. Biol. Inorg. Chem.*, **13**, 335–347, (2008).

85. Tran, Q., Furger, E., Alberto, R., *Org. Biomol. Chem.*, **11**, 3247–3254, (2013).

86. Collet, G., Grillon, C., Nadim, M., Kieda, C., *Gene*, **525**, 208–216, (2013).

87. Ruiz-Sánchez, P., Mundwiler, S., Alberto, R.,. *Chimia*, **61**, 190–193, (2007).

Chapter 4

4. Vitamin B_{12} Conjugation Strategies

4.1 Rationale

Considering the unexpected challenges encountered during the implementation of the originally planned conjugation strategy discussed in **Chapter 3**, an alternative methodology was adapted to obtain conjugates of the type {B_{12}–Co–C≡C–Ph–Inp–dtc–M} and {FLUO-B_{12}–Co–C≡C–Ph–Inp–dtc–M}(M = Au(III)/Pt(II), FLUO = **FLUO1**/**FLUO2**). Typically, the attachment of phenylacetylide moieties on vitamin B_{12} involves the reduction of Cbl(III) to Cbl(I) with suitable electrophiles. Although effective, these reactions are limited and very complex.[1–3] However, in 2013 Gryko *et al*.,[4] proposed an alternative procedure to the straightforward ligand exchange reaction on cobalamins under mild conditions. Based on this, a stepwise methodology was planned for the preparation of phenylacetylide-containing metal-dithiocarbamato complexes with the general formula [HC≡C–Ph–Inp–dtc–M](M = Au(III)/Pt(II)), and their subsequent attachment to the axial β-upper site of vitamin B_{12}. The feasibility of such a synthetic approach was first evaluated with the preparation of the BOC-protected N-(4-ethynylphenyl)piperidine-4-carboxamide. The newly synthesized compound was fully characterized and successfully attached to the axial β-upper site of vitamin B_{12} **B_{12}-1** (**Figure 4.1**).

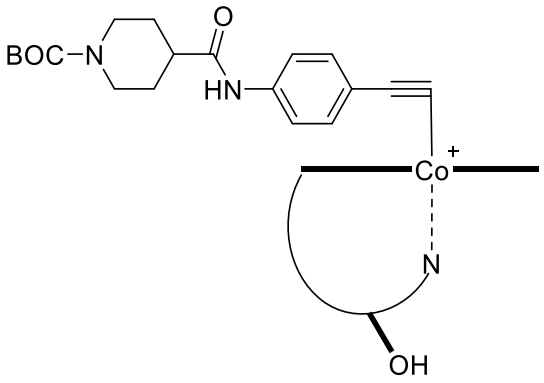

Figure 4.1: Schematic representation of the model **B_{12}-1** conjugate.

Then, through well-established transmetalation (see **Chapter 3**) and protection/ deprotection techniques, the model gold(III)-dithiocarbamato complex of the type [$AuBr_2$(dtc-Inp-Ph)] **Au0** was successfully synthesized (**Figure 4.2**) and characterized by IR, mono- and multidimensional NMR spectroscopy.

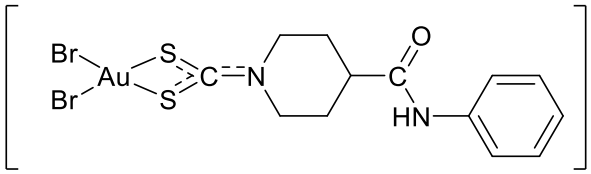

Figure 4.2: Schematic representation of the newly synthesized **Au0**.

Subsequently, two finely tailored gold(III)-dithiocarbamato phenylacetylide precursors were designed, synthesized, and characterized, are containing the terminal triple bond required for the ligand exchange reaction on the axial β-upper site of vitamin B_{12}. The object [$AuBr_2$(dtc-Inp-Ph-C≡CH)] **Au2** and [Au(Bnpy)(dtc-Inp-Ph-C≡CH)](PF_6) **Au4** complexes were prepared via the transmetallation reaction between the zinc(II) intermediate [Zn(dtc-Inp-Ph-C≡C-TIPS] **Zn4** with K[$AuBr_4$] and [Au(Bnpy)Cl_2], respectively (**Figure 4.3**).

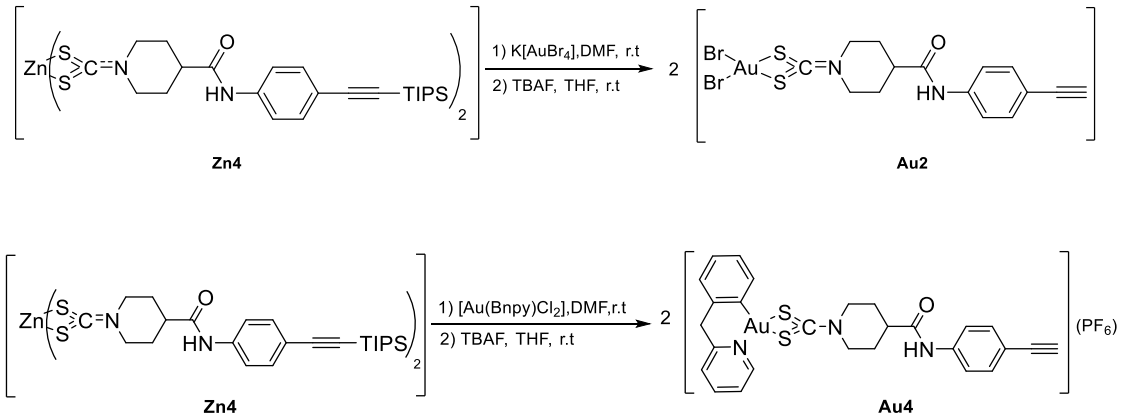

Figure 4.3: General synthetic route to the preparation of the target **Au2** and **Au4** via transmetallation reaction with the intermediate **Zn4**, and subsequent removal of the TIPS protecting group.

Next, the novel phenylacetylide-containing platinum(II)-dithiocarbamato complex [Pt(dppe)(dtc-Inp-Ph-C≡CH)](PF_6) **Pt16** was synthetized by reacting **Pt15** with **Zn4** (**Figure 4.4**).

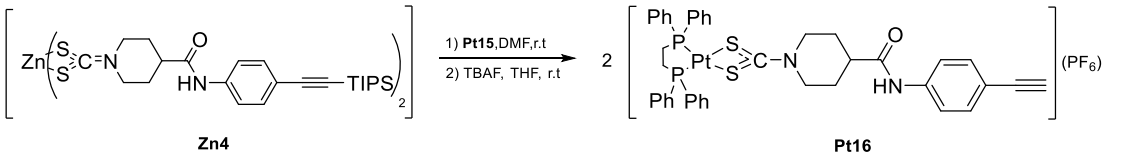

Figure 4.4: General synthetic route to the preparation of the target **Pt16** via transmetallation reaction with the intermediate **Zn4**, and subsequent removal of the TIPS protecting group.

Attachment of complexes **Au2**, **Au4**, and **Pt16** to the axial β-upper site of vitamin B_{12} is currently being attempted by our collaborator Prof. Fabio Zobi at the University of Fribourg (Switzerland). The preparation of the model bioconjugates **B_{12}-Au2**, **B_{12}-Au4**, and **B_{12}-Pt16** would be carried out via an optimized and straightforward ligand exchange reaction in presence of CuAcO and DBU in DMA at room temperature (**Figure 4.5**).[5]

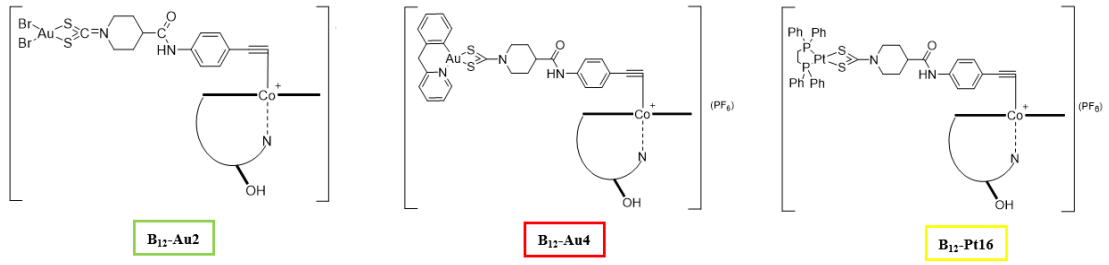

Figure 4.5: Schematic representation of the model bioconjugates **B_{12}-Au2**, **B_{12}-Au4** and **B_{12}-Pt16 (**ongoing).

The subsequent step would involve, the reaction of the previously synthesized fluorescent [B_{12}-5'-(FLUO)] (FLUO = **FLUO-1** and **FLUO-2**) derivatives (see **Chapter 2**) with **Au2**, **Au4**, and **Pt16** with the view to obtain two series of novel fluorescent vitamin B_{12}-based derivatives of the type [FLUO-B_{12}–Co–C≡C–Ph–Inp–dtc–M] (M = Au(III)/Pt(II)) (**Figure 4.6**).

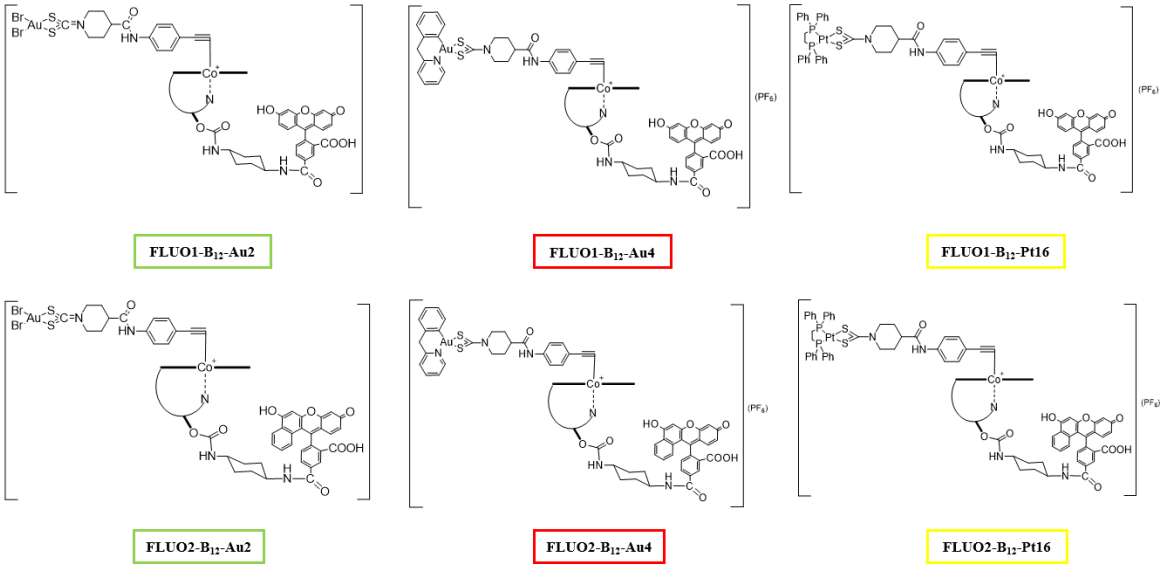

Figure 4.6: Schematic representation of the novel bioconjugates with the general formula [FLUO-B_{12}–Co–C≡C–Ph–Inp–dtc–M] (M = Au(III)/Pt(II)) (ongoing).

4.2 Synthesis

For detailed experimental conditions and full characterization see **Chapter 7**. For structures numbering see **Figure 4.32**.

4.2.1 Preparation of the model B_{12}-1 scaffold

Initially, the synthetic plan involved the preparation of the model BOC-protected organic ligand BOC-N-(4-ethynylphenyl)piperidine-4-carboxamide (**Figure 4.7**), according to well-known amide formation techniques. Amide bonds typically result from the coupling of carboxylic acids and amines in the presence of various coupling reagents.[6-15] The object compound was prepared by reacting BOC-isonipecotic acid with 1-ammino-4-ethynylbenzene, in presence of dicyclohexylcarbodiimide (DCC) and the additive 1-hydroxy-1H benzotriazole (HOBt) at room temperature for two days.[16-20] Purification on silica gel with EtOAc/PET 1:2 yielded 82% of the desired amide as a fine white powder. The successful formation of the compound was confirmed by IR, mono- and multidimensional NMR.

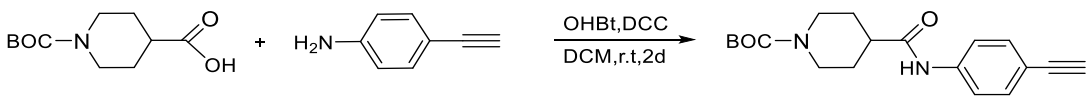

Figure 4.7: Synthesis of the BOC-protected N-(4-ethynylphenyl)piperidine-4-carboxamide.

Attachment of the previously formed amide on the axial β-upper site of vitamin B_{12} (**Figure 4.8**) was performed in Prof. Zobi's group, following a modified reduction-free synthesis of stable acetylide cobalamins.[21-27] This method involved the use of a catalytic amount of CuOAc and DBU in DMA at room temperature for 4 hours. The crude residue was then dissolved in a 1:1 mixture of methanol and water, filtered and purified by preparative HPLC. The eluting band containing the desired **B_{12}-1** was isolated and lyophilized.[4,5]

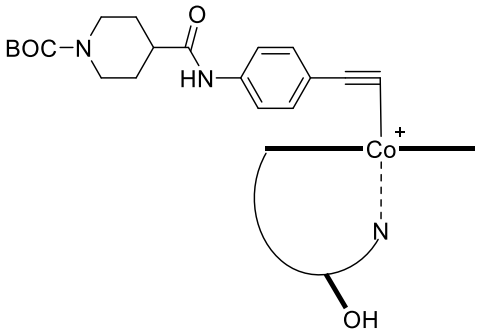

Figure 4.8: Schematic representation of the model **B_{12}-1**.

The model acetylide-containing **B_{12}-1** was characterized with ^{1}H, $^{13}C\{^{1}H\}$, and multidimensional NMR. Despite the size and the complexity of the compound NMR spectroscopy provided insights into the chemical structure. As expected, the spectral pattern of vitamin B_{12} was substantially preserved, while the methyl group $C^{20}H_3$ showed a slight downfield shift of about 0.12 ppm. High-intensity peaks in the region 6-7.5 ppm were assigned to the aromatic protons of the ethynylphenyl moiety (**Figure 4.9**).[26]

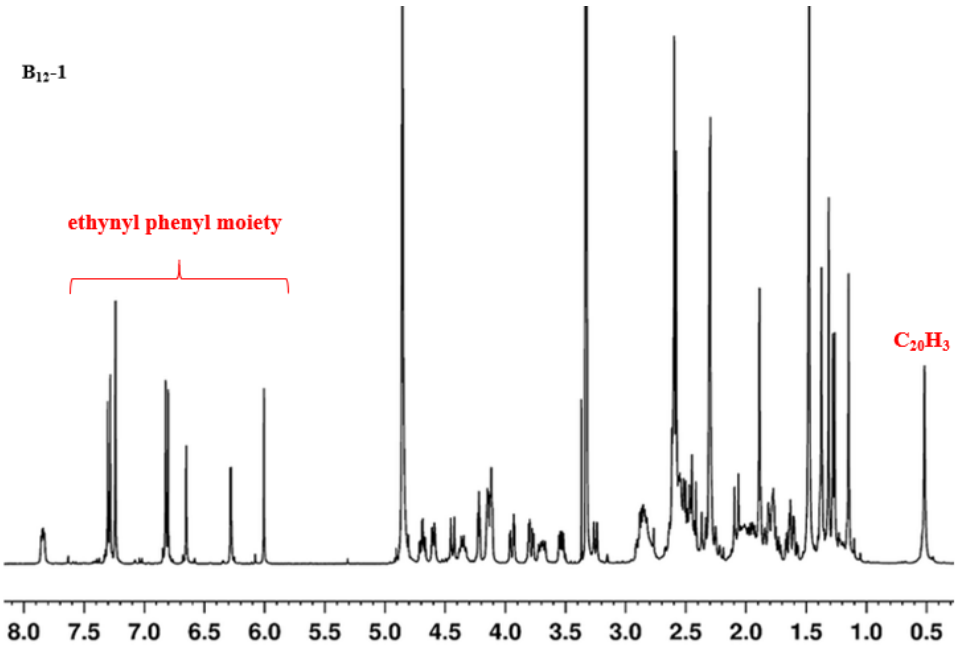

Figure 4.9: ^{1}HNMR spectrum in CD_3OD of **B_{12}-1**.

The UV-Vis spectrum of **B_{12}-1** (**Figure 4.10**) returned λ_{max} values at 361, 523, and 551 nm consistent with the coordination of an alkynyl function to the cobalt (III) center of vitamin B_{12}.

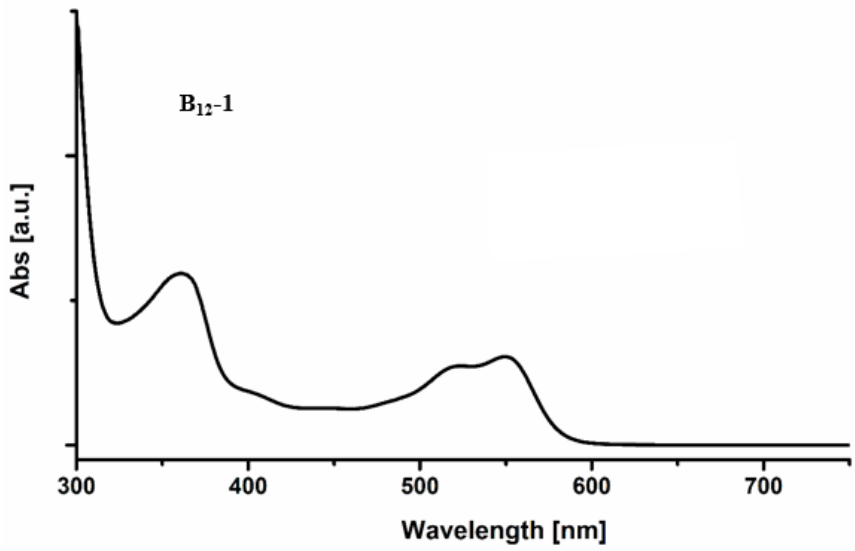

Figure 4.10: UV-Vis spectrum of **B_{12}-1** in methanol.

Characteristic IR bands at 3344 and 3205 cm^{-1} (ν(N-H)$_{amide\ \&\ corrin\ ring}$) were recorded for **$B_{12}$-1**. Bands at 2919, 2851, and 1404 cm^{-1} ν(C-H) indicated the successful formation of the target acetylide cobalamin. Additionally, vibrations at 1731, 1664, and 1574 cm^{-1} confirmed the presence of ν(C=O)$_{carboxylic\ acid}$ and ν(C=O)$_{amide\ \&\ corrin\ ring}$, respectively (**Figure 4.11**).[30,31]

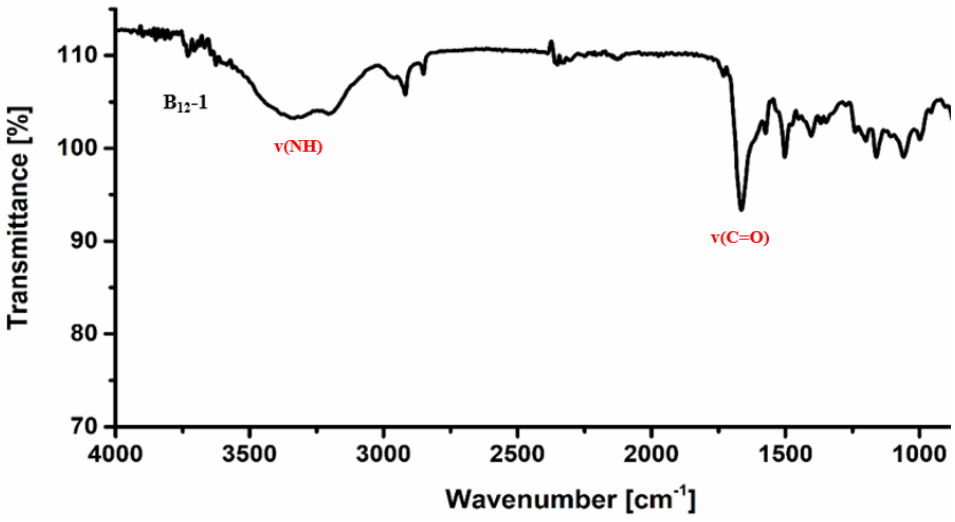

Figure 4.11: Mid IR in CsI of **B_{12}-1**.

Furthermore, the characteristic $[M+Na]^+$ = 1678.4 fraction of **B_{12}-1** was revealed in the positive mode of analytical HPLC with a retention time of 28.0 minutes (**Figure 4.12**).

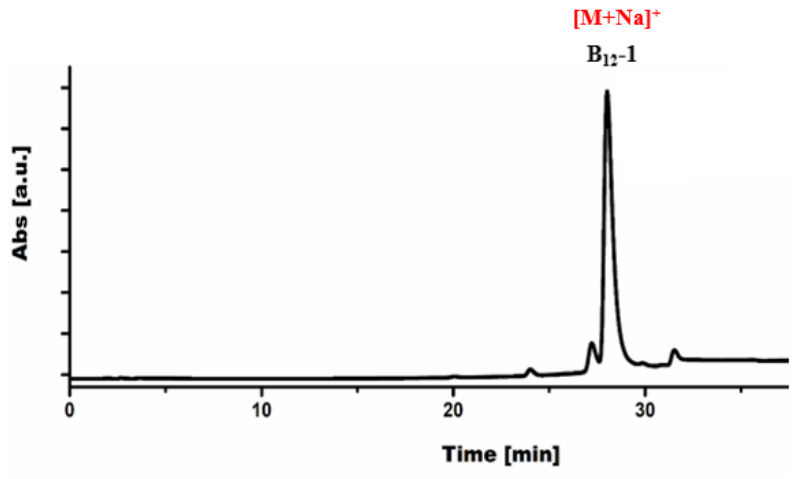

Figure 4.12: Chromatogram of **B_{12}-1**.

The successful generation of compound **B_{12}-1** confirmed the suitability of the bioconjugation strategy. Therefore, the subsequent steps would have involved the removal of the BOC protection followed by the conversion of the piperidine's ammino function into a dithiocarbamate moiety to eventually coordinated to a metal scaffold. Several attempts were carried out to remove the BOC protecting group but, unexpectedly, all led to the cleavage of the Co-C bond. Therefore, an alternative synthetic route was desired, based on the pre-generation of the metal-dithiocarbamato scaffold {M(dtc-Inp-Ph-C≡C-H)} to the subsequently conjugated to the cobalt (III) center of vitamin B_{12} through the terminal unsaturated carbon atom.

4.2.2 Preparation of the zinc(II)-dithiocarbamato complexes

The synthesis of the metal-dithiocarbamato scaffolds was achieved through a transmetallation reaction between the zinc(II) intermediate [Zn(dtc-Inp-Ph-C≡C-TIPS)$_2$] (**Zn4**) with the relevant metal salt/precursor. Given that such reaction had never been attempted before, its feasibility was first investigated by using a model ligand deprived of the alkynyl groups, to identify the optimal experimental conditions to the generation of the zinc(II)-dithiocarbamato intermediate. The model zinc(II) complex [Zn(dtc-Imp-Ph)$_2$] (**Zn3**) was obtained through a multistep reaction, first involving the synthesis of the BOC-protected N-phenyl-4-piperidine-carboxamide according to a modified literature procedure (**Figure 4.13**).[32,33]

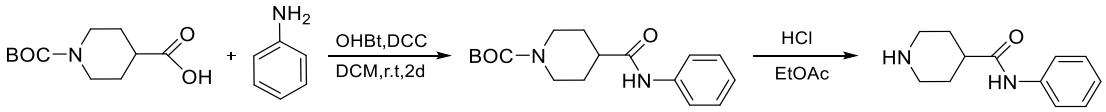

Figure 4.13: Synthesis of N-phenyl-4-piperidinecarboxamide.

Then, the intermediate **Zn3** was obtained via a one-pot reaction with carbon disulfide, under basic conditions and [$Zn(OAc)_2 \cdot 2H_2O$] in a 2:1 ligand-to-metal ratio in DMF (**Figure 4.14**).[34] Addition of H_2O afforded the desired zinc(II) complex in the form of an off-white solid (85% yield).

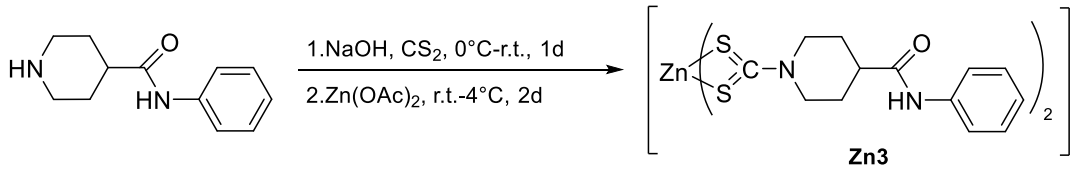

Figure 4.14: General synthetic route for the preparation of the target zinc(II) intermediate **Zn3**.

The target compound **Zn3** was characterized employing IR, mono- and multinuclear NMR spectroscopy. In the mid-IR spectrum, the appearance of the characteristic band ν(N-CSS) at 1440 cm^{-1} confirms the formation of the dithiocarbamato moiety. According to the Bonati-Ugo method,[31] the recording of a single band at 953 cm^{-1} assigned to the ν_a(SCS) indicated symmetric bidentate coordination to the metal center. Moreover, the diagnostic absorption bands at 3295, 1655, and 751 cm^{-1} denote the presence of the ν(NH), ν(C=O), and δ(C=C) vibrations, respectively (**Figure 4.15**).

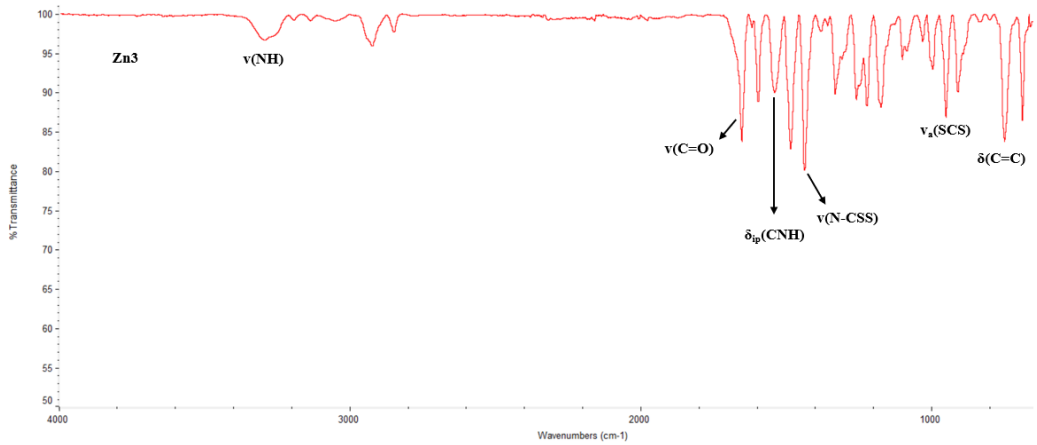

Figure 4.15: Mid-IR spectrum in CsI disk of **Zn3**.

The ^1H chemical shifts of the newly synthesized zinc(II) intermediate were present at 1.68 ($C^{3',5'}H_{ax}$), 1.91($C^{3',5'}H_{ax}$), 2.62 ($C^{2',6'}H_{ax}$), 2.53 (C^4H), 4.89 ($C^{2',6'}H_{eq}$), 7.03(p-

H), 7.29 (m-H), 7.59 (o-H) and 10.0 (NH $_{amide}$), respectively (**Figure 4.16**), supporting the formation of **Zn3**.

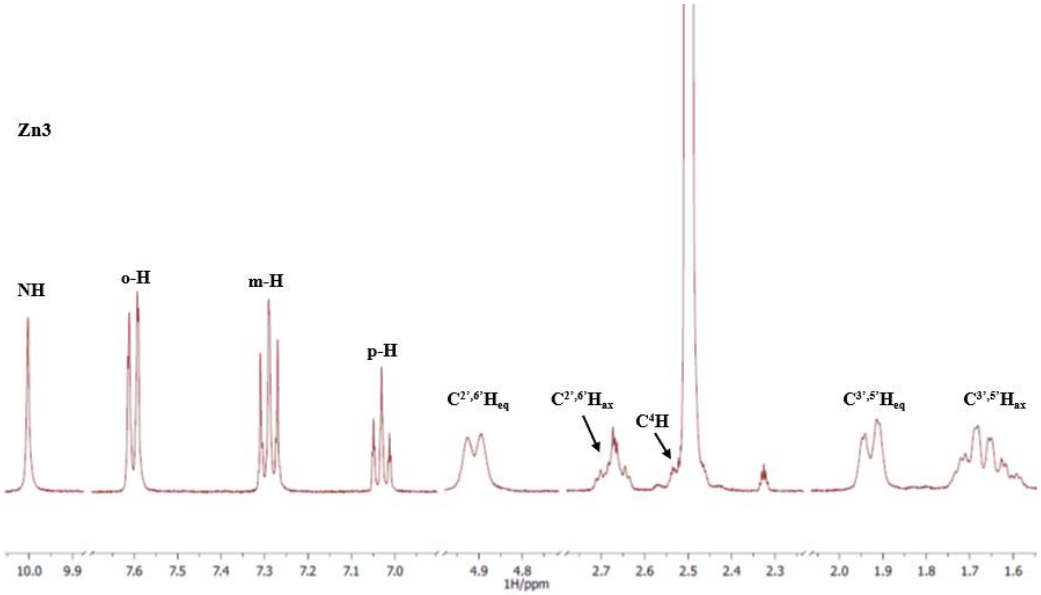

Figure 4.16: ^{1}HNMR spectrum in DMSO-d_6 of **Zn3**.

The same approach was used to obtain the actual target zinc (II) intermediates [Zn (dtc-Inp-Ph-C≡C-TIPS)$_2$] (**Zn4**). Initially, a simple, mild, and efficient procedure for the amidation of the N-protected isonipecotic acid and 4-iodoaniline with $SOCl_2$ yielded 79% of the desired amide.[35,36] Subsequently, a Sonogashira reaction (also called the Sonogashira-Hagihara reaction) in the presence of a palladium(0) catalyst, copper(I) cocatalyst, and DIPA generated 66% of the target TIPS-protected terminal alkyne.[37-42] The final step of the organic synthesis involved the deprotection of the BOC group with TFA in DCM. While, afforded 75% of the target 4-((4-((triisopropylsilyl)ethynyl)phenyl)carbamoyl)piperidin-1-ium 2,2,2-trifluoroacetate in the form of a fine white powder (**Figure 4.17**).

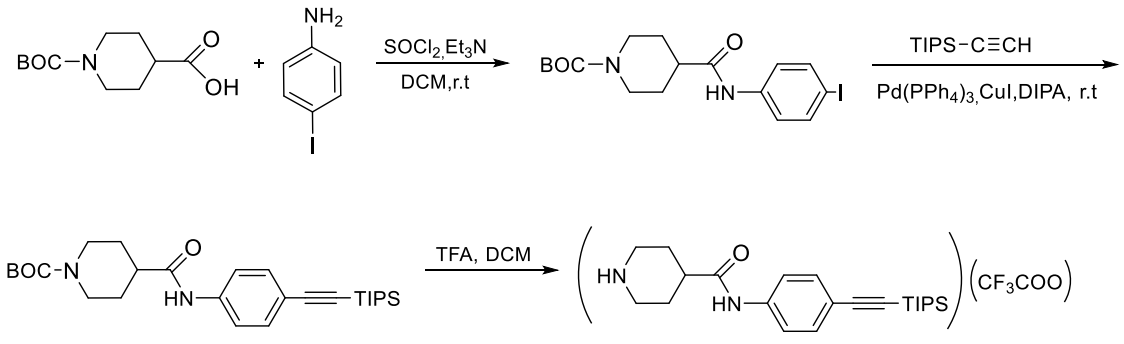

Figure 4.17: Synthesis of 4-((4-((triisopropylsilyl)ethynyl)phenyl)carbamoyl)piperidin-1-ium 2,2,2-trifluoroacetate.

Then, the intermediate **Zn4** isolated via a one-pot reaction with carbon disulfide, under basic conditions, and $[Zn(OAc)_2 \cdot 2H_2O]$ in a 2:1 ligand-to-metal ratio in DMF (**Figure 4.18**). The addition of H_2O afforded the desired zinc(II) complex in the form of an off-white solid (70% yield).

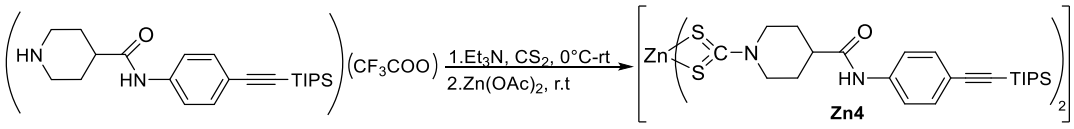

Figure 4.18: General synthetic route for the preparation of the target zinc(II) intermediate **Zn4**.

In the far-IR spectrum, the peak at 541 cm^{-1} was assigned to the $\nu_s(SCS)$, while the peak at 380 cm^{-1} arises from the antisymmetric stretching $\nu_a(ZnS_4)$ (**Figure 4.19**).[43,44]

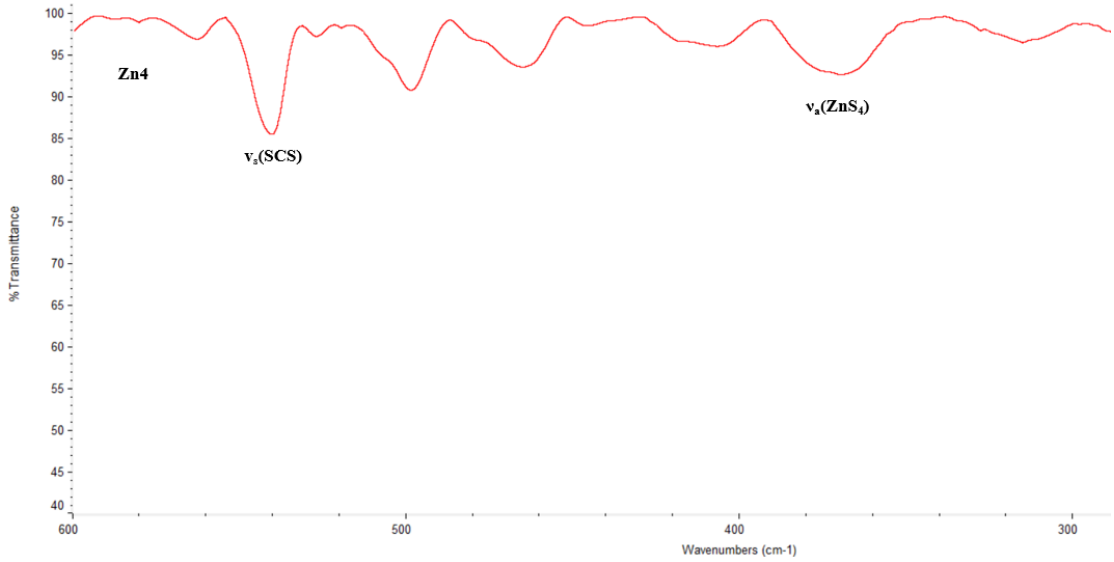

Figure 4.19: Far IR in CsI disk spectrum of **Zn4**.

The ^1H chemical shifts of the newly synthesized zinc(II) intermediate were recorded at 1.67 ($C^{3',5'}H_{ax}$), 1.95 ($C^{3',5'}H_{ax}$), 3.29 ($C^{2',6'}H_{ax}$), 2.53 (C^4H), 4.91 ($C^{2',6'}H_{eq}$), 7.40 (m-H), 7.64 (o-H) and 10.2 (NH_{amide}), respectively (**Figure 4.20**), in agreement with those observed for **Zn3** but with the extra addition of the TIPS peak.

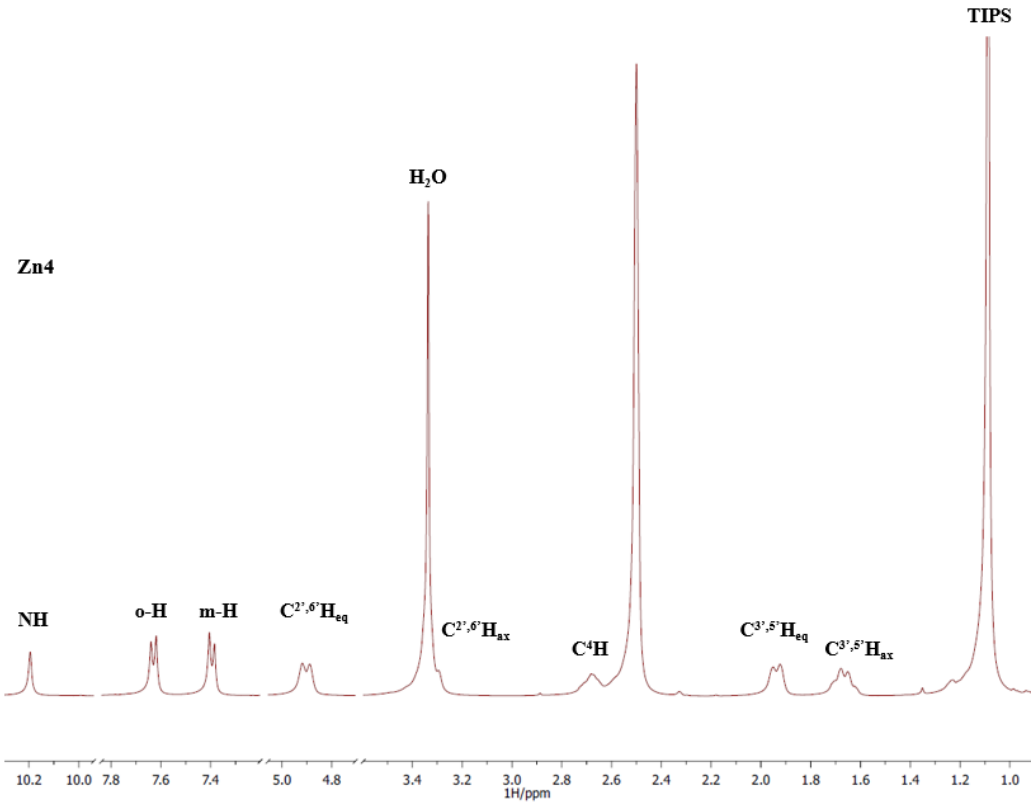

Figure 4.20: ^{1}HNMR spectrum in DMSO-d_6 of **Zn4**.

4.2.3 Preparation of the gold(III)-dithiocarbamato complexes

The model gold(III) complex **Au0** was synthesized through the well-established transmetallation reaction of **Zn3** with K[$AuBr_4$], to verify the feasibility of the synthetic method. The Zn(II)-Au(III) transmetallation took place in DMF in a 2:1 ligand-to-metal ratio for 17 hours.[34] The novel complex [$AuBr_2$(dtc-Inp-Ph)] **Au0** was isolated in almost quantitative yield after the addition of H_2O and multiple washings with MeOH (**Figure 4.21**). The desired compound was isolated as an orange solid and characterized with FT-IR and NMR spectroscopy.

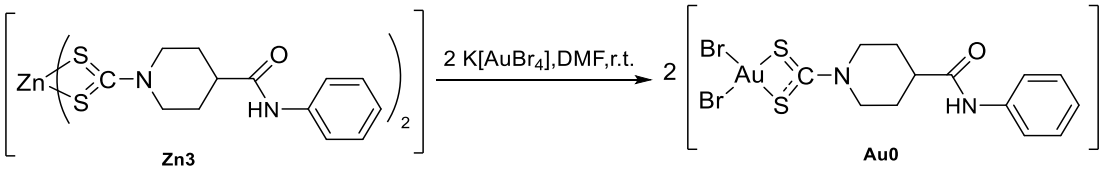

Figure 4.21: Synthesis of the dibromo-gold(III)-dithiocarbamato model compound **Au0** *via* transmetallation.

The model compound **Au0** was characterized by IR, mono- and multinuclear NMR

spectroscopy. In the mid-IR spectrum, the appearance of a band at 1547 cm^{-1} confirmed the stretching vibration ν(N-CSS). According to the Bonati-Ugo method, the recording of a single band at 946 cm^{-1} ν_a(SCS) confirming the expected chelating coordination mode. Moreover, the diagnostic absorption bands at 3400, 1668, and 759 cm^{-1} denoted the presence of the ν(NH), ν(C=O), and δ(C=C) vibrations, respectively. In the far-IR spectrum, the peak at 511 cm^{-1} was assigned to the ν_s(SCS), while the peak at 392 cm^{-1} indicates the stretching $\nu_{a/s}$(S-Au-S). Additionally, the $\nu_{a/s}$(Br-Au-Br) vibration was recorded at 222 cm^{-1} (**Figure 4.22**).[31,45,46]

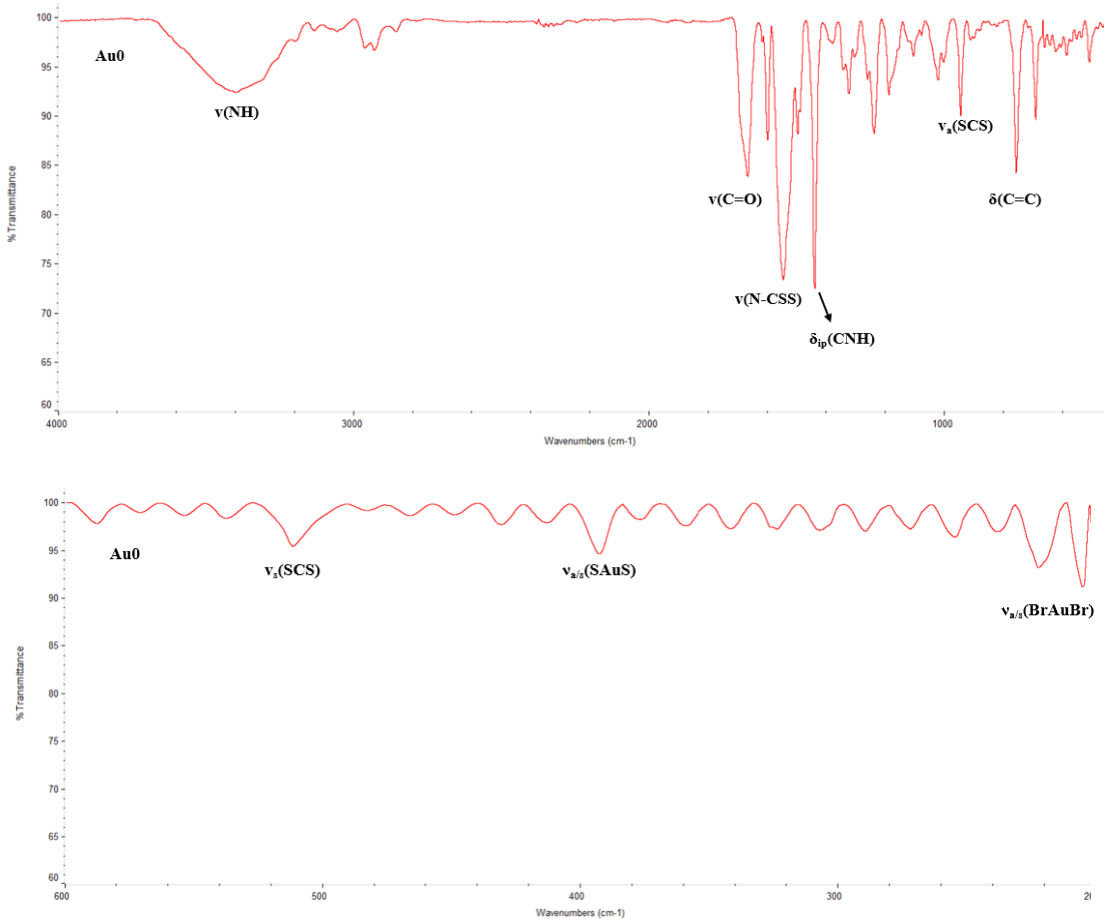

Figure 4.22: Mid-IR and Far-IR spectra with CsI disk of **Au0** derivative.

Further insights into the structure of **Au0** were provided by the study of mono- and multidimensional NMR. In comparison with the **Zn3** intermediate, the chemical shifts of the model **Au0** showed a downfield shifting. More precisely, the peaks at 1.82 ($C^{3',5'}H_{ax}$), 2.09 ($C^{3',5'}H_{ax}$), 2.89 ($C^{4}H$), 4.18 ($C^{2',6'}H_{eq}$), 7.04(p-H), 7.30 (m-H), 7.58 (o-H) and 10.02 (NH_{amide}) ppm were slightly shifted, while the signal at 3.62

($C^{2',6'}H_{ax}$) recorded the greatest shift (**Figure 4.23**).

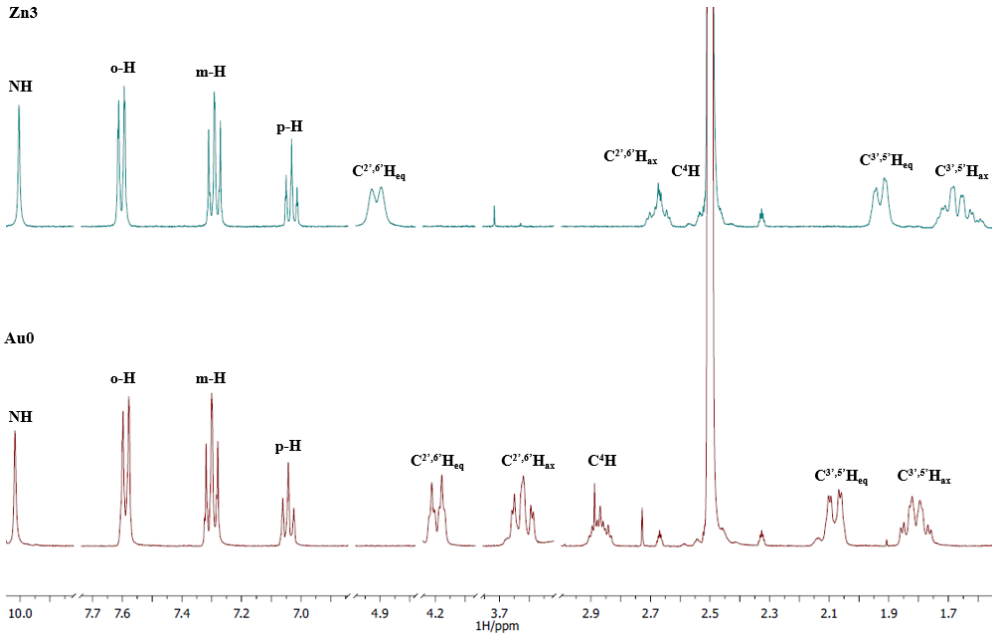

Figure 4.23: Comparative ^{1}H NMR spectra in DMSO-d_6 of **Zn3** and **Au0**.

After the successful preparation of the model compound **Au0**, isolation of the target complex [$AuBr_2$(dtc-Inp-Ph-C≡CH)] **Au2** was achieved (**Figure 4.24**). The object gold(III)-dithiocarbamato derivative was isolated *via* transmetallation from the corresponding intermediate **Zn4** and K[$AuBr_4$]. The zinc(II)-gold(III) transmetallation took place in DMF at room temperature. The zinc(II)-gold(III) reaction in 1:2 ratio yielded **Au1** in 95% yield, after precipitation in H_2O and multiple washings with MeOH. Next, the complex **Au1** was TIPS-deprotected with TBAF in THF to afford **Au2** in 87% yield as an off-white powder.[34,47-49]

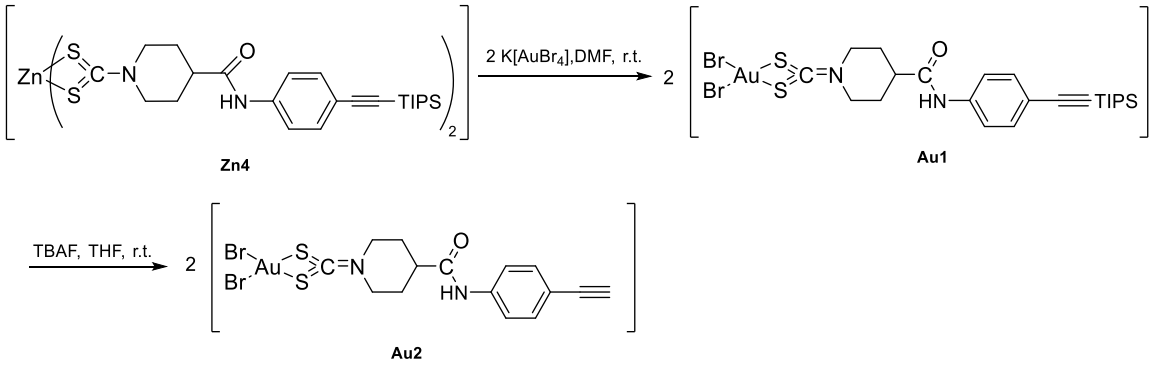

Figure 4.24: Synthesis of the dibromo-gold(III)-dithiocarbamato complex **Au2** after transmetallation and TIPS-deprotection techniques.

Complex **Au2** was characterized by IR, mono- and multinuclear NMR spectroscopy. In the mid-IR spectra, the appearance of bands at 1562 1513 and 2102 cm^{-1} confirmed the stretching vibrations ν(N-CSS), δ_{ip} (CNH_{amide}), and ν(C≡C), respectively. According to the Bonati-Ugo method, the recording of a single band at 1022 cm^{-1} indicated the stretching of dithiocarbamates ν_a(SCS). Moreover, the diagnostic bands at 3275, 1694, and 837 cm^{-1} denote the presence of the ν(NH), ν(C=O), and δ(C=C) vibrations, respectively. In the far-IR spectrum, the peak at 511 cm^{-1} was assigned to the ν_s(SCS) while the peak at 387 cm^{-1} indicates the antisymmetric stretching $\nu_{a/s}$(S-Au-S). Additionally, the $\nu_{a/s}$(Br-Au-Br) vibration was recorded at 233/222 cm^{-1} (**Figure 4.25**). [31,45,46]

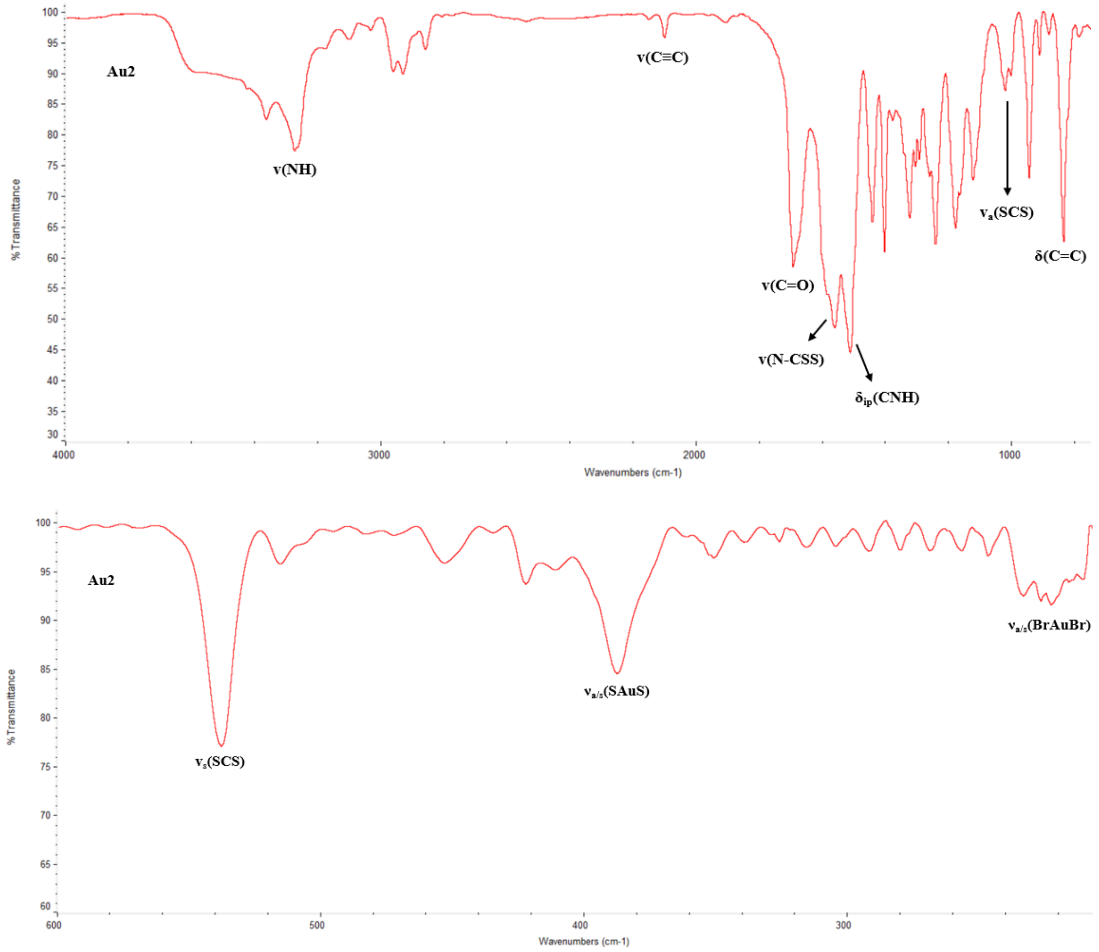

Figure 4.25: Mid-IR and Far-IR spectra with CsI disk of **Au2** derivative.

Further insights into the structure of **Au2** provided by the study of mono- and multidimensional NMR. The chemical shifts of the novel **Au2** were recorded at 1.84 ($C^{3',5'}H_{ax}$), 2.10 ($C^{3',5'}H_{ax}$), 2.87 ($C^{4}H$), 3.65 ($C^{2',6'}H_{ax}$), 4.10 (C≡CH), 4.21 ($C^{2',6'}H_{eq}$),

7.43 (m-H), 7.62 (o-H) and 10.2 (NH_{amide}) ppm (**Figure 4.26**).

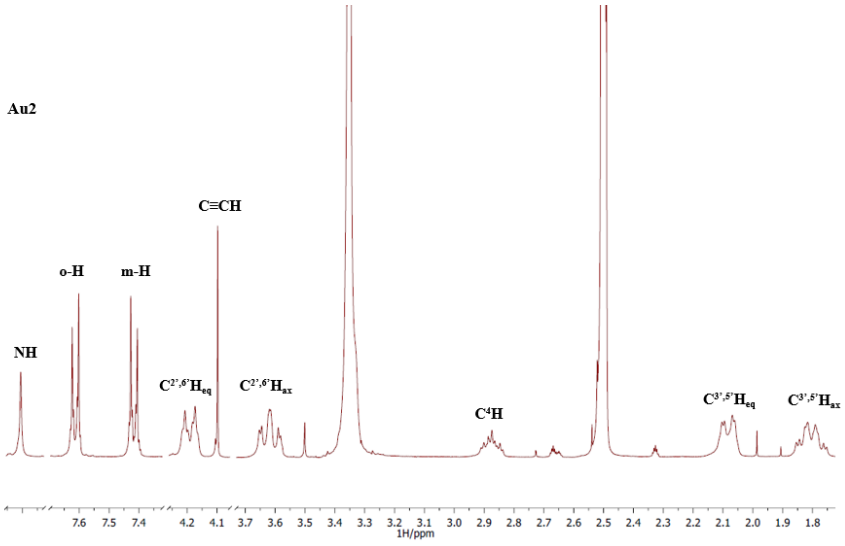

Figure 4.26: ^{1}H-NMR spectrum in DMSO-d_6 of **Au2**.

Similarly, isolation of the organometallic [Au(Bnpy)(dtc-Inp-Ph-C≡CH)](PF_6) **Au4** was achieved (**Figure 4.27**). The object gold(III)-dithiocarbamato derivative was isolated *via* transmetallation from the corresponding intermediate **Zn4** and the organometallic compound [Au(Bnpy)Cl_2]. The zinc(II)-gold(III) transmetallation took place in DMF at room temperature with KPF_6 as a counterion to maintain charges neutrality. The zinc(II)-gold(III) reaction in 1:2 ratio yielded 91% of **Au3** after precipitation in H_2O and multiple washings with MeOH. Next, the TIPS-protected complex **Au3** was deprotected with TBAF in THF to afford **Au4** in 67% yield, in the form of a fine yellow powder.[34,47-51]

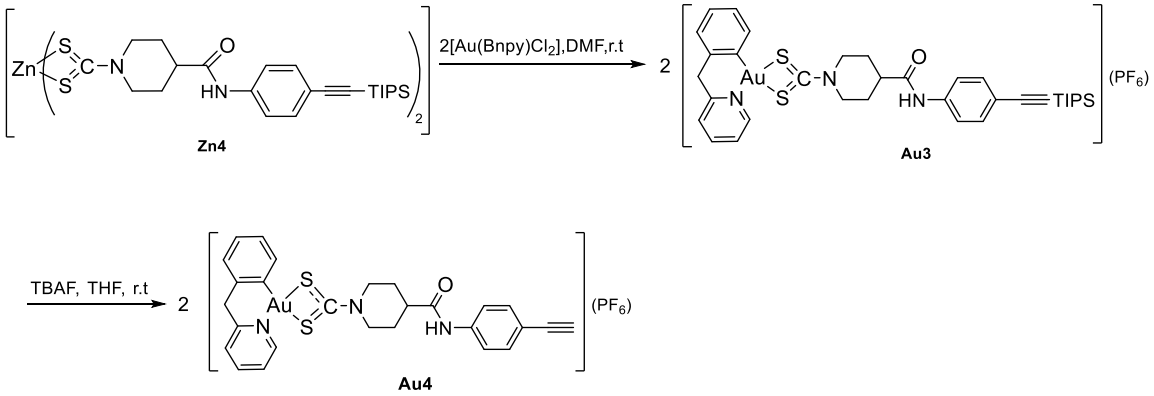

Figure 4.27: Synthesis of the organometallic-gold(III)-dithiocarbamato **Au4** following transmetallation and deprotection techniques.

In the same manner, complex **Au4** was characterized by FT-IR, mono- and multinuclear NMR spectroscopy. In the mid-IR spectra, the appearance of the characteristic bands at 1593 1522 and 2103 cm^{-1} confirms the stretching vibration ν(N-CSS), $\delta_{ip}(CNH_{amide})$, and ν(C≡C), respectively. The recording of a single band at 1026 cm^{-1} indicated the antisymmetric stretching of dithiocarbamates $\nu_a(SCS)$. Moreover, the diagnostic absorption bands at 3289, 1686, and 843 cm^{-1} denote the presence of the ν(NH), ν(C=O), and $\nu_a(PF_6^-)$ vibrations, respectively. In the far-IR spectrum, the peaks at 558 and 540 cm^{-1} were assigned to the $\delta_{ip}(PF_6^-{}_{scissoring})$ and $\nu_s(SCS)$, while the peak at 397 cm^{-1} indicates the antisymmetric stretching $\nu_{a/s}$(S-Au-S) (**Figure 4.28**). [31,45,46,52,53] Due to particular structural similarities the ^1H NMR spectrum of **Au4** is omitted for clarity.

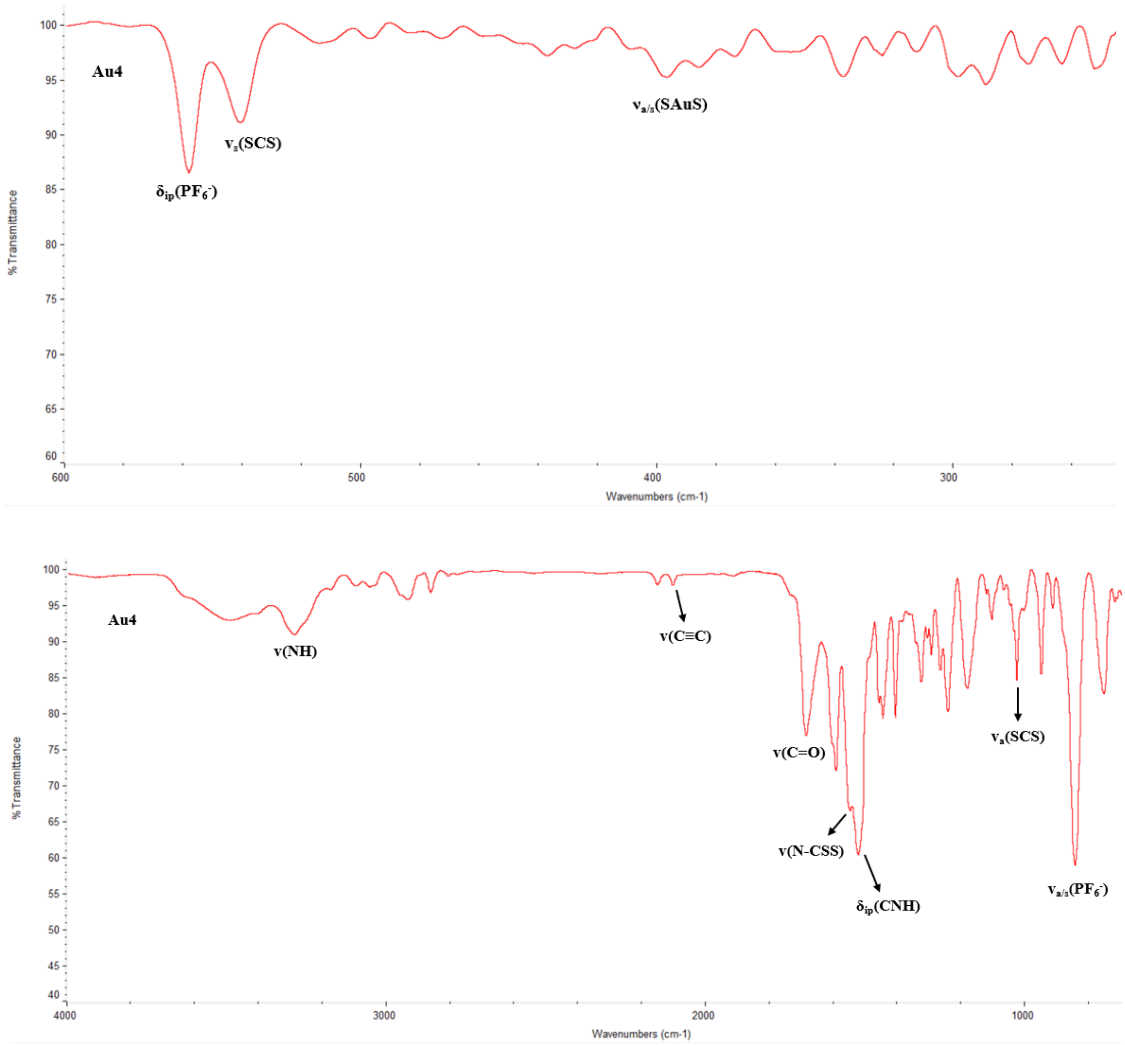

Figure 4.28: Mid-IR and FAR-IR spectra with CsI disk of **Au4** derivative.

4.2.4 Preparation of the platinum(II)-dithiocarbamato complexes

Likewise, isolation of the platinum(II)-dithiocarbamato complex [Pt(dppe)(dtc-Inp-Ph-C≡CH)](PF_6) **Pt16** was achieved (**Figure 4.29**). The novel platinum(II) derivative isolated *via* transmetallation from the corresponding intermediate **Zn4** and the pre-prepared precursor [$PtCl_2$(dppe)] **Pt15**. The zinc(II)-platinum(II) transmetallation took place in DMF at room temperature with KPF_6 as a counterion to maintain charges neutrality. The zinc(II)-platinum(II) reaction in 1:2 ratio yielded 97% of **Pt15** after precipitation in H_2O and multiple washings with MeOH. Next, the TIPS-protected complex **Pt16** was deprotected with TBAF in THF to afford **Pt16** in 89% yield, in the form of a fine white powder. [34,47-49,54]

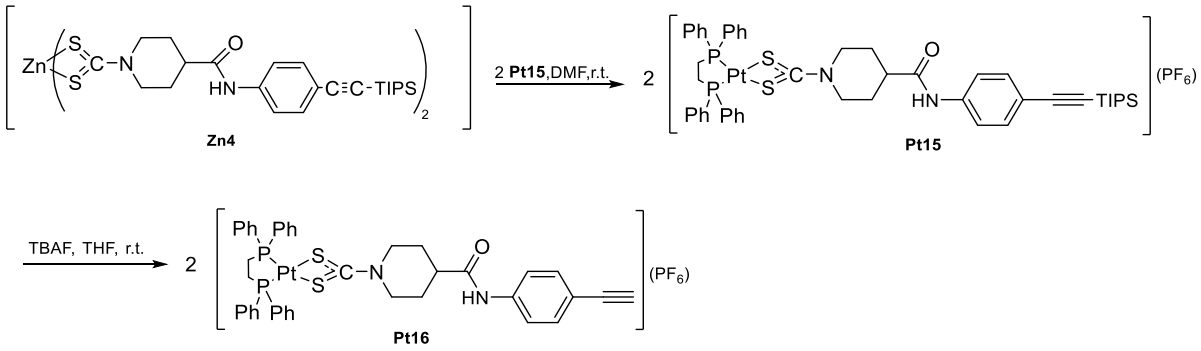

Figure 4.29: Synthesis of the platinum(II)-dithiocarbamato **Pt16** following transmetallation and deprotection techniques.

In the same manner, complex **Pt16** was characterized employing FT-IR, mono- and multinuclear NMR spectroscopy. In the mid-IR spectra, the appearance of the characteristic bands at 1528, 1436, and 2103 cm^{-1} confirmed the stretching vibration ν(N-CSS), ν(C=C), and ν(C≡C), respectively. According to the Bonati-Ugo method, the recording of a single band at 1027 cm^{-1} indicated the antisymmetric stretching of dithiocarbamates ν_a(CSS). Moreover, the diagnostic absorption bands at 3435, 1628, and 1106 cm^{-1} denote the presence of the ν(NH), ν(C=O), and ν_a(P-Ph) vibrations, respectively. In the far-IR spectrum, the peaks at 533 and 493 cm^{-1} were assigned to the $\delta_{ip}(PF_6^-{}_{scissoring})$ and ν_a(P-Pt-P), while the peak at 380 cm^{-1} indicates the antisymmetric stretching ν(S-Pt-S) (**Figure 4.30**). [31,45,46,52,53]

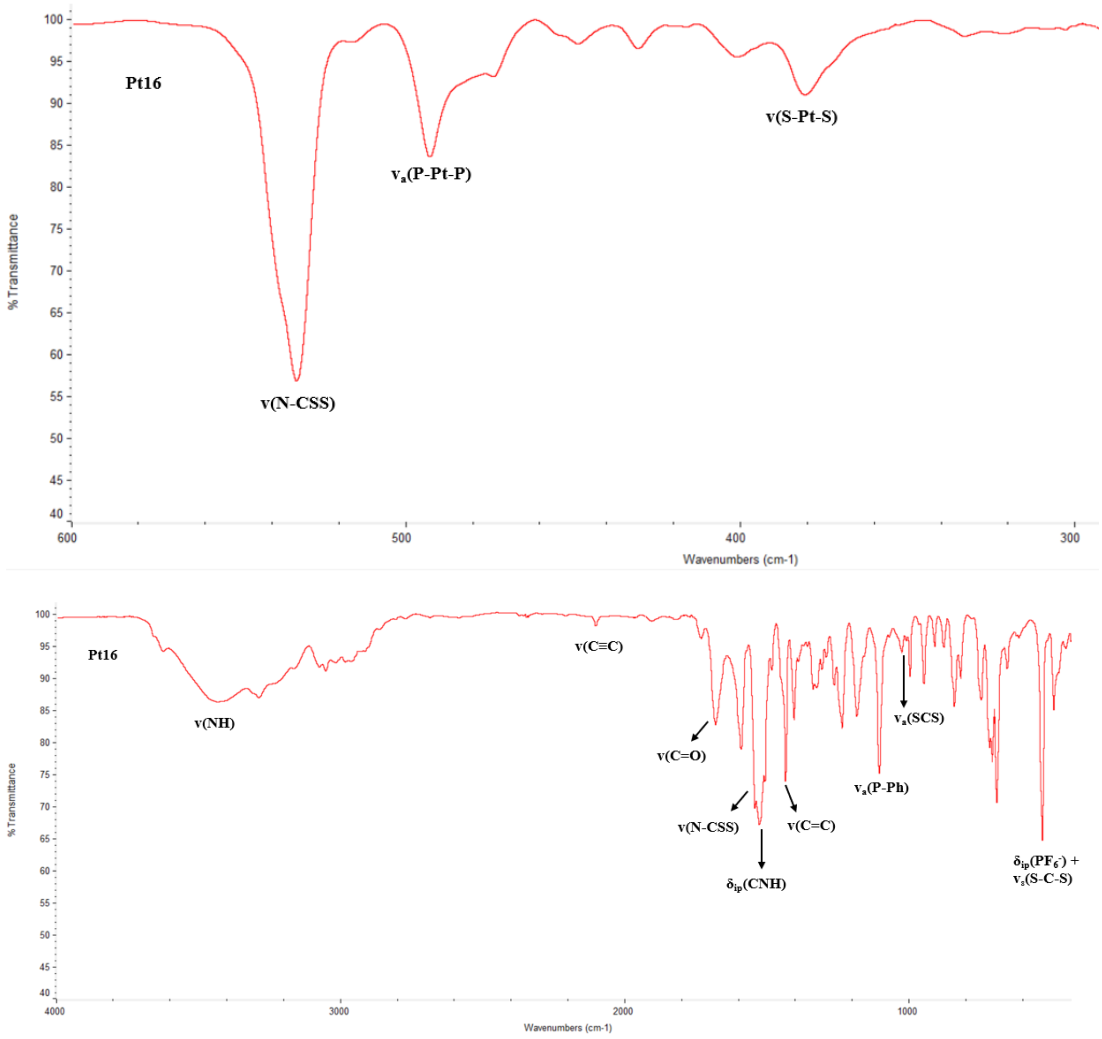

Figure 4.30: Mid-IR and Far-IR spectra with CsI disk of **Pt16** derivative.

Further insights into the structure of **Pt16** provided by the study of mono- and multidimensional NMR. The chemical shifts of the novel **Pt16** were recorded at 1.67 ($C^{3',5'}H_{ax}$), 2.02 ($C^{3',5'}H_{ax}$), 2.87 (P-C_2H_4-P+C^4H), 3.43 ($C^{2',6'}H_{ax}$), 4.10 (C≡CH), 4.37 ($C^{2',6'}H_{eq}$), 7.41 (m-H), 7.62 (P-Ph + o-H), 7.79 (P-Ph) and 10.3 (NH_{amide}) ppm (**Figure 4.31**).

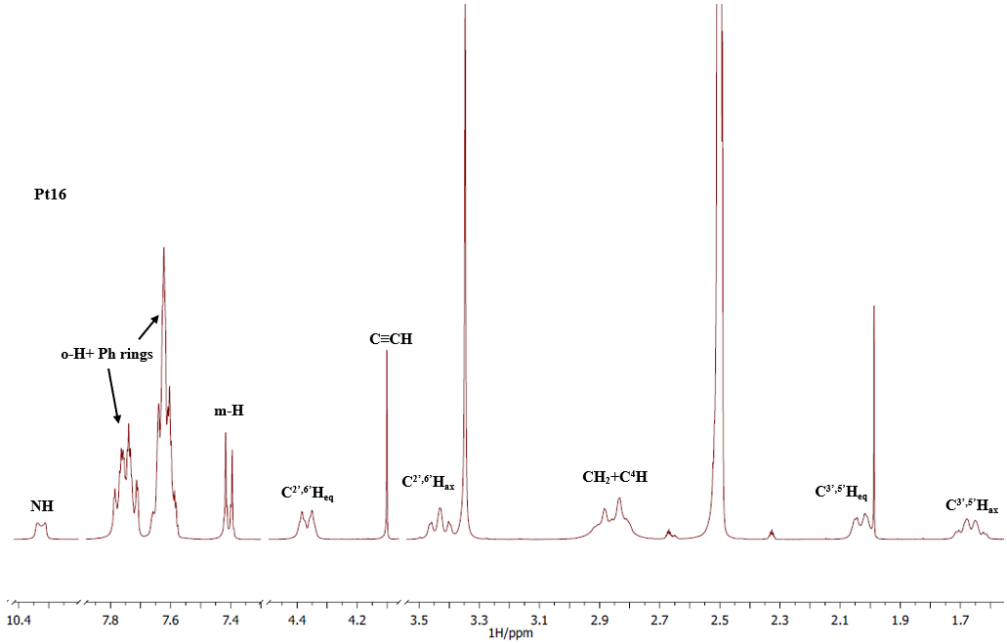

Figure 4.31: ^{1}H-NMR spectrum in DMSO-d_6 of **Pt16**.

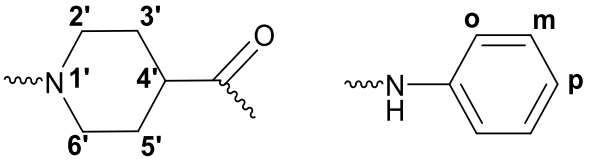

Figure 4.32: Numbering scheme of the isonipecotic ring (left) and the aniline ring (right).

4.3 Vitamin B_{12}-metal conjugated: preliminary results

Following the successful preparation of the metal-dithiocarbamato-alkynyl scaffold **Au2**, **Au4** and **Pt16** the subsequent steps would have involved their conjugation to the vitamin B_{12} fluorescent derivatives B_{12}-5'-(FLUO-1) (**3**) and B_{12}-5'-(FLUO-2) (**4**) **(**discussed in **Chapter 2**) to obtain the target fluorescent vitamin B_{12}-metal conjugates (**Figure 4.6**). This part of the project was supposed to be carried out in collaboration with Prof. Fabio Zobi at the University of Fribourg (Switzerland). However, due to the lockdown caused by the outbreak of COVID-19 and the subsequent closure of the universities worldwide the practical implementation was dramatically delayed, and preliminary attempts were performed only with the platinum (II) derivatives **Pt16**. To confirm the feasibility of the synthetic strategy previously employed (see **Chapter 4.2.1**) conjugation was first attempted between **Pt16** and vitamin B_{12} (see **Chapter 7** for details). **Pt16** and vitamin B_{12} were

reacted in DMA for 48 hours at room temperature in presence of a catalytic amount of CuOAc and DBU, leading to the precipitation of a shiny dark purple residue. The crude was then washed several times with H_2O, methanol, DCM, and diethyl ether, and purification was attempted by preparative HPLC. Regardless of the eluents employed, unexpectedly the residue proved insoluble in all common organic solvents, thus making its chromatographic purification unfeasible. Given its slight solubility in DMSO, NMR analysis in DMSO-d_6 was attempted. Although the analysis of the ^1H NMR spectrum proved inconclusive due to the large overlap of the peaks and their low intensity, some insights were provided by $^{31}P\{1H\}$NMR. A ^{31}P peak was recorded at 44.3 ppm (**Figure 4.33**) and assigned to the chelating diphosphine ligand coordinated to the platinum(II) center, whereas the peak of the starting precursor **Pt16** was at 41.9 ppm.[54]

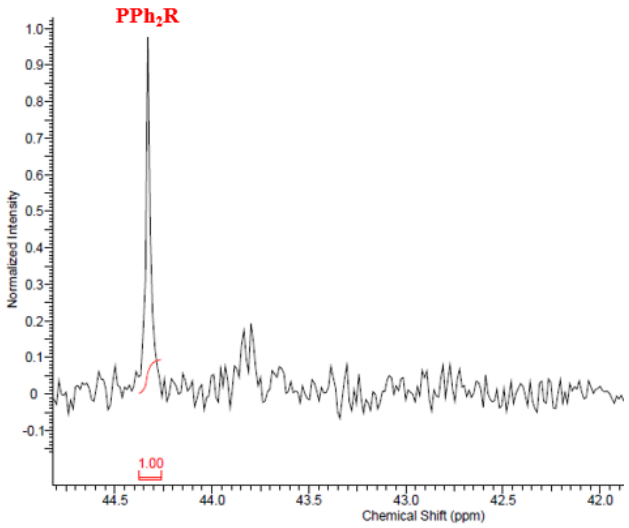

Figure 4.33: $^{31}P\{^1H\}$NMR spectrum in DMSO-d_6 of the reaction crude

To identify the residue obtained, UV-Vis analysis was also carried out and the spectrum was compared with that of pure vitamin B_{12} recorded under the same experimental conditions (**Figure 4.34**).

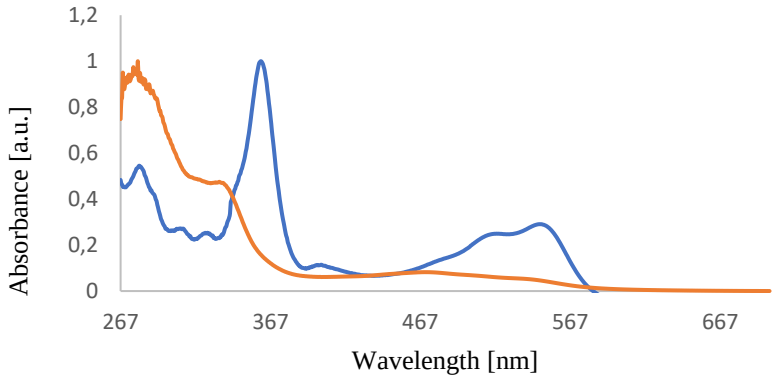

Figure 4.34: UV-Vis spectra in DMSO (1 mg/mL) of reaction crude (orange) and vitamin B_{12} (blue). Intensity has been normalized to the maxima.

It is clear that the two compounds are different, and the absorption pattern and maxima of the unidentified reaction crude are consistent with the coordination of an unsaturated terminal phenyl-alkyl carbon to the cobalt (III) center of vitamin B_{12}.[5] Characterization in solid was performed by IR spectroscopy which allowed the identification of some diagnostic bands (**Figure 4.35**)

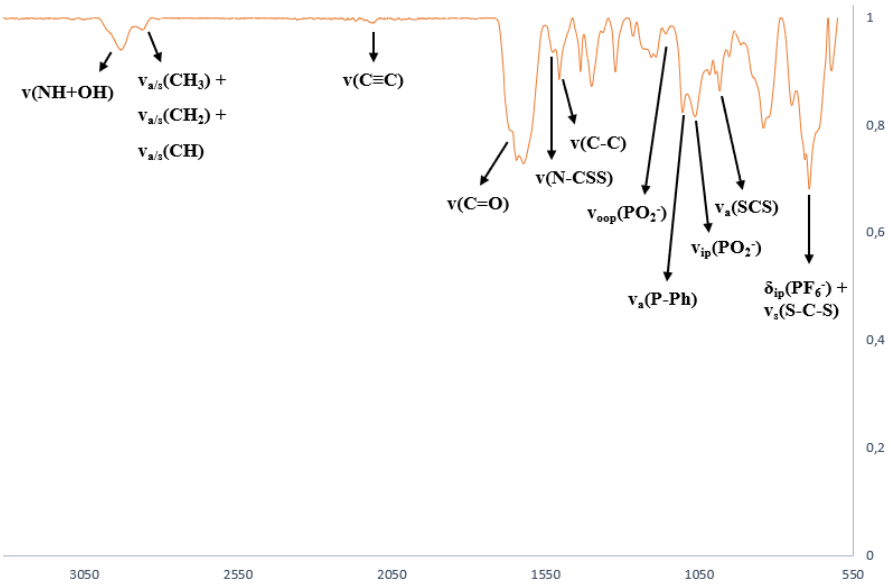

Figure 4.35: FT-IR spectrum with CsI disk of the reaction crude

Apart from the vibrations in common with the vitamin B_{12} (see **Chapter 2**), new bands at 1525 cm^{-1} and 983 cm^{-1} (assigned to ν(N-CSS) and ν_a(SCS) respectively) are consistent with the presence of the dithiocarbamate scaffold coordinated to a metal

center. Moreover, the absence of ν(C≡N) at 2138 cm^{-1} (assigned to the free cyano-group of vitamin B_{12}) or at ~ 2200 cm^{-1} (assigned to the cyano- group coordinating to the platinum (II) center), and the concomitant appearance of a weak band at 2115 cm^{-1} (expected for ν(C≡C-Co)) support the formation of an organometallic bond C≡C-Co.[31,45,46,52-56] Although not fully conclusive, altogether these experimental results would suggest the generation of the vitamin B_{12}-platinum (II) derivatives **B_{12}-Pt16** showed in **Figure 4.5**. This would be further confirmed by the presence in the mass spectrum of a peak at 809.5 m/z fully consistent with the $[(B_{12}\text{-Pt16})+H+2Na]^{3+}$ fragment (**Figure 4.36**).

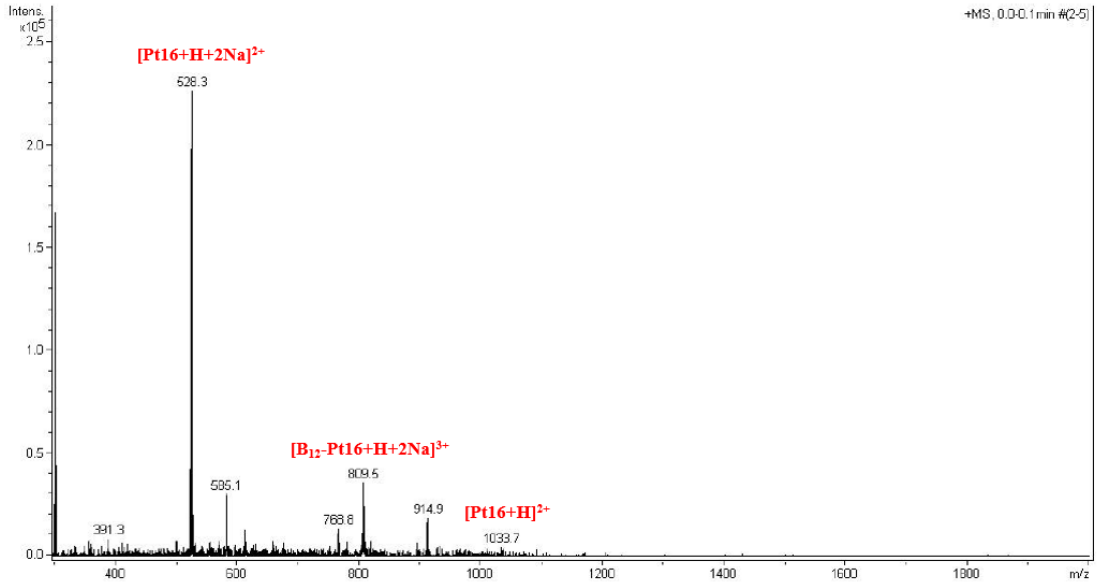

Figure 4.36: Mass spectrum of the reaction crude.

Although not fully conclusive, these encouraging preliminary results seem to confirm the feasibility of the proposed conjugation strategy. The same synthetic procedure is currently being applied to the gold (III) precursor **Au2** and **Au4** in the hope to overcome the solubility issues experienced with **P16**.

4.4 Conclusions

Three novel metal-dithiocarbamato-alkynyl complexes (namely, **Au2**, **Au4**, and **Pt16**) have been prepared and fully characterized. Conjugation of the platinum(II) derivative to vitamin B_{12} has been attempted and, although more challenging than expected, provided insights into the generation of this new class of vitamin B_{12}-metal conjugates. Should the conjugation of the gold(III) derivatives **Au2** and **Au4** to vitamin B_{12} be successful, the reaction will be extended to the fluorescent derivatives

B_{12}-5'-(FLUO-1) (3) and **B_{12}-5'-(FLUO-2)** (4) (see **Chapter 2**) previously obtained, to prepare the final target fluorescent conjugates originally identified.

4.5 References

1. Baldwin, A., Betterton, A., Pratt, M., *Dalton Trans*., 217-223, (1983).

2. Corsi, M., Murthy, N., Young, G., Karlin, D., *Inorg. Chem.,* **38**, 848–858 (1999).

3. Ruetz, M., Salchner, R., Wurst, K., Fedosov, S., Kräutler, B., *Angew. Chem., Int. Ed.,* **52**, 11406–11409, (2013).

4. Chromiński, M., Lewalska, A., Gryko, D., *Chem. Commun.,* **49**, 11406–11408, (2013).

5. Rossier, J., Hauser, D., Kottelat, E., Rothen-Rutishauser, B., Zobi, F., *Dalton Trans.,* **46**, 2159–2164, (2017).

6. Jursic, B., Zdravkovdki, Z., *Synth. Commun*., **23**, 2761–2770, (1993).

7. Gotor, V., *Bioorg. Med. Chem.,* **7**, 2189–2197, (1999).

8. Van Rantwijk, F., Hacking, M., Sheldon, R., *Monatsh. Chem.,* **131**, 549–569, (2000).

9. Bodanszky, M., *J. Protein Chem*., **25**, 449–474, (1985).

10. Bodanszky, M., *Peptide Res.,* **5**, 134–139, (1992).

11. Han, S., Kim, Y., *Tetrahedron*, **60**, 2447–2467, (2004).

12. Humphrey, J., Chamberlin, A., *Chem. Rev.,* **97**, 2243–2266, (1997).

13. Katritzky, A., Suzuki, K., Singh, S., Arkivoc, **vii**, 36-55, (2004).

14. Montalbetti, C., Falque, V., *Tetrahedron*, **61**, 10827–10852, (2005).

15. Najera, C., *Synlett*, **9**, 1388–1403, (2002).

16. Sheehan, J., Hess, G., *J. Am. Chem. Soc.*, **77**, 1067–1068, (1955).

17. Meiser, F., Cortez, C., Caruso, F., *Angew. Chem.Int.Ed*, **43**, 5954–5957, (2004).

18. Moraillon, A., Gouget-Laemmel, A., Ozanam, F., Chazalviel, J., *J. Phys. Chem. C*,

112, 7158–7167, (2008).

19. Koenig, W., Geiger, R., *Chem. Ber.*, **103**, 788–798, (1970).

20. Koenig, W., Geiger, R., *Chem. Ber.*, **103**, 2024–2033, (1970).

21. Ruetz, M., Gherasim, C., Gruber, K., Fedosov, S., Krautler, B., *Angew. Chem. Int.Ed*, **52**, 2606–2610, (2013).

22. Banerjee, R., Chemistry and Biochemistry of B_{12}, Chapter 1, (1999).

23. Pratt, J., Inorganic Chemistry of Vitamin B_{12}, Chapter 1, (1972).

24. Proinsias, K., Giedyk, M., Gryko, D., *Chem. Soc. Rev*., **42**, 6605–6619, (2013).

25. Baldwin, D., Betterton, E., Pratt, J., *Dalton Trans.*, 225–229, (1983).

26. Jonsdottir, S., Klar, G., *Acta Chem. Scand.*, **51**, 797–799, (1997).

27. Ruetz, M., Salchner, R., Wurst, K., Fedosov, S., Krautler, B., *Angew. Chem*., **52**, 11406–11409, (2013).

28. Sreeruttun, R., Ramasami, P., Wannere, C., Simmonett, A., Schaefer, H., *Phys. Chem. A*, **13**, 2838–2845, (2008).

29. Samadi-Maybodi, A., Darzi, S., *Spectrochim. Acta A*, **70**, 1167–1172, (2008).

30. Nakamoto, K., Theory and Applications in Inorganic Chemistry, Part A, (2008).

31. Bonati, F., Ugo, R., *J. Organomet. Chem.*, **10**, 257–268, (1967).

32. Valeur, E., Bradley, M., *Chem. Soc. Rev.*, **38**, 606–631, (2009).

33. Han, G., Tamaki, M., Hruby, V., *J. Peptide Res*., **58**, 338-341, (2001).

34. Lecina, J., Carrer, A., Álvarez-Larena, A., Mazzi, U., Suades, J., *Organometallics*, **31**, 5884−5893, (2012).

35. Leggio, A., Belsito, E., De Luca, G., Di Gioia, M., Leotta, V., *et.al.*, *RSC Adv.*, **6**, 34468-34475, (2016).

36. Montalbetti, C., Falque, V., *Tetrahedron*, **61**, 10827–10852, (2005).

37. Chinchilla, R., Nájera, C., *Chem. Rev.*, **107**, 874–922, (2007).

38. Li, J., Sonogashira Reaction, Chapter 1-3, (2021)

39. Eckhardt, M., Fu, G., *J. Am. Chem. Soc*., **125**, 13642-13643, (2003).

40. Hundertmark, T., Littke, A., Buchwald, S., Fu, G., *Org. Lett.,* **2**, 1729-1731, (2000).

41. Panda, B., Sarkar, T., *Synthesis*, **45**, 817-829, (2013).

42. Capani, J., Chochran, J., Liang, J., *J. Org. Chem.*, **84**, 9378-9384, (2019).

43. Wiercigroch, E., Szafraniec, E., Czamara, K., Pacia, M., Majzner, K., *et al.*, *Spectrochim. Acta A*, **185**, 317–335, (2017).

44. Picquart, M., Abedinzadeh, Z., Grajcar, L., Baron, M., *Chem. Phys.,* **228**, 279–291, (1998).

45. Boscutti, G., Feltrin, L., Lorenzon, D., Sitran, S., Aldinucci, D., *et al., Inorg. Chim. Acta,* **393**, 304–317, (2012).

46. Forghieri, F., Preti, C., Tassi, L., Tosi, G., *Polyhedron*, **7**, 1231–1237, (1988).

47. Jacquemard, U., Bénéteau, V., Lefoix, M., Routier, S., Mérour, J., *et al.*, *Tetrahedron*, **44**, 10039-10047, (2004).

48. Kaburagi, Y., Kishi, Y., *Org. Lett*., **4**, 723–726, (2007).

49. Yan, H., Oha, J., Song, C., *Org. Biomol. Chem*., **9**, 8119-8121, (2011).

50. Bertrand, B., Spreckelmeyer, S., Bodio, E., Cocco, F., Picquet, M., *et al.*, *Dalton Trans.*, **44**, 11911–11918, (2015).

51. Shaw, A., Tilset, M., Heyn, R., Jakobsen, S., *J. Coord. Chem.*, **64**, 38–47, (2011).

52. Taylor, J., Odel, A., Raethel, A., *Spectrochim. Acta A,* **24**, 1855–1861, (1968).

53. Daasch, W., Smith, C., *Anal. Chem.,* **23**, 853–868, (1951).

54. Dopke, C., Oemke, H., *Inorganica Chim. Acta,* **376**, 638–640, (2011).

55. Adamczyk, M., Fishpaugh, J., Heuser, K., *Bioconjug. Chem.*, **8**, 253–255, (1997).

56. Wang, L., *Spectrochim. Acta A Mol. Biomol. Spectrosc.,* **57**, 1781–1791, (2001

Chapter 5

5. Design, Synthesis and Characterization of Novel Fluorescent Pt(II)- and Au(III)-based Dithiocarbamato *L*-tyrosyl Ester Derivatives as Potent Anticancer Agents

5.1 Background

Amino acids (AA), a category of low mass organic compounds, were identified at the start of the 19th century.[1] Members of this biologically important class of molecules present common structural characteristics, including a carboxyl group (-COOH), an amino group (-NH_2), and an organic side chain (R = aliphatic, acyclic, aromatic, hydroxyl or sulfur). The carbon atom directly connected to the carboxyl group is called α-carbon, and when the amino group is in direct connection with the α-carbon, the AA is called alpha-(α-)-amino acid (**Figure 5.1**). Based on the above, amino acids classified as beta (β-), gamma- (γ-), and delta- (δ-). Amino acids are existing in two optically active forms (D and L) due to the asymmetric a-carbon. Interestingly, the dominant configuration of the amino acids is the L.

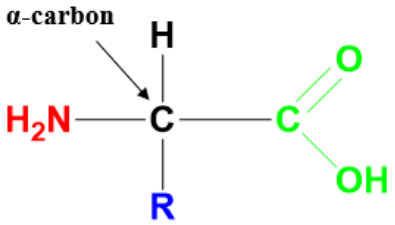

Figure 5.1: General structure of an α-amino acid in its molecular form.

From the plethora of amino acids, only twenty of these have gotten involved in protein synthesis (**Figure 5.2**). Namely, these are the essential amino acids (i.e., lysine, methionine, valine, tryptophan, isoleucine, histidine, phenylalanine, threonine, leucine, and arginine) and the non-essential (i.e., cysteine, tyrosine, serine, alanine, asparagine, amino acid, glutamic acid, glycine, lysine, and proline).[2] Humans are unable to synthesize essential amino acids, while they sufficiently produce the non-essential.

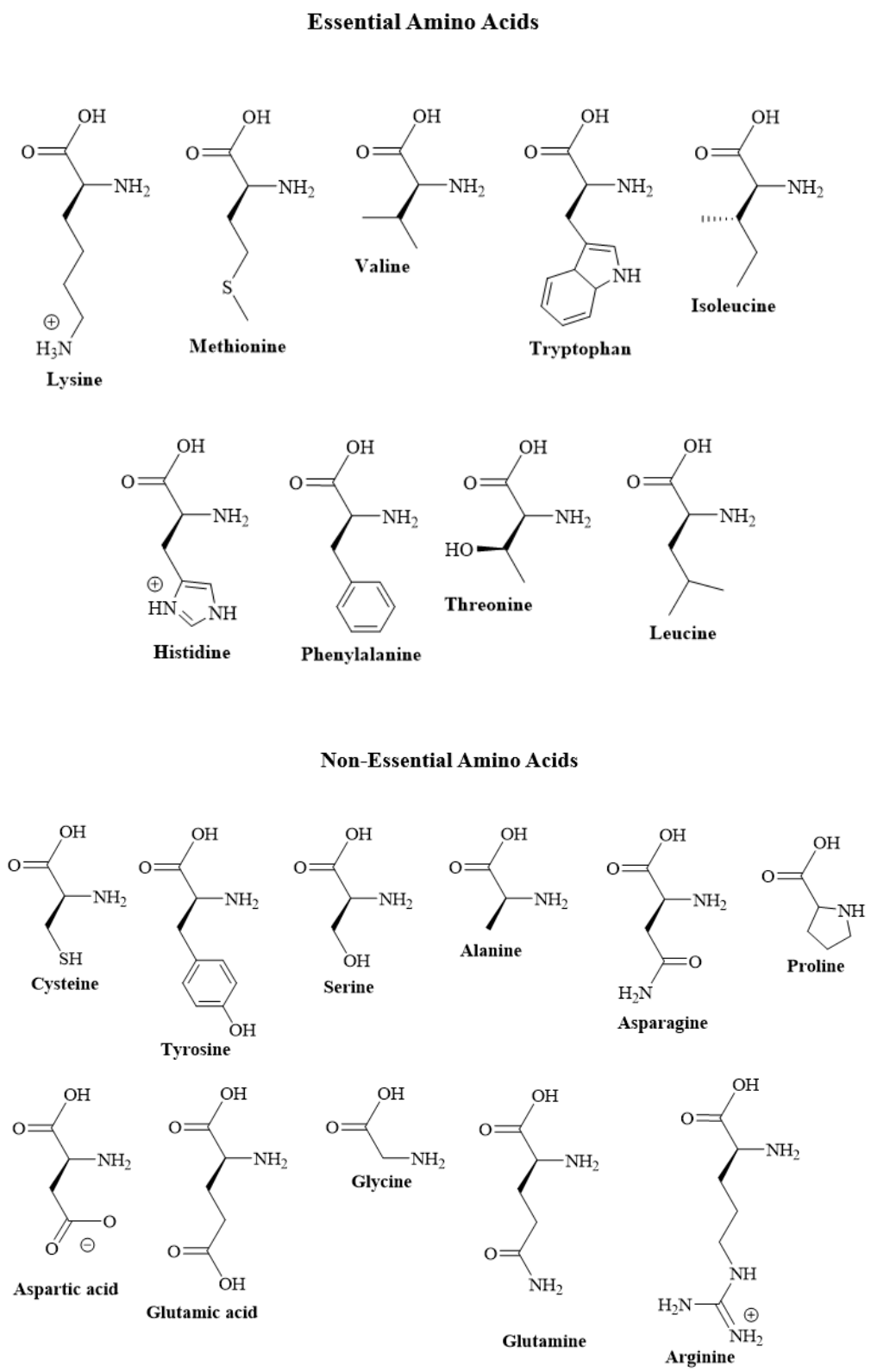

Figure 5.2: Chemical structures of the twenty proteinogenic amino acids.

Nowadays, numerous scientific studies focusing on amino acids due to their importance in multiple biological pathways. Amino acids could act as alternative

fuels, redox balance derivatives, homeostatic regulators, modulators of processes related to gene expression, and mediators of immune responses linked to tumorigenesis and metastasis. So far, amino acids have been proven vital for the successful treatment of genetic defects.[3] Interestingly, the idea of adapting naturally occurring amino acids, and their synthetic analogs as potential therapeutics is becoming increasingly popular in cancer research.

5.1.1 Briefly the role of amino acids in tumors

Apart from their role as building blocks of proteins, certain amino acids present additional functionalities. To date, scientific studies have revealed critical aspects about their importance in tumors microenvironment.[4,5] In short, branched-chain amino acids (i.e., valine, leucine, isoleucine) and threonine can fuel the tricarboxylic acid cycle and act as ad hoc energy supply. Moreover, branched-chain amino acids and lysine promote gene expression and support tumor growth. Also, proline involves in tumor progression. Additionally, glycine, glutamine, aspartate, serine, and methionine serve as carbon and nitrogen donors for purine biosynthesis, while phenylalanine assists nonessential amino acids biosynthesis. After the accumulation of reactive oxygen species, glycine and cysteine promote redox balance. Interestingly, tyrosine and alanine control metabolic enzyme signaling, arginine alters gene expression, while tryptophan promotes immunosuppression. Furthermore, methionine, serine, and glycine promote epigenetic regulation and posttranscriptional modification by influencing the methionine cycle.

5.1.2 Platinum(II)- and gold(I/III)-based complexes incorporating amino acids

Metal-based therapeutics demonstrate various electronic and structural features, oxidation states, coordination geometries, and types of ligands, which make them promising candidates for clinical uses. Due to their unique properties and novel mechanisms of action, these compounds are proposed as therapeutic or diagnostic agents to treat various chronic diseases e.g., cancer.[22,23] Medicinal inorganic chemistry geared toward such therapeutics by identifying several desired

characteristics of the metal ion (e.g., nature, oxidation state, and stability) and the ligands (i.e., type, properties, and pharmacological profile). Up to the present moment, there are numerous examples of platinum- and gold-based therapeutics, while also copper, vanadium, ruthenium, rhodium, nickel, palladium, iron, and cobalt complexes have been reported.[24–28] So far, there are several examples of proteinogenic molecules as ligands for metal complexes, which are presenting good chelating properties, favorable pharmacological profile, and promising antitumor activity. Amino acids and derivatives (e.g., amino acid ester Schiff bases and various amino acid esters) tend to form stable five- and six-membered chelates through the amino and carboxylate groups with different metal ions. However, specific atoms present on the amino acid's side chains may also act as binding sites.[29] Moreover, modifications on amino acid esters with alternative groups incorporating various binding modes (i.e., dithiocarbamato moieties) have led to stable cytotoxic complexes.

Extensive research on platinum(II)-based cancer therapeutics with biologically important ligands led to several mixed ligand platinum(II)-AA complexes (AA = glycine and alanine) with purine/pyrimidine bases (adenine, guanine, hypoxanthine cytosine, and uracil).[30] Next, new platinum complexes of the type [Pt(2,2-bipyridine)(AA)]$^+$ (AA= histidine, lysine, asparagine, phenylalanine, tryptophan, tyrosine, glycine, alanine, leucine, serine, cysteine, methionine and glutamine) were developed, showing growth inhibition against P-388 lymphocytic leukemia cells (**Figure 5.3**).[31]

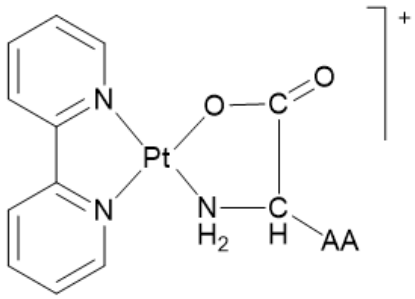

Figure 5.3: General schematic representation of [Pt(2,2-bipyridine)(AA)]$^+$ type of complexes.

Progression on the field was led to the idea of conjugating fluorescent organic dyes or strongly luminescent metal complexes to weakly- or non-luminescent clusters to allow cellular imaging. Indeed, species with the general formula [Pt(phen)(AA)]$^+$ (AA

= glycine, alanine, leucine, phenylalanine, tyrosine, and tryptophan) were examined by fluorescence spectroscopy, which were shown intercalative binding mode in calf thymus DNA at low concentrations (**Figure 5.4**).[32]

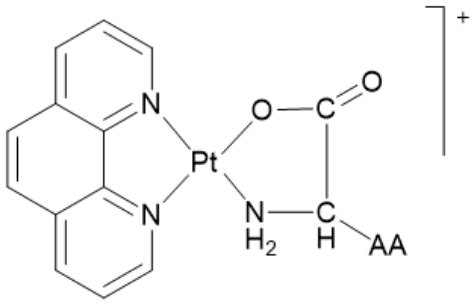

Figure 5.4: Chemical structure of $[Pt(phen)(AA)]^+$ derivatives.

Following the above-stated method, several dual-action systems were prepared. Interestingly, the [Pt(C^N)(AA)] (C^N = 2-(2'-thienyl) pyridine, AA= phenylalanine, tryptophan, glycine) complexes could function both as luminescent probes and anticancer agents. More precisely, these clusters demonstrated high binding affinity and selectivity towards human serum albumin (HSA) with enhanced photoluminescence at 562 nm. Amongst all, the complex [Pt(C^N)(phe)] presented an IC_{50} value of up to 1 μM against several cancer cell lines (**Figure 5.5**).[33]

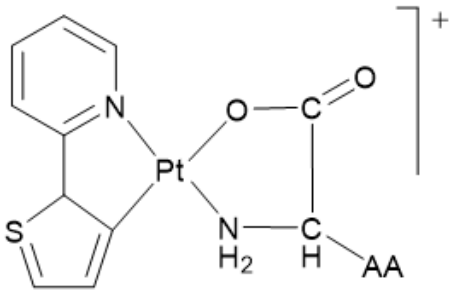

Figure 5.5: Chemical structure of the multifunctional [Pt(C^N)(AA)] type of complexes.

Furthermore, long amino acidic and amide chain platinum complexes of the type $[PtCl_2\{NH_2(CH_2)_nCOOH]\}_2]$ (n = 5, 10) proposed as potent anticancer pharmaceuticals.[34] Alternative strategies suggest the preparation of platinum(II) complexes containing reduced amino acid ester Schiff bases (**Figure 5.6**). This class of compounds tested on salmon sperm DNA and investigated employing UV and CD spectroscopies. All the newly prepared platinum(II) Schiff base scaffolds

demonstrated an intercalation type of binding mode with DNA and cytotoxic activity against a panel of selected human carcinoma cell lines.[35]

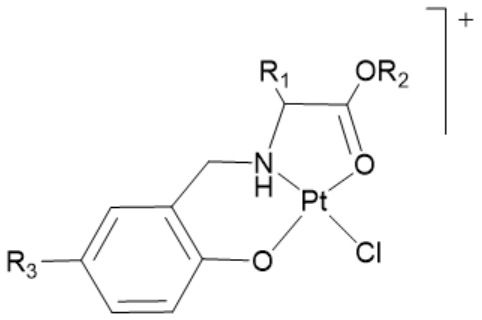

R_1= Bn, Pr^i,
R_2= Me, Et, H,
R_3= H, Cl, Br,

Figure 5.6: General structure of the platinum(II)-amino acid ester Schiff bases.

Analogously, there are a few gold-based complexes incorporating amino acids or dipeptides as ligands.[36] Recently, novel robust gold(I) complexes with thiolates and methyl ester aminoacidic moieties (**Figure 5.7**) were isolated, displaying sufficient IC_{50} values in vitro against A549, Hep-G2, HeLa, MCF-7, and NIH-3T3 cell lines.[37]

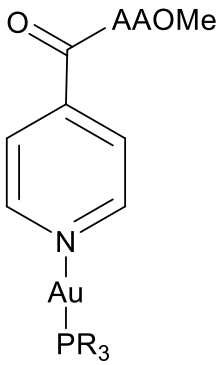

AA= L-valine methyl ester, L-alanine methyl ester, L-phenylalanine methyl ester
R_3 = PPh_3, PPh_2py

Figure 5.7: Chemical structure of the gold(I)-methyl ester-AA scaffolds.

In 2010, a new class of gold(III)-peptidodithiocarbamato compounds of the general type [AuX_1X_2(pdtc)] (X = halogen, pseudo-halogen; pdtc = peptidodithiocarbamato) derivatives of 2 to 5 esterified amino acids, including glycine, alanine, proline, serine sarcosine, a-amino isobutyric and phenylalanine were reported, demonstrating

outstanding cytotoxic activity and enhanced selectivity towards peptide transporters PEPT1 and PEPT2. In vitro cytotoxicity of the novel gold(III) compounds was evaluated toward PC3 and DU145, ovarian adenocarcinoma 2008, C13, and L540 cancer cell lines (**Figure 5.8**).[38]

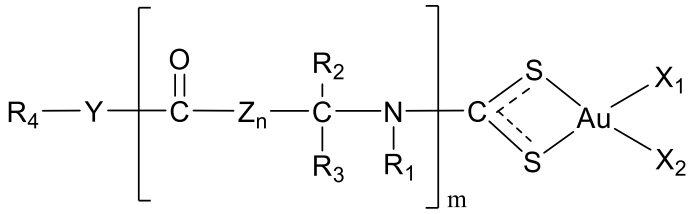

X_1,X_2 = Cl, Br, CN, SCN
m = 2,3,4,5
R_1 = H, CH_3, C_2-C_6 alkyl, C_3-C_6 cycloalkyl, phenyl, CH_2
R_2 = H, CH_3, C_2-C_6 alkyl, C_3-C_6 cycloalkyl, phenyl
R_3 = H, CH_3, CH_2-C=CH-NH-(C_6H_4), $CH(CH_3)_2$, $(CH_2)_2$
Z_n (n = 0,1) = -C-(R_5,R_6), R_5, R_6 = H, CH_3, C_2-C_6 alkyl, C_3-C_6 cycloalkyl, phenyl
Y = O, S, NR_7, R_7 = H, CH_3, C_2-C_6 alkyl, C_3-C_6 cycloalkyl, phenyl
R_4 = H, CH_3, C_2-C_6 alkyl, C_3-C_6 cycloalkyl, phenyl, $(CH_2CH_2O)_PH$, p=1,2,3,4

Figure 5.8: Chemical structure of the cytotoxic gold(III)-peptidodithiocarbamato complexes.

5.2 Strategy

This side project involved the design and synthesis of novel platinum(II)- and gold(III)-containing luminescent chemotherapeutics via a straightforward transmetallation technique. Because *L*-tyrosine lacks sensitivity to environmental changes such as polarity, two fine-tuned artificial analogs of the amino acid (*L*-tyrosine methyl ester and *L*-tyrosine ethyl ester) were adapted for the preparation of the target metal complexes. Isolation of the novel platinum(II)-dithiocarbamato amino acid ester derivatives **Pt17** and **Pt18** occurred via the transmetallation reaction of the pre-prepared precursors **Pt15** and zinc(II) intermediates [Zn(dtc-*L*-Tyr-OMe)$_2$] (**Zn5**) and [Zn(dtc-*L*-Tyr-OEt)$_2$] (**Zn6**) (**Figure 5.9**).

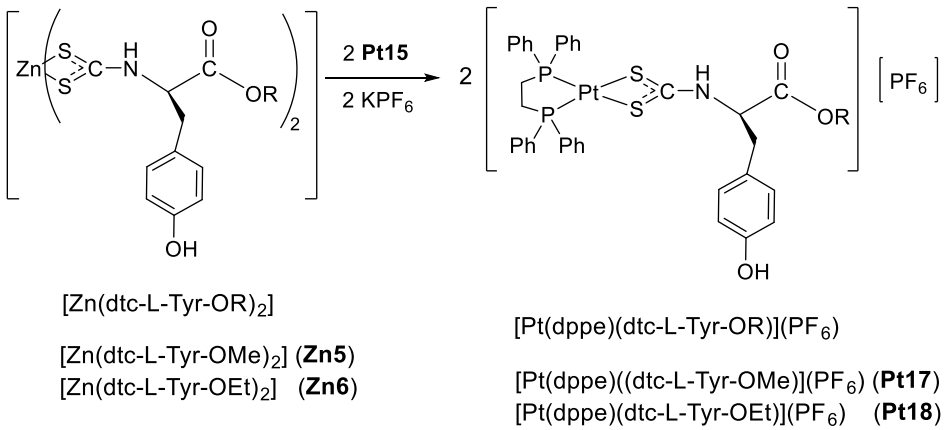

Figure 5.9: General reaction scheme for the preparation of **Pt17** and **Pt18**.

The novel gold(III)-dithiocarbamato amino acid ester derivatives **Au5** and **Au6** were prepared analogously after transmetallation of the zinc(II) intermediates with the organometallic compound [Au(Bnpy)Cl2] (**Figure 5.10**).

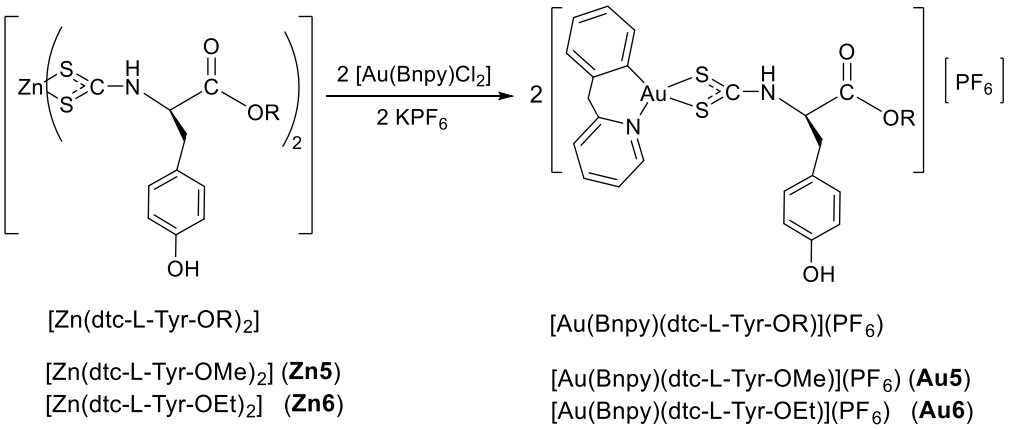

Figure 5.10: General route for the preparation of **Au5** and **Au6**.

All the newly isolated compounds were characterized employing IR, mono- and multidimensional NMR and fluorescence spectroscopy. Evaluation of their *in vitro* cytotoxic activity toward selected human tumor and non-tumor cell lines is currently in progress.

5.3 Synthesis

During my PhD, alongside my research project, I had the opportunity to carry out an original side project, which is highly connected with the platinum(II) and gold(III)

chemistry already developed within the group. In the present study, four novel naturally fluorescent metal-based dithiocarbamato amino acid ester derivatives have been successfully synthesized. I contributed to this by re-synthesizing the zinc(II)-dithiocarbamato intermediates (**Zn5**, **Zn6**) already developed from Rosy Polisicchio, preparing the starting **Pt15** and [Au(Bnpy)Cl_2], optimizing the experimental conditions in order to generate the target **Pt17**, **Pt18** and **Au5, Au6** complexes and performing their full spectroscopic characterization.

5.3.1 Preparation of the zinc(II)-dithiocarbamato *L*-tyrosyl ester derivatives

For detailed experimental conditions and full characterization see **Chapter 7**.

Generation of the object dithiocarbamate derivatives occurred via a one-pot reaction with carbon disulfide (CS_2) under basic conditions and low temperature in DMF. Once the desired dithiocarbamate ligands were successfully prepared in solution, subsequently reacted with [Zn$(OAc)_2 \cdot 2H_2O$] in a 2:1 ligand-to-metal ratio for 24 hours, to obtain the corresponding [Zn(dtc-*L*-Tyr-OMe)$_2$] (**Zn5**) and [Zn(dtc-*L*-Tyr-OEt)$_2$] (**Zn6**) derivatives (**Figure 5.11**). After completion of the reaction, the addition of H_2O afforded the desired complexes in the form of off-white solids in yields over 85%. The target compounds were characterized employing IR, mono- and multinuclear NMR spectroscopy.

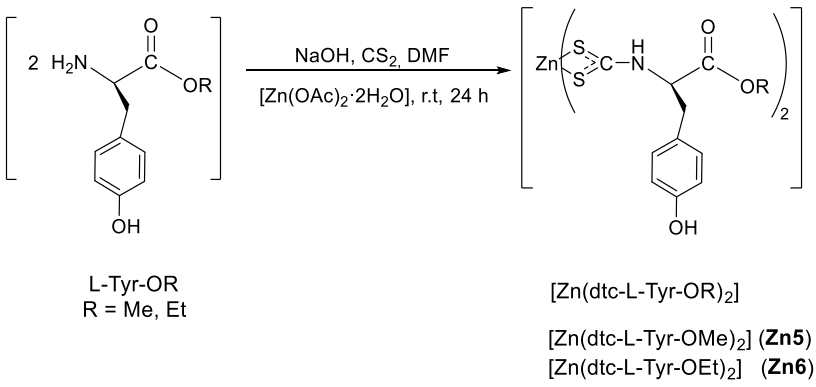

Figure 5.11: Synthetic path for the preparation of the intermediate complexes **Zn5** and **Zn6**.

In the mid-IR spectra, the appearance of a characteristic band at 1519 cm^{-1} confirms the stretching vibration ν(N-CSS).[39,40] According to the Bonati-Ugo method, recording of a single band at 1026 cm^{-1} indicates the antisymmetric stretching of

dithiocarbamates ν_a(CSS).[41] Moreover, diagnostic absorption bands at 3230, 1740, and 1110 cm^{-1} denote the presence of the ν(NH+OH), ν(C=O), and ν(C-O_{ester}) vibrations of the L-tyrosine ester moiety. The far-IR spectra from 400 to 200 cm^{-1} revealed an intense peak at 320 cm^{-1} which points out the antisymmetric stretching $\nu_a(ZnS_4)$ (**Table 5.1**).[42]

Complex	ν(C=O)	ν(C-O_{ester})	ν(N-CSS)	$\nu_{a/s}$(SCS)	$\nu_a(ZnS_4)$
Zn5	1754	1113	1435	1060/521	374
Zn6	1738	1114	1519	1026/524	324

Table 5.1: Selected IR absorptions with CsI disk of complexes **Zn5** and **Zn6**.

Comparisons between the starting materials and zinc(II) intermediates provided further evidence of successful formation. The ^{1}H-NMR of **Zn5** indicated the downfield shifting of protons H^c and H^d (**Figure 5.12**) from 3.47 to 4.61 ppm and 2.69 to 2.95 ppm, respectively. Additionally, the NH_2 group experiences a great shift from 1.72 ppm to 10.24 ppm. Also, in the spectrum of **Zn6**, the signature downfield shifting of the NH_2 group from 1.68 towards 10.21 ppm was observed. Moreover, downfield trend was observed for protons H^b and H^c from 2.69 to 4.06 ppm and 3.45 to 4.56 ppm, respectively. In the $^{13}C\{^1H\}$ NMR spectra of **Zn5** and **Zn6**, the diagnostic peak of the -NCSS group was present at 207 ppm (**Table 5.2**).

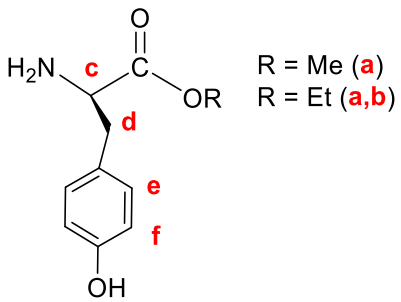

Figure 5.12: Labeling scheme of the starting *L*-tyrosine-OR esters.

Complex	^{1}H NMR (ppm)			^{13}C NMR (ppm)	
	NH	H^c	H^d	NCSS	C=O
Zn5	10.24	4.61	2.95	207.20	170.83
Zn6	10.21	4.06	4.56	207.17	170.64

Table 5.2: Selected ^{1}H and $^{13}C\{1H\}$ NMR resonances of the intermediates **Zn5** and **Zn6**.

5.3.2 Synthesis and characterization of the novel platinum(II)-dithiocarbamato *L*-tyrosyl ester complexes

For detailed experimental conditions and full characterization see **Chapter 7**.

The object complexes were synthesized through the well-known transmetallation reaction of **Zn5** and **Zn6** with the **Pt15** complex. The Zn(II)-Pt(II) transmetallation took place in DMF in a 2:1 ligand-to-metal ratio for 17 hours with KPF_6 as counterion to maintain charges neutrality. The novel complexes [Pt(dppe)(dtc-*L*-Tyr-OMe)](PF_6) **Pt17** and [Pt(dppe)(dtc-*L*-Tyr-OEt)](PF_6) **Pt18** were isolated with yields above 90% after the addition of H_2O and multiple washings with MeOH (**Figure 5.13**). The desired compounds were isolated as off-white crystalline solids and characterized by IR, NMR, and fluorescence spectroscopy. Due to the particular structural similarities and equivalent spectral patterns of **Pt17** and **Pt18**, the mid- and far-IR, ^{1}H, and $^{13}C\{^{1}H\}$ NMR spectra of the novel complex **Pt18** presented below as an example.

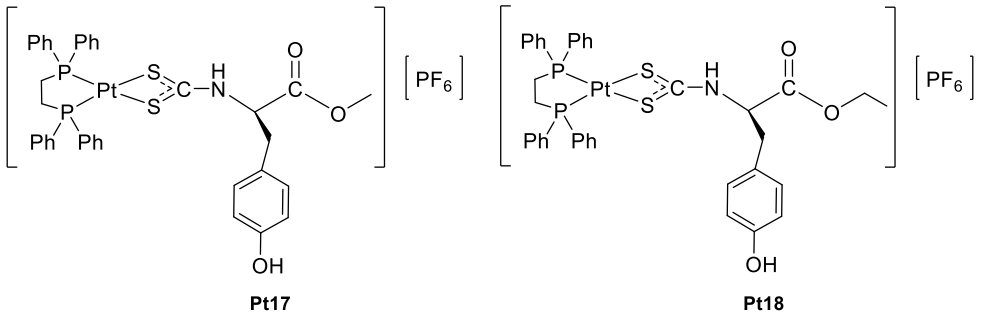

Figure 5.13: Schematic representation of complexes **Pt17** and **Pt18**.

Recording of the infrared spectra of the newly synthesized compounds revealed characteristic absorption frequencies at 1740, 1107, 1026 cm^{-1} which were assigned to the v(C=O), v_a(P-Ph), and v_a(SCS), respectively. The bond between the platinum metal center and the phosphorus atoms of the dppe presented a broad stretching signal at 490 cm^{-1} (v_a(P-Pt-P)). The signal at 401 cm^{-1} of the v(S-Pt-S) indicated successful coordination of the dithiocarbamato moiety. The sharp bands at 841 and 558 cm^{-1} were the signature $v_a(PF_6^-)$ and $\delta_{ip}(PF_6^-)$ vibrations of the counterion PF_6^- (**Table 5.3, Figure 5.14**).[42,43,44]

Complex	ν(C=O)	ν_a(P-Ph)	ν_a(SCS)	$\nu_a(PF_6^-)$	ν_a(S-Pt-S)	ν_a(P-Pt-P)
Pt17	1747	1107	1026	841	401	491
Pt18	1740	1107	1026	841	402	492

Table 5.3: Selected IR absorptions with CsI disk of **Pt17** and **Pt18**.

Then, the platinum complexes were characterized employing ^{1}H, $^{13}C\{^{1}H\}$ and multidimensional NMR. Comparing the chemical shifts of the newly synthesized species with the starting zinc(II) intermediates, a slight downfield shifting tendency was observed due to the increase of the electron density upon the addition of the dppe ligand. Specifically, groups closer to the reaction center, such as the H^c, showed a shifting of about 0.2 ppm (**Figure 5.15**). The overlapped signals at 7.60-7.74 ppm were assigned to the phenyl rings of the organophosphine ligand and confirmed the successful preparation of the desired complexes. Additionally, the NH group experiences a slight shift of 0.1 ppm, while the OH group experiences a shifting of about 1.6 ppm (**Table 5.4**).

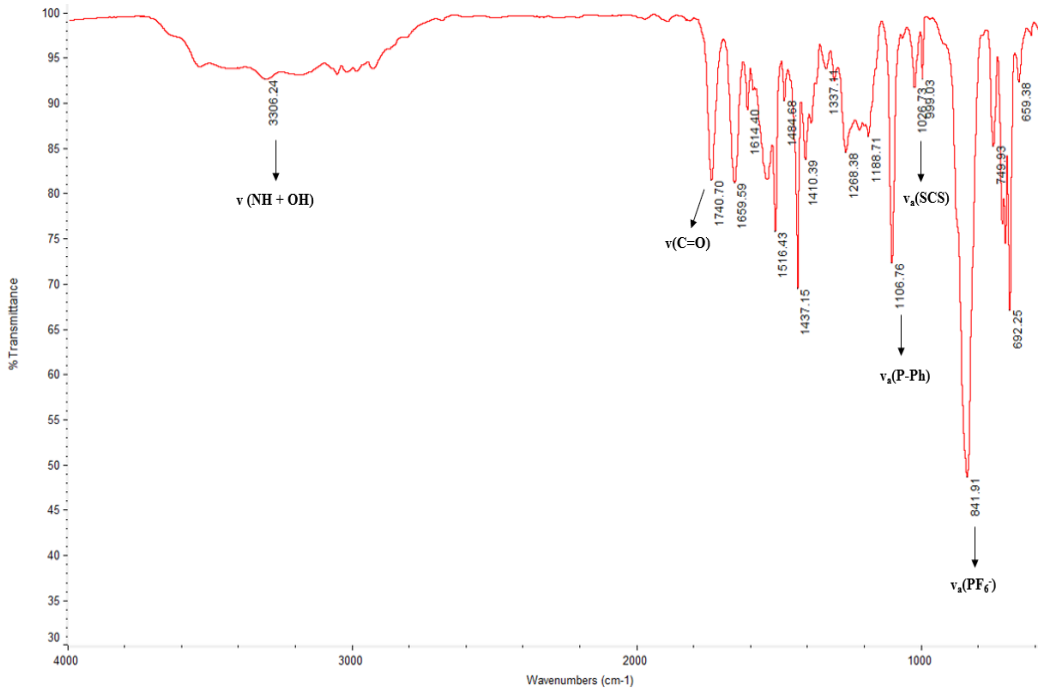

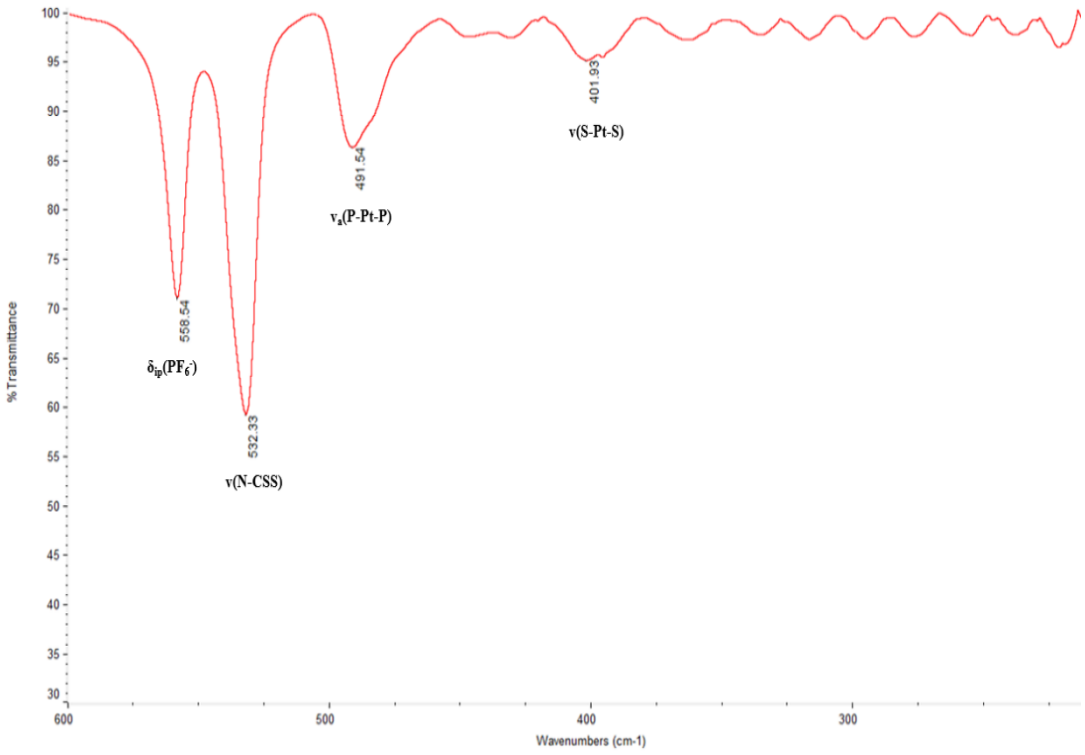

Figure 5.14: Mid-IR (top, 4000-400 cm^{-1})and Far-IR (bottom, 600-200 cm^{-1}) spectra with CsI disk of **Pt18**.

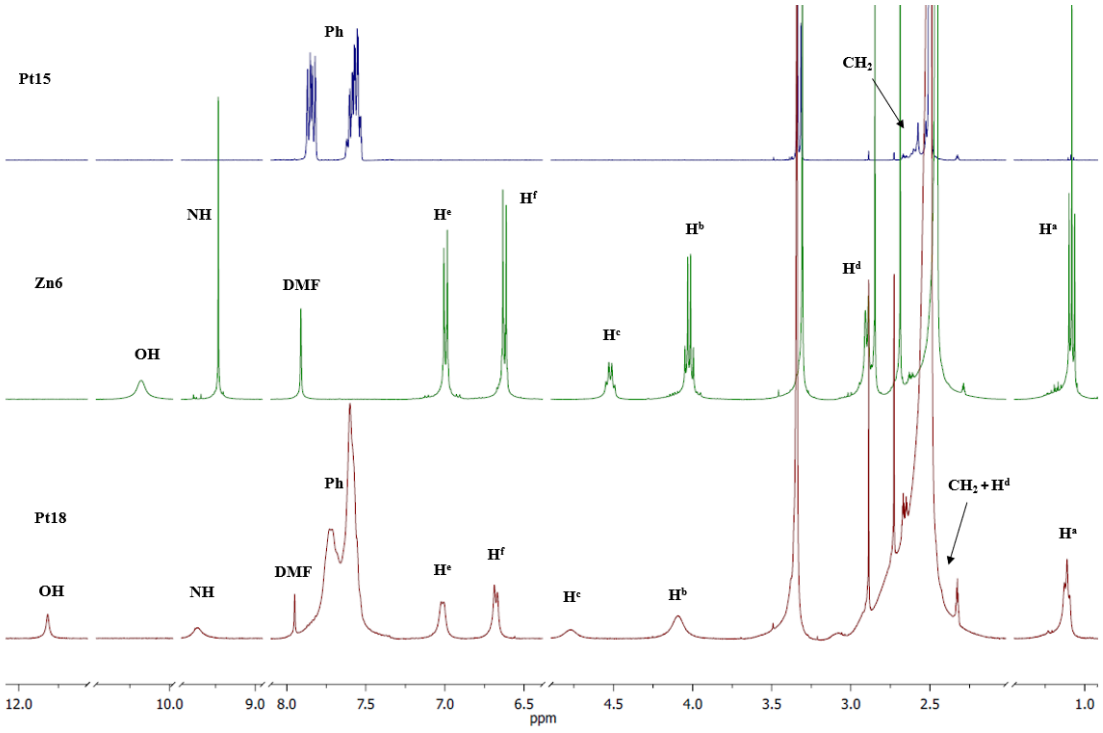

Figure 5.15: Comparative ^{1}H NMR spectra in DMSO-d_6 of **Pt15**, **Zn6** and **Pt18**.

The presence of characteristic signals in the $^{13}C\{^{1}H\}$ NMR spectra was a further evidence of the successful generation of **Pt17** and **Pt18**. Indeed, the diagnostic signal of the dithiocarbamato moiety, observed at 190 ppm, showing that the dithiocarbamic signal was shifted compared to the signal of the corresponding zinc(II) analogs (207 ppm) (**Figure 5.16**). The low-intensity peak at 169 ppm was assigned to the C=O group, while the C-OH was detected at 156 ppm. Furthermore, the signals of the phenyl rings and the CH_2 groups of the dppe ligand were present at 129-132 and 26-27 ppm, respectively (**Table 5.4**).

Complex	**^{1}H NMR (ppm)**			**^{13}C NMR (ppm)**		
	NH	H^c	H^d	NCSS	C=O	Ph rings
Pt17	9.37	4.83	3.12	192.23	169.28	129.54-132.73
Pt18	9.36	4.76	3.08	190.74	168.93	129.38-132.84

Table 5.4: Selected ^{1}H, ^{13}C{1H} NMR resonances of **Pt17** and **Pt18**.

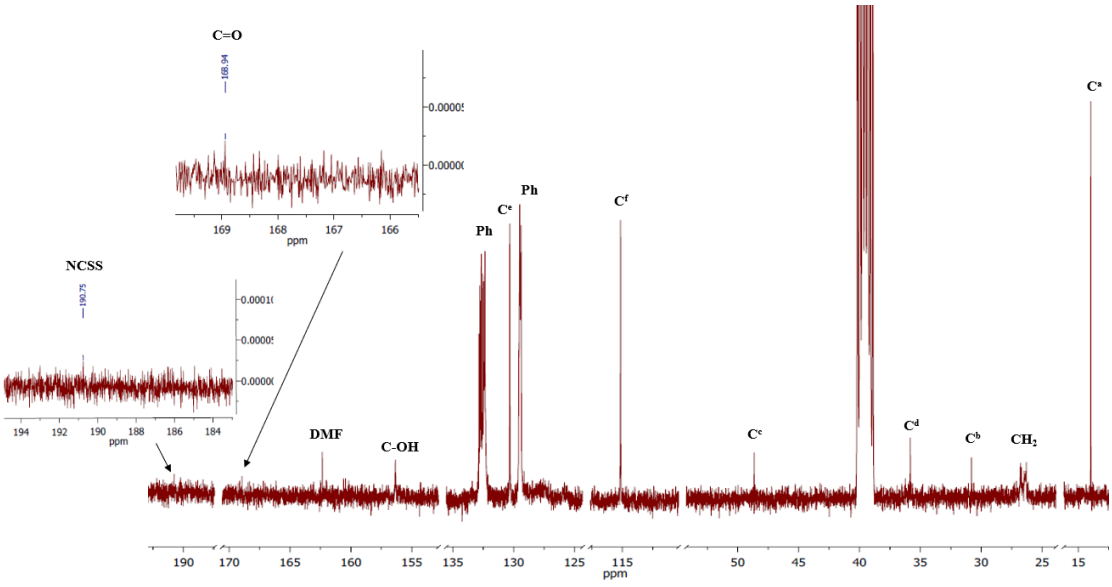

Figure 5.16: $^{13}C\{^{1}H\}$NMR spectrum of **Pt18** in DMSO-d_6.

Moreover, both the excitation and emission spectra were recorded for **Pt17** and **Pt18** (**Figure 5.17**). Typically, the energy differences in the absorption and emission spectra are similar, thus the Gaussian bands are approximately mirrored images of each other. Since the sample of interest was irradiated with a wide spectrum of wavelengths, a range of allowed transitions between the various vibrational energy

levels of the excited states emerged. In particular, the absorption spectrum of **Pt17** contains peaks at 328 and maximum at 376 nm while **Pt18** at 327 and maximum at 376 nm. Upon excitation at 370 nm, scanning of the region from 400 to 700 nm, revealed their emission spectral profile. Both complexes demonstrated the same transitions for absorption and emission, and as a result, the fluorescence spectra adhered to the mirror image rule as broadband with a maximum at 438 nm and an overlapped peak at 494 nm for **Pt17** and 423 and 468 nm for **Pt18**, respectively. The difference between the maximum wavelengths in the excitation and emission spectra is generally known as Stokes's shift, which gives a value of 62 nm for **Pt17** and 47 nm for **Pt18**. Both complexes demonstrated a good response to the long-wave UV radiation spectrum with intense absorption at 376 nm, while each compound exhibits violet light emission in the visible electromagnetic spectral region.

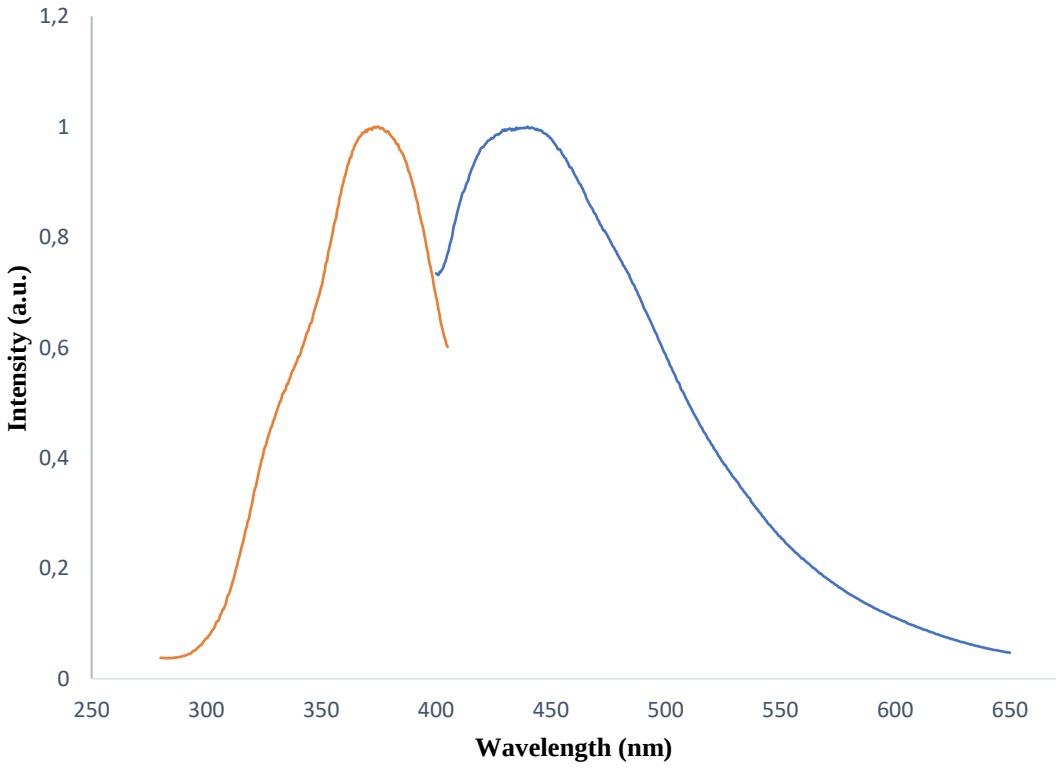

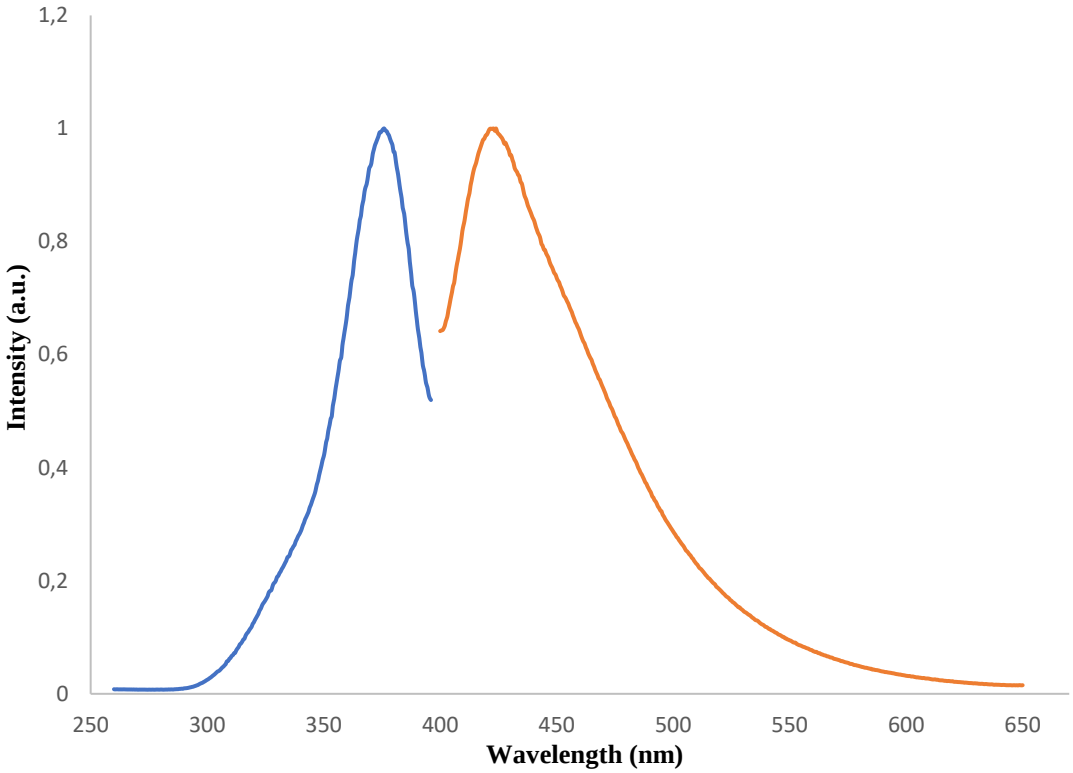

Figure 5.17: Top: Combination of absorption (left) and emission (right) spectra of **Pt17**. Bottom: Absorption (left) and emission (right) spectra of **Pt18**. The intensity has been normalized to the maxima. All measurements took place in HPLC grade DMSO solution, C = 1μg/ml.

5.3.3 Synthesis and characterization of the novel gold(III)-dithiocarbamato *L*-tyrosyl ester derivatives

For detailed experimental conditions and full characterization see **Chapter 7**.

After the successful isolation of the target **Pt17** and **Pt18** complexes, preparation of the organometallic gold(III) complexes **Au5** and **Au6** was also achieved (**Figure 5.18**). The synthesis of the target complexes was accomplished through transmetallation reaction of the starting reagent [Au(Bnpy)Cl_2] and the corresponding zinc(II)-dithiocarbamato intermediates **Zn5** and **Zn6** in a 2:1 ligand-to-metal ratio.[45,46a] The aforementioned one-pot reaction took place in DMF at room temperature where KPF_6 was added in slight excess to maintain charges balance. After 17 hours, the addition of H_2O and multiple washings with MeOH yielded the novel organometallic complexes [Au(Bnpy)(dtc-*L*-Tyr-OMe)](PF_6) (**Au5**) and

[Au(Bnpy)(dtc-*L*-Tyr-OEt)](PF_6) (**Au6**) in yields above 85% in the form of a fine yellow powder.

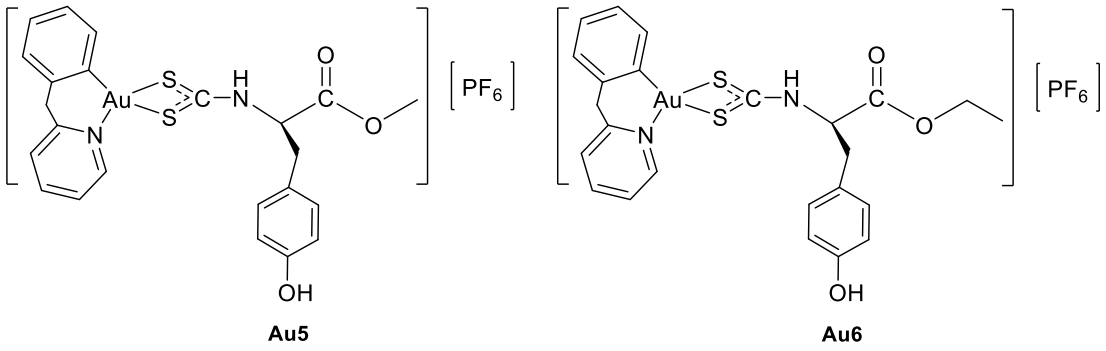

Figure 5.18: Schematic representation of the complexes **Au5** and **Au6**.

For both complexes, infrared spectroscopy revealed the diagnostic stretching vibration of the ν(C=O) at 1740 $cm^{-1}$and the antisymmetric stretching ν_a(SCS) at 1026 cm^{-1}. The appearance of the typical bands of the aromatic rings in the regions between 1612-1440 cm^{-1} and 755 cm^{-1} ($\nu(C–C)_{aromatic}$ and δ_{oop}(C-H), respectively) indicated the successful transmetallation. The sharp bands at 843 and 558 cm^{-1} were the signature $\nu_a(PF_6^-)$ and $\delta_{ip}(PF_6^-)$ vibrations of the counterion PF_6^-. Additionally, the medium intensity peak at 437 cm^{-1} was assigned to the $\nu_{a/s}$(S-Au-S) vibration (**Table 5.5, Figure 5.19**).[41, 42,46b]

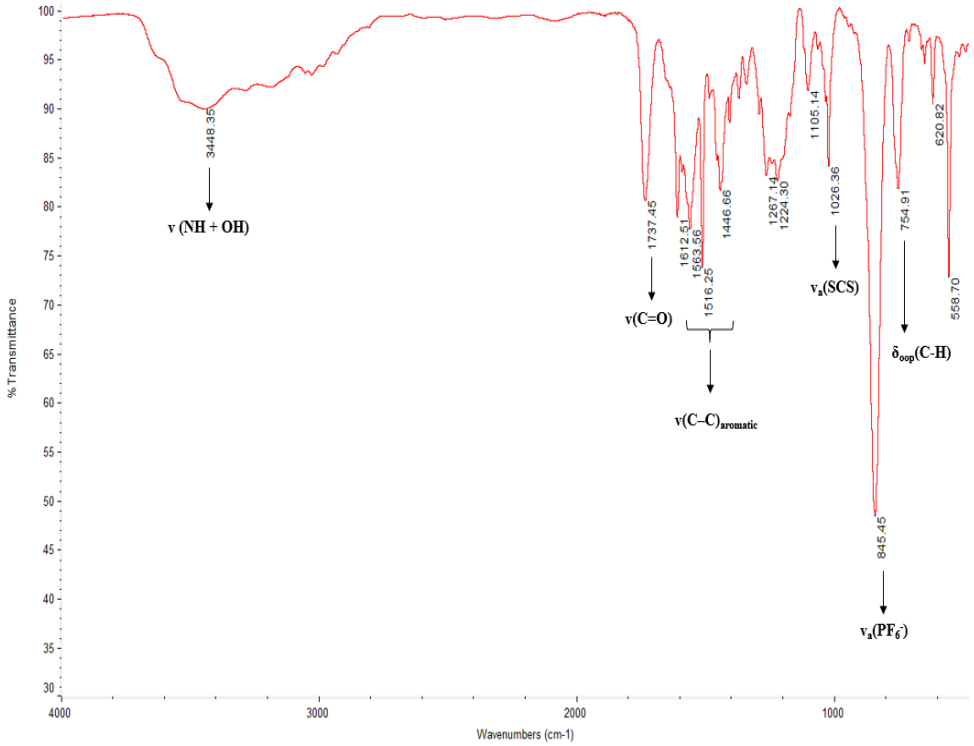

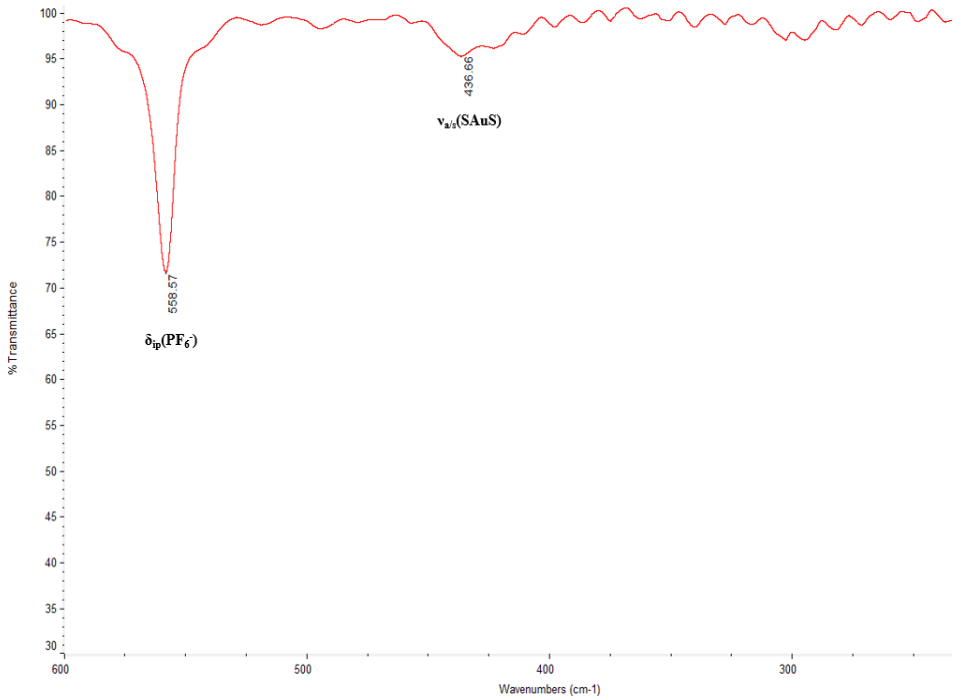

Figure 5.19b: Mid-IR (top, 4000-600 cm^{-1}) and Far-IR (bottom, 600-200 cm^{-1}) spectra with CsI disk of **Au6** derivative.

Complex	ν(C=O)	ν_a(SCS)	$\nu_a(PF_6^-)$	δ_{oop}(C-H)	$\nu_{a/s}$(S-Au-S)
Au5	1745	1026	843	755	437
Au6	1737	1026	845	754	436

Table 5.5: Selected IR absorptions with CsI disk of **Au5** and **Au6**.

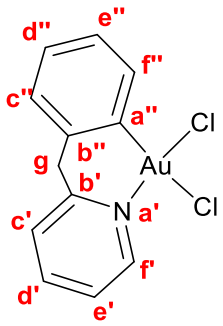

Figure 5.20: Labeling scheme of the starting reagent [Au(Bnpy)Cl_2].

Further insights into the structure of **Au5** and **Au6** gave the study of mono- and multidimensional NMR. A general slight upfield shift of the protons $H^{c''}$-$H^{f''}$ and $H^{c'}$-

$H^{f'}$ (**Figure 5.20**) observed while the protons H^{g} were present at 4.46 ppm. Protons H^{b} and H^{c} of the *L*-tyrosine ester (**Figure 5.12**) were overlapped at 4.09 ppm (**Figure 5.21**). In the $^{13}C\{^{1}H\}$ the diagnostic peak arising from the –NCSS carbon was recorded at 205 ppm for **Au5** and 203 ppm for **Au6**. The low-intensity peak at 168 ppm was assigned to the C=O group, while the C-OH signal was present at 156 ppm (**Figure 5.22**). Selected ^{1}H, $^{13}C\{^{1}H\}$ NMR resonances of the newly formed organometallic gold(III) complexes are given in **Table 5.6**.

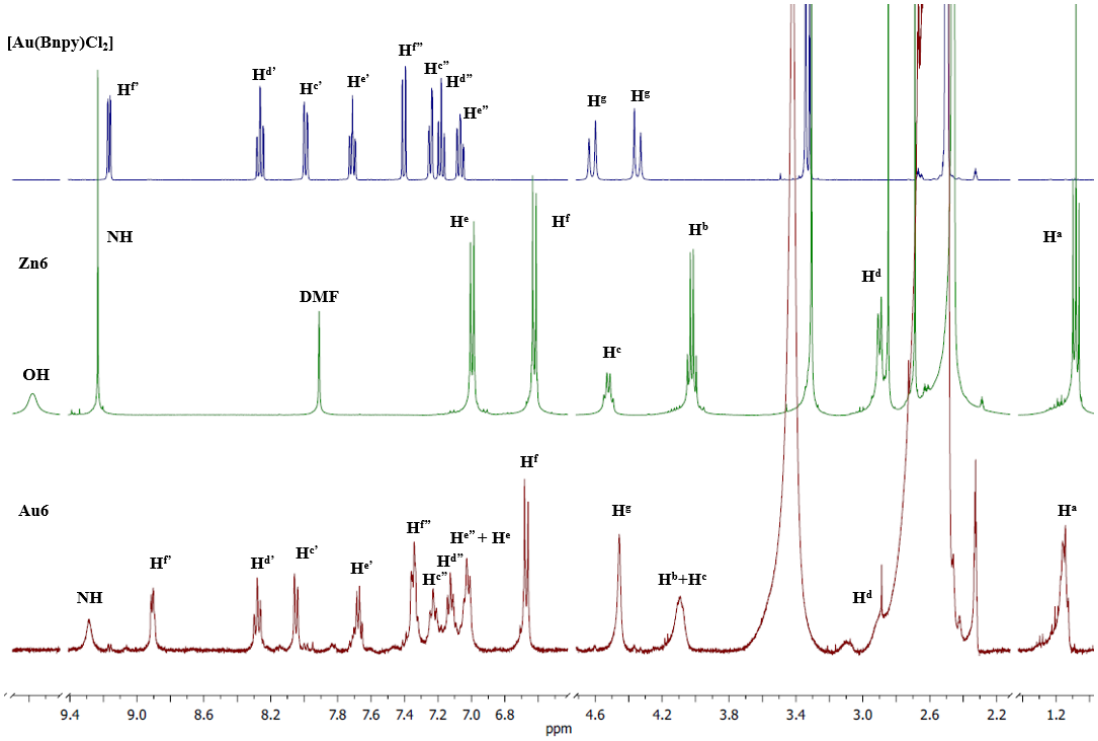

Figure 5.20: Comparative ^{1}H-NMR spectra of [Au(Bnpy)Cl_2], **Zn6** and **Au6** in DMSO-d_6.

Complex	^{1}H NMR (ppm)			^{13}C NMR (ppm)		
	NH	H^{c}	H^{g}	NCSS	C=O	C^{g}
Au5	9.33	4.85	4.48	215.89	168.19	46.06
Au6	9.29	4.09	4.46	213.71	167.68	46.06

Table 5.6: Selected ^{1}H, $^{13}C\{1H\}$ NMR resonances of **Au5** and **Au6**.

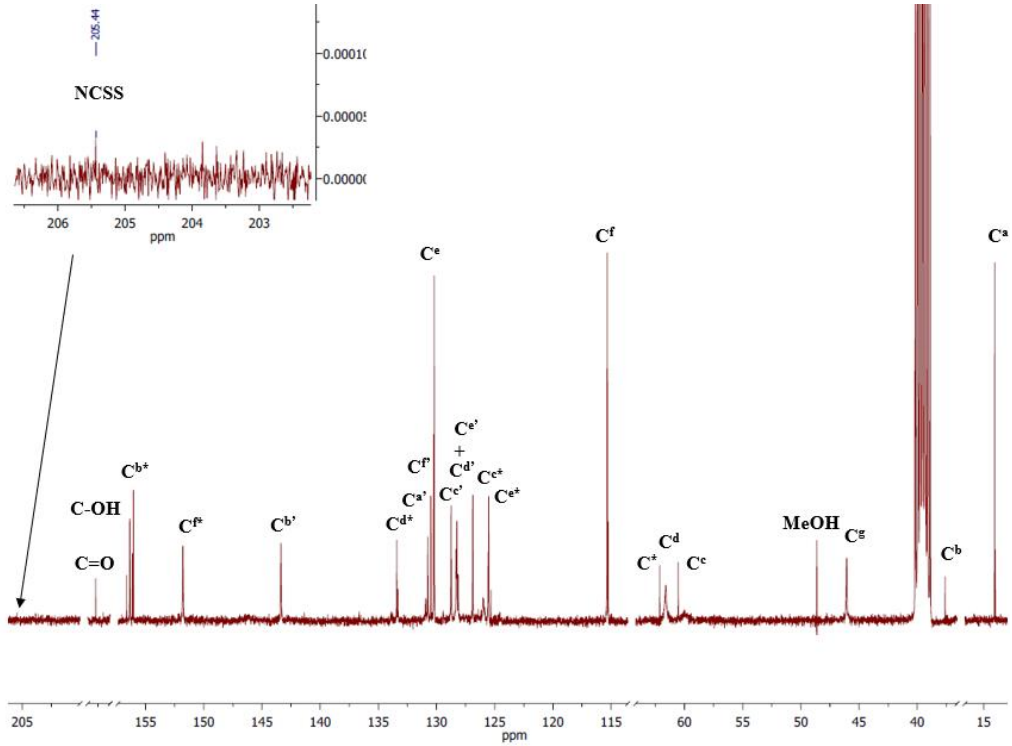

Figure 5.22: $^{13}C\{^{1}H\}$NMR spectrum of **Au6** in DMSO-d_6.

Additionally, fluorescence spectroscopy measurements were performed in the region from 250 to 700 nm (**Figure 5.23**). Absorption maxima were recorded at 334 and 394 nm for **Au5** and intense fluorescence emission was recorded as broadband with a maximum at 443 nm, while two more peaks were recorded at 530 and 670 nm. Interestingly, the emitted photons were shifted to longer wavelengths, thus resulting in a Stokes Shift value of 49 nm. **Au6** presented similar behavior with absorption maxima at 366 and 395 nm and fluorescence emission at 449, 489, and 672 nm. The Stokes shifting, in this case, was equal to 54 nm. The complexes demonstrated a good response to the long-wave UV radiation spectrum and exhibited violet light emission.

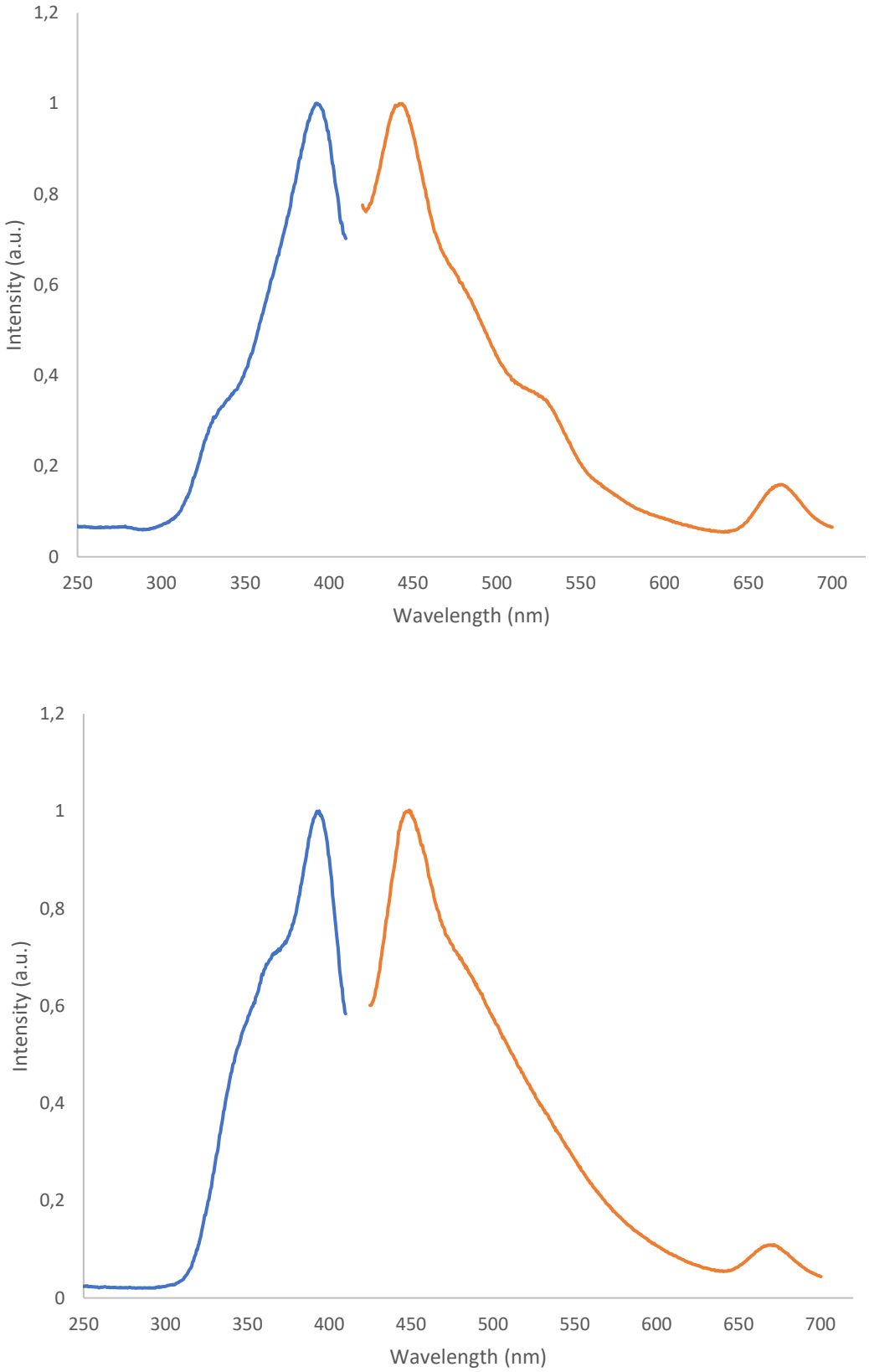

Figure 5.21: Top: Combination of absorption (left) and emission (right) spectra of **Au5**. Bottom: Absorption (left) and emission (right) spectra of **Au6**. The intensity has been normalized to the maxima. All measurements took place in HPLC grade DMSO solution, C = 1μg/ml.

5.4 Conclusions

Over the past years, amino acids have gained significant critical attention in cancer research. Several significant findings emerged about their role in tumor metabolism as nutrients, inhibitors, and epigenetic regulators. In an attempt to enhance our understanding towards the potential of amino acids in anticancer research, we designed four novel naturally fluorescent metal-dithiocarbamato *L*-tyrosine ester complexes of the type [M(dtc-*L*-Tyr-ester)(L)](PF_6), (M= Pt(II)/Au(III); dtc = dithiocarbamate; L: dppe = 1,2-bis(diphenylphosphino)ethane, Bnpy = benzylpyridine). In principle, the fluorescent aminoacidic substrates are expected to allow visualization of transport and cellular distribution of the novel **Pt17**, **Pt18**, **Au5**, and **Au6** complexes through fluorescence spectroscopy. The successful isolation of the object compounds were confirmed by several spectroscopic measurements. Fluorescence spectroscopy depicted sufficient photoluminescence at the long-wavelength region of the electromagnetic spectrum (>420 nm). Future studies include evaluation of their in vitro antiproliferative activity towards a panel of human tumor cell lines. Moreover, biological investigations about their mechanism of action and interactions with biological macromolecules will occur. Additionally, synthesis, characterization and biological assessment of the analogous gold(I)-based complexes of the general formula [Au(dtc-*L*-Tyr-ester)(L)], (dtc = dithiocarbamate; L: PPh_3 = triphenylphosphine, $BImEt_2$ = 1,3-diethylbenzimidazol-2-ylidene) would be worthwhile.

5.6 References

1. Vickery, B., Schmidt, A., *Chem. Rev.*, **9**, 169–318, (1931).
2. Akram, M., *et al., J. Med. Plants Res.*, **5**, 3997–4000, (2011).
3. Massey, A., Blakeslee, H., Pitkow, S., *Amino Acids*, **14**, 271–300, (1998).
4. Lukey, J., Katt, P., Cerione, A., *Drug Discov. Today*, **22**, 796–804, (2017).
5. a) Lieu, L., Nguyen, T., Rhyne, S., Kim, J., *Mol. Med.*, **52**, 15–30, (2020); b) Johannes, F., Vykoukal, V., Ostrin, J., *Frontiers in Oncology*, **10**, 1-8, (2020).
6. Abuchowski, A., *Cancer Biochem. Biophys.*, **7**, 175–186, (1984).
7. Wetzler, M., Sanford, B., Kurtzberg, J., De Oliveira, D., Frankel, S., *et al.*, *Blood*, **109**, 4164–4167, (2007).
8. Leu, Y., Wang, S., *Cancer*, **70**, 733–736, (1992).
9. Savoca, K. V. Davis, F., McCoy, R., Palczuk, C., *Cancer Biochem. Biophys.*, **7**, 261–268, (1984).
10. Gross, I., Demo, S., Dennison, J., Chen, L., Chernov-Rogan, T., *et al.*, *Mol. Cancer Ther.*, **13**, 890–901, (2014).
11. Xiang, Y., Stine, Z., Xia, J., Lu, Y., O'Connor, R., *et al., J. Clin. Investig.*, **125**, 2293–2306, (2015).
12. Pacold, E., Brimacombe, K., Chan, S., Rohde, J., Lewis, C., *et al., Nat. Chem. Biol.*, **12**, 452–458, (2016).
13. Anglin, J. Zavareh, R., Sander,P., Haldar, D., Mullarky, E., *et al., Bioorg. Med. Chem. Lett.*, **28**, 2675–2678, (2018).
14. Tonjes, M., Barbus, S., Park, Y., Wang, W., Schlotter, M., *et al., Nat. Med.*, **19**, 901–908, (2013).
15. Kandasamy, P., Gyimesi, G., Kanai, Y., Hediger, A., *Trends Biochem. Sci.* **43**, 752–789, (2018).
16. Gout, W., Buckley, A., Simms, C., Bruchovsky, N., *Leukemia*, **15**, 1633–1640,

(2001).

17. Schulte, L., Fu, A., Zhao, P., Li, J., Geng, L., Smith, S., *et al.*, *Nat. Med.*, **24**, 194–202, (2018).

18. Yun, W., Lee, S., Park, M., Kim, J., Yu, S., Park, M., *et al.*, *J. Pharm. Sci.*, **124**, 208–217, (2014).

19. Zhao, Y., Wang, L., Pan, J., *Intractable Rare Dis. Res.*, **4**, 165–169, (2015).

20. Chiangjong, W., Chutipongtanate, S., Hongeng, S., *Int. J. Oncol.*, **57**, 678–696, (2020).

21. Xie, M., Liu, D., Yang, Y., *Open Biol.* **10**, 7, (2020).

22. Anthony, J., Bolitho, E., Bridgewater, H., Carter, O., Donnelly, J., *Chem. Sci.*, **11**, 12888-12917, (2020).

23. Yousuf, I., Bashir, M., *Adv. Met. Prep. Appl. Med. Chem.*, Chapter 1, (2020).

24. Jung, Y., Lippard, S., *Chem. Rev.*, **107**, 1387–1407, (2007).

25. Kim, E., Rye, P., Essigmann, J., Croy, R., *J. Inorg. Biochem.*, **103**, 256–261, (2008).

26. Lazarević, T., Rilak, A., Bugarčić, Z., *Eur. J. Med. Chem.*, **142**, 8–31, (2017).

27. Leon, I., Cadavid-Vargas, J., Di Virgilio, A., Etcheverry, S., *Curr. Med. Chem.*, **24**, 112–148, (2017).

28. Li, D., Tian,J., Gu, W., Liu, X., Yan, S., *J. Inorg. Biochem.*, **104**, 171–179, (2010).

29. Iakovidis, A., Hadjiliadis, N., *Coord. Chem. Rev.*, **135**, 17–63, (1994).

30. Khan, T., Kumari, V., Goud, N., *J. Coord. Chem.*, **12**, 19–25, (1982).

31. Kumar, L., Kandasamy, N., Srivastava, T., Amonkar, A., Adwankar, M., *et al.*, *J. Inorg. Biochem.*, **23**, 1–11, (1984).

32. Mital, R., Srivastava, S., *Amino Acids*, **40**, 111-120, (1990).

33. Siu, M., Ma, L., Che, M., *Chem. Commun.*, **1**, 1025–1027, (2005).

34. Wagner-Schuh, B., Beck, W., *J. Inorg. and Gener. Chemistry*, **643**, 632–635,

(2017).

35. Yan, Q., Yuan, Z., Liu, G., Fu, B., *et al., Appl. Organomet. Chem.*, **31**, 1–9, (2017).

36. Gutiérrez. A., Bernal, J., Villacampa, M., Cativiela, C., Laguna, A., *et al., Eur. J. Inorg. Chem.*, **52** ,6473–6480, (2013).

37. Fernández-Moreira, V., Herrera, P., Gimeno, C., *Pure Appl. Chem.*, **91**, 247–269, (2019).

38. Fregona, D., Ronconi, L., Formaggio, F., Ping, D., Aldinucci, D., WO 2010/105691 A1, (2010).

39. Aravamudan, G., Brown, H. Venkappayya, D., *J. Chem. Soc. A*, **36**, 2744–2747, (1971).

40. Prakasam, B., Ramalingam, K., Bocelli, G., Cantoni, A., *Polyhedron*, **26**, 4489–4493, (2007).

41. Bonati, F., Ugo, R., *J. Organomet. Chem.*, **10**, 257–268, (1967).

42. Nakamoto, K., Infrared and Raman Spectra of Inorganic and Coordination Compounds, Part A, (2008).

43. Taylor, J., Odell, L., Raethel, A., *Spectrochim. Acta Part A Mol. Spectrosc.*, **24**, 1855–1861, (1968).

44. Daasch, W., Smith, C., *Anal. Chem.*, **23**, 853–868, (1951).

45. Shaw, A., Tilset, M., Heyn, R., Shaw, P., Tilset, M., *et al., J. Coord. Chem.*, **64**, 38–47, (2011).

46. a) Bertrand, B., Spreckelmeyer, S., Bodio, E., Cocco, F., *et al., Dalt. Trans.*, **44**, 11911–1191, (2015); b) Boscutti, G., Feltrin, L., Lorenzon, D., Sitran, S., Aldinucci, D., *et al., Inorg. Chim.Acta*, **393**, 304–317, (2012).

Chapter 6

6. Design, Synthesis and Biological Evaluation of Novel Platinum(II)-glycoconjugates

6.1 Background

Numerous studies on cancer therapy portray the use of a drug (or combination of drugs), which preferentially targets tumor cells, without having any significant toxic effect on healthy tissues.[1-3] As such, the research focus turned to selective and structurally diverse compounds, which potentially demonstrate improved therapeutic effectiveness and minor systemic and/or specific toxicity. To date, molecular biology has introduced various potential bio-targets for cancer therapy, such as the transmembrane glucose transporters (GLUTs).[4,5]

6.1.1 Tumor glycolysis: a brief overview

The process of glucose conversion into pyruvate followed by lactate production, known as glycolysis (**Figure 6.1**), has been proposed as an attractive therapeutic target for cancer therapy.[6-8]

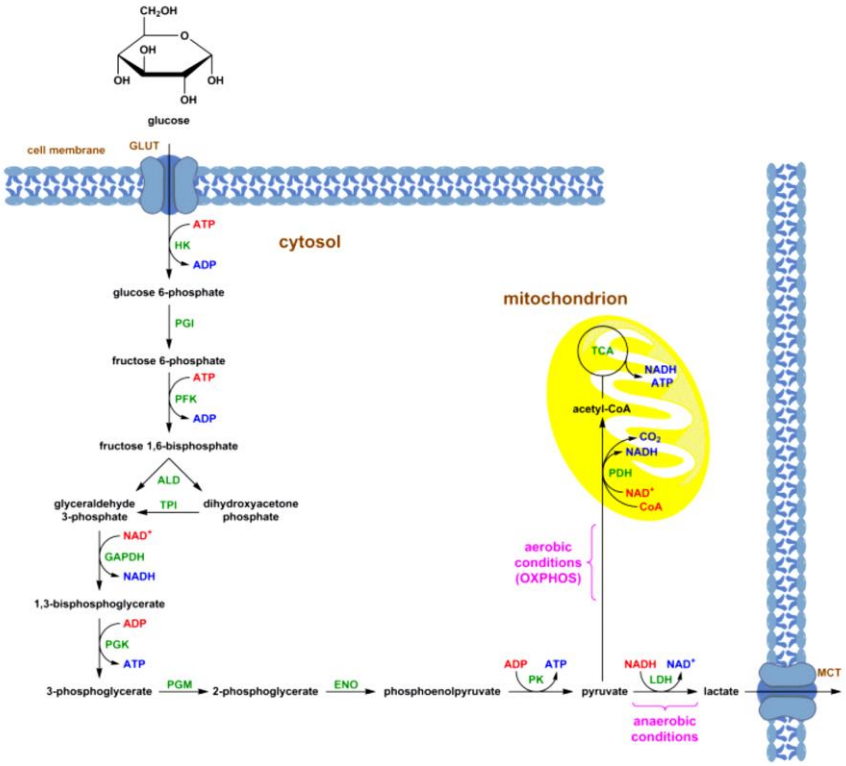

Figure 6.1: Schematic overview of the glycolytic pathway (GLUT: glucose transporter; ATP: adenosine- 5'-triphosphate; HK: hexokinase; ADP: adenosine-5'-diphosphate; PGI:

phosphoglucoseisomerase; PFK: phosphofructokinase; ALD: aldolase; TPI: triosephosphate isomerase; NAD^+: nicotinamide adenine dinucleotide - oxidized form; GAPDH: glyceraldehyde-3-phosphate dehydrogenase; NADH: nicotinamide adenine dinucleotide - reduced form; PGK: phosphoglycerate kinase; PGM: phosphoglycerate mutase; ENO: enolase; PK: pyruvate kinase; LDH: lactate dehydrogenase; MCT: monocarboxylate transporter; OXPHOS: oxidative phosphorylation; CoA: coenzyme A; PDH: pyruvate dehydrogenase; TCA: tricarboxylic acid (Krebs) cycle. [9]

Glucose, in healthy cells, undergoes under glycolytic pathway producing 36 molecules of adenosine triphosphate (ATP), the "cellular energy currency", in aerobic environment. On the other hand, in hypoxia condition, tumour cell environment, the same metabolic procedure stop to the production of pyruvate, which is converted to lactate, subsequently acidifying the extracellular environment (**Figure 6.2**).[10,11] Due to the inefficiency of this metabolic procedure, the tumor cells need to intake more glucose through membrane proteins (glucose transporters, GLUTs) and accelerate the metabolic rate of glycolysis.

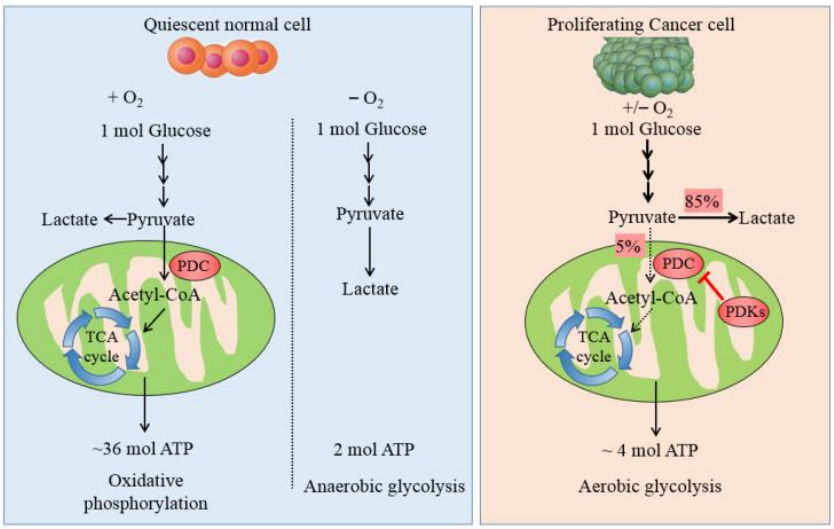

Figure 6.2: Schematic illustration of the metabolic pathway of glucose in normal (left) and tumor cells (right).[12]

6.1.2 GLUTs: glucose transporters

Under hypoxia conditions, hypoxia-inducible factor 1 (HIF-1, also known as ARNT) potentiates the transcription of several enzymes and the overexpression of glucose transporters 1 and 3 (GLUT1 and GLUT3).[13] The family of these membrane proteins consists of 14 different isoforms and their features categorized them into three classes. More precisely, Class 1 (GLUT1-GLUT4) is selective for glucose transport, whereas Class 2 (GLUT5) and Class 3 (GLUT6, GLUT8, GLUT10) show a preference for other sugars.[14-16] In vitro, vivo and clinical studies have indicated specific

biomolecules in glycolytic pathways as potential candidates in targeted anticancer therapy, such as the membrane proteins GLUT1 and GLUT3. Transporter GLUT1 shows a very high affinity for glucose and promotes its shuttle between blood and organs. Analogously, GLUT3 has a vital role in the carbohydrate's receipt and supports the maintenance of the glycolytic energy metabolism in cell regions of limited substrate supply.[17,18] Due to the increased demand for glucose in tumor cells, the overexpression of GLUT1 and GLUT3 reinforces the sugar's uptake and contributes to enhanced glycolysis. As such, synthetic methods are suggesting the attachment of anticancer agents on sugar scaffolds, in order to target tumor glycolysis. Compounds of this type have already entered Phase I-III clinical trials, and many others are undergoing preclinical evaluation.[19,20]

6.1.3 Targeting glucose transporters

So far, various compounds have been developed as specific inhibitors for biomolecules with key roles in glycolysis, which are currently on trial or have been approved as therapeutic agents against cancer.[21-23] Specifically, there are novel compounds able to inhibit the glycolytic pathway, reduce the glucose uptake and cell growth in vitro and in vivo, or induce apoptosis (e.g., WZB117 and STF-31, WZB27 and WZB115, 2-deoxy-D-glucose (2-DG), shRNA, anti-GLUT1 monoclonal antibody, antidiabetics, and hormones).[24-27] Alternative approaches are suggesting the design and development of anticancer agents that can be transported into cancer cells through GLUTs. Thus, exerting their activity directly inside, without inhibiting the membrane protein. These glycoconjugates are considered pro-drugs, where the structural features of the glucose-like scaffold conceal the attached anticancer drug.[28] This delicate model demonstrates successful applications such as the glycoconjugate 2-glucose-SNAP (SNAP: S-nitroso-N-acetylpenicillamine), which had up to 5000-fold higher cytotoxicity toward ovarian carcinomas in vitro compared with the non-conjugated SNAP precursor.[29] Also, glufosfamide is currently undergoing Phase III clinical trials (**Figure 6.3**).

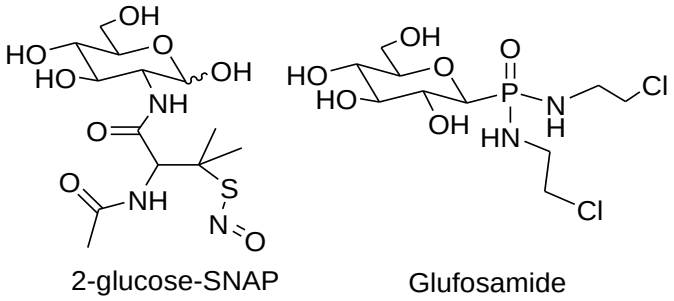

Figure 6.3: Chemical structures of 2-glucose-SNAP and glufosfamide.

Additionally, adriamycin (doxorubicin) conjugated with a glucose analog (2-amino-2-deoxy-d-glucose) and succinic acid (2DG-SUC-ADM) was designed to target tumor cells through GLUT1, and proved effective against many types of solid tumors in clinical applications (**Figure 6.4**).[30]

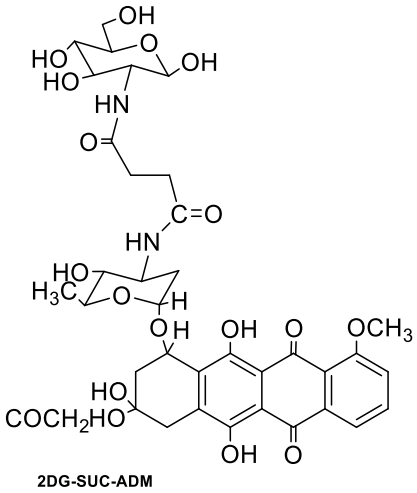

Figure 6.4: Chemical structure of the drug 2DG-SUC-ADM.

6.1.4 Metal-based glycoconjugates

Apart from the organic glycoconjugates, there are several glucose-like metallodrugs with well-defined pharmacological profiles. The sensing of the glucose unit by GLUTs is strongly dependent on where the metal-containing scaffold bonds on the carbohydrate ligand. As such, the presence of a free anomeric group of the glycomimetic moiety oblige the recognition by GLUTs.[9,19,31] In particular, the research groups of Tsubomura and Keppler have reported the synthesis of a series of cisplatin and cisplatin-like glycoconjugates (**Figure 6.5**) that demonstrate anticancer activity comparable to cisplatin.[32,33]

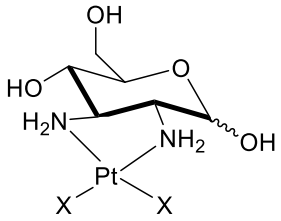

Figure 6.5: Chemical structures of cisplatin-like glycoconjugates.

Likewise, Hanessian and Wang investigated the same type of metal complexes derivatized with diaminohydroxypyrano and/or diaminometoxypyrano ligands (**Figure 6.6**).[34]

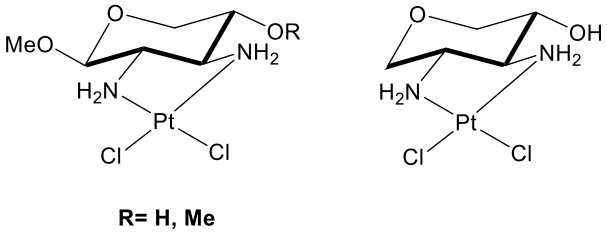

Figure 6.6: Chemical structures of cisplatin-diaminomethoxypyrano (left) and -diaminohydroxypyrano (right) conjugates.

Chen and co-workers synthesized cisplatin analogs bearing a monosaccharide moiety connected through different diaminopropano spacers and found that complexes containing α-anomers were overall more active than the corresponding β-anomers (**Figure 6.7**).[35,36]

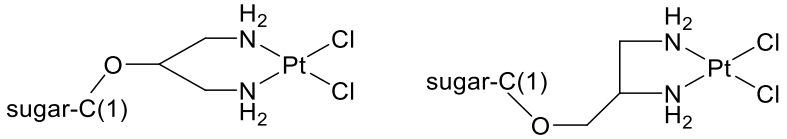

Figure 6.7: Chemical structures of cisplatin monosaccharide moieties, sugars: glucose, galactose, mannose, both α and β anomers.

Similar studies on glycosylated analogs of well-known chemotherapeutic agents displayed increased cytotoxicity in all the tested human carcinoma cell lines.[37-40] Additionally, glyco-functionalized organoplatinum derivatives show cytotoxic activity slightly higher than the reference drug cisplatin. Remarkably, the cationic water-soluble fluorescent organoplatinum compound [Pt(terpy)(glycosylated arylacetylide)]$^{+}$ proved to be an exception since it is 100-fold more active than

cisplatin and 8-fold more cytotoxic than the corresponding non-glycosylated analog (**Figure 6.8**).[41,42]

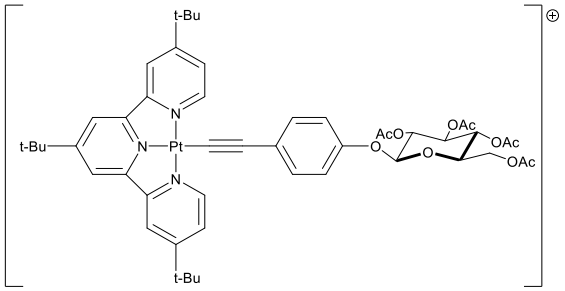

Figure 6.8: Chemical structure of the active [Pt(terpy)(glycosylated arylacetylide)]$^{+}$ complex.

It is worthwhile to mention that palladium(II) has attracted great interest in terms of anticancer potential due to its chemical similarities with platinum(II).[43] Interestingly, the amino-pyridine palladium(II) complex (**Figure 6.9**) presented greater in vitro and in vivo anticancer activity compared to its platinum(II) analog.[44]

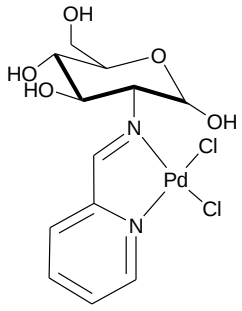

Figure 6.9: Chemical structure of [$PdCl_2$(L)] (L = 2-deoxy-2-[(2-pyridinylmethylene) amino]-α-D-glucopyranose).

Gold(I) complexes directly bound to a glucose-like scaffold have well-known antiproliferative properties. Specifically, auranofin (**Figure 6.10**) was extensively studied and showed promising anticancer activity in vitro. Moreover, N-heterocyclic (NHC) carbene gold(I) complexes presented stability under physiological-like conditions, thus appraised as potential cancer chemotherapeutics.[45]

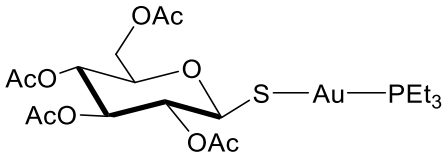

Figure 6.10: Chemical structure of auranofin.

Recently, the gold(III)-dithiocarbamato complex [$AuBr_2$(SSC-Inp-OEt)] proved cytotoxic toward several cancer cell lines, thus the analogous [$AuBr_2$(SSC-Inp-GlcN1)] glycoconjugate was synthesized.[46,47] An unanticipated finding was the antiproliferative activity against several cancer cell lines, with IC_{50} values ranging from 0.1 to 0.8 μM, of some trinuclear ruthenium(0)-carbonyl derivatives of bicyclophosphito-glucofuranoside (**Figure 6.11**).[48]

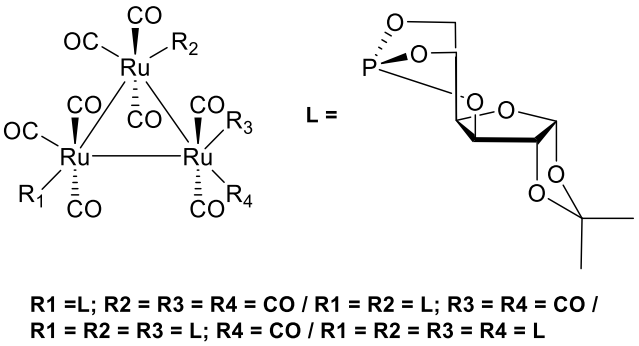

R1 =L; R2 = R3 = R4 = CO / R1 = R2 = L; R3 = R4 = CO /
R1 = R2 = R3 = L; R4 = CO / R1 = R2 = R3 = R4 = L

Figure 6.11: Chemical structure of the trinuclear ruthenium(0)-carbonyl complexes.

Glyco-functionalized mononuclear and binuclear copper(II) complexes tested in vitro, and although the results were somewhat promising, no further studies were performed to date.[49,50] Several titanocene derivatives with ribofuranosides were synthesized and tested toward a panel of human tumor cell lines.[51] Among all, the complex with two cyclopentadienyl ligands turned out to demonstrate activity comparable to cisplatin in human KB3-1 cervix carcinoma and murine L929 aneuploid fibrosarcoma cells (**Figure 6.12**). Additionally, molybdocene analogs investigated, but they have overall poor in vitro cytotoxic activity.[52]

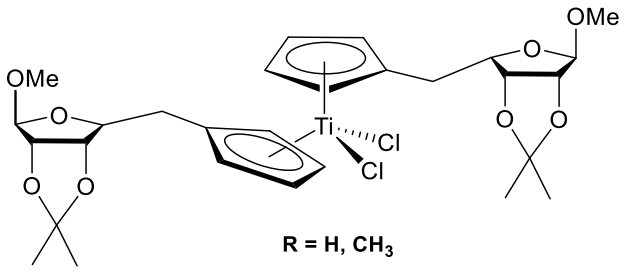

Figure 6.12: Chemical structure of the functionalized titanocene derivative.

According to Itoh and co-workers,[53] development of mono- and di-ferrocenyl derivatives (**Figure 6.13**) conjugated to various sugar moieties proved promising cytotoxic agents, with IC_{50} values in the low micromolar range. On the other hand, the attachment of carbohydrates to ^{99m}Tc-containing scaffolds generated by Schibli and co-workers yielded glycoconjugates with high stability in vitro, but their cellular uptake proved low and not mediated by a GLUT1-dependent process.[54]

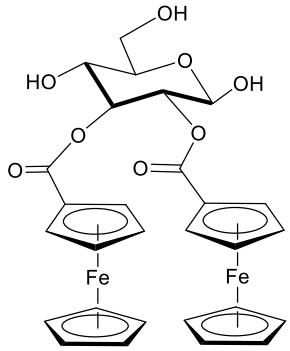

Figure 6.13: Chemical structure of the glyco-functionalized ferrocenyl derivative.

6.2 Strategy

Relying on the extensive research of former members of the research group on the development of novel gold(III) containing chemotherapeutics of the general formula $[AuBr_2(GLUdtc)]$ (GLU = glucose-like substrate; dtc = dithiocarbamato moiety) which are targeting glucose transporters (GLUTs). Synthesis of the analogous platinum(II)-glycoconjugates $[Pt(dppe)(GLUdtc)](PF_6)$ (dppe: bis(diphenylphosphino)ethane; GLU = glucose-like substrate; dtc = dithiocarbamato moiety) was planned.[55] This strategy was included in the pre-generation of zinc(II)-dithiocarbamato glycoconjugate precursors and the subsequent transfer of the whole dithiocarbamato ligand to the desired metal center via a transmetallation reaction.[56-58] From a synthetic perspective, insertion of an amino acidic rigid linker between the

dithiocarbamato function and the conjugated sugar provides the direct conversion of the amino terminus into an –NCSS group without affecting the carbohydrate scaffold. Besides, the carboxylic function can be easily activated with N,N,N′,N′-tetramethyl-O-(N-succinimidyl)uranium tetrafluoroborate (TSTU) and subsequently coupled to an amino sugar (**Figure 6.14**).[59] From a biological point of view, the rigid linker would reduce the steric hindrance around the anomeric site of the sugar, and allow at least in principle, its recognition by GLUTs.

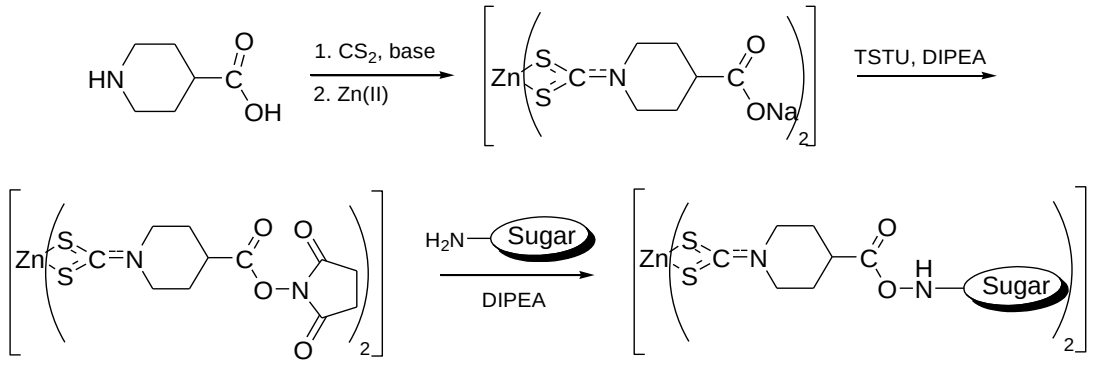

Figure 6.14: General synthetic route for the preparation of zinc(II)-dithiocarbamato glycoconjugates.

The initial plan involved the use of the $(PPh_4)[PtCl_3(NH_3)]$ (**Pt3**) (see **Chapter 3**) precursor for the transmetallation of the corresponding zinc(II)-dithiocarbamato glycoconjugate intermediates,[55] $[Zn(dtc\text{-}Inp\text{-}NH_2)_2]$ (**Zn7**), $[Zn(dtc\text{-}Inp\text{-}GlcN2)_2]$ (**Zn8**), $[Zn(dtc\text{-}Inp\text{-}GlcN3)_2]$ (**Zn9**) and $[Zn(dtc\text{-}Inp\text{-}GlcN4)_2]$ (**Zn10**), (dtc: dithiocarbamate, R= Inp-NH2:isonipecotamide, GlcN2:1-O-methyl-2-amino-2-deoxy-(α,β)-D glucopyranoside, GlcN3:1-O-methyl-6-amino-6-deoxy-α-D-glucopyranoside, GlcN4:2-aminoethyl-β-D-glucopyranoside). Despite the numerous attempts and exploitation of different experimental conditions, the expected mono-dithiocarbamato derivatives of the type $[PtCl(dtc\text{-}Inp\text{-}R)(NH_3)]$ were not obtained. Instead, the full replacement of both the chloride and the amino ligands with two dithiocarbamato ligands was observed (**Figure 6.15**).

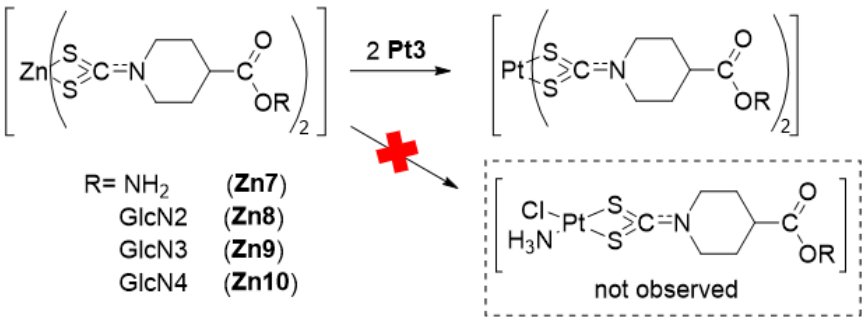

Figure 6.15: General scheme of the zinc(II)-platinum(II) transmetalation reaction.

As such, an alternative strategy was designed, which suggests the use of the **Pt15** (see **Chapter 4**).[60] Due to the enhanced affinity of the organophosphine (dppe) for the metal ion, a complex of greater stability can be obtained, which prevents the formation of the bis-dithiocarbamato derivatives. This ligand can potentially prevent an approaching nucleophile and enhance the chance to reach its pharmacological target intact. Once this synthetic strategy applied, a total of four novel platinum(II)-diphosphine glycoconjugates obtained, namely, [Pt(dppe)(dtc-Inp-NH_2)](PF_6) (**Pt19)**, [Pt(dppe)(dtc-Inp-GlcN2)](PF_6) (**Pt20**), [Pt(dppe)(dtc-Inp-GlcN3)](PF_6) (**Pt21**) and [Pt(dppe)(dtc-Inp-GlcN4)](PF_6) (**Pt22**). After the successful completion of the synthesis, preliminary biological evaluation of the novel platinum(II)-based derivatives (**Figure 6.16**) occurred.

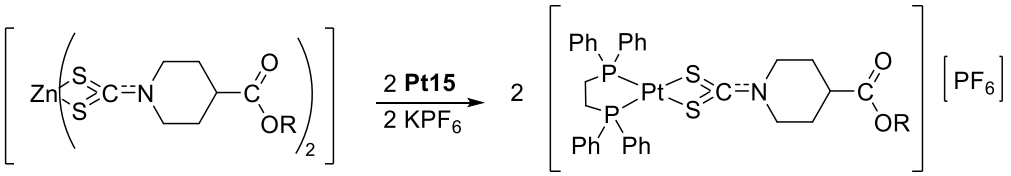

[Zn(dtc-Inp-R)$_2$]

[Zn(dtc-Inp-NH2)$_2$] (**Zn7**)
[Zn(dtc-Inp-GlcN2)$_2$] (**Zn8**)
[Zn(dtc-Inp-GlcN3)$_2$] (**Zn9**)
[Zn(dtc-Inp-GlcN4)$_2$] (**Zn10**)

[Pt(dppe)(dtc-Inp-R)](PF_6)

[Pt(dppe)(dtc-Inp-NH_2)](PF_6) (**Pt19**)
[Pt(dppe)(dtc-Inp-GlcN2)](PF_6) (**Pt20**)
[Pt(dppe)(dtc-Inp-GlcN3)](PF_6) (**Pt21**)
[Pt(dppe)(dtc-Inp-GlcN4)](PF_6) (**Pt22**)

Figure 6.16: General synthetic route for the preparation of **Pt19**-**Pt22**.

6.3 Synthesis

During my Ph.D., alongside my research project, I had the opportunity to carry out a side project highly connected with the carbohydrate chemistry already developed within the group. To date, several gold(III)-dithiocarbamato glycoconjugates have been isolated, however, isolation of their platinum(II)-based analogs proved challenging. As such, an alternative synthesis followed. I contributed to this, by re-synthesizing compounds already developed within the research group **Zn7-Zn10**, optimizing the experimental conditions to generate the novel platinum precursors **Pt19-Pt22**, and perform their preliminary biological evaluation towards a panel of human tumor cell lines.

6.3.1 Carbohydrate precursors

For detailed experimental conditions and full characterization see **Chapter 7**.

The first synthetic step includes the carbohydrate precursors (GlcN2, GlcN3, GlcN4),[61-63] which were readily available and previously synthesized according to well-established literature procedures by Dr. Andrea Pettenuzzo. Based on structural characteristics, three different amino sugar precursors were selected. Particularly, the **GlcN2** (1-O-methyl-2-amino-2-deoxy-(α,β)-D-glucopyranoside), **GlcN3** (1-O-methyl-6-amino-6-deoxy-α-D-glucopyranoside) and **GlcN4** (2-Aminoethyl-β-D-glucopyranoside) (**Figure 6.17**).

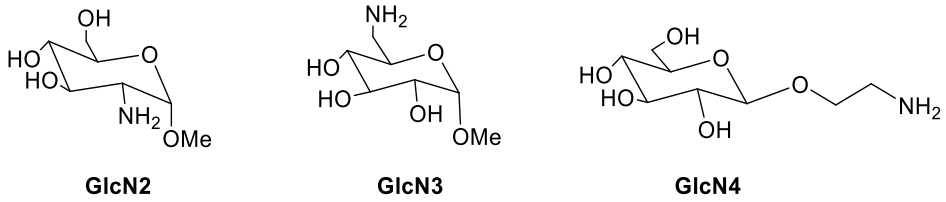

Figure 6.17: Chemical structures of the amino sugar precursors of the present study.

6.3.2 Synthesis of the zinc(II)-dithiocarbamato glycoconjugates

For detailed experimental conditions and full characterization see **Chapter 7**. For structure numbering see **Figure 6.21**.

Initially, the isonipecotamide-dithiocarbamato ligand was prepared in situ as a sodium salt (Na(dtc-InpNH$_2$)·MeOH following a well-established synthetic protocol.[64] Once the desired dithiocarbamate ligand generated in solution, subsequently reacted with [Zn(OAc)$_2$·2H$_2$O] in a 2:1 ligand-to-metal ratio to obtain **Zn7** (**Figure 6.18**).

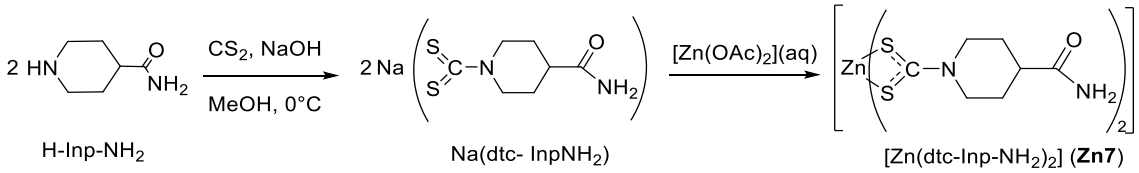

Figure 6.18: Synthetic route for the preparation of **Zn7**.

Complex **Zn7** was characterized employing IR, as well as mono- and multinuclear NMR. In the mid-IR spectrum, appearance of a characteristic band at 1492 cm^{-1} confirmed the presence of the ν(N-CSS).[65,66] Recording of a single band at 1007 cm^{-1} indicated the ν_a(CSS).[67] The far IR spectrum, revealed an intense peak at 392 cm^{-1} which pointed out the asymmetric stretching $\nu_a(ZnS_4)$ (**Table 6.1**).[68] Further evidence of the successful formation of **Zn7**, constitutes the downfield shifting trend of the proton signals, compared with the starting materials. This tendency was mainly observed for the equatorial protons $C^{2',6'}H$, cis-NH, and trans-NH. Additionally, the characteristic dithiocarbamic carbon peak was recorded at 202 ppm (**Table 6.2**). To synthesize the zinc(II)-dithiocarbamato glycoconjugates **Zn8**-**Zn10**, the intermediate complex $Na_2[Zn(dtc\text{-}Inp\text{-}O)_2]\cdot 2H_2O$ was initially prepared through an optimized literature procedure,[56] and subsequently its carboxylic function was activated with TSTU to yield the $[Zn(dtc\text{-}Inp\text{-}OSu)_2]$ intermediate (**Figure 6.19**).

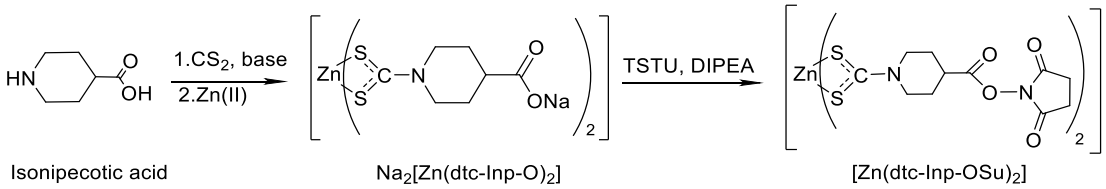

Figure 6.19: Stepwise synthesis of the zinc(II) intermediate $[Zn(dtc\text{-}Inp\text{-}OSu)_2]$.

Then, an excess of each glucose-like scaffolds was reacted with activated zinc(II) precursor in anhydrous DMF under basic conditions and yielded the corresponding **Zn8**, **Zn9**, and **Zn10** complexes (**Figure 6.20**).

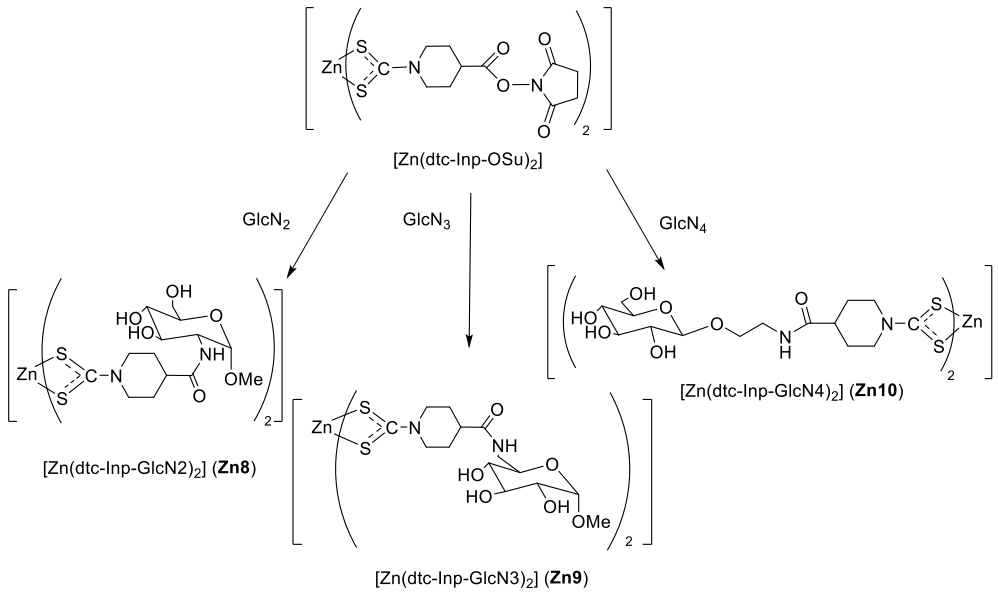

Figure 6.20: Synthesis of the zinc(II)-dithiocarbamato glycoconjugates **Zn8**-**Zn10**.

IR spectroscopic characterization of **Zn8**-**Zn10** revealed that atoms close to the newly formed amide bond display the most affected signals compared to the starting materials. Characteristic absorption bands of the intermediate [Zn(dtc-Inp-OSu)$_2$], such as the succinimidyl ester (ν_{ip}(C=O$_{succinimidyl}$), ν_{oop}(C=O$_{succinimidyl}$)) and ν(C=O$_{ester}$) at 1817, 1780 and 1737 cm^{-1}, respectively) and the amino/ammonium group of the modified carbohydrates **GlcN2**-**GlcN4** ($\nu_a(NH_3^+)$, $\nu_s(NH_3^+)$, $\delta_a(NH_3^+)$, $\delta_s(NH_3^+)$, $\nu(NH_2)$ and $\delta(NH_2)$ at 3090, 2840, 1620, 1580, 3260 and 1600 cm^{-1}, respectively) disappeared. [56,69] Recordings of new intense bands at 1640 (ν(C=O)) and 1550 (δ_{ip}(CNH)) cm^{-1} indicated the formation of an amide group.[70] Vibrations of groups that are away from the substitution center, (e.g., ν(N–CSS), ν_a(SCS), ν_s(SCS) and $\nu_a(ZnS_4)$) remained unchanged (**Table 6.1**).

Complex	ν(C=O)	δ_{ip}(CNH)	ν(N-CSS)	$\nu_{a/s}$(SCS)	$\nu_a(ZnS_4)$
[Zn(dtc-Inp-OSu)$_2$]	1737	-	1496	990/562	397
Zn7	1667	1649	1492	1007/531	391
Zn8	1645	1557	1494	950/576	382
Zn9	1637	1543	1494	1010/564	366
Zn10	1647	1556	1494	1004/563	386

Table 6.1: Selected IR absorptions (CsI disk, wavenumber in cm^{-1}) of **Zn7**-**Zn10**.

Similar observations arise from the ^{1}H and ^{13}C{^{1}H} NMR (**Table 6.2**) of the **Zn7**-**Zn10** glycoconjugates. Interestingly, groups closer to the newly formed amide bond demonstrate a downfield shift. More precisely, these are the peaks of the C$^{4'}$H of the isonipecotic ring and the C_2H (for **Zn8**), the C_6H_2 (for **Zn9**), and the CH_2 group bound to the nitrogen of the aminoethylene linker (for **Zn10**).

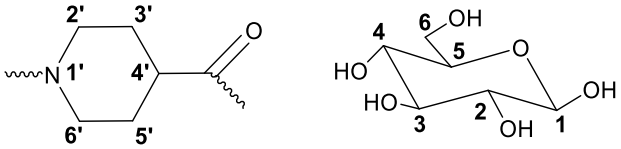

Figure 6.21: Numbering scheme of the isonipecotic ring (left) and the glucose ring (right).

Complex	^{1}H NMR (ppm)	^{13}C NMR (ppm)

	NH	$C^{2',6'}H_{eq}$	C^1H	NCSS	C=O	C^1	$C^{2',6'}$
[Zn(dtc-Inp-OSu)$_2$]	-	4.72	-	203.30	170.17/ 169.90	-	49.87
Zn7	7.36/ 6.87	4.82	-	202.29	175.60	-	50.72
Zn8	7.80	4.82	4.54	202.23	173.91	97.88	50.80
Zn9	7.97	4.83	4.51	202.22	173.78	99.64	50.74
Zn10	7.89	4.83	4.13	202.65	173.69	103.17	50.54

Table 6.2: Selected ^{1}H and ^{13}C{1H} NMR resonances (400 MHz, DMSO-d_6) of **Zn7**-**Zn10**.

6.3.3 Synthesis of the novel platinum(II)-glycoconjugates

For detailed experimental conditions and full characterization see **Chapter 7**.

Dithiocarbamates present interesting bonding characteristics, binding modes, structural features and a wide range of biological applications.[71,72] For what concerns the present study, the initial target was the generation of the mono-dithiocarbamato derivatives of the type [PtCl(dtc-Inp-R)(NH_3)], through the transmetallation reaction of **Pt3** (see **Chapter 3**) and the corresponding zinc(II)-dithiocarbamato glycoconjugate intermediates **Zn7-Zn10**. Although the ligand exchange procedure was successful, the expected complexes were not obtained, due to the full replacement of both the chloride and the amino ligands with two dithiocarbamato ligands. Therefore, key modifications to the synthetic strategy occurred and **Pt15** was selected. The organophosphine (dppe) is potentially a significant phosphorus donor ligand and chelating agent due to the presence of a backbone (ethane in this case) that connects the two phosphino groups, as such, it can act as a bidentate ligand with the central platinum(II) atom. Due to the enhanced affinity of the chelating bis-phosphine ("soft" Lewis base) ligand for the platinum(II) center ("soft" Lewis acid), a stable five-member ring forms upon coordination of the ligand to the metal ion.[73] In the literature, there are specific examples of this platinum(II) complex, which can react with various dithiocarbamates to generate complexes of the type [Pt(dppe)(dtc-R)].[74] Although the purpose of this study is unrelated to the present discussion, it is worthwhile to mention that even using an excess of the dtc species, the bulky diphosphine group of dppe remains connected to the central metal atom. To that extent, during the transmetallation reaction with the zinc(II) intermediates (**Zn8**-

Zn10), at least in principle, the organophosphine will prevent the formation of the bis-dithiocarbamato derivatives by remaining attached to the metal center and allowing the coordination of only one dtc-based ligand. Additionally, findings that support the potential of this synthetic model were reported from Tahir *et al.*, who synthesized a family of square planar heteroleptic platinum(II) dithiocarbamates with the general formula [Pt(dtc)LCl] (dtc=4-(4-methoxyphenyl)piperazine-1-carbodithioate and 4-(furan-2-carbonyl)piperazine-1-carbodithioate; L = tri-(4-flourophenylphosphine) and tri-(4-chlorophenylphosphine)), whose in vitro anticancer activity against five different cancer cell lines revealed the high potency of the complexes.[75] Following the above considerations, the desired platinum(II)-dithiocarbamato glycoconjugates were isolated *via* transmetallation from the corresponding zinc(II) intermediates and **Pt15**. Initially, to verify the feasibility of the proposed method, the zinc(II) isonipecotamide (Inp-NH_2) dithiocarbamate (**Zn7** as model compound) undergo transmetallation reaction with **Pt15** complex. The zinc(II)-platinum(II) transmetallation took place in DMF at room temperature with KPF_6, and zinc(II)-platinum(II) in 1:2 ratio yielded the platinum(II) counterpart [Pt(dppe)(dtc-Inp-NH_2)](PF_6) (**Pt19**) in 78% yield, after precipitation in Et_2O and multiple washings with MeOH (**Figure 6.22**).

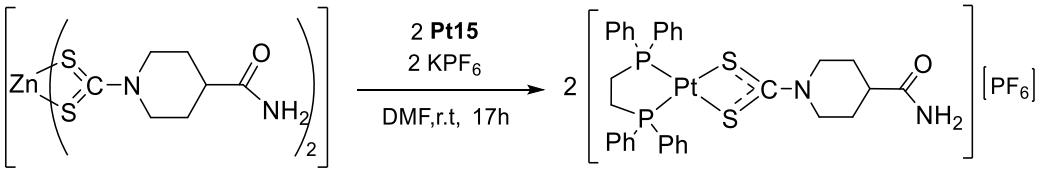

[Zn(dtc-Inp-NH_2)$_2$] (**Zn7**) [Pt(dppe)(dtc-Inp-NH_2)](PF_6) (**Pt19**)

Figure 6.22: Synthesis of the platinum(II)-dithiocarbamato model compound **Pt19**.

After the successful generation of the model **Pt19**, the same experimental procedure adapted for the preparation of its platinum(II)-glycosylated analogues, [Pt(dppe)(dtc-Inp-GlcN2)](PF_6) (**Pt20**), [Pt(dppe)(dtc-Inp-GlcN3)](PF_6) (**Pt21**) and [Pt(dppe)(dtc-Inp-GlcN4)](PF_6) (**Pt22**) which were isolated in a range of yields 58-98% (**Figure 6.23**).

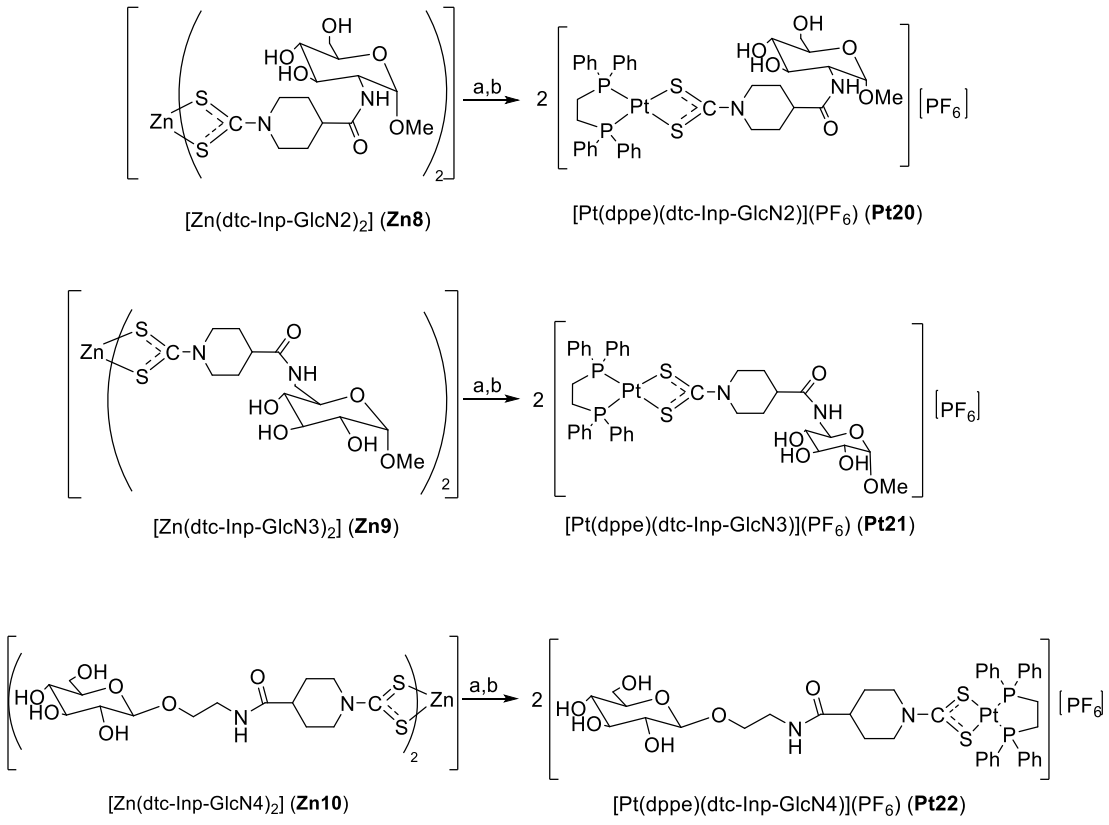

Figure 6.23: Synthesis of the platinum(II)-dithiocarbamato glycoconjugates **Pt20**-**Pt22** *via* transmetallation.

IR spectroscopy proved useful to identify characteristic groups of the newly synthesized compounds. Recording of the mid-IR spectrum revealed a characteristic absorption frequency at 1107 cm^{-1} which was assigned to the asymmetrical stretching ν_a(P-Ph). The bond between the platinum metal center and the phosphorus atoms of the dppe ligand gave a broad signal at 492 cm^{-1} (ν_a(P-Pt-P)). The appearance of bands at 1536, 999, and 394 cm^{-1} (ν(N-CSS), ν_a(SCS), and ν(S-Pt-S), respectively) indicated the successful formation of **Pt19-Pt22** (**Table 6.3**).[68,76,77] Additionally, the sharp band at 841 cm^{-1} was the characteristic vibration of the counterion PF_6^- (**Figure 6.24**).

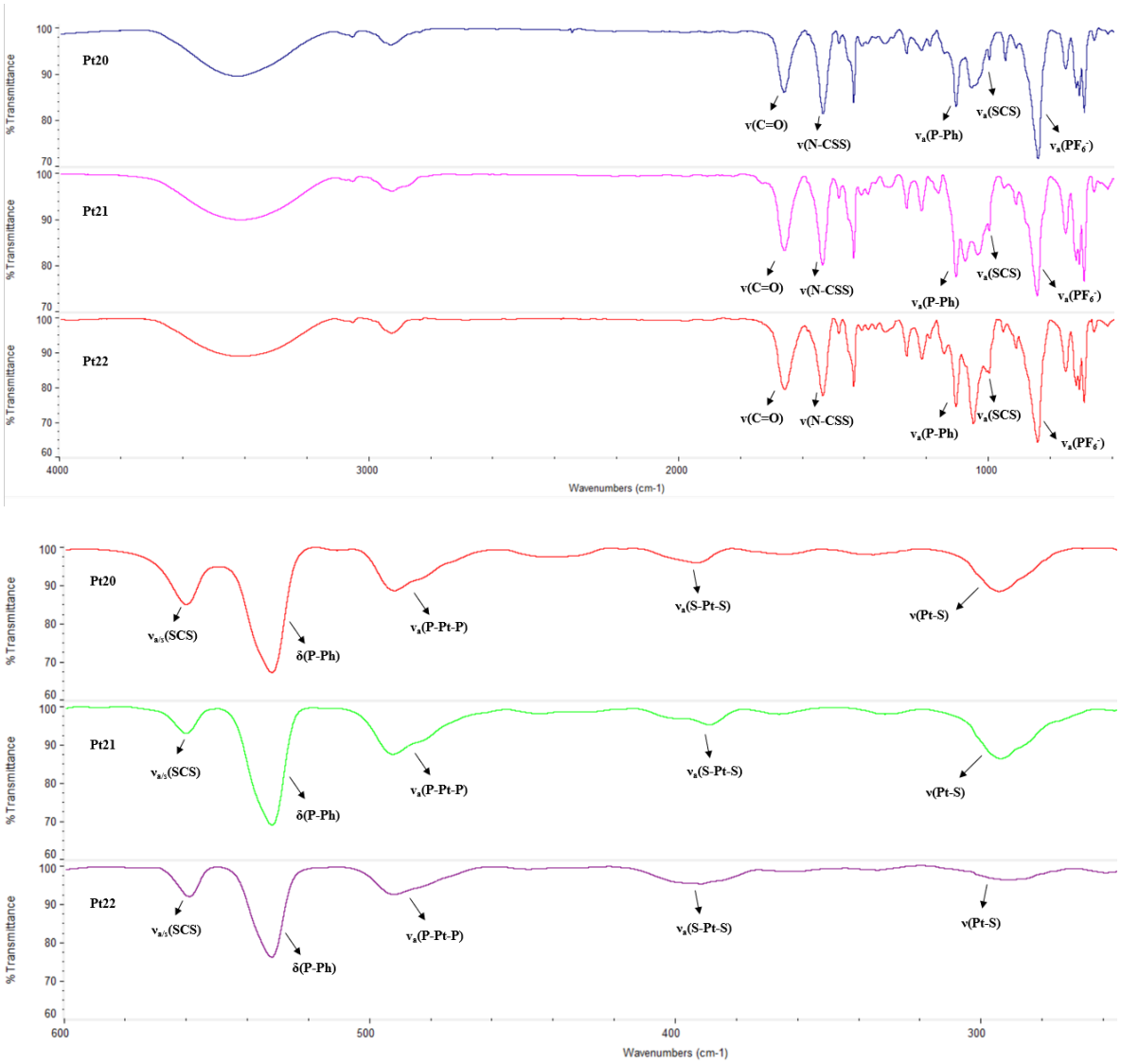

Figure 6.24: Mid-IR (top) and Far-IR (bottom) spectra with CsI disk of **Pt19-Pt22**.

Complex	ν(C=O)	ν(CNH)	ν(N-CSS)	$\nu_{a/s}$(SCS)	ν_a(S-Pt-S)	ν_a(P-Pt-P)
Pt19	1672	1536	999	558	394	492
Pt20	1662	1536	998	559	391	492
Pt21	1659	1537	999	560	394	492
Pt22	1660	1538	999	560	389	493

Table 6.3: Selected FT-IR absorptions (CsI disk, wavenumber in cm^{-1}) of **Pt19-Pt22**.

The platinum complexes were characterized with ^{1}H, $^{13}C\{^{1}H\}$, multidimensional, and $^{31}P\{^{1}H\}$NMR. Interestingly, groups closer to the reaction center, such as the equatorial protons $C^{2',6'}H$, show a shifting of about 0.5 ppm (**Figure 6.25**). The chemical shifts of the dppe phenyl rings were observed at 7.89-7.60 ppm (**Table 6.4**).

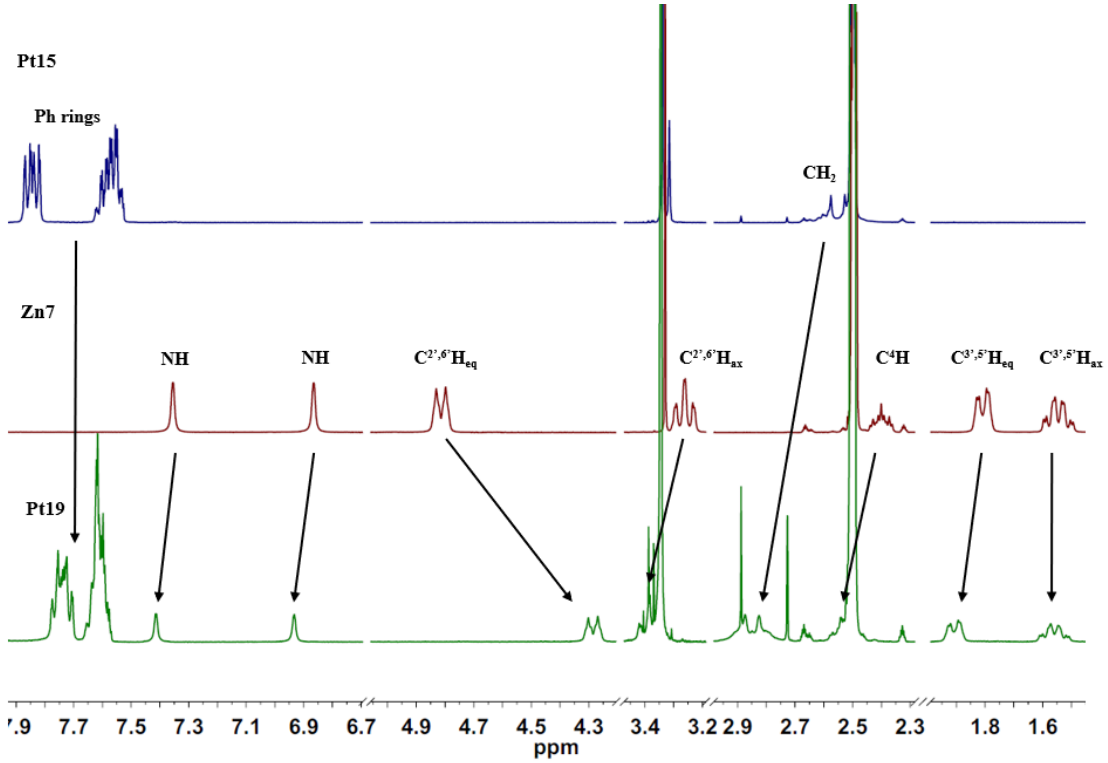

Figure 6.25: Comparative ^{1}H NMR spectra in DMSO-d_6 of **Pt14**, **Zn7** and **Pt19**.

In the $^{13}C\{^{1}H\}$ NMR spectra, characteristic chemical shifts confirmed the successful generation of **Pt19**-**Pt22**. As concerns the dithiocarbamato isonipecotic side, the diagnostic peak arising from the –NCSS carbon recorded at 200 ppm, showing that the dithiocarbamic signal is shifted compared to the peak of the corresponding zinc(II) derivatives (202 ppm) (**Figure 6.26**). Furthermore, the signals of the phenyl rings and the two CH_2 groups of the dppe ligand are present at 129-132 and 25-30 ppm, respectively (**Table 6.4**).

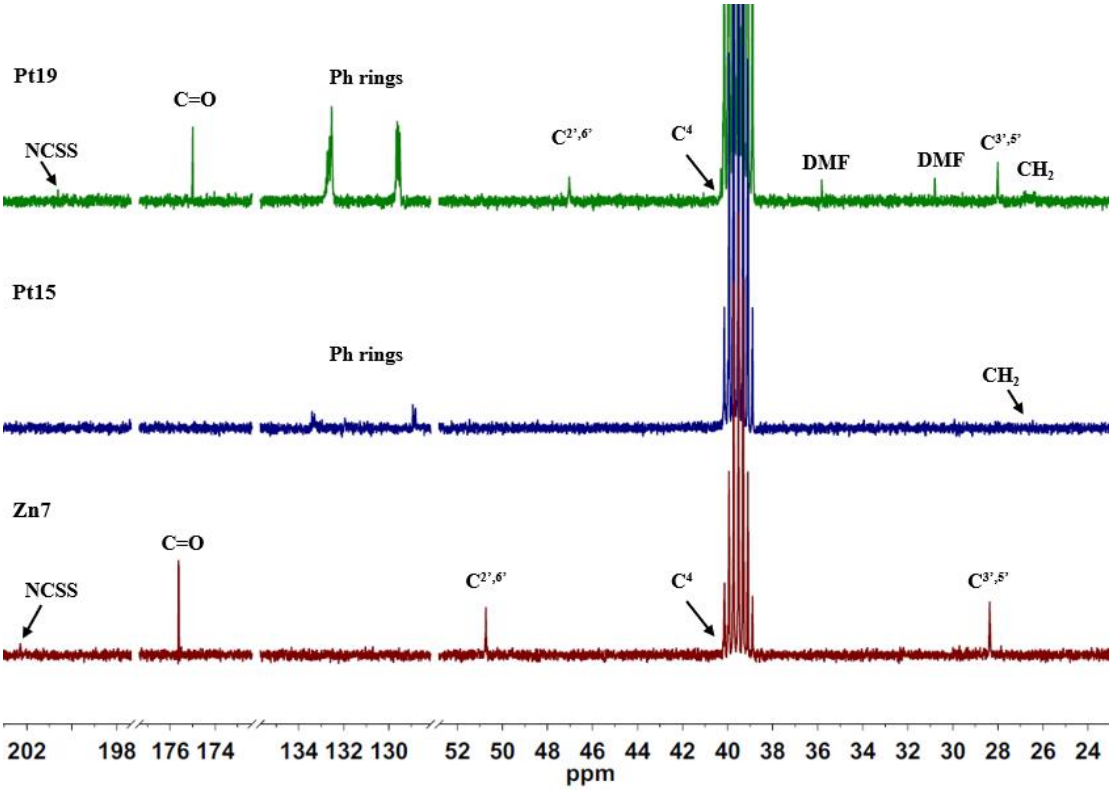

Figure 6.26: Comparative $^{13}C\{^{1}H\}$NMR spectra in DMSO-d_6 of **Pt15**, **Zn7** and **Pt19**.

Likewise, in the $^{31}P\{H\}$ NMR (**Figure 6.27**) the chemical shift of the starting organophorshine platinum complex agrees with the reported literature at 41.90 ppm, while in the spectra of the newly synthesized complexes, it is present at around 45.09 ppm (**Table 6.4**).[60] Additionally, the quintet splitting pattern at -143 ppm assigned to the counterion PF_6^-.

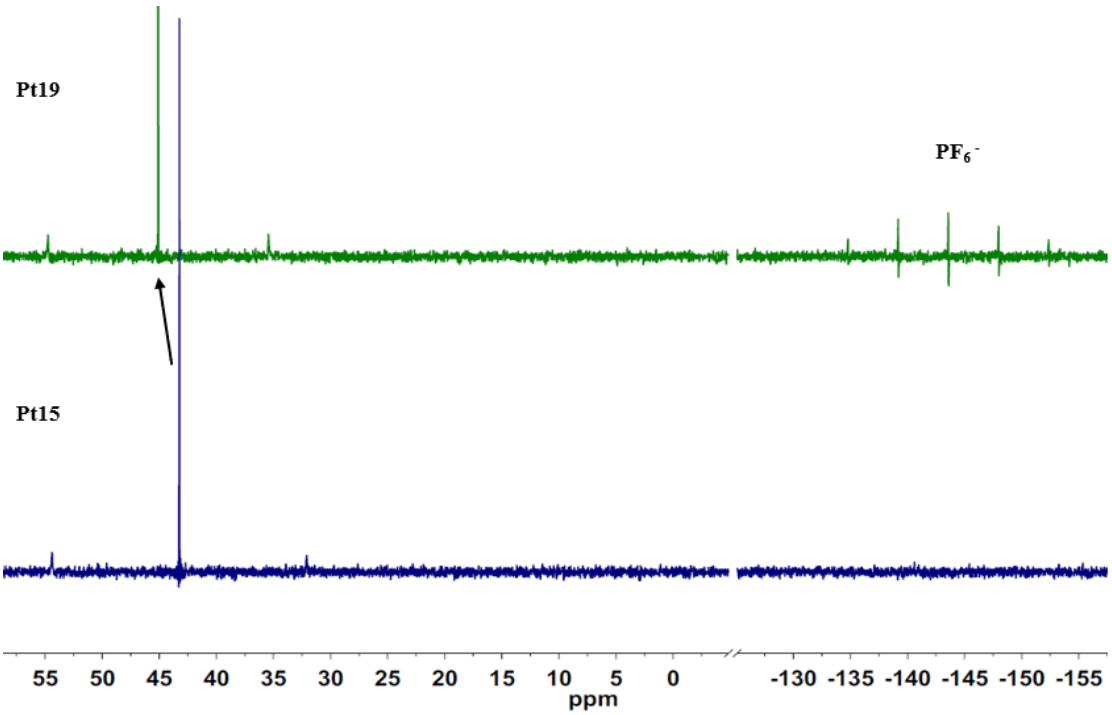

Figure 6.27: Comparative $^{31}P\{^{1}H\}$NMR spectra in DMSO-d_6 of **Pt15** and **Pt19**.

Complex	^{1}H NMR (ppm)			^{13}C NMR (ppm)			^{31}P{H} NMR (ppm)	
	NH	$C^{2',6'}H_{eq}$	$C^{1}H$	NCSS	C=O	$C^{2',6'}$	P-Pt	PF_6^-
Pt19	4.41/6.93	4.30	-	200.53	174.99	48.03	45.09	-143.59
Pt20	7.88	4.33	4.54	200.64	173.34	47.02	45.07	-143.62
Pt21	8.02	4.32	4.50	200.68	173.19	50.16	45.09	-143.61
Pt22	8.05	4.31	4.12	200.66	173.13	46.99	45.06	-143.60

Table 6.4: Selected ^{1}H, ^{13}C{1H} (400 MHz, DMSO-d_6) and ^{31}P{1H} (500 MHz, DMSO-d_6) NMR resonances of **Pt19**-**Pt22**.

6.4 Biological evaluation of the novel Platinum(II)-glycoconjugates

The biological evaluation of the novel **Pt19**–**Pt22** occurred during an Erasmus internship, in the Department of Pharmaceutical and Pharmacological Sciences at the University of Padova, under the supervision of Prof. Lisa Dalla Via.

6.4.1 Materials and methods

Antiproliferative activity assay performed for all the platinum complexes on the following human cancer cell lines, under standard cell culture conditions:

- A2780: cisplatin-sensitive ovarian cancer cells[78]
- A2780cis: cisplatin-resistant ovarian cancer cells[79]

Cell lines

The chosen cell lines A2780 and A2780cis (**Figure 6.28**) were cultured in RPMI-1640 (R6504, Sigma-Aldrich) medium, containing 10% fetal bovine serum (Biowest). Furthermore, before use, additions of two antibiotics (100 μg / mL of penicillin sodium salt and 100 μg / mL of streptomycin sulfate) and an antifungal (0.25 μg / mL of amphotericin B) (A5955, Sigma-Aldrich) occurred. The cell cultures were kept in an incubator (Forma Scientific model 3111) at 37°C (5% CO_2), and the hood used for their handling was an ICN Faster model Ultrasafe 48. Cisplatin 1 μM (Sigma-Aldrich) was added to the A2780cis cell line to maintain the resistant cells.

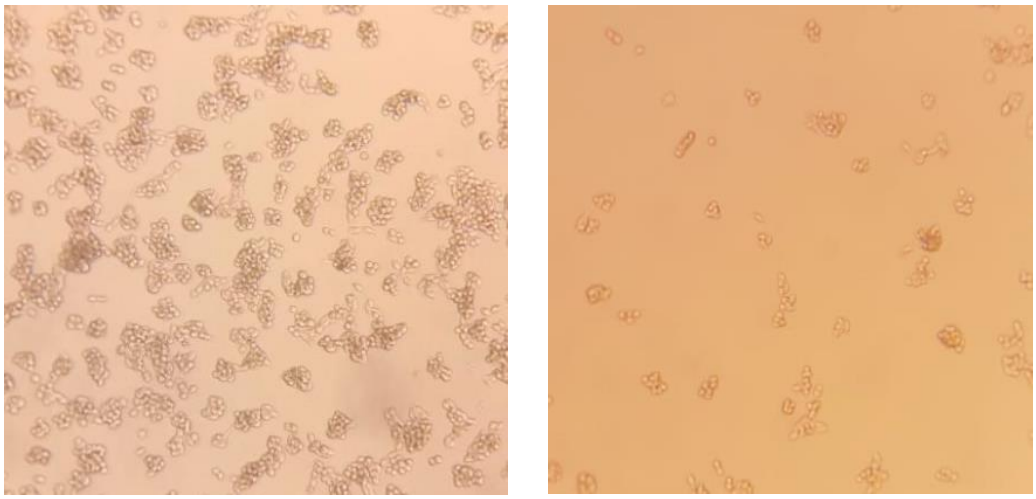

Figure 6.28: A2780 (left) and A2780cis (right) cancer cells under standard conditions (10 times magnification using an optical microscope).

Solutions and material

- PBS buffer (Phosphate Buffer Saline): 0.1 M NaCl (Merck), 0.002 M KCl (Merck), 0.008 M $Na_2HPO_4 \cdot 2H_2O$ (Sigma-Aldrich) and KH_2PO_4 (Merck).

- Trypsin-EDTA: 10 mM trypsin (Sigma-Aldrich), 0.3 mM EDTA (Sigma-Aldrich) in PBS buffer.
- Trypan Blue: (T6146-25G, Sigma-Aldrich) 0.1% w / v in PBS buffer.
- Cisplatin (P4394, Sigma-Aldrich): 4 mM stock solution in 0.9% sterile NaCl.

Method

To determine the anti-proliferative activity, $5 \cdot 10^4$ cells per well cultured, using sterile 24-well plates. After 24 hours of incubation at 37°C, **Pt19**-**Pt22** complexes in solutions of concentrations between 1 and 20 μM, were added to the culture medium. The volume of solvent (DMSO) was less than 0.5% of the total volume of the well. To exclude possible effects of the solvent, one of the reference wells (untreated cells) treated with an amount of DMSO equal to the maximum volume used in the experiment. For each compound, three tests were carried out, in duplicate, for each treatment. After 48 hours of incubation, the cells counted following a well-established method. Initially the culture medium removed, and the cells remained attached to the bottom of the well. Subsequently, the cells washed with 1mL of PBS 1X, and detached after the addition of 200 μL of the Trypsin-EDTA solution. Next, an adequate volume of Trypan Blue dye was added. Finally, the sample examined under an optical microscope, using Burker chambers to determine the number of cells. Utilization of the Trypan Blue dye determined the number of viable cells present in the cell suspension. In general, living cells possess intact cell membranes that exclude certain dyes, whereas dead cells do not. As a result, discrimination of the living cells occurred. The cytotoxicity of each metal complex was expressed in terms of IC_{50} values, i.e., the concentration of complex (expressed in μM) capable of inhibiting the cell growth by 50% compared to a control population.

6.4.2 Study of the antiproliferative activity

The antiproliferative activity of complexes **Pt19**-**Pt22** evaluated in vitro on two human tumor cell lines, A2780 (cisplatin-sensitive ovarian cancer cells) and A2780cis (cisplatin-resistant ovarian cancer cells). The cell cultures treated as described in the Materials and Methods section. Determinations occurred after incubation of the cells for 48 hours in the presence of the metal complexes. The solubility of **Pt19** and **Pt20**

in the cell cultures proved to be challenging. During the counting process, the formation of amorphous crystals was observed (**Figure 6.29**). Specifically, on the A2780 cell line, **Pt19** gives crystals at concentrations above 12 μM and **Pt20** at concentrations above 15 μM. Likewise, on A2780cis cells, crystals formation was observed at concentrations above 8 μM and 12 μM, respectively. Interestingly, **Pt19** is active against the cisplatin-resistant ovarian cancer cell line A2780cis, and both precursors were cytotoxic against A2780.

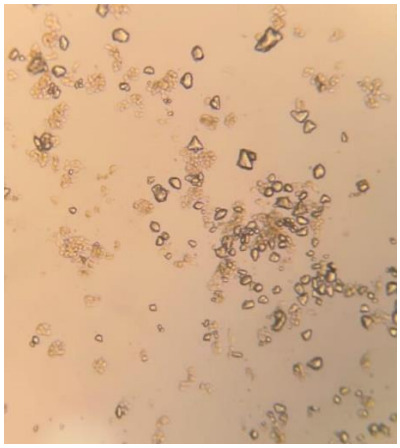

Figure 6.29: Example of the amorphous crystals' formation of complex **Pt19** on the A2780 human cancer cell line.

Interestingly, complexes **Pt19**-**Pt22** presented cytotoxic activity against the A2780 cells and complexes **Pt19**, **Pt21**, and **Pt22** on the A2780cis cell line. The IC_{50} value of each complex demonstrated pharmacological significance, with values lower than 20 μM (**Table 6.5**).

Complex	**IC_{50} [μM, 72 h]**	
	A2780	**A2780cis**
Pt19	**8.5 ± 1.4**	**6.0 ± 0.9**
Pt20	**15.5 ± 3.3**	**>20**
Pt21	**9.8 ± 0.7**	**6.5 ± 2.0**
Pt22	**10.8 ± 0.4**	**16.1 ± 4.0**

Table 6.5: IC_{50} values (in μM) of the **Pt19**-**Pt22** complexes on A2780 and A2780cis cancer cell lines.

6.5 Conclusions

Stimulated by the promising anticancer activity of several novel gold(III)-glycoconjugates reported from Ronconi's group, four new platinum(II) glycomimetic analogs **Pt19**-**Pt22** were synthesized and fully characterized. Notably, each complex features a diphosphine ligand which demonstrates a favorable toxicological profile, and a dithiocarbamato glucose-containing scaffold (apart from the model non-glycosylated **Pt19**) coordinated to the metal center. The aforementioned structural characteristics may contribute to resistance against a possible nucleophilic attack at the metal center by surrounding sulfur-containing entities, thus enhance the chances of the complexes to reach their biological target (GLUTs) intact. Once the platinum(II)-glycoconjugates successfully identified from the glucose transporters and internalized, they can, at least on a theoretical basis, exert their cytotoxic effect directly into the tumor cell. The in vitro antiproliferative activity of **Pt19**-**Pt22** evaluated towards a panel of human tumor cell lines. Overall, the family of the novel platinum(II) complexes **Pt19**-**Pt22** proved cytotoxic against the A2780 ovarian cancer cell line and **Pt19**, **Pt21**, and **Pt22** against the resistant cell line A2780cis, with GI_{50} values lower than 20 μM.

6.6 References

1. Smith, H., Introduction to the Principles of Drug Design and Action, Chapter 1-2, (1998).
2. Cooper, G., Elements of Human Cancer, Chapter 1,(1992).
3. Vasir, K., Labhasetwar, V., *Technol. Cancer Res. Treat.*, **4**, 363–374, (2005).
4. Macheda, L., Rogers, S., Best, J., *J. Cell. Physiol.*, **202**, 654–662, (2005).
5. Krzeslak, A., Wojcik-Krowiranda, K., Forma, E., Jozwiak, P., Romanowicz, H., *et al.*, *Pathol. Oncol. Res.*, **18**, 721–728, (2012).
6. Berg, J., Stryer, L., *Biochemistry*, Chapter 1, (2002).
7. Jinmei-Tian, K., *J. Cancer Sci. Ther.*, **10**, 140–142, (2018).
8. Ganapathy-Kanniappan, S., Geschwind, J., *Mol. Cancer*, **12**, 1–11, (2013).

9. Pettenuzzo, A., Pigot, R., Ronconi L., *Metallodrugs*, **1**, 36–61, (2016).

10. Pfeiffer, T., Schuster, S., Bonhoeffer, S., *Science*, **292**, 504–507, (2001).

11. Heiden, V., Cantley, L., Thompson, C., *Science*, **324**, 1029–1033, (2009).

12. Kim, Y., Hollenbaugh, J., Kim, D., Kim, B., *Plos One*, **6**, (2011).

13. Denko, C., *Nat. Rev. Cancer*, **8**, 705–713, (2008).

14. Mueckler, M., Thorens, B., *Mol. Aspects Med.*, **34**, 121–138, (2013).

15. Zhao, Q., Keating, A., *Curr. Genomics*, **8**, 113–128, (2007).

16. Macheda, L., Rogers, S., Best, J., *J. Cell. Physiol.*, **202**, 654–662, (2005).

17. Vaupel, P., Kallinowski, F., Okunieff, P., *Cancer Res.*, **49**, 6449–6465, (1989).

18. Simmons, A., *Fetal and Neonatal Physiology*, Chapter 1, (2017).

19. Granchi, C., Minutolo,F., *ChemMedChem*, **7**, 1318–1350, (2012).

20. Porporato, E., Dhup, S., Dadhich, R., Copetti, T., Sonveaux, P., *et al., Front. Pharmacol.*, **2**, 1–18, (2011).

21. Barbosa, M., Martel, F., *Cancers*, **12**, 154, (2020).

22. Luengo, A., Gui, D., Van der Heiden, M., *Cell Chem. Biol.*, **24**, 1161–1180, (2017).

23. Qian, Y., Wang, X, Chen, X., *World J. Transl. Med.*, **3**, 37-57, (2014).

24. Chan, A., *Sci. Transl. Med.*, **3**, 85, (2011).

25. Liu, Y., Zhang, W., Cao, Y., Liu, Y., Bergmeier, S., *et al.*, *Cancer Lett.*, **298**, 176–185, (2010).

26. Siebeneicher, H., Cleve, A., Rehwinkel, H., Neuhaus, R., Heisler, R., *et al.*, *ChemMedChem.*, **11**, 2261–2271, (2016).

27. Aykin-Burns, N., Ahmad, I., Zhu, Y., Oberley, L., Spitz, D., *et al.*, *Biochem. J.*, **418**, 29–37, (2009).

28. Calvaresi, C., Hergenrother, P., *Chem. Sci.*, **4**, 2319–2333, (2013).

29. Cantuaria, G., Magalhaes, A., Angioli, R., Mendez, L., Mirhashemi, R., Wang, J., *et al., Cancer,* **88**, 381–388, (2000).

30. Cao, J., Cui, S., Li, S., Du, C., Tian, J., *Cancer Res.*, **73**, 1362–1373, (2013).

31. Lin, S., Tungpradit, R., Sinchaikul, S., Feng-Ming. A., Liu, D., *et al., J. Med. Chem.*, **51**, 7428–7441, (2008).

32. Tsubomura, T., Ogawa, M., Yano, S., Kobayashi, K., Sakurai, T., *et al., Inorg. Chem.*, **29**, 2622–2626, (1990).

33. Berger, I., Nazarov, A., Hartinger, C., Groessl, M., Valiahdi, S., *et al., ChemMedChem*, **2**, 505–514, (2007).

34. Hanessian S., Wang, J., *Can. J. Chem.,* **71**, 886–895, (1993).

35. Chen, Y., Heeg, M., Braunschweiger,P., Xie, W., Wang, P., *et al., Angew. Chemie.*, **38**, 1768–1769, (1999).

36. Mikata, Y., Shinohara, Y., Yoneda, K., Nakamura, Y., Brudziñska, I., *et al., Bioorganic Med. Chem. Lett.*, **11**, 3045–3047, (2001).

37. Tromp, A., Evan, S., Boom,M., Timmers,S., *Bioorg. Med. Chem. Lett.*, **14**, 4273–4276, (2004).

38. Möker, J., Thiem, J., *European J. Org. Chem.,* **28**, 4842–4847, (2009).

39. Möker, J., Thiem, J., *Carbohydr. Res.*, **348**, 14–26, (2012).

40. Möker, J., Thiem, J., *J. Carbohydr. Chem.*, **31**, 702–710, (2012).

41. Gasser, G., Ott, I., Metzler-Nolte, N., *J. Med. Chem.*, **54**, 3–25, (2011).

42. Sun, Y., Dik-Lung, M., Lai-Ming, E., *Dalt. Trans.*, **43**, 4884–4892, (2007).

43. Garoufis, A., Hadjikakou, S., Hadjiliadis, N., *Coord. Chem. Rev.,* **253**, 1384–1397, (2009).

44. Tanaka, M., Mizuno, M., Toyokuni, S., Maruyama, S., Kodera, Y., *et al., Cancer,* **13**, 1640-1648, (2013).

45. a) Madeira, J., Gibson, D., Kean, W., Klegeris, A., *Inflammopharmacol.*, **20**, 297-306, (2012); b) Marzano, C., Gandin, V., Folda, A., Scutari, G., Bindoli, A., *et al.*, *Free Radic. Biol. Med.*, **15**, 872-881, (2007); c) Nakaya, A., Morihiko, S., Akihiro, M., Hideo, U., Yasuo,I., *et al., Leuk. Res.*, **35**, 243-249, (2011); d) Park, J., In-Sook, K., *J. Pharmacol*., **146**, 506-513, (2005); e) Mirabelli, C., Johnson, R., Sung, C., Faucette, L., Muirhead, K., *et al., Cancer Res.*, **45**, 32-39, (1985); f) Simon, M., Vibert, G., Lorber, A., *Cancer Res.*, **41**, 94-97, (1981); g) Baker, V., Barnard, P., Berners-Price, S., Brayshaw, S., Hickey, J., *et al., J. Organomet. Chem.,* **690**, 5625–5635, (2005).

46. Shen, W., Pouliot, L., Hall, M., Gottesman, M., *Pharmacol. Rev.*, **64**, 706–721, (2012).

47. Hartmann, K., Pettenuzzo, A., Ronconi, L., Rouge, J., *Appl. Mater. Interfaces*, **209**, 1063–1069, (2020).

48. Nazarov, A., Baquié, M., Nowak-Sliwinska, P., Zava, O., Beijnum, J., *et al.*, *Sci. Rep.*, **3**, 1–7, (2013).

49. Sathisha, P., Budagumpi, S., Kulkarni, V., Kurdekar, S., Revankar, K., *et al.*, *Eur. J. Med. Chem.,* **45**, 106–113, (2010).

50. Pellei, M., Papini, G., Trasatti, A., Giorgetti, M., Tonelli, D., *et al., Dalt. Trans.,* **40**, 9877–9888, (2011).

51. Erker, G., *DE102006053690A1*, (2008).

52. Waern, B., Dillon, C., Harding, M., *J. Med. Chem.*, **48**, 2093–2099, (2005).

53. Itoh, T., Shirakami, S., Ishida, N., Yamashita, Y., Takashi, Y., *et al.*, *Bioorganic Med. Chem. Lett.*, **10**, 1657–1659, (2000).

54. Schibli, R., Dumas, C., Petrig, J., Spadola, L., Scapozza, L., *et al., Bioconjug. Chem.,* **16**, 105–112, (2005).

55. Pettenuzzo, A., Montagner, D., McArdle, P., Ronconi. L., *Dalt. Trans.*, **47**, 10721–10736, (2018).

56. Lecina, J., Carrer, A., Álvarez-Larena, A., Mazzi, U., Melendez-Alafort, L., Suades, J.,*Organometallics*, **31**, 5884–5893, (2012).

57. Pearson, G., *J. Am. Chem. Soc.*, **85**, 3533–3539, (1963).

58. Hogarth, G., *Progress in Inorganic Chemistry*, Chapter 2, (2005).

59. Valeur, E., Bradley, M., *Chem. Soc. Rev.*, **38**, 606–631, (2009).

60. Dopke, C., Oemke, H., *Inorganica Chim. Acta*, **376**, 638–640, (2011).

61. Gao, F., Yan, X., Tushar, S., Baettig, O., Ait-Mohand-Brunet, S., *J. Med. Chem.*, **49**, 5273–5281, (2006).

62. Wiebe, L., US20070021380A1, (2007).

63. Šardzík, R., Noble, G., Weissenborn, M., Martin, A., Webb, S., *et al.,J. Org. Chem.*, **6**, 699–703, (2010).

64. Nyamen, D., *Dalt. Trans.*, **41**, 8297–8302, (2012).

65. Aravamudan, G., Rajasekhar P., Adeola, A., Ndifon,T., Warner, J., **27**, 2744–2747, (1971).

66. Arul Prakasam, B., *Polyhedron*, **26**, 4489–4493, (2007).

67. Bonati, F., Ugo, R., *J. Organomet. Chem.*, **10**, *257–268*, (1967).

68. Nakamoto, K., Infrared and Raman Spectra of Inorganic and Coordination Compounds, Part A, (2008).

69. Wiercigroch, E., Szafraniec, E., Czamara, K., Pacia, M., Majzner, K., *Spectrochim. Acta A Mol, Biomol. Spectrosc.*, **185**, 317–335, (2017).

70. Picquart, M., Abedinzadeh, Z., Grajcar, L., Baron, M., *et al., Chem. Phys.*, **228**, 279–291, (1998).

71. Adokoh, K., *RSC Adv.*, **10**, 2975–2988, (2020).

72. Odularu, T., Ajibade, P., *Bioinorg. Chem. Appl.,* **2019**, 15, (2019).

73. Manohar, A., Karpagavel, K., Murugan, A., *Int. J. ChemTech Res.,* **6**, 474–480, (2014).

74. Keter, K., Guzei, I., Darkwa, J., *Inorg. Chem. Commun.,* **27**, 60–63, (2013).

75. Amir, K., Rehman, Z., Hayat, F., Khan, S., Hogarth,G., *RSC Adv.,* **6**, 110517–110524, (2016).

76. Taylor, J., Odel, A., Raethel, A., *Spectrochim. Acta Part A Mol. Spectrosc.,* **24**, 1855–1861, (1968).

77. Daasch, W., Smith, C., *Anal. Chem.,* **23**, 853–868, (1951).

78. Hamilton, C., Hamilton, T.,Ozols, F., *Semin.Oncol*, **11**, 285-298, (1984).

79. Ozols, F., Young, R., Hamilton, T., *Cancer Res.*, **47**, 414–418, (1987).

80. Sarto, M., Anti-proliferative activity and study of the mechanism of action of new organometallic glycoconjugates, Master Thesis, (2019).

81. Skoog, A., Fundamentals of Analytical Chemistry, Chapter 2, (2005).

82. Gumuş, F., *J. Med. Chem.,* **52**, 1345–1357 (2009).

83. Nitiss, L., *Nat. Rev. Cancer,* **9**, 338–350, (2009).

General Conclusions

Chapter 2 of the present Thesis reports an optimized synthetic methodology for preparing two novel luminescent vitamin B_{12}-based carriers of potential anticancer drugs. A stepwise experimental procedure followed for the generation of fluorophores **FLUO-1**, **FLUO-2**, their corresponding activated esters **FLUO-1a** and **FLUO-2a**, and the functionalized intermediate **2**. A combination of the active fluorophores and **2** under mild conditions in the dark resulted in the target fluorescent vitamin B_{12}-based derivatives. Subsequently, the original research plan involved the generation of platinum(II)-dithiocarbamato scaffolds containing (at least) one metal-coordinated chloride to be replaced by the cyano group of vitamin B_{12}, to obtain the desired vitamin B_{12}-metal conjugates. **Chapter 3** summarizes all the synthetic attempts that have been carried out in this regard, most of which unfortunately failed. Consequently, the overall research program had a screening halt, and we were forced to identify suitable alternative options, including a complete change of course (**Chapter 4**). As such, three novel metal-dithiocarbamato-alkynyl complexes (namely, **Au2**, **Au4**, and **Pt16**) have been prepared and fully characterized. So far, conjugation of **Pt16** derivative to vitamin B_{12} has been attempted and, although more challenging than expected, provided insights into the generation of this new class of vitamin B_{12}-metal conjugates. Additionally, to enhance our understanding of the potential of amino acids in anticancer research, we designed four novel naturally fluorescent metal-dithiocarbamato *L*-tyrosine ester complexes, namely **Pt17**, **Pt18**, **Au5**, and **Au6**. The successful isolation of the object compounds was confirmed by several spectroscopic measurements. Fluorescence spectroscopy depicted sufficient photoluminescence at the long-wavelength region of the electromagnetic spectrum (>420 nm). Moreover, four new platinum(II) glycomimetic analogs **Pt19**-**Pt22** were synthesized and fully characterized. Notably, each complex features a diphosphine ligand which demonstrates a favorable toxicological profile, and a dithiocarbamato glucose-containing scaffold (apart from the model non-glycosylated **Pt19**) coordinated to the metal center. The in vitro antiproliferative activity of **Pt19**-**Pt22** evaluated towards a panel of human tumor cell lines. Overall, the family of the novel platinum(II) complexes **Pt19**-**Pt22** proved cytotoxic against the A2780 ovarian cancer cell line and **Pt19**, **Pt21**, and **Pt22** against the resistant cell line A2780cis, with GI_{50} values lower than 20 μM.

Chapter 7

7. Experimental

List of compounds synthesized in this research work

Fluorophores

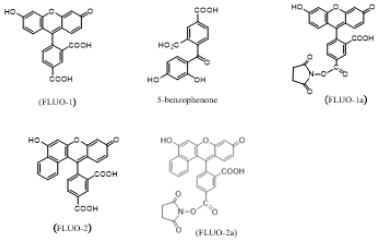

Vitamin B_{12}-based Compounds

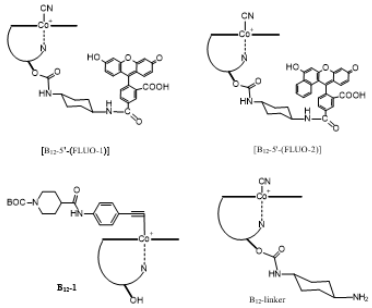

Ligands

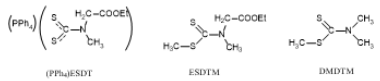

Ligands

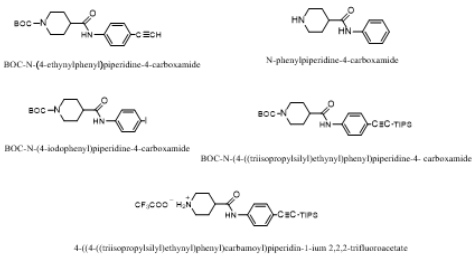

Zn(II) Complexes

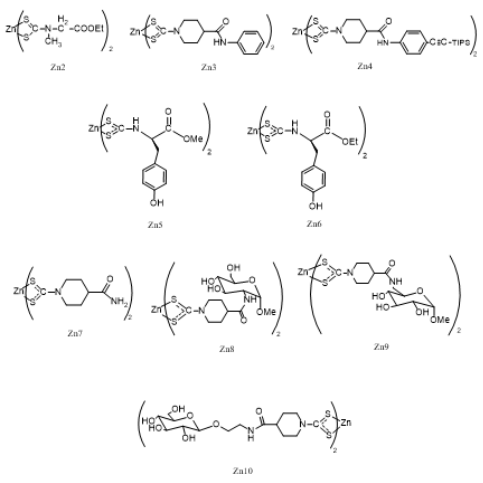

Pt(II) Complex

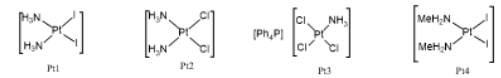

Pt1

Pt2

Pt3

Pt4

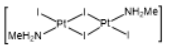

Pt5

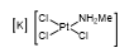

Pt6

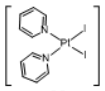

Pt7

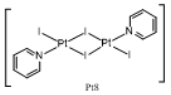

Pt8

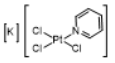

Pt9

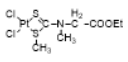

Pt10

Pt11

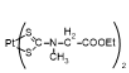

Pt12

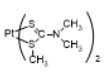

Pt14

Pt15

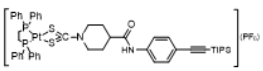

Pt16

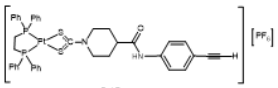

Pt17

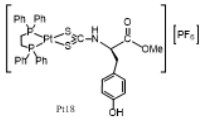

Pt18

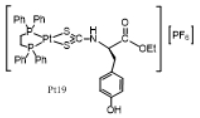

Pt19

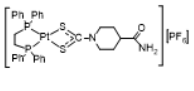

Pt20

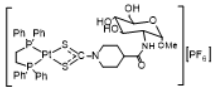

Pt21

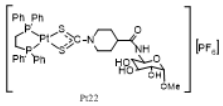

Pt22

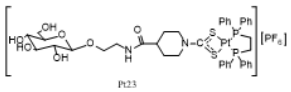

Pt23

Au(III) Complex

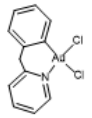

[Au(bpy)Cl$_2$]

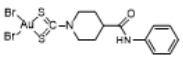

Au0

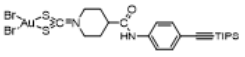

Au1

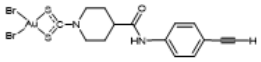

Au2

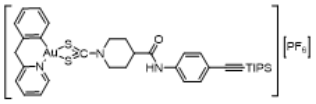

Au3

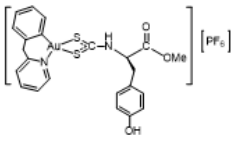

Au5

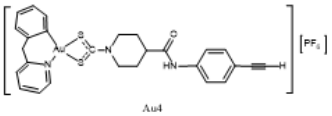

Au4

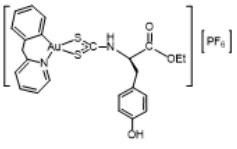

Au6

7.1 Materials

CN-Cbl, $MeSO_3H$, benzene-1,3-diol, naphthalene-1,3-diol, trimellitic anhydride chloride,Na_2SO_4, HCl, NaOH, KOH, EDAC, TSTU, aniline, 4-iodoaniline, $SOCl_2$, N-hydroxysuccinimide,trans-1,4-diaminocyclohexane,CS_2, $(Et_4N)Cl$,$(Et_4N)F$, NaCl, CDT, CDI, dppe, $AgNO_3$, $Na(S_2CN(CH_3)_2)$,(Triisopropyisilyl)acetylene, 4-ethynylaniline, 4-[(Trimethylsilyl)ethynyl]aniline,isonipecotamide, isonipecotic acid,MeI, DIPEA, DIPA, Et_3N, 2-benzylpyridine, TFA, L-tyrosine methyl ester, L-tyrosine ethyl ester, GlcN2, GlcN3, GlcN4, KPF_6, $K[AuBr_4]\cdot 2H_2O$, $Na[AuCl_4]\cdot 2H_2O$, $PtCl_2$, $K_2[PtCl_4]$,$[Zn(OAc)_2]\cdot 2H_2O$, KI, CH_3NH_2 (40%), pyridine, $HClO_4$ (70%), ethyl sarcosinate hydrochloride, NH_4Cl, $(Ph_4P)Cl$, CuAcO, DBU, DCC, HOBt, $Pd(PPh_4)_3$,CuI, DMA, PBS buffer, $Na_2HPO_4\cdot 2H_2O$, KH_2PO_4, Trypsin (10 mM), EDTA (0.3 mM), Trypan Blue (0.1% w/v), Cisplatin (4 mM), P_2O_5,CsI, KBr, KCl, DMF, anhydrous DMSO, THF, EtOH, MeOH, Acetone, MeCN, DCM, Chloroform, diethyl ether, EtOAc, Petroleum ether, hexane, n-pentane, CD_3OD, $CDCl_3$, D_2O, DMSO-d_6, DMF-d_7,CD_3COCD_3.

7.2 Instrumentation

Chromatography: Thin layer chromatography (TLC) was performed on silica gel Merck60F_{254} precoated aluminum sheets. Spots were visualized by direct UV irradiation at 254nm or developed by exposure to potassium permanganate staining solutions as appropriate. Flash column chromatography was performed on Sigma Aldrich 60 Å silica gel (40-63 μm, 230-400 mesh) as stationary phase using the appropriate eluent.

IR Spectroscopy: FT-IR spectra of the newly synthesized species were recorded from thin films at room temperature on a Perkin Elmer Spectrum 100 FT-IR spectrophotometer, equipped with a UATR accessory in the range 4000-650 cm^{-1} (32 scans, resolution 4 cm^{-1}). FT-IR spectra of the metal complexes were recorded with CsI disks at room temperature on a Perkin Elmer Frontier FT-IR/FIR spectrophotometer in the range 4000-600 cm^{-1} (32 scans, resolution 4 cm^{-1}) and in the range 600-200 cm^{-1}(32 scans, resolution2 cm^{-1}). Data processing was carried out using OMNIC version 5.1 (Nicolet Instrument Corporation).

NMR Spectroscopy: All NMR spectra were acquired in the appropriate deuterated solvent at room temperature on a JEOL 400 MHz NMR ECX-400 spectrometer equipped with z-field gradients. ^{1}H and ^{13}C chemical shifts were referenced to TMS at 0.00 ppm via internal referencing to the residual peak of the deuterated solvent employed. ^{31}P chemical shifts were referenced to an external standard of 85% H_3PO_4 at 0 ppm. ^{1}H and $^{13}C\{^{1}H\}$signals were assigned with the aid of [^{1}H,^{1}H] COSY, ^{13}C, [^{1}H,^{13}C] HSQC and [^{1}H,^{13}C] HMBC experiments. Typical acquisition parameters for 1D ^{1}H NMR spectra (^{1}H:399.78 MHz): 16 transients, spectral width 6.0 kHz, 16k data points, relaxation delay 1.0s. Spectra were processed using exponential weighting with a resolution of 0.5 Hz and a line-broadening threshold of 0.1 Hz. Typical acquisition parameters for 2D [^{1}H,^{1}H] COSY NMR spectra (1H: 399.78 MHz): 512 transients of 2 scans per block, spectral width3.8/3.8 kHz, 640/256 data points, relaxation delay 1.0 s. Spectra were processed using sine weighting with a resolution of 4.8/9.8 Hz and a line-broadening threshold of 0.8/1.5Hz. Typical acquisition parameters for 1D $^{13}C\{^{1}H\}$ NMR spectra (^{13}C: 100.53 MHz): 512 transients, spectral width 25.1 kHz, 32k data points, relaxation delay 2.0 s. Spectra were processed using exponential weighting with a resolution of 2.0 Hz and a line-broadening threshold of 2.5 Hz. Typical acquisition parameters for 2D [^{1}H,^{13}C] HMQC NMR spectra(^{1}H: 399.78/^{13}C: 100.53 MHz): 1k transients of 4 scans per block, spectral width 4.8/7.7kHz, 1k/1k data points, relaxation delay 1.0 s. Spectra were processed using cosine-square weighting with a resolution of 1.0/3.0 Hz and a line-broadening threshold of 0.3/1.0 Hz. Typical acquisition parameters for 2D [^{1}H,^{13}C] HMBC NMR spectra (^{1}H: 399.78/^{13}C:100.53 MHz): 1.2k transients of 4 scans per block, spectral width 8.0/25.1 kHz, 2k/2k data points, relaxation delay 1.0 s. Spectra were processed using sine-square weighting with a resolution of 0.3/1.0 Hz and a line-broadening threshold of 0.3/1.0 Hz. Whenever specified, NMR spectra were acquired in the appropriate deuterated solvent at room temperature on a VarianVNMRS500 MHz AR spectrometer or on an Agilent DD2 NMR 600 MHz ASC spectrometer (equipped with cold probe), equipped with z-field gradients. ^{1}H and ^{13}C chemical shifts were referenced to TMS at 0.00 ppm via internal referencing to the residual peak of the deuterated solvent employed. Data processing was carried out using MestReNova version 12.0 (Mestrelab Research S.L).

HPLC: Agilent 6400 Series Triple Quadrupole LC/MS with normal flow LC/MS, binary pump, quaternary pump and autosampler. Quadrupole mass analyzer with four parallel rods to which specific DC and RF voltages are applied. The rods are labeled (+) and (–) in reference to the DC voltages applied to them. Gas pressure of 2 Torr. Utilization of C18 LC columns. Spectral range to 90-2000m/z. Dual electrospray ionization source and an Agilent 1260 UPLC liquid chromatography. Mass resolution of up to 20,000 and standard mass range of up to 3,200 m/z. Sample concentrations of 1 mg/mL for molecules below 1,000 Da. Mobile phases: MeOH/H_2O (0.01% TFA).

Fluorescence Spectroscopy: The fluorescence spectra were obtained using the Cary Eclipse Fluorescence Spectrophotometer which incorporates a xenon flash lamp and captures a data point every 12.5 ms and scans at 24,000 nm/min. Wavelength range from 275 to 750 nm. Measure polarization as a function of temperature using the thermal software application in the Agilent Cary WinFLR software. Angle selections include 0°, 90°, 55° (magic angle), and 35°. Probe range: –10 ℃ to +100 ℃. Probe size: 1.5 mm diameter, 15 mm long. Photometric performance: fiber optics. Temperature control between 20–60 °C, using the water thermostatic cell holder. Reproducible temperature control: ± 0.05 °C.

7.3 Chapter 2 – Experimental

Synthesis of 5-benzophenone:

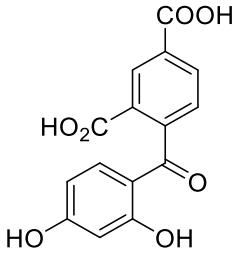

1,3-Dioxo-1,3-dihydroisobenzofuran-5-carboxylic acid (20 g, 0.104 mol) and resorcinol (23 g,0.208 mol) were dissolved in methanesulfonic acid (100 mL) and the mixture was stirred under reflux at 80 °C overnight. The mixture was cooled down to 0 °C and a light-yellow precipitate was observed. The precipitate was dissolved in hot EtOH (200 mL) and then water was added, and a yellowish precipitate was

observed. The precipitate was filtered and dried under vacuum over P_2O_5 obtaining 36.5 g of crude 5(6)-benzophenone as a yellowish powder. The crude compound was suspended in an aqueous solution of NaOH (200 g NaOH in 200 g H_2O) and was stirred under reflux at 80 °C overnight, obtaining a transparent and colorless solution. Then ice (300 g) was added in the solution. Subsequently, an aqueous solution of HCl 12 M was added dropwise (until pH 1-2) under stirring obtaining a white precipitate. Subsequently, the mixture was left at 5 °C overnight. The precipitate was filtered and dried under vacuum over P_2O_5 obtaining a crude mixture of isomers of 5(6)-carboxyfluorescein (1:1 ratio) as an off-white solid. The off-white solid was fractionally crystallized by dissolving it in MeOH (50 mL) and subsequently adding H_2O (750 mL). The mixture was left to stand at room temperature for three weeks obtaining a yellow crystalline solid of 5-benzophenone (8.3 g, 26% yield). $C_{15}H_{10}O_7$, MW: 302,24: C, 59.61; H, 3.34; O, 37.05. FT-IR (CsI disk, $\tilde{\nu}_{max}$, cm^{-1}): 3439 (br, v, $OH_{alcohol}$), 3065 (br, v, $OH_{carboxylic\ acid}$), 2470 (br, v, $OH_{carboxylic\ acid}$), 1691(s, v, C=O), 1580 (s, v, $C{=}O_{carboxylic\ acid}$), 1455 (s, δ, $OH_{alcohol}$), 1300 (m, , δ, $OH_{carboxylic\ acid}$), 1208 (s, v, C-O), 875 (m, δ, C=C), 767 (m, δ, C-C).^{1}H NMR (400 MHz, DMSO-d_6): δ = 13.54 (2H, -COOH),12.01 (1H, -OH), 10.75 (1H, -OH), 8.16 (1H, H^a), 8.09 (1H, H^b), 7.85 (1H, H^c), 6.99 (1H, H^d), 6.34–6.29 (2H, H^e, H^f) ppm. ^{13}C NMR (100 MHz, DMSO-d_6): δ = 199.4, 166.7, 166.5, 165.6, 164.7, 140.7, 135.2, 134.3, 133.8, 130.9, 130.8, 128.4, 113.6, 108.9, 103.0 ppm. MS (ESI^+): calcd. for $[M + H]^+$ 303.0 and found 302.9.

Synthesis of 5-carboxyfluorescein (FLUO-1):

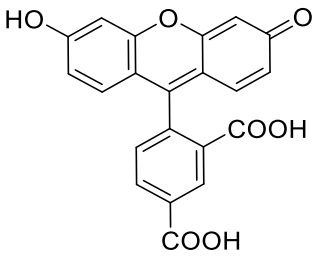

5-benzophenone (500 mg, 1.65 mmol) and resorcinol (200 mg, 1.82 mmol) were dissolved in methanesulfonic acid (10 mL) and was stirred at room temperature overnight. Iced water (50 mL) was added in the mixture while stirring obtaining an orange precipitate. The precipitate was filtered and then was dissolved in an aqueous

solution of NaOH 2M (40 mL). An aqueous solution of HCl 2M (30 mL) was added to the basic solution obtaining an orange solid. The solid was filtered and then was firstly re-precipitated in EtOH/H_2O and then in NaOH/HCl. The solid was filtered and dried under vacuum over P_2O_5 yield the title compound as an orange solid (604mg, 97% yield). $C_{21}H_{12}O_7$, MW: 376,32: C, 67.03; H, 3.21; O, 29.76. FT-IR (CsI disk, $\tilde{\nu}_{max}$, cm^{-1}): 3439 (br, v, $OH_{alcohol}$), 3065 (br, v, $OH_{carboxylic\ acid}$), 2470 (br, v, $OH_{carboxylic\ acid}$), 1691(s, v, C=O), 1580 (s, v, $C{=}O_{carboxylic\ acid}$), 1455 (s, δ, $OH_{alcohol}$), 1300 (m, , δ, $OH_{carboxylic\ acid}$), 1208 (s, v, C-O), 875 (m, δ, C=C), 767 (m, δ, C-C).^{1}H NMR (400 MHz, D_2O (NaOD)): δ = 8.21 (1H, H^a), 8.00 (1H, H^b), 7.24 (1H, H^c), 7.13 (2H, H^d), 6.58 (2H, H^e), 6.54 (2H, H^f) ppm.^{13}C NMR (100 MHz, D_2O (NaOD)): δ = 180.6, 174.7, 174.5, 158.7, 139.56, 137.4, 134.1, 131.4, 130.1, 129.4, 128.4, 122.9, 112.2, 103.6 ppm. MS (ESI^+): calcd. for $[M + H]^+$ 376.32 and found 377.1.

Synthesis of 5-carboxyfluorescein-N-hydroxysuccinimide ester (FLUO-1a):

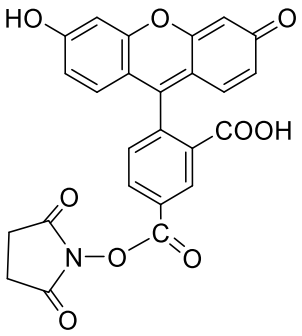

5-carboxyfluorescein (200mg, 0.53 mmole) was dissolved in dry DMF (3 mL). EDAC (173mg, 0.90 mmole) and N-hydroxysuccinimide (73.4mg, 0.64 mmole) were added and the mixture was stirred under N_2 overnight. Acetone (18 mL) and 0.05 M sodium phosphate buffer (25 mL) were added to the mixture. The mixture was extracted with a mixture of diethyl ether (100 mL) and ethyl acetate (50 mL). The organic phase was collected and was extracted with water (3×60 mL) and brine (1×75 mL).The resulting organic solution was dried with anhydrous sodium sulfate and then the solvent was removed by rotary evaporation under reduced pressure to obtain the desired compound as a bright orange solid (163mg, 65% yield). $C_{25}H_{15}NO_9$, MW: 473,39: C, 63.43; H, 3.19; N, 2.96; O, 30.42. FT-IR (CsI disk, $\tilde{\nu}_{max}$, cm^{-1}): 3060 (br, v, $OH_{alcohol}$), 1745(s, v, C=O), 1594 (s, v, $C{=}O_{carboxylic\ acid}$), 1458 (s, δ, $OH_{alcohol}$), 1369 (m, δ, $OH_{carboxylic\ acid}$), 1206 (s, v, C-OSu), 851 (m, δ, C=C), 756 (m, δ, C-C).^{1}H NMR (400

MHz, D_2O (NaOD)): δ = 8.25 (1H, H^a), 8.02 (1H, H^b), 7.25 (1H, H^c), 7.15 (2H, H^d), 6.60 (2H, H^e), 6.55 (2H, H^f), 2.93 (4H, -OSu) ppm. ^{13}C NMR (100 MHz, D_2O (NaOD)): δ = 180.6, 174.7, 174.5, 158.7, 139.6, 137.4, 134.1, 131.4, 130.0, 129.4, 128.4, 122.9, 112.2, 103.6, 25.4 ppm. MS (ESI^+): calcd. for $[M + H]^+$ 473.39 and found 474.3.

Synthesis of 5-carboxy-([a]-seminaphtho)-fluorescein (FLUO-2):

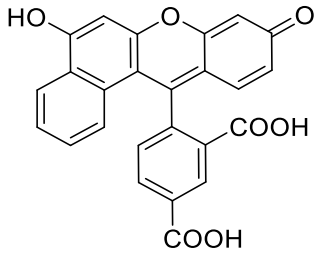

4-(2,4-dihydroxybenzoyl)isophthalic acid (200 mg, 0.66 mmol) andnaphthalene-1,3-diol (204 mg, 1.27 mmol) were dissolved in methanesulfonic acid (10 mL) and was stirred at room temperature overnight. Iced water (50 mL) was added in the mixture while stirring obtaining an orange precipitate. The precipitate was filtered and then was dissolved in an aqueous solution of NaOH 2M (40 mL). An aqueous solution of HCl 2M (30 mL) was added to the basic solution obtaining an orange solid. The solid was filtered and then was firstly re-precipitated in EtOH/H_2O and then in NaOH/HCl. The solid was filtered and dried under vacuum over P_2O_5 yield the title compound as an orange solid (170mg, 72% yield). $C_{25}H_{14}O_7$. MW: 426,38: C, 70.42; H, 3.31; O, 26.27. FT-IR (CsI disk, $\tilde{\nu}_{max}$, cm^{-1}): 3425 (br, v, $OH_{alcohol}$), 3067 (br, v, $OH_{carboxylic\ acid}$), 2432 (br, v, $OH_{carboxylic\ acid}$), 1685 (s, v, C=O), 1580 (s, v, $C{=}O_{carboxylic\ acid}$), 1463 (s,δ, $OH_{alcohol}$), 1307 (m, ,δ, $OH_{carboxylic\ acid}$), 1226 (s, v, C-O), 849 (m, δ, C=C), 759 (m,δ, C-C). ^{1}HNMR (400 MHz, D_2O (NaOD)): δ = 8.22 (1H, H^a), 8.10 (1H, H^j), 7.78 (1H, H^g), 7.37–7.28 (1H, H^b), 7.08 (1H, H^d), 6.88 (1H, H^c), 6.81–6.74 (1H, H^f), 6.71 (1H, H^e), 6.47 (2H, H^h, H^i), 6.33 (1H, H^f) ppm. ^{13}C NMR (100 MHz, D_2O (NaOD)): δ = 180.4, 176.9, 174.5, 174.0, 163.0, 155.7, 155.0, 138.6, 138.1, 137.1, 131.6, 130.8, 130.2, 129.8, 129.5, 129.4, 128.6, 126.7, 126.3, 124.7, 121.2, 111.7, 109.8, 103.1, 101.3 ppm. MS (ESI^+): calcd. for $[M + H]^+$ 427.1 and found 427.1.

Synthesis of 5-carboxy-([a]-seminaphtho)-fluorescein N-hydroxysuccinimide ester (FLUO-2a):

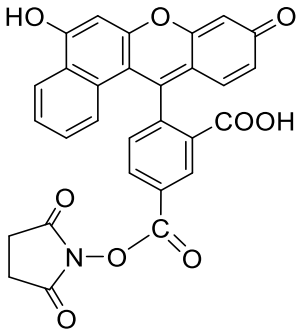

5-carboxy-([a]-seminaphtho)-fluorescein (170mg, 0.40mmole) was dissolved in dry DMF (3 mL). EDAC (130 mg, 0.68 mmole) and N-hydroxysuccinimide (55 mg, 0.48 mmole) were added and the mixture was stirred under N_2 overnight. Acetone (18 mL) and 0.05 M sodium phosphate buffer (25 mL) were added to the mixture. The mixture was extracted with a mixture of diethyl ether (100 mL) and ethyl acetate (50 mL). The organic phase was collected and was extracted with water (3×60 mL) and brine (1×75 mL).The resulting organic solution was dried with anhydrous sodium sulfate and then the solvent was removed by rotary evaporation under reduced pressure to obtain the desired compound as a bright orange solid (135mg, 79.8% yield). $C_{29}H_{17}NO_9$, MW: 523,45: C, 66.54; H, 3.27; N, 2.68; O, 27.51. FT-IR (CsI disk, $\tilde{\nu}_{max}$, cm^{-1}): 3065 (br, v, $OH_{alcohol}$), 1732 (s, v, C=O), 1589 (s, v, $C{=}O_{carboxylic\ acid}$), 1463 (s, δ, $OH_{alcohol}$), 1373 (m, δ, $OH_{carboxylic\ acid}$), 1207 (s, ν, C-OSu),848 (m, δ, C=C), 754 (m, δ, C-C). ^{1}H NMR (400 MHz, D_2O (NaOD)): δ = 8.22 (1H, H^a), 8.10 (1H, H^j), 7.78 (1H, H^g), 7.37–7.28 (1H, H^b), 7.08 (1H, H^d), 6.88 (1H, H^c), 6.81–6.74 (1H, H^f), 6.71 (1H, H^e), 6.47 (2H, H^h, H^i), 6.33 (1H, H^f), 2.92 (4H, -OSu) ppm. ^{13}C NMR (100 MHz, D_2O (NaOD)): δ = 180.4, 176.9, 177.2, 174.5, 174.0, 163.0, 155.7, 155.0, 138.6, 138.1, 137.1, 131.5, 130.8, 130.2, 129.8, 129.5, 129.4, 128.6, 126.7, 126.3, 124.7, 121.2, 111.7, 109.8, 103.1, 101.3, 25.5 ppm. MS (ESI^+): calcd. for $[M + H]^+$ 523.45 and found 524.5.

Synthesis of vitamin B_{12}-linker (2):

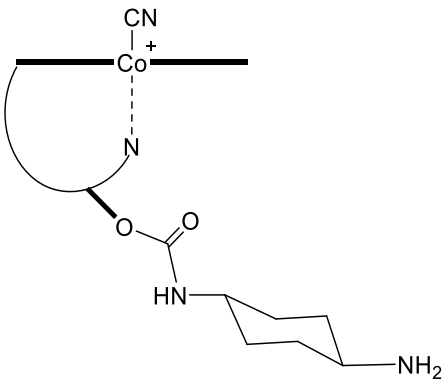

Vitamin B_{12} (2.00 g, 1.38 mmole), CDI (2.00 g, 1.38 mmole) and trans-1,4-diaminocyclohexane (1.58 g, 1.38 mmole) were dissolved in anhydrous DMSO. The mixture was stirred for 24 hours and then was added slowly to a vigorously stirring mixture of $EtO_2/CHCl_3$ (1:1). A red precipitate was observed which was filtered and then washed with acetone (50 mL). The crude compound was purified by column chromatography with $MeOH/MeCN/H_2O$ (1:0.225:0.025), yielding compound (**2**) as a fine pink crystalline powder (1.33 g, 73 %). $C_{70}H_{100}CoN_{16}O_{15}P$, MW: 1495,57: C, 56.22; H, 6.74; Co, 3.94; N, 14.99; O, 16.05; P, 2.07. FT-IR (CsI disk, $\tilde{\nu}_{max}$, cm^{-1}): 3430 (br, v, N-H), 3195 (br, v, O-H), 2960 (m, v, C-H), 2137 (w, v, C-N), 1667 (s, v, C=O + δ, N-H overlapped), 1638 (br, δ, $N\text{-}H_{corrin\ ring}$), 1576/1504/1466 (br, v, $C{=}C_{corrin\ ring}$), 1213 (s, v, C-O), 1203(w, v_{oop}, PO_2^-),1109 (s, v, P=O), 918 (m, δ, O-H), 620 (m, δ, Co-CN), 466 (m, v, $Co\text{-}N_{corrin\ ring}$). ^1H NMR (400 MHz, DMSO-d_6): δ = 8.60 (1H, NH_{amide}), 7.76/7.11 (2H, $N^{29}H$), 7.64/7.14 (2H, $N^{63}H$), 7.60 (2H, $N^{59}H$) 7.54/6.91 (2H, $N^{52}H$), 7.54/7.01 (2H, $N^{40}H$), 7.34/6.76 (2H, $N^{34}H$), 7.31 (1H, H^{B7}), 7.01 (1H, H^{B2}), 6.68/6.50 (2H, $N^{45}H$), 6.45 (1H, H^{B4}), 6.27 (1H, H^{R1}), 5.90 (1H, $C^{10}H$), 4.67 (1H, $C^{3}H$), 4.49 (1H, H^{R3}), 4.10 (1H, H^{Pr2}), 3.93 (1H, $C^{19}H$), 3.90 (1H, H^{R2}), 3.88 (1H, H^{R4}), 3.70 (1H, $C^{8}H$), 3.57/2.68 (2H, H^{Pr1}), 3.57 (2H, H^{R5}), 3.13 (1H, $C^{13}H$), 2.74 (1H, $C^{18}H$), 2.64/2.01 (2H, $C^{42}H$), 2.47 (3H, $C^{35}H$), 2.46 (4H, $C^{56}H$, $C^{60}H$,), 2.44/1.74 (2H, $C^{37}H$), 2.43 (3H, $C^{53}H$), 2.39/2.29 (2H, $C^{49}H$), 2.22 (2H, $C^{31}H$), 2.16/2.03 (2H, $C^{26}H$) 2.16 (6H, H^{B10}, H^{B11}), 1.93/1.62 (2H, $C^{48}H$), 1.78/1.66 (2H, $C^{30}H$), 1.78/0.92 (2H, $C^{41}H$), 1.75 (2H, $C^{55}H$), 1.70 (3H, $C^{36}H$), 1.33 (3H, $C^{47}H$), 1.22 (3H, $C^{54}H$), 1.17 (3H, $C^{25}H$), 1.05 (3H, $C^{46}H$), 1.04 (3H, H^{Pr3}), 0.32 (3H, $C^{20}H$). ^{13}C NMR (100 MHz, DMSO-d_6): δ = 15.0, 15.6, 16.4, 16.5,18.7, 19.9, 25.6, 25.8, 27.2, 30.7, 31.1, 31.6,

33.9, 35.1, 38.0, 40.4, 42.1, 46.6, 47.4, 48.6, 48.9,50.3, 53.0, 53.8, 54.9, 58.6, 63.0, 68.8, 70.5, 74.9, 84.4, 86.0, 93.5, 103.1, 105.9, 116.6, 129.7,131.3, 132.7, 136.5, 142.2, 149.2, 155.4, 164.6, 165.4, 171.0, 171.1, 172.6, 173.0, 173.7, 175.1,178.2, 179.5.

Synthesis of [B_{12}-5'-(FLUO-1)] (3):

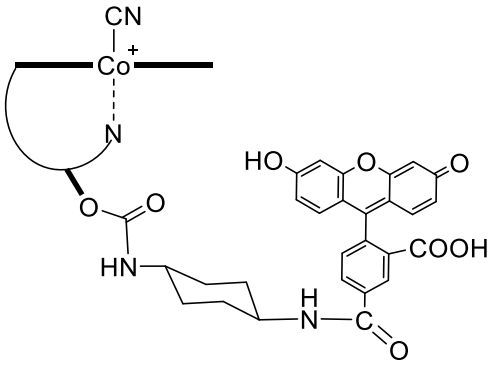

Compound (**2**)(50 mg, 0.03 mmole), **FLUO-1a** (23 mg, 0.04 mmole) and DIPEA (4.66μL) were dissolved in DMSO (3 mL). The mixture was stirred at room temperature under N_2 in a dark place for24 hours. The mixture was added to a vigorously stirring solution of DCM/Et_2O (1:1). A red precipitate was formed and then it was filtered. The crude compound was purified by column chromatography with MeOH/MeCN/H_2O (1:0.225:0.025), yielding compound (**3**) as a red crystalline solid (36 mg, 57% yield). $C_{91}H_{110}CoN_{16}O_{21}P$, MW: 1853,88: C, 58.96; H, 5.98; Co, 3.18; N, 12.09; O, 18.12; P, 1.67. FT-IR (CsI disk, $\tilde{\nu}_{max}$, cm^{-1}): 3452 (br, v, N-H+ br, $\nu_{a/s}$, NH_2), 3298 (br, v, O-H), 2930 (m, v, C-H +w, $\nu_{a/s}$, CH_2 + w, $\nu_{a/s}$, CH_3), 2138 (w, v, C-N), 1666 (br, v, C=O + br, v, $C=O_{amide\ II}$+ δ, N-H_{amide} overlapped), 1573 (δ, N-H_{amide}), 1648 (br, δ, N-$H_{corrin\ ring}$), 1582/1498/1493 (br, v, $C=C_{corrin\ ring}$+ v, $C=N_{corrin\ ring}$ overlapped), 1213 (s, v, C-O), 1190(w, ν_{oop}, PO_2^-),1103 (s, v, P=O + w, ν_a, P-Ph), 998 (m, δ, O-H+ s, ν_{ip}, PO_2^-), 618 (m, δ, Co-CN), 464 (m, v, Co-$N_{corrin\ ring}$). ^{1}H NMR (400 MHz, DMSO-d_6): δ = 10.23 (1H, OH_{FLUO}), 8.62 (1H, NH_{amide}), 8.47 (1H, H^a), 8.23 (1H, H^b), 7.76/7.11 (2H, $N^{29}H$), 7.64/7.14 (2H, $N^{63}H$), 7.60 (2H, $N^{59}H$) 7.54/6.91 (2H, $N^{52}H$), 7.54/7.01 (2H, $N^{40}H$), 7.34/6.76 (2H, $N^{34}H$), 7.31 (1H, H^{B7}), 7.09 (1H, H^c), 7.01 (1H, H^{B2}), 6.68/6.50 (2H, $N^{45}H$), 6.45 (1H, H^{B4}), 6.27 (1H, H^{R1}), 5.90 (1H, $C^{10}H$), 4.67 (1H, C^3H), 4.49 (1H, H^{R3}), 4.10 (1H, H^{Pr2}), 3.93 (1H, $C^{19}H$), 3.90 (1H, H^{R2}), 3.88 (1H, H^{R4}), 3.70 (1H, C^8H), 3.57/2.68 (2H, H^{Pr1}), 3.57 (2H, H^{R5}), 3.13 (1H,

$C^{13}H$), 2.74 (1H, $C^{18}H$), 2.64/2.01 (2H, $C^{42}H$), 2.47 (3H, $C^{35}H$), 2.46 (4H, $C^{56}H$, $C^{60}H$,), 2.44/1.74 (2H, $C^{37}H$), 2.43 (3H, $C^{53}H$), 2.39/2.29 (2H, $C^{49}H$), 2.22 (2H, $C^{31}H$), 2.16/2.03 (2H, $C^{26}H$) 2.16 (6H, H^{B10}, H^{B11}), 1.93/1.62 (2H, $C^{48}H$), 1.78/1.66 (2H, $C^{30}H$), 1.78/0.92 (2H, $C^{41}H$), 1.75 (2H, $C^{55}H$), 1.70 (3H, $C^{36}H$), 1.33 (3H, $C^{47}H$), 1.22 (3H, $C^{54}H$), 1.17 (3H, $C^{25}H$), 1.05 (3H, $C^{46}H$), 1.04 (3H, H^{Pr3}), 0.33 (3H, $C^{20}H$).

Synthesis of [B_{12}-5'-(FLUO-2)] (4):

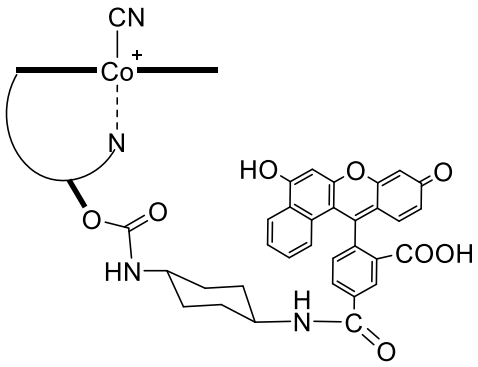

Compound (**2**) (10 mg, 0.006 mmole), **FLUO-2a** (6 mg, 0.01 mmole) and DIPEA (1 μL) were dissolved in DMSO (1 mL). The mixture was stirred at room temperature under N_2 in a dark place for24 hours. The mixture was added to a vigorously stirring solution of DCM/Et_2O (1:1). A red precipitate was formed and then it was filtered. The crude compound was purified by column chromatography with MeOH/MeCN/H_2O (1:0.225:0.025), yielding compound (**4**) as a red crystalline solid (4.9 mg, 48% yield). $C_{95}H_{112}CoN_{16}O_{21}P$, MW: 1903,94: C, 59.93; H, 5.93; Co, 3.10; N, 11.77; O, 17.65; P, 1.63. FT-IR (CsI disk, $\tilde{\nu}_{max}$, cm^{-1}): 3478 (br, v, N-H+ br, $v_{a/s}$, NH_2), 3295 (br, v, O-H), 2947 (m, v, C-H +w, $v_{a/s}$, CH_2 + w, $v_{a/s}$, CH_3), 2159 (w, v, C-N), 1652 (br, v, $C=O_{amide\ I}$ +br, v, $C=O_{amide}$ + δ, $N\text{-}H_{amide}$ overlapped), 1570 (δ, $N\text{-}H_{amide}$), 1690 (br, δ, $N\text{-}H_{corrin\ ring}$), 1564/1512/1428 (br, v, $C=C_{corrin\ ring}$+ v, $C=N_{corrin\ ring}$ overlapped), 1217 (s, v, C-O), 1168(w, v_{oop}, PO_2^-),1105 (s, v, P=O + w, v_a, P-Ph), 965 (m, δ, O-H+ s, v_{ip}, PO_2^-), 619 (m, δ, Co-CN), 458 (m, v, $Co\text{-}N_{corrin\ ring}$). ^1H NMR (400 MHz, DMSO-d_6, ppm): δ = 10.08 (1H, OH_{FLUO}), 8.62 (1H, NH_{amide}), 8.32 (1H, H^a), 7.76/7.11 (2H, $N^{29}H$), 7.64/7.14 (2H, $N^{63}H$), 7.60 (2H, $N^{59}H$) 7.54/6.91 (2H, $N^{52}H$), 7.54/7.01 (2H, $N^{40}H$), 7.34/6.76 (2H, $N^{34}H$), 7.31 (1H, H^{B7}), 7.23 (1H, H^b), 7.01 (1H, H^{B2}), 6.80 (1H, H^c), 6.68/6.50 (2H, $N^{45}H$), 6.45 (1H, H^{B4}), 6.27 (1H, H^{R1}), 5.90 (1H, $C^{10}H$), 4.67 (1H, C^3H), 4.49 (1H, H^{R3}), 4.10 (1H, H^{Pr2}), 3.93 (1H, $C^{19}H$), 3.90 (1H,

H^{R2}), 3.88 (1H, H^{R4}), 3.70 (1H, $C^{8}H$), 3.57/2.68 (2H, H^{Pr1}), 3.57 (2H, H^{R5}), 3.13 (1H, $C^{13}H$), 2.74 (1H, $C^{18}H$), 2.64/2.01 (2H, $C^{42}H$), 2.47 (3H, $C^{35}H$), 2.46 (4H, $C^{56}H$, $C^{60}H$,), 2.44/1.74 (2H, $C^{37}H$), 2.43 (3H, $C^{53}H$), 2.39/2.29 (2H, $C^{49}H$), 2.22 (2H, $C^{31}H$), 2.16/2.03 (2H, $C^{26}H$) 2.16 (6H, H^{B10}, H^{B11}), 1.93/1.62 (2H, $C^{48}H$), 1.78/1.66 (2H, $C^{30}H$), 1.78/0.92 (2H, $C^{41}H$), 1.75 (2H, $C^{55}H$), 1.70 (3H, $C^{36}H$), 1.33 (3H, $C^{47}H$), 1.22 (3H, $C^{54}H$), 1.17 (3H, $C^{25}H$), 1.05 (3H, $C^{46}H$), 1.04 (3H, H^{Pr3}), 0.32 (3H, $C^{20}H$).

7.4 Chapter 3 – Experimental

Synthesis of *cis*-[Pt(NH$_3$)$_2$I$_2$] (Pt1):

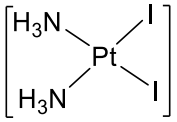

An aqueous solution (2 mL) of KI (1.1509 g, 6.93 mmol) was added to an aqueous solution (15 mL) of $K_2[PtCl_4]$ (1.1509 g, 0.693 mmol) obtaining a dark brown solution. After 30 min, an aqueous solution (3 mL) of NH_4Cl (76.2 mg, 1.425 mmol) was added to the mixture. The pH was adjusted to 10 upon a dropwise addition of an aqueous solution of KOH 2M leading to the formation of a yellow precipitate. The yellow solid was subsequently filtered, washed with cold water, ethanol and diethyl ether and dried under vacuum over P_2O_5 (850 mg, 86% yield). $H_6I_2N_2Pt$, MW: 482,95: H, 1.25; I, 52.55; N, 5.80; Pt, 40.39. FT-IR (CsI disk, $\tilde{\nu}_{max}$, cm^{-1}): 488.87 (ν_a, Pt-N), 479.22 (ν_s, Pt-N), 243.98 (δ, N-Pt-N), 3280.32 (ν_a, NH_3), 3261 (ν_s. NH_3), 761.74 (ρ, NH_3). ^{1}H NMR (400 MHz, DMSO-d_6): δ = 4.67 (6H, NH_3).

Synthesis of *cis*-[Pt(NH$_3$)$_2$Cl$_2$] (Pt2):

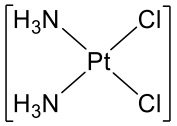

To an aqueous solution (15 mL) of **Pt1**(291 mg, 0.6 mmol), an aqueous solution (1 mL) of $AgNO_3$ (203.8 mg, 1.2 mmol)was added and a white precipitate of AgCl was observed. The mixture was heated in absence of light at 55 ˚C overnight. The mixture

was filtered to remove AgCl and then NaCl (141 mg, 2.41 mmol) was added to the filtrate. The mixture was stirred for 1 hour and a yellow solid was formed. The mixture was kept overnight at 4˚C. The yellow solid was filtered, washed with cold water and diethyl ether and dried under vacuum over P_2O_5 (150 mg, 26% yield). $Cl_2H_6N_2Pt$, MW: 300,05: Cl, 23.63; H, 2.02; N, 9.34; Pt, 65.02. FT-IR (CsI disk, $\tilde{\nu}_{max}$, cm^{-1}): 323 ($\nu_{as,}$ Pt-Cl), 251 (δ, N-Pt-N), 3289.96 ($\nu_{a,}$ NH_3), 3210.9 (ν_s. NH_3), 798.39 (ρ, NH_3). ^{1}H NMR (400 MHz, DMSO-d_6): δ = 5.99 (6H, NH_3).

Synthesis of $(Ph_4P)[PtCl_3(NH_3)]$ (Pt3):

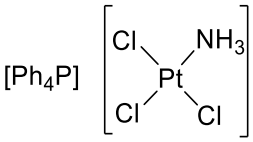

A solution of **Pt2** (48 mg, 0.16 mmol) in water (5 mL) was treated under stirring with Et_4Cl (37 mg, 0.22 mmol). The solution was stirred at 100˚C under N_2. After 6 hours the mixture cooled down to room temperature and a mixture (1:1) of ethyl acetate/hexane (80 mL) was added and kept overnight at -10˚C. The mixture then came to room temperature, water (15 mL) was added, and then was filtered. To the filtrate, $(PPh_4)Cl$ (60 mg, 0.16 mmol) in water (1 mL) was added and the solution was left overnight at 4˚C. The precipitation was filtered, washed with cold water and diethyl ether and dried under vacuum over P_2O_5 (32 mg, 63% yield). $C_{24}H_{23}Cl_3NPPt$, MW: 657,86: C, 43.82; H, 3.52; Cl, 16.17; N, 2.13; P, 4.71; Pt, 29.65. FT-IR (CsI disk, $\tilde{\nu}_{max}$, cm^{-1}): 3322.75 (ν_a, NH_3), 3264.89 (ν_s, NH_3), 3056.62 (ν, C-H), 1434.78 (ν, C=C), 527.44 (δ_{oop}, PPh_4), 327.84 (ν, Pt-Cl). ^{1}H NMR (400 MHz, DMSO-d_6): δ = 7.96 (4H, para-CH), 7.81 (8H, meta-CH), 7.73 (8H, ortho-CH).

Synthesis of *cis*-$[PtI_2(MeNH_2)_2]$ (Pt4):

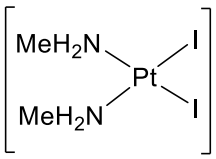

KI (1 g, 6 mmol) was added under stirring to an aqueous solution (20 mL) of $K_2[PtCl_4]$ (249 mg, 0.6 mmol). After 90 min, methylamine (0.0965 ml, 12 mmol) was

added, and the solution was left for a further 3 hours. The precipitation was filtered, washed with cold water and diethyl ether and dried under vacuum over P_2O_5 (127 mg, 51% yield). $C_2H_{10}I_2N_2Pt$, MW: 511,01: C, 4.70; H, 1.97; I, 49.67; N, 5.48; Pt, 38.18. FT-IR (CsI disk, $\tilde{\nu}_{max}$, cm^{-1}): 475.27 (ν_s, Pt-N), 1069.62 (ν, N-CH_3), 1562.06 (δ, N-H), 3212.63 (ν_s, NH_3), 3245.61 (ν_a, NH_3). ^{1}H NMR (400 MHz, Acetone-d_6): δ = 4.49 (4H, NH_2); 2.65 (6H, CH_3).

Synthesis of $[Pt(MeNH_2)I_2]_2$ (Pt5):

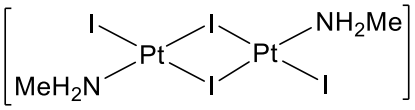

$HClO_4$ (103 mg, 1.02 mmol) previously dissolved in 6 mL of EtOH was added under constant stirring to **Pt4** (150 mg, 0.29 mmol). After being left overnight, the brown precipitate was filtered and washed with a 1:1mixture of EtOH:H_2O and left to dry under vacuum over P_2O_5 (93 mg, 36% yield). $C_2H_{10}I_4N_2Pt_2$, MW: 959,90: C, 2.50; H, 1.05; I, 52.88; N, 2.92; Pt, 40.65. FT-IR (CsI disk, $\tilde{\nu}_{max}$, cm^{-1}): 475.37 (ν_s, Pt-N), 486.94 (ν_a, Pt-N), 254.56 (ν_s, N-Pt-N), 1070.3 (ν, N-CH_3), 1563.06 (δ, N-H), 3210.69 (ν_s, NH_3), 3251.4 (ν_a, NH_3). ^{1}H NMR (400 MHz, Acetone-d_6): δ = 4.39 (4H, NH_2), 2.65 (3H, CH_3), 2.50 (3H, CH_3).

Synthesis of $K[Pt(MeNH_2)Cl_3]$ (Pt6):

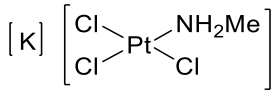

An aqueous solution (6 mL) of **Pt5** (82 mg, 0.086 mmol) was added to an aqueous solution of $AgNO_3$ (88 mg, 0.58 mmol). The mixture was left under constant stirring in absence of light at 50˚C for 4 days. The solution was then filtered and KCl (64 mg, 0.86 mmol) was added in the filtrate. The mixture was left for constant stirring at 50˚C in the dark for 24 hours. The solution was then filtered, washed with H_2O and left to dry under vacuum over P_2O_5 (46 mg, 52% yield). CH_5Cl_3KNPt, MW: 371,59: C, 3.23; H, 1.36; Cl, 28.62; K, 10.52; N, 3.77; Pt, 52.50. FT-IR (CsI disk, $\tilde{\nu}_{max}$, cm^{-1}):

314.49 (ν_s, Pt-Cl), 333.42 (ν, Pt-Cl), 1079.98 (ν, C-N), 1585.44 (δ, N-H), 3251.21 (ν, N-H). ^{1}H NMR (400 MHz, Acetone-d_6): δ = 5.74 (2H, NH_2), 4.30 (3H, CH_3).

Synthesis of *cis*-[$PtI_2(py)_2$] (Pt7):

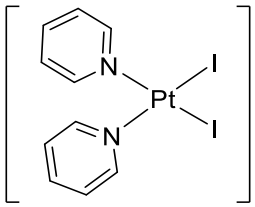

KI (1 g, 6 mmol) was added under constant stirring to an aqueous solution (8 mL) of $K_2[PtCl_4]$ (250 mg, 0.6 mmol). After 90 min, 145 μL (1.8 mmol) of pyridine were added and the solution was left for further 3 hours. The precipitation was filtered, washed with cold water and diethyl ether and dried under vacuum over P_2O_5 (136 mg, 56% yield). $C_{10}H_{10}I_2N_2Pt$, MW: 607,10: C, 19.78; H, 1.66; I, 41.81; N, 4.61; Pt, 32.13. FT-IR (CsI disk, $\tilde{\nu}_{max}$, cm^{-1}): 3021.89 (ν_s, C-H), 3035.90 (ν_s, C-H), 461.01 (ν_a, Pt-N), 447.37 (ν_s, Pt-N), 244.55 (δ, N-Pt-N). ^{1}H NMR (400 MHz, Acetone-d_6): δ = 8.98 (4H, ortho-CH), 7.98 (4H, meta-CH), 7.52 (2H, para-CH).

Synthesis of $[Pt(py)I_2]_2$ (Pt8):

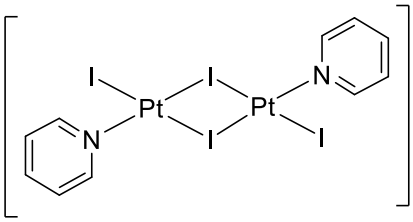

An ethanolic solution of $HClO_4$ (115 mg, 1.15 mmol) was added under constant stirring to an aqueous solution of **Pt7** (200 mg, 0.32 mmol). After 17 hours, the brown precipitate was filtered and washed with a 1:1mixture of EtOH:H_2O and was left to dry under vacuum over P_2O_5 (116 mg, 39% yield). $C_{10}H_{10}I_4N_2Pt_2$, MW: 1055,99: C, 11.37; H, 0.95; I, 48.07; N, 2.65; Pt, 36.95. FT-IR (CsI disk, $\tilde{\nu}_{max}$, cm^{-1}): 451.26 (ν_s, Pt-N), 757.89 (ν, py C-H), 1070 (δ, py C-H), 1448.38 (ν, py-ring). ^{1}H NMR (400 MHz, Acetone-d_6): δ = 8.95 (4H, ortho-CH), 8.03 (4H, meta-CH), 7.58 (2H, para-CH).

Synthesis of K[Pt(py)Cl$_3$] (Pt9):

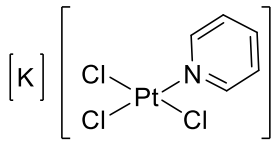

An aqueous solution (5 mL) of **Pt8** (100 mg, 0.23 mmol) was added to an aqueous solution of $AgNO_3$ (242 mg, 1.4 mmol). The mixture was left under constant stirring in the absence of light at 50˚C for 4 days. The solution was then filtered and KCl (177 mg, 2.38 mmol) was added in the filtrate. The mixture was left for constant stirring at 50˚C in the dark for 1 more day. The solution was then filtered, washed with H_2O and left to dry under vacuum over P_2O_5, yielding the corresponding yellow powder of **Pt9** (43 mg, 43% yield). $C_5H_5Cl_3KNPt$, MW: 419,63: C, 14.31; H, 1.20; Cl, 25.34; K, 9.32; N, 3.34; Pt, 46.49. FT-IR (CsI disk, $\tilde{\nu}_{max}$, cm^{-1}): 328.8 (ν, Pt-Cl), 764.86 (ν, py C-H), 1361.25 (ν, C-N), 1606.02 (ν, py-ring). ^{1}H NMR (400 MHz, Acetone-d_6): δ = 8.96 (2H, ortho-CH), 7.84 (2H, meta-CH), 7.30 (1H, para-CH).

Synthesis of (PPh$_4$)ESDT

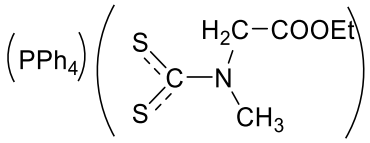

4 mL (6.51 mmol) of NaOH were added dropwise to an aqueous solution of sarcosine ethyl ester hydrochloride (996.3 mg, 6.48 mmol) at 0˚C (pH=6). Subsequently, the solution was treated dropwise with CS_2 (400 μL, 6.62 mmol) (pH=9). After 2 hours (PPh_4)Cl (504 mg, 3.25 mmol) was added to the solution under stirring at room temperature. The solution was then stirred for 30 min and the precipitation of a yellow solid was observed. The solution was filtered, and the yellow solid was washed with cold water and dried under vacuum over P_2O_5, yielding (PPh_4)ESDT as a fine yellow powder (650 mg, 73% yield). $C_{30}H_{30}NO_2PS_2$, MW: 531,67: C, 67.77; H, 5.69; N,

2.63; O, 6.02; P, 5.83; S, 12.06. FT-IR (CsI disk, $\tilde{\nu}_{max}$, cm^{-1}):2980 (ν, C-H), 1731.76 (ν, C=O), 1434.78 (ν, N-CSS), 1268.93 (ν_a, CSS) + (ρ, CSS) + (ν_a, C-N-C), 1193.72 (ν_a, CSS), 1029.94 (ν, N-CH_3). ^{1}H NMR (400 MHz, DMSO-d_6): δ = 7.97 (4H, t, para-CH), 7.81 (8H, dd, meta-CH), 7.77 (8H, dd, ortho-CH), 4.95 (2H, s, N-CH_2), 4.07 (2H, q, O-CH_2), 3.39 (3H, s, N-CH_3), 1.18 (3H, t, CH_3). ^{13}C NMR (100 MHz, DMSO-d_6): δ = 135.4, 134.6, 130.5, 118.1/117.2, 59.8, 56.1, 14.2.

Synthesis of ESDTM:

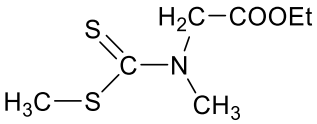

To an ethanolic (10mL) solution of sarcosine ethyl ester (1g, 6.5mmol) and CS_2 (196μL, 3.25mmol), a 1:1 ethanol/H_2O solution of NaOH (260mg, 6.5mmol) was added and subsequently the mixture was treated with MeI (203 μL, 3.25mmol). The solution stirred for 1 hour and then H_2O (100mL) was added under vigorous stirring until white precipitate was observed. The solution stayed at 4°C overnight. The white flocculent crystalline solid collected by vacuum filtration, washed with H_2O and dried under vacuum over P_2O_5 (820 mg, 82% yield). $C_7H_{13}NO_2S_2$. MW: 207,31: C, 40.56; H, 6.32; N, 6.76; O, 15.44; S, 30.93.FT-IR (CsI disk, $\tilde{\nu}_{max}$, cm^{-1}): 3076 (br, ν, C-H), 1758 (s, ν, C=O), 1453 (s, ν, N-CSS), 1219 (br, ν_a, CSS + w, ρ, CSS+ w, ν_a, C-N-C overlapped), 1190 (s, ν_a, CSS), 1012 (w, ν, N-CH_3). ^{1}H-NMR (400 MHz, DMSO-d_6): δ = 4.80 (2H, N-CH_2), 4.50 (3H, N-CH_3), 4.22 (2H, OCH_2CH_3), 2.64 (3H, S-CH_3), 1.29 (3H, OCH_2CH_3).^{13}C NMR (100 MHz, DMSO-d_6): δ = 59.7, 56.2, 42.5, 14.5, 14.3.

Synthesis of DMDTM:

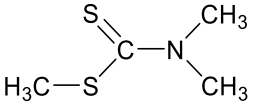

DMDTM was prepared upon the reaction of Na($S_2CN(CH_3)_2$) with MeI in EtOH/H_2O. The oily product dissolved in diethyl ether, washed with H_2O and dried over

anhydrous Na_2SO_4. The solvent was then removed under reduced pressure and the title compound was recrystallized from n-pentane (85mg, 75% yield). $C_4H_9NS_2$, MW: 135,24: C, 35.52; H, 6.71; N, 10.36; S, 47.41. FT-IR (CsI disk, $\tilde{\nu}_{max}$, cm^{-1}): 2985 (br, ν, C-H), 1794 (s, ν, C=O), 1511 (s, ν, N-CSS), 1252 (br, ν_a, CSS + w, ρ, CSS+ w, ν_a, C-N-C overlapped), 1153 (s, ν_a, CSS), 1026 (w, ν, N-CH_3).^{1}H-NMR(400 MHz, DMSO-d_6): δ = 1.23 (3H, S-CH_3), 3.34/3.46 (N-CH_3). ^{13}C NMR (100 MHz, DMSO-d_6): δ = 42.6, 12.4.

Synthesis of Pt(ESDTM)Cl_2 (Pt10):

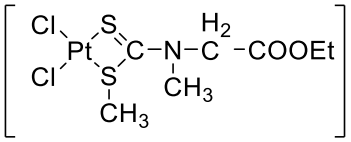

$PtCl_2$ (200mg, 0.8mmol) and ESDTM (156mg, 0.8mmol) were dissolved in benzene. The mixture stirred vigorously in absence of light for 24 hours. The solution filtrated and evaporated to dryness to yield a yellow oil. Multiple washings with n-pentane converted the oily product to a bright yellow solid which dried under vacuum over P_2O_5 (101mg, 31.8% yield). $C_7H_{13}NO_2PtS_2$, MW: 402,39: C, 20.89; H, 3.26; N, 3.48; O, 7.95; Pt, 48.48; S, 15.93. FT-IR (CsI disk, $\tilde{\nu}_{max}$, cm^{-1}): 3076 (br, ν, C-H), 1758 (s, ν, C=O), 1453 (s, ν, N-CSS), 1219 (br, ν_a, CSS + w, ρ, CSS + w, ν_a, C-N-C overlapped), 1190 (s, ν_a, CSS), 1012 (w, ν, N-CH_3), 546 (s, ν_s, S-C-S), 434 (w, ν, S-Pt-S)355 (w, ν, Pt-Cl), 315(w, ν_s, Pt-Cl). ^{1}H-NMR (400 MHz, DMSO-d_6): δ = 4.75 (2H, N-CH_2), 4.44 (3H, N-CH_3), 4.21 (2H, OCH_2CH_3), 2.54 (3H, S-CH_3), 1.28 (3H, OCH_2CH_3). ^{13}C NMR (100 MHz, DMSO-d_6): δ = 59.7, 56.2, 42.5, 14.3.

Synthesis of [Pt(TMDT)Cl_2] (Pt11):

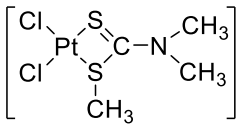

Pt11 was prepared by stirring a suspension of $PtCl_2$ (100mg, 0.4mmol) and **DMDTM** (56mg,0.8mmol) dissolved in DCM (2mL) and the mixture was stirred for 3 hours at room temperature. The reaction went on gradual formation of a red solution and a

yellow-solid, which was filtered and washed carefully with DCM (20mL), n-pentane (20mL) and dried under vacuum over P_2O_5 (133 mg, 70% yield). $C_4H_9NPtS_2$, MW: 330,33: C, 14.54; H, 2.75; N, 4.24; Pt, 59.06; S, 19.41. FT-IR (CsI disk, $\tilde{\nu}_{max}$, cm^{-1}): 2985 (br, ν, C-H), 1794 (s, ν, C=O), 1511 (s, ν, N-CSS), 1252 (br, ν_a, CSS + w, ρ, CSS+ w, ν_a, C-N-C overlapped), 1153 (s, ν_a, CSS), 1026 (w, ν, N-CH_3), 565 (s, ν_s, S-C-S), 435 (w, ν, S-Pt-S), 325 (w, ν, Pt-Cl), 317 (w, ν_s, Pt-Cl). ^{1}H NMR (400 MHz, DMSO-d_6): δ = 3.26 (6H, N-CH_3), 2.64 (3H, S-CH_3). ^{13}C NMR (100 MHz, DMSO-d_6): δ = 201.8, 12.2.

Synthesis of Pt(ESDT)$_2$ (Pt12)

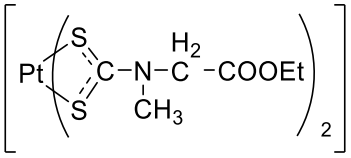

Pt12 was isolated by reacting **Pt3** (0.05 mmol) and **(PPh$_4$)ESDT** (0.05 mmol) in anhydrous benzene under vigorous stirring for 24 hours, in the dark. After this time, by addition of n-pentane a red oil was separated which was decanted and treated with further n-pentane. The resulting yellow powder was filtered, washed with n-pentane and dried under reduced pressure. The complex was recrystallized from a n-pentane/DCM solution obtaining compound **Pt12** in 75% yield. $C_{12}H_{20}N_2O_4PtS_4$, MW: 774.72: C, 18.60; H, 2.60; N, 3.62; O, 8.26; Pt, 50.36; S, 16.55. FT-IR (CsI disk, $\tilde{\nu}_{max}$, cm^{-1}): 2985 (ν, C-H), 1743 (ν, C=O), 1527 (ν, N-CSS), 1279 (ν_a, CSS) + (ρ, CSS) + (ν_a, C-N-C), 1208 (ν_a, CSS), 1037 (ν, N-CH_3), 568 (s, ν_s, S-C-S), 436 (w, ν, S-Pt-S).^{1}H NMR (400 MHz, DMSO-d_6): δ = 4.44 (2H, N-CH_2), 4.18 (2H, O-CH_2),3.19-3.20 (3H,N-CH_3), 1.22-1.23 (3H, CH_3). ^{13}C NMR (100 MHz, DMSO-d_6): δ = 59.7, 56.1, 15.2.

Synthesis of [Zn(ESDT)$_2$] (Zn2)

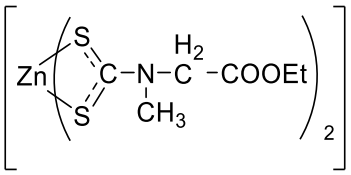

CS_2 (360 μL, 5.92 mmol) was added dropwise under stirring to an aqueous solution (10mL) of sodium hydroxide (233 mg, 5.82 mmol) and ESDT*HCl (893.5 mg, 5.82 mmol) at 0°C. The mixture was stirred for 1.5 hours (pH 10 to 6) and subsequently was added dropwise to a [$Zn(OAc)_2 \cdot 2H_2O$] (635.7 mg, 2.89 mmol) solution. Immediate precipitation of a white precipitate occurred which was then centrifuged and washed with water and dried under vacuum over P_2O_5 (563 mg, 43% yield). $C_{12}H_{20}N_2O_4S_4Zn$, MW: 257,65: C, 27.97; H, 3.91; N, 5.44; O, 12.42; S, 24.89; Zn, 25.38. FT-IR (CsI disk, $\tilde{\nu}_{max}$, cm^{-1}): 2979 (ν, C-H), 2933 (ν, C-H), 1735 (ν, C=O), 1497 (ν, NCSS), 1196 (ν, C-OEt), 968 (ν, SCS), 372 (ν_a, ZnS_4). ^{1}H NMR (400MHz, DMSO-d_6): δ = 4.94 (2H, s, N-CH_2), 4.08 (2H, q, O-CH_2), 3.35 (3H, s, N-CH_3), 1.19 (3H, t, CH_3). ^{13}C NMR (100MHz, DMSO-d_6): δ = 59.73, 56, 14.19/14.17.

7.5 Chapter 4 – Experimental

Synthesis of [Pt(dppe)Cl_2] (Pt15):

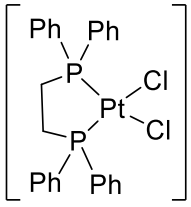

K_2PtCl_4 (222mg, 0.5mmol) and dppe (224.4mg, 0.5mmol) were loaded into microwave tube, a 1:1 mixture of chloroform/EtOH (6mL) was added and the solution stirred at 145°C for 1 hour. The mixture stirred for an additional 1 hour. The solvent removed and the off-white solid loaded into a clean microwave tube with DMF (3mL) and irradiated under the same conditions for 6 minutes. Diethyl ether (30mL) added into the tube and the solution stayed at 4°C overnight. After this time, white crystals collected by vacuum filtration and dried under vacuum over P_2O_5 (380mg, 71% yield). $C_{26}H_{26}Cl_2P_2Pt$, MW: 666,43: C, 46.86; H, 3.93; Cl, 10.64; P, 9.30; Pt, 29.27.FT-IR (CsI disk, $\tilde{\nu}_{max}$, cm^{-1}): 3061.72 (v, C-H), 1435.94 (v, C=C), 1184.89 (δ_{ip} C-H), 1106.37 ($\nu_q\nu_{ib}$ P-Ph_2), 822.05 (δ_{oop} C-H), 705.15 ($\nu_m\nu_{ib}$ P-Ph_2), 534.17 ($\delta_y\nu_{ib}$ P-Ph_2), 493.68 (ν_a P-Pt-P), 461.70 (ν_s P-Pt-P), 439.28 (ν_t P-Ph_2), 313.54 (ν_a $PtCl_2$), 239.42 (ν_s $PtCl_2$).^{1}H NMR (400 MHz, DMSO-d_6): δ = 7.84 (8H, ortho-CH), 7.47 (4H,

para-CH), 7.45 (8H, meta-CH), 2.37 (4H, CH_2).^{13}C NMR (100 MHz, DMSO-d_6): δ = 135.5, 132.1, 129.1. ^{31}P NMR (400MHz, DMSO-d_6): δ = 41.8.

Synthesis of [Au(bpy)Cl$_2$]:

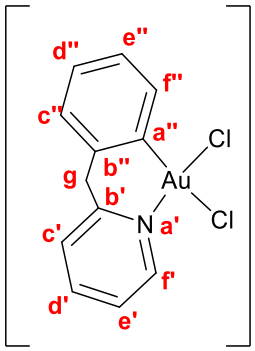

An acetonitrile solution (5 mL) of compound 2-benzylpyridine (80.8 µL, 0.503 mmol) was added dropwise to an aqueous solution (5 mL) of Na[$AuCl_4$]·2H_2O (200 mg, 0.503 mmol) at room temperature, observing yellow precipitation. The yellow precipitate was filtered and washed with water. Subsequently, the yellow precipitation was diluted in a solution of H_2O/MeCN (10 mL, 1:1) and stirred under reflux for 3 h. The solution was left to cool down to room temperature, observing a white precipitate. The white precipitate was filtered and washed with water. Recrystallisation of the white solid in a solution of Et_2O/ DCM (1:1) resulted in the compound [Au(bpy)Cl_2] (147 mg, 67 %) as an off-white solid. $C_{12}H_{10}AuCl_2N$, MW: 436,09: C, 33.05; H, 2.31; Au, 45.17; Cl, 16.26; N, 3.21. FT-IR (CsI disk, ῡmax, cm-^{1}): 3116/3050 (w, ν, C-H aromatic), 2978/2911 (w, ν, C-H aliphatic), 1610 (m, ν, quadrant), 1566 (m, ν, quadrant), 1460 (m, ν, semicircle), 1438 (s, ν, semicircle), 1026 (s, δ_{ip}, CH rocking), 751 (vs, δ, adjacent H wagging), 359 (m, ν, Au-Cl trans to N), 350 (w, ν, Au-Cl trans to N), 294 (s, ν, Au-Cl trans to C). ^{1}H NMR (400 MHz DMSO-d_6): δ = 9.17 (1H, $H^{f'}$), 8.26 (1H, $H^{d'}$), 7.99(1H, $H^{c'}$), 7.71 (1H, $H^{e'}$), 7.40 (1H, $H^{f''}$), 7.24(1H, $H^{c''}$), 7.18 (1H, $H^{d''}$), 7.07 (1H, $H^{e''}$), 4.61, (2H, H^{g}). ^{13}C NMR (100 MHz, DMSO-d_6): δ = 155.7, 152.1, 143.3, 141.1, 132.7, 132.0, 128.6, 128.0, 126.9, 126.4, 124.5, 46.1.

Synthesis of BOC-N-(4-ethynylphenyl)piperidine-4-carboxamide:

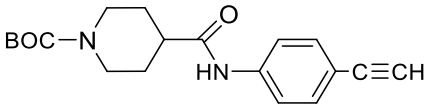

BOC-Isonipecotic acid (251 mg, 0.63 mmol) and 4-ethynylaniline(251 mg, 0.63 mmol) were reacted with DCC(251 mg, 0.63 mmol)and HOBt (251 mg, 0.63 mmol)under N_2 at ambient temperature for two days in dry DCM. The crude brown oil was collected after evaporation of DCM purified on silica gel with EtOAc/PET in ratio 1:2 to afford the amide in the form of a fine white powder (218 mg, 82% yield). $C_{14}H_{15}N_2O$, MW: 266,11: C, 67.70; H, 5.68; N, 10.53; O, 12.02. FT-IR (CsI disk, $\tilde{\nu}_{max}$, cm^{-1}): 3459 (br, $\nu_{a/s}$, NH_2), 1666 (vs, ν, $C{=}O_{amide\ I}$), 1648 (s, δ_{ip}, CNH). ^1H NMR (400 MHz, DMSO-d_6, ppm): δ = 10.10 (1H, NH), 7.98 (2H, o-H), 7.69 (2H, m-H), 4.00(4H, $C^{2',6'}H_{eq}$), 3.59 (1H, C≡CH), 3.39 (4H, $C^{2',6'}H_{ax}$), 2.77 (2H, $C^{4'}H$), 1.77 (4H, $C^{3',5'}H_{eq}$), 1.48 (4H, $C^{3',5'}H_{ax}$), 1.38 (9H, BOC). ^{13}C NMR (100 MHz, DMSO-d_6, ppm): δ = 174.4, 173.3, 132.4, 127.9, 118.8, 110.0, 83.7, 78.7, 56.1, 51.5, 42.8, 28.1, 18.6.

Synthesis of B_{12}-1

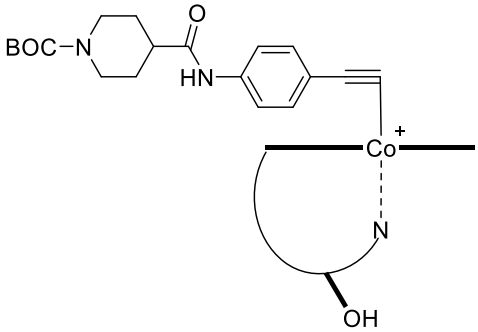

B_{12}-1 derivative was synthetized following a slightly modified ligand exchange procedure. A mixture of vitamin B_{12} (50 mg, 0.037 mmol), CuOAc (0.45 mg, 0.0037 mmol) and BOC-N-(4-ethynylphenyl)piperidine-4-carboxamide (48 mg, 0.148 mmol) was stirred in DMA (2 ml) until dissolution. Then, DBU (9.0 µl, 0.060 mmol) was added and the solution was stirred at room temperature for 4 hours. The crude was precipitated by dropwise addition to a stirring 1:1solution of Et_2O/DCM (50 ml). After filtration, the residue was dissolved in a 1:1mixture of MeOH/H_2O (2 ml), filtered through a 0.45µm microfilter and purified by preparative HPLC. The eluting

band containing the desired product was isolated, evaporated and lyophilized (18.7 mg, 31%). $C_{82}H_{111}CoN_{15}O_{17}P$, MW: 1681,47: C, 58.00; H, 6.45; Co, 3.70; N, 13.18; O, 16.05; P, 1.94. ^{1}H NMR (400 MHz, MeOD, ppm): δ = 7.31 (1H, H^{B7}), 7.01 (1H, H^{B2}), 6.45 (1H, H^{B4}), 6.27 (1H, H^{R1}), 5.90 (1H, $C^{10}H$), 4.67 (1H, $C^{3}H$), 4.49 (1H, H^{R3}), 4.10 (1H, H^{Pr2}), 3.93 (1H, $C^{19}H$), 3.90 (1H, H^{R2}), 3.88 (1H, H^{R4}), 3.70 (1H, $C^{8}H$), 3.57/2.68 (2H, H^{Pr1}), 3.57 (2H, H^{R5}), 3.13 (1H, $C^{13}H$), 2.74 (1H, $C^{18}H$), 2.64/2.01 (2H, $C^{42}H$), 2.47 (3H, $C^{35}H$), 2.46 (4H, $C^{56}H$, $C^{60}H$,), 2.44/1.74 (2H, $C^{37}H$), 2.43 (3H, $C^{53}H$), 2.39/2.29 (2H, $C^{49}H$), 2.22 (2H, $C^{31}H$), 2.16/2.03 (2H, $C^{26}H$) 2.16 (6H, H^{B10}, H^{B11}), 1.93/1.62 (2H, $C^{48}H$), 1.78/1.66 (2H, $C^{30}H$), 1.78/0.92 (2H, $C^{41}H$), 1.75 (2H, $C^{55}H$), 1.70 (3H, $C^{36}H$), 1.33 (3H, $C^{47}H$), 1.22 (3H, $C^{54}H$), 1.17 (3H, $C^{25}H$), 1.05 (3H, $C^{46}H$), 1.04 (3H, H^{Pr3}), 0.45 (3H, $C^{20}H$).

Synthesis of N-phenylpiperidine-4-carboxamide:

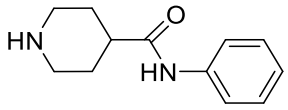

BOC-Isonipecotic acid (251 mg, 0.63 mmol) and aniline(251 mg, 0.63 mmol) reacted with DCC(251 mg, 0.63 mmol)and HOBt (251 mg, 0.63 mmol) under N_2 at ambient temperature for two days in dry DCM. The crude brown oil was collected after evaporation of DCM, deprotected with 6N HCl in EtOAc, purified on silica gel with EtOAc/PET in ratio 1:2 to afford the amide in the form of a fine white powder(230 mg, 87% yield). $C_{12}H_{16}N_2O$, MW: 204,27: C, 70.56; H, 7.90; N, 13.71; O, 7.83. FT-IR (CsI disk, $\tilde{\nu}_{max}$, cm^{-1}): 3422 (br, $\nu_{a/s}$, NH_2), 1663 (vs, ν, $C{=}O_{amide\ I}$), 1667 (s, δ_{ip}, CNH). ^{1}H NMR (400 MHz, DMSO-d_6, ppm): δ = 9.80 (1H, NH), 7.58 (2H, o-H), 7.27 (2H, m-H), 7.00 (1H, p-H), 2.95 (4H, $C^{2',6'}H_{eq}$), 2.47 (4H, $C^{2',6'}H_{ax}$), 2.39 (2H, $C^{4'}H$), 1.64 (4H, $C^{3',5'}H_{eq}$), 1.51 (4H, $C^{3',5'}H_{ax}$). ^{13}C NMR (100 MHz, DMSO-d_6, ppm): δ = 174.3, 132.2, 127.4, 117.6, 111.1, 51.5, 42.7, 28.1.

Synthesis of[Zn(dtc-Inp-an)$_2$] (Zn3)

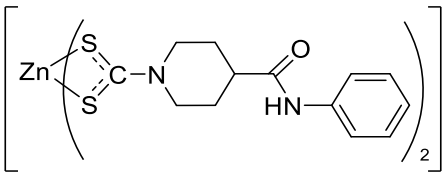

CS_2 (360 μL, 5.92 mmol) was added dropwise under stirring to an aqueous solution (10mL) of sodium hydroxide (233 mg, 5.82 mmol) and N-phenylpiperidine-4-carboxamide (652 mg, 5.82 mmol) at 0°C. The mixture was stirred for 1.5 hours (pH 10 to 6) and subsequently was added dropwise to the $[Zn(OAc)_2 \cdot 2H_2O]$ (635.7 mg, 2.89 mmol) aqueous solution. Immediate precipitation of a white precipitate occurred which was then centrifuged and washed with water and dried under vacuum over P_2O_5 (436 mg, 45% yield). $C_{26}H_{30}N_4O_2S_4Zn$. MW: 624,17 : C, 45.29; H, 4.39; N, 8.13; O, 4.64; S, 18.60; Zn, 18.96. FT-IR (CsI disk, $\tilde{\nu}_{max}$, cm^{-1}): 3215 (br, $\nu_{a/s}$, NH_2), 1659 (vs, ν, $C{=}O_{amide}$), 1645 (s, δ_{ip}, CNH), 1440 (ν, NCSS), 953 (ν, SCS), 370 (ν_a, ZnS_4).^{1}H NMR (400 MHz, DMSO-d_6): δ = 10.0 (1H, NH), 7.59 (2H, o-H), 7.29 (2H, m-H), 7.03 (1H, p-H), 2.89(4H, $C^{2',6'}H_{eq}$), 2.62 (4H, $C^{2',6'}H_{ax}$), 2.54 (2H, $C^{4'}H$), 1.91 (4H, $C^{3',5'}H_{eq}$), 1.68 (4H, $C^{3',5'}H_{ax}$). ^{13}C NMR (100 MHz, DMSO-d_6): δ = 173.7, 139.4, 128.6, 122.9, 119.0, 45.6, 43.6, 29.4.

Synthesis of BOC-N-(4-iodophenyl)piperidine-4-carboxamide

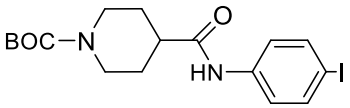

To a dry DCM solution of BOC-Isonipecotic acid (100mg, 0.436mmol), 4-iodoaniline (95.5mg, 0.63 mmol) and Et_3N (182.3 μL, 1.308 mmol), $SOCl_2$ (32 μL, 0.436 mmol) was added and was stirred for 3h under N_2 at ambient temperature. The crude mixture was extracted with an aqueous solution of $NaHSO_4$ 5% w/v, and the organic phase was collected and evaporated to afford a light-yellow oil. The crude mixture was purified by column chromatography in silica gel with EtOAc/PET (1:10), yielding the amide as a colorless oil (80 mg, 79 % yield). $C_{18}H_{23}IN_2O_3$, MW: 367,98: C, 42.43; H, 3.83; I, 34.49; N, 7.61; O, 8.70. ^{1}H NMR (400 MHz, $CDCl_3$): δ = 7.60 (2H, o-H), 7.47 (1H, NH), 7.30 (2H, m-H), 4.17 (4H, $C^{2',6'}H_{eq}$), 2.76 (4H, $C^{2',6'}H_{ax}$), 2.40 (2H, $C^{4'}H$), 1.85 (4H, $C^{3',5'}H_{eq}$), 1.67 (4H, $C^{3',5'}H_{ax}$), 1.46 (9H, BOC). ^{13}C NMR ($CDCl_3$, δ, ppm): 172.7, 154.7, 137.9, 137.6, 121.7, 87.5, 79.8, 44.3, 43.1, 28.5, 28.4.

Synthesis of BOC-N-(4-((triisopropylsilyl)ethynyl)phenyl)piperidine-4-carboxamide

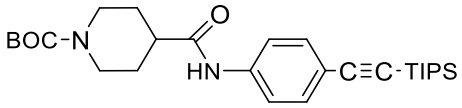

To a DIPA solution (10 mL) of (Triisopropyisilyl)acetylene (325.3 μL, 1.45 mmol), BOC-N-(4-iodophenyl)piperidine-4-carboxamide (264 μL, 1.32 mmol) and CuI (5mg, 0.026mmol), $Pd(PPh_4)_3$ (30.5mg, 0.026mmol) was added and was stirred for 20 min at room temperature under N_2. The mixture was filtered, and the filtrate was concentrated to dryness. The crude mixture was purified by column chromatography in silica gel, yielding the TIPS-protected terminal alkyne as a colorless oil (422.3 mg, 66 % yield). $C_{29}H_{44}N_2O_3Si$, MW: 422,45: C, 68.24; H, 8.35; N, 6.63; O, 7.57; Si, 6.65. ^{1}H NMR (400 MHz, $CDCl_3$, ppm): δ = 7.47 (2H, o-H), 7.42 (2H, m-H), 7.40 (1H, NH), 4.18 (2H, $C^{2',6'}H_{eq}$), 2.77 (2H, $C^{2',6'}H_{ax}$), 2.41 (2H, $C^{4'}H$), 1.87 (2H, $C^{3',5'}H_{eq}$), 1.68 (4H, $C^{3',5'}H_{ax}$), 1.46 (9H, BOC), 1.11 (21H, TIPS). ^{13}C NMR (100 MHz, $CDCl_3$, ppm): δ = 172.6, 154.7, 137.8, 132.8, 119.3, 106.6, 90.1, 79.8, 44.4, 42.9, 28.5, 28.4, 18.6, 11.3.

Synthesis of 4-((4-((triisopropylsilyl)ethynyl)phenyl)carbamoyl)piperidin-1-ium 2,2,2-trifluoroacetate:

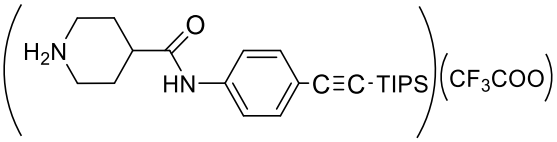

BOC-N-(4-((triisopropylsilyl)ethynyl)phenyl)piperidine-4-carboxamide (327 mg, 0.675 mmol) was deprotected with TFA (100.3 μL, 1.35 mmol) in DCM (2 ml) for two hours. The deprotection afforded the target compound in the form of a white powder (mg, 75%). $C_{25}H_{37}F_3N_2O_3S$, MW: 498,66: C, 60.22; H, 7.48; F, 11.43; N, 5.62; O, 9.63; Si, 5.63. FT-IR (CsI disk, $\tilde{\nu}_{max}$, cm^{-1}): 3228 (br, $\nu_{a/s}$, NH), 1672 (vs, ν, $C{=}O_{amide}$), 1663 (s, δ_{ip}, CNH). ^{1}H NMR (400 MHz, $CDCl_3$): δ = 10.3 (1H, NH), 8.44 (2H, NH_2), 7.62 (2H, o-H), 7.40 (2H, m-H), 3.35(2H, $C^{2',6'}H_{eq}$), 2.93 (2H, $C^{2',6'}H_{ax}$), 2.62 (2H, $C^{4'}H$), 1.94 (2H, $C^{3',5'}H_{eq}$), 1.74 (4H, $C^{3',5'}H_{ax}$), 1.09 (21H, TIPS). ^{13}C NMR (100 MHz, $CDCl_3$): δ = 172.3, 137.7, 132.4, 119.0, 107.4, 88.7, 42.5, 39.9, 25.1, 18.5, 10.8.

Synthesis of [Zn(dtc-Inp-ph-C≡C-TIPS)$_2$] (Zn4)

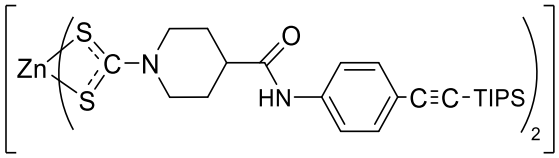

CS_2 (96 μL, 1.59 mmol) was added dropwise under stirring to a DMF solution (10 mL) of the 4-((4-((triisopropylsilyl)ethynyl)phenyl)carbamoyl)piperidin-1-ium-2,2,2-trifluoroacetate (612.3 mg, 1.23 mmol) and Et_3N (857 μL, 6.15 mmol) at 0°C. The mixture was stirred for 1.5 hours (pH 10 to 6) and subsequently was added dropwise into a DMF solution of $[Zn(OAc)_2{\cdot}2H_2O]$ (162 mg, 0.738 mmol) and was stirred for 30 min.. Diethyl ether was added to the mixture and a white precipitate occurred which was then centrifuged and washed with water and dried under vacuum over P_2O_5 (580 mg, 96% yield). FT-IR (CsI disk, $\tilde{\nu}_{max}$, cm^{-1}): 3228(br, $\nu_{a/s}$, NH), 1672 (vs, ν, $C{=}O_{amide}$), 1663 (s, δ_{ip}, CNH), 1439 (ν, NCSS), 541 (s, ν_a, SCS), 380 (w, ν_a, ZnS_4).^{1}H NMR (400 MHz, DMSO-d_6): δ = 10.2 (1H, NH), 7.62 (2H, o-H), 7.41 (2H, m-H), 4.92(4H, $C^{2',6'}H_{eq}$), 3.29 (4H, $C^{2',6'}H_{ax}$), 2.67 (2H, $C^{4'}H$), 1.95 (4H, $C^{3',5'}H_{eq}$), 1.68 (4H, $C^{3',5'}H_{ax}$), 1.09 (21H, TIPS). ^{13}C NMR (100 MHz, DMSO-d_6): δ = 202.5, 172.8, 139.8, 132.4, 119.0, 116.7, 107.4, 88.7, 50.6, 41.4, 28.2, 18.6, 10.8.

Synthesis of [Au(dtc-Inp-an)$_2$] (Au0)

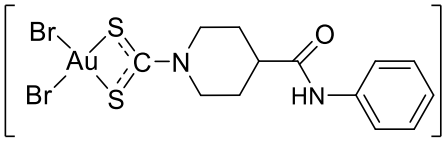

A DMF solution (2 mL) of **Zn3** (100 mg, 0.16 mmol) was added dropwise under stirring to a DMF solution (2 mL) of $K[AuBr_4]$ (189 mg, 0.32mmol) at room temperature. The mixture was stirred for 17 hours. Upon addition of water (60 mL), the formation of an orange precipitate was observed, which was then washed with MeOH and dried under vacuum over P_2O_5 (275 mg, 97% yield). $C_{13}H_{15}AuBr_2N_2OS_2$, MW: 636,17: C, 24.54; H, 2.38; Au, 30.96; Br, 25.12; N, 4.40; O, 2.51; S, 10.08. FT-IR (CsI disk, $\tilde{\nu}_{max}$, cm^{-1}):3215 (br, $\nu_{a/s}$, NH_2), 1659 (vs, ν, $C{=}O_{amide}$), 1645 (s, δ_{ip},

CNH), 1440 (ν, NCSS), 953 (ν, SCS), 370 (ν_a, ZnS_4).^{1}H NMR (400 MHz, DMSO-d_6): δ = 10.02 (1H, NH), 7.58 (2H, o-H), 7.30 (2H, m-H), 7.04 (1H, p-H), 4.18(4H, $C^{2',6'}H_{eq}$), 3.62 (4H, $C^{2',6'}H_{ax}$), 2.89 (2H, $C^{4'}H$), 2.09 (4H, $C^{3',5'}H_{eq}$), 1.82 (4H, $C^{3',5'}H_{ax}$). ^{13}C NMR (100 MHz, DMSO-d_6): δ = 193.09, 171.8, 139.1, 129.0, 123.7, 119.5, 48.8, 41.8, 27.7.

Synthesis of [$AuBr_2$ (dtc-Inp-ph-C≡C-TIPS)] (Au1)

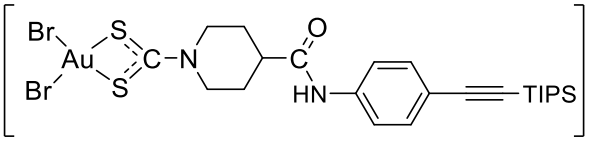

A DMF solution (2 mL) of **Zn4** (100 mg, 0.148 mmol) was added dropwise under stirring to a DMF solution (2 mL) of K[$AuBr_4$] (176 mg, 0.297mmol) at room temperature. The mixture was stirred for 17 hours. Upon addition of water (60 mL), the formation of an orange precipitate was observed, which was then washed with MeOH and dried under vacuum over P_2O_5 (258 mg, 96% yield). $C_{24}H_{35}AuBr_2N_2OS_2Si$, MW: 816,54: C, 35.30; H, 4.32; Au, 24.12; Br, 19.57; N, 3.43; O, 1.96; S, 7.85; Si, 3.44. FT-IR (CsI disk, $\tilde{\nu}_{max}$, cm^{-1}): 3215 (br, $\nu_{a/s}$, NH_2), 1659 (vs, ν, $C{=}O_{amide}$), 1645 (s, δ_{ip}, CNH), 1440 (ν, NCSS), 953 (ν, SCS), 370 (ν_a, ZnS_4). ^{1}H NMR (400 MHz, DMSO-d_6): δ = 10.22 (1H, NH), 7.63 (2H, o-H), 7.42 (2H, m-H), 4.21(4H, $C^{2',6'}H_{eq}$), 3.62 (4H, $C^{2',6'}H_{ax}$), 2.88 (2H, $C^{4'}H$), 2.10 (4H, $C^{3',5'}H_{eq}$), 1.81 (4H, $C^{3',5'}H_{ax}$)1.09 (21H, TIPS). ^{13}C NMR (100 MHz, DMSO-d_6): δ = 202, 172.6, 139.6, 132.5, 119.02, 116.5, 107.5, 88.6, 50.4, 41.3, 28.1, 18.6, 10.8.

Synthesis of [$AuBr_2$(dtc-Inp-ph-C≡C)] (Au2)

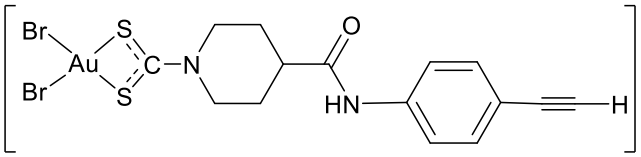

Into a dry THF solution (2 mL) of **Au1** (250 mg, 0.37 mmol), TBAF (311µl, 0.42 mmol) was added at room temperature and the mixture was stirred for 1 hour under

N_2. After this time, the solvent was evaporated, and the off-white residue was washed with water (60 mL). Subsequently, the solid was washed with MeOH and EtOAc and dried under vacuum over P_2O_5 (194 mg, 80% yield). $C_{15}H_{15}AuBr_2N_2OS_2$, MW: 660,19: C, 27.29; H, 2.29; Au, 29.83; Br, 24.21; N, 4.24; O, 2.42; S, 9.71. FT-IR (CsI disk, $\tilde{\nu}_{max}$, cm^{-1}):3435 (br, v, NH $_{amide}$), 2104 (w, v, C≡C), 1628 (s, v, C=O $_{amide}$), 1528 (vs, v, N-CSS), 1436 (m, v, C=C), 1106 (s, ν_a, P-Ph), 1027 (m, ν_a, SCS), 533 (s, δ_{ip} PF_6^- scissoring + ν_s, S-C-S overlapped), 493 (m, ν_a, P-Pt-P), 380 (w, v, S-Pt-S). ^{1}H NMR (400 MHz, DMSO-d_6): δ = 10.3 (s, 1H, NH $_{amide}$), 7.71-7.79 (m, 8H, P-Ph), 7.57-7.66 (m, 14H, P-Ph +H^8), 7.41 (d, 2H, H^9), 4.37 (m, 2H, $H^{2,6eq}$), 4.10 (s,1H, H^{12}), 3.43 (m,2H, $H^{2,6ax}$), 2.81-2.91 (m,5H, P-C_2H_4-P+H^4), 2.02 (m,2H, $H^{3,5eq}$), 1.67 (m, 2H, $H^{3,5ax}$). ^{13}C NMR (100 MHz, DMSO-d_6): δ = 201.0, 172.3, 139.7, 127.1-132.8, 119.0, 116.3, 83.6, 80.0, 46.9, 41.6, 27.9, 26.3, 26.8.

Synthesis of [Au(bpy)(dtc-Inp-ph-C≡C-TIPS)] (Au3)

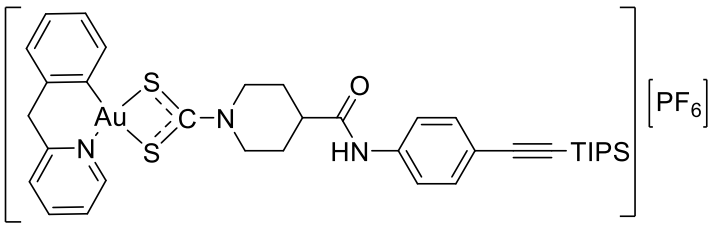

A DMF solution (2 mL) of **Zn4** (137 mg, 0.204 mmol) was added dropwise under stirring to a DMF solution (2 mL) of [Au(bpy)Cl_2] (178 mg, 0.408mmol) at room temperature. After 30 minutes KPF_6 (75 mg, 0.408mmol) was added. The mixture was stirred for 17 hours. Upon addition of water (60 mL), the formation of a yellow precipitate was observed, which was then washed with MeOH and dried under vacuum over P_2O_5 (294 mg, 79 % yield). $C_{36}H_{45}AuF_6N_3OPS_2Si$, MW: 969,91: C, 44.58; H, 4.68; Au, 20.31; F, 11.75; N, 4.33; O, 1.65; P, 3.19; S, 6.61; Si, 2.90. FT-IR (CsI disk, $\tilde{\nu}_{max}$, cm^{-1}):3348(br, $\nu_{a/s}$, NH), 1657 (vs, ν, C=O_{amide}), 1662 (s, δ_{ip}, CNH), 1441 (ν, NCSS), 952 (ν, SCS), 1026 (m, ν_a, SCS), 842 (s, $\nu_{a/s}$, PF_6^-),578 (w, νs, SCS), 558 (s, δip, $PF_6^-$$_{scissoring}$), 408 (w, $\nu_{a/s}$, SAuS). ^{1}H NMR (400 MHz, DMSO-d_6): δ = 10.3 (s, 1H, NH $_{amide}$), 9.00-8.99 (d,1H, H^f), 8.33(m, 1H, H^d), 8.10 (d,1H, H^c), 7.73 (m, 1H, H^e), 7.73-7.65 (d, 2H, H^8), 7.43-7.39 (m, 3H, H^9 + H $^{f'}$+$H^{c'}$), 7.29 (m, 1H, $H^{d'}$), 7.17 (1H, $H^{e'}$), 4.47 (s, 2H, H^g), 4.38-4.34(4H, $C^{2',6'}H_{eq}$), 3.78-3.64 (4H,

$C^{2',6'}H_{ax}$), 3.08 (2H, $C^{4'}H$), 2.16 (4H, $C^{3',5'}H_{eq}$), 1.75 (4H, $C^{3',5'}H_{ax}$)1.09 (21H, TIPS). ^{13}C NMR (100 MHz, DMSO-d_6): δ = 192, 172, 156, 151, 145, 143, 139, 133, 132, 130, 129, 128.6, 128.3, 127, 125, 119, 116, 83, 80, 53, 50, 41, 28.3, 28.

Synthesis of [Au(bpy)(dtc-Inp-ph-C≡C)] (Au4)

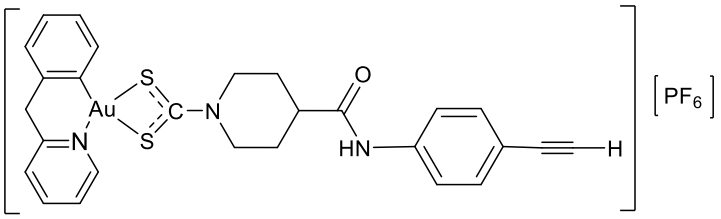

To a dry THF solution (2 mL) of **Au3** (250 mg, 0.257 mmol), TBAF (303 µl, 0.33 mmol) was added at room temperature. The mixture was stirred for 1 hour under N_2. After this time, the solvent was evaporated, and the off-white residue was washed with water (60 mL). Subsequently, the solid was washed with MeOH and EtOAc and dried under vacuum over P_2O_5 (194 mg, 80% yield). $C_{27}H_{25}AuN_3OS_2$, MW: 668,60: C, 48.50; H, 3.77; Au, 29.46; N, 6.28; O, 2.39; S, 9.59. FT-IR (CsI disk, $\tilde{\nu}_{max}$, cm^{-1}):3289 (br, v, NH $_{amide}$), 2103 (w, v, C≡C), 1686 (s, v, C=O $_{amide}$), 1593 (s, v, N-CSS), 1522 (s, δ_{ip}, CNH $_{amide}$), 1026 (m, ν_a, SCS), 843 (s, ν_a, PF_6^-), 558 (s, δ_{ip} PF_6^- scissoring), 540 (m, ν_s, S-C-S), 397 (w, $\nu_{a/s}$, S-Au-S). ^1H NMR (400 MHz, DMSO-d_6): δ = 10.3 (1H, NH), 9.01 (1H, H^f), 8.33(1H, H^d), 8.09 (1H, H^c), 7.73 (1H, H^e),7.65 (2H, o-H), 7.44-7.39 (3H, H^9 + $H^{f'}$+$H^{c'}$), 7.30 (1H, $H^{d'}$), 7.17 (1H, $H^{e'}$), 4.55 (2H, H^g), 4.47-4.35(4H, $C^{2',6'}H_{eq}$), 4.11 (1H, -C≡CH) 3.78-3.67 (4H, $C^{2',6'}H_{ax}$), 2.93 (2H, $C^{4'}H$), 2.14 (4H, $C^{3',5'}H_{eq}$), 1.77 (4H, $C^{3',5'}H_{ax}$).^{13}C NMR (100 MHz, DMSO-d_6): δ = 192, 172, 156, 151, 145, 143, 139, 133, 132, 130, 129, 128.6, 128.3, 127, 125, 119, 116, 83, 80, 53, 50, 41, 28.3, 28.01.

Synthesis of [Pt(dppe)(dtc-Inp-ph-C≡C-TIPS)] (Pt15)

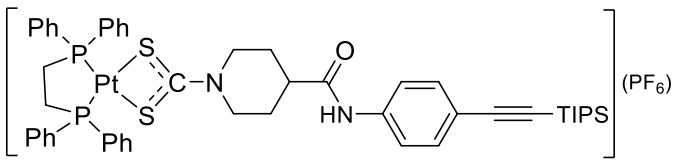

A DMF solution (2 mL) of **Zn4** (200 mg, 0.203 mmol) was added dropwise under stirring to a DMF solution (2 mL) of [Pt(dppe)Cl_2] (270 mg, 0.406mmol) at room temperature. After 30 minutes KPF_6 (73 mg, 0.406mmol) was added. The mixture was stirred for 17 hours. Upon addition of water (60 mL), the formation of a white precipitate was observed, which was then washed with MeOH and dried under vacuum over P_2O_5 (336 mg, 87% yield). $C_{50}H_{59}F_6N_2OP_3PtS_2Si$, MW: 1198,24: C, 50.12; H, 4.96; F, 9.51; N, 2.34; O, 1.34; P, 7.75; Pt, 16.28; S, 5.35; Si, 2.34. FT-IR (CsI disk, $\tilde{\nu}_{max}$, cm^{-1}):3454 (br, v, NH $_{amide}$), 2118 (w, v, C≡C), 1643 (s, v, C=O $_{amide}$), 1557 (vs, v, N-CSS), 1439 (m, v, C=C), 1108 (s, ν_a, P-Ph), 1025 (m, ν_a, SCS), 534 (s, δ_{ip} PF_6^- $_{scissoring}$ + ν_s, S-C-S overlapped), 493 (m, ν_a, P-Pt-P), 382 (w, v, S-Pt-S).^{1}H NMR (400 MHz, DMSO-d_6): δ = 10.4 (1H, NH), 7.71-7.79 (8H, P-Ph), 7.58-7.66 (14H, P-Ph +o-H), 7.39 (2H, m-H), 4.36 (4H, $C^{2',6'}H_{eq}$), 3.43 (4H, $C^{2',6'}H_{ax}$), 2.83-2.91 (2H, $C^{4'}H$), 2.04 (4H, $C^{3',5'}H_{eq}$), 1.67 (4H, $C^{3',5'}H_{ax}$), 1.08 (21H, TIPS).^{13}C NMR (100 MHz, DMSO-d_6, ppm): δ = 200.9, 172.3, 139.7, 127.2-132.8, 119.0, 116.7, 88.7, 46.9, 41.5, 27.9, 18.6, 10.8.

Synthesis of [Pt(dppe)(dtc-Inp-ph-C≡C)] (Pt16)

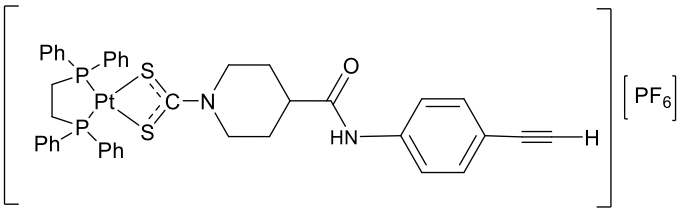

To a dry THF solution (2 mL) of **Zn4** (317 mg, 0.26 mmol), TBAF (345 µl, 0.34 mmol) was added at room temperature. The mixture was stirred for 1 hour under N_2. After this time, the solvent was evaporated, and the off-white residue was washed with water (60 mL). Subsequently, the solid washed with MeOH and EtOAc and dried under vacuum over P_2O_5 (302 mg, 87% yield). $C_{41}H_{39}N_2OP_2PtS_2$, MW: 896,93: C, 54.90; H, 4.38; N, 3.12; O, 1.78; P, 6.91; Pt, 21.75; S, 7.15. FT-IR (CsI disk, $\tilde{\nu}_{max}$, cm^{-1}):3435 (br, v, NH $_{amide}$), 2104 (w, v, C≡C), 1628 (s, v, C=O $_{amide}$), 1528 (vs, v, N-CSS), 1436 (m, v, C=C), 1106 (s, ν_a, P-Ph), 1027 (m, ν_a, SCS), 533 (s, δ_{ip} PF_6^- $_{scissoring}$ + ν_s, S-C-S overlapped), 493 (m, ν_a, P-Pt-P), 380 (w, v, S-Pt-S).^{1}H NMR (400 MHz, DMSO-d_6): δ = 10.4 (1H, NH), 7.71-7.79 (8H, P-Ph), 7.57-7.66 (14H, P-Ph + o-H), 7.41 (2H, m-H), 4.37 (4H, $C^{2',6'}H_{eq}$), 3.43 (4H, $C^{2',6'}H_{ax}$), 2.81-2.91 (2H, $C^{4'}H$), 2.02

(4H, $C^{3',5'}H_{eq}$), 1.67 (4H, $C^{3',5'}H_{ax}$).^{13}C NMR (100 MHz, DMSO-d_6): δ = 201.0, 172.3, 139.7, 132.8, 127.1, 119.0, 116.3, 83.6, 80.0, 46.9, 41.6, 27.9, 26.8, 26.3.

7.6 Chapter 5 – Experimental

Synthesis of [Zn(dtc-*L*-Tyr-OMe)](Zn5)

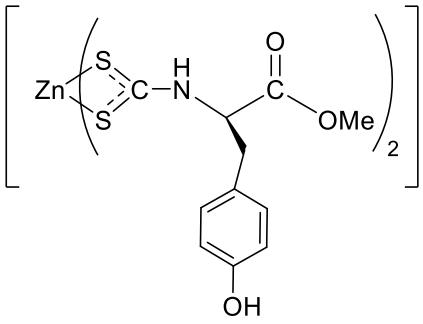

CS_2 (123 μL, 2.04 mmol) was added dropwise under stirring to a DMF solution (10mL) of sodium hydroxide (81 mg, 2.04 mmol) and L-tyrosine methyl ester (400 mg, 2.04 mmol) at 0 °C. The yellow mixture was stirred for 5 min (pH 12 to 6) which subsequently it was added to a DMF solution of $[Zn(OAc)_2 \cdot 2H_2O]$ (112 mg, 0.50 mmol) and was stirred overnight. After this time, upon addition of water, a white precipitate was observed which was centrifuged, and the bulk of the supernatant discarded. A yellow sticky product was observed, which was dried under vacuum over P_2O_5 (270 mg, 87.1% yield). $C_{22}H_{24}N_2O_6S_4Zn_2$, MW: 606.44: C, 39.35; H, 3.60; N, 4.17; O, 14.30; S, 19.10; Zn, 19.47. FT-IR (CsI disk, $\tilde{\nu}_{max}$, cm^{-1}): 3019.75 (ν, OH), 3950 (ν, NH), 1753.27 (ν, C=O), 1490 (ν, NCSS), 1053.56 (ν_{as}, SCS), 542.52 (ν_s, SCS), 371.08 (ν_a, ZnS_4).^{1}H NMR (400 MHz, DMSO-d_6): δ = 10.23 (OH), 9.27 (NH), 7.04 (2H, H^e), 6.66 (2H, H^f), 4.60 (1H,H^c), 3.61 (2H, H^d), 1.95(3H,H^a). ^{13}C NMR (100 MHz, DMSO-d_6): δ = 30.8, 52.1, 63.4, 115.2, 127.0, 129.9, 156.1, 170.8, 207.2.

Synthesis of [Zn(dtc-*L*-Tyr-OEt)] (**Zn6**)

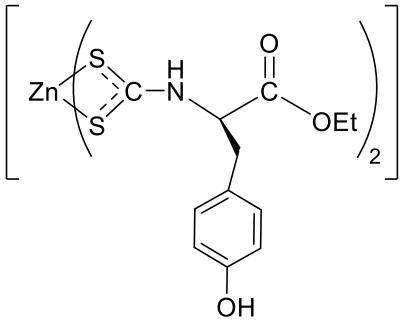

CS_2 (114 μL, 1.91 mmol) was added dropwise under stirring to a DMF solution (10mL) of sodium hydroxide (40 mg, 1.91 mmol) solution of L-tyrosine ethyl ester (400 mg, 1.91 mmol) at 0 °C. The yellow mixture was stirred for 5 min (pH 12 to 6) which subsequently was added to a DMF solution of $[Zn(OAc)_2 \cdot 2H_2O]$ (105 mg, 0.50 mmol) was added and was stirred overnight. After this time, upon addition of water, a white precipitate was observed which was centrifuged, and the bulk of the supernatant discarded. A yellow sticky product was observed, which was then dried under vacuum over P_2O_5, (222 mg, 73% yield). $C_{24}H_{28}N_2O_6S_4Zn_2$, MW: 634.5: C, 41.21; H, 4.03; N, 4.00; O, 13.72; S, 18.33; Zn, 18.69. FT-IR (CsI disk, $\tilde{\nu}_{max}$, cm^{-1}): 3367.93 (ν, OH; ν, NH), 2980.15 (ν, CH), 1767.57 (ν, C=O), 1552.14 (ν, NCSS), 1022.26 (ν_{as}, SCS), 543.57 (ν_s, SCS), 374.39 (ν_a, ZnS_4).^{1}H NMR (400 MHz, DMSO-d_6): δ = 10.21 (OH), 9.27 (NH), 7.04 (2H,H^e), 6.66 (2H,H^f),4.56 (1H,H^c), 4.06 (2H,H^d), 2.94 (2H,H^b), 1.12 (3H,H^a).^{13}C NMR (100 MHz, DMSO-d_6): δ = 14.1, 30.8, 60.8, 63.4, 115.1, 126.9, 130.0, 156.10, 170.4, 207.2.

Synthesis of [Pt(dppe)(dtc-*L*-Tyr-OMe)](PF$_6$)(Pt17)

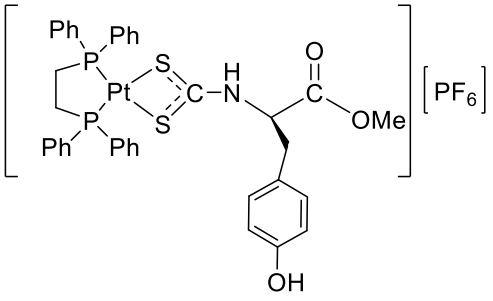

A DMF solution (2 mL) of **Zn5** (100 mg, 0.16 mmol) was added dropwise under stirring to a DMF solution (2 mL) of **Pt14** (219 mg, 0.32mmol) at room temperature. After 30 minutes KPF_6 (61 mg, 0.32mmol) was added. The mixture was stirred for 17 hours. Upon addition of water (60 mL), the formation of an off-white precipitate was

observed, which was then washed with MeOH and dried under vacuum over P_2O_5 (311 mg, 96% yield). $C_{37}H_{38}F_6NO_3P_3PtS_2$, MW: 1010,83: C, 43.96; H, 3.79; F, 11.28; N, 1.39; O, 4.75; P, 9.19; Pt, 19.30; S, 6.34. FT-IR (CsI disk, $\tilde{\nu}_{max}$, cm^{-1}): 3307 (br, v, NH+OH), 1747 (s, v, C=O), 1517 (s, δ_{ip}, CNH), 1437 (m, δ, C-$H_{methyl\ group}$), 1107 (s, v, C-O_{ester}), 1026 (m,v_a, SCS), 841 (s, v_a, PF_6^-), 692 (s, δ, C=C), 558 (s, δ_{ip} PF_6^-), 532 (s, v_s, S-C-S), 491 (m, v_a, P-Pt-P), 401 (w, v, S-Pt-S). ^{1}H NMR (400 MHz, DMSO-d_6): δ = 11.83 (1H, OH), 9.37 (1H, NH), 7.57-7.74 (20H, Ph), 7.01-7.03 (2H,H^e), 6.68-6.70 (2H, H^f), 4.83 (1H, H^c), 3.65 (3H, H^a), 3.10-3.12 (1H, H^d), 2.74-2.93 (5H, H^d + PCH_2). ^{13}C NMR (100 MHz, DMSO-d_6): δ = 192.3, 169.3, 156.4, 132.5-132.7, 130.3, 129.5-130.3, 127, 115.2, 64.0, 52.7, 35.8, 26.4-26.8.

Synthesis of [Pt(dppe)(dtc-*L*-Tyr-OEt)](PF_6) (Pt18)

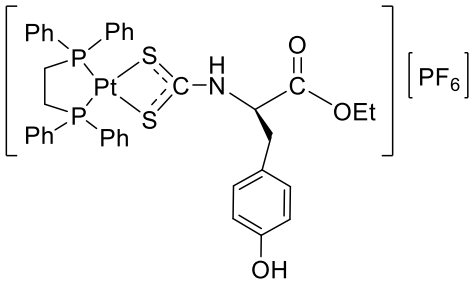

A DMF solution (2 mL) of **Zn6** (12.4 mg, 0.02 mmol) was added dropwise under stirring to a DMF solution (2 mL) of **Pt14** (26 mg, 0.04mmol) at room temperature. After 30 minutes KPF_6 (7.2 mg, 0.4mmol) was added. The mixture was stirred for 17 hours. Upon addition of water (60 mL), the formation of an off-white precipitate was observed, which was then washed with MeOH and dried under vacuum over P_2O_5 (36.4 mg, 98% yield). $C_{38}H_{40}F_6NO_3P_3PtS_2$, MW: 1024,86: C, 44.53; H, 3.93; F, 11.12; N, 1.37; O, 4.68; P, 9.07; Pt, 19.04; S, 6.26. FT-IR (CsI disk, $\tilde{\nu}_{max}$, cm^{-1}):3306 (br, v, NH+OH), 1740 (s, v, C=O), 1516 (s, δ_{ip}, CNH), 1437 (m, δ, C-$H_{methyl\ group}$), 1106 (s, v, C-O_{ester}), 1026 (m,v_a, SCS), 841 (s, v_a, PF_6^-), 692 (s, δ, C=C), 558 (s, δ_{ip} PF_6^-), 532 (s, v_s, S-C-S), 491 (m, v_a, P-Pt-P), 401 (w, v, S-Pt-S).^{1}H NMR (400 MHz, DMSO-d_6) δ = 11.82 (1H, OH), 9.36 (1H, NH), 7.60-7.73 (20H, Ph), 7.01-7.02 (2H,H^e), 6.67-6.69 (2H,H^f), 4.76 (1H,H^c), 4.09 (2H,H^b), 3.08 (1H,H^d), 2.74-2.93 (4H, P-C_2H_4-P), 1.11 (3H, H^a). ^{13}C NMR (100 MHz, DMSO-d_6): δ = 190.7, 168.9, 156.3, 132.3-132.8, 130.31, 129.4-129.5, 115.1, 48.6, 35.8, 26.3-26.8, 14.0.

Synthesis of [Au(Bnpy)(dtc-*L*-Tyr-OMe)](PF$_6$) (Au5)

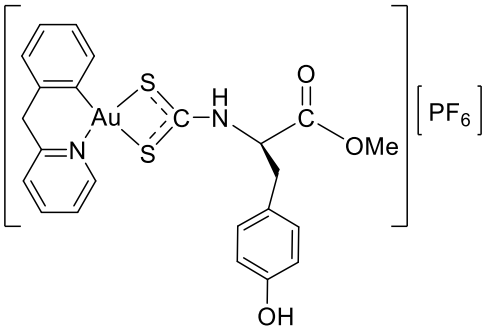

A DMF solution (2 mL) of **Zn5** (80 mg, 0.13 mmol) was added dropwise under stirring to a DMF solution (2 mL) of Au(bpy)Cl_2 (115 mg, 0.26mmol) at room temperature. After 30 minutes KPF_6 (49 mg, 0.26mmol) was added. The mixture was stirred for 17 hours. Upon addition of water (60 mL), the formation of an off-white precipitate was observed, which was then washed with MeOH and dried under vacuum over P_2O_5 (179 mg, 85% yield). $C_{23}H_{22}AuF_6N_2O_3PS_2$, MW: 780,49: C, 35.39; H, 2.84; Au, 25.24; F, 14.60; N, 3.59; O, 6.15; P, 3.97; S, 8.22. FT-IR (CsI disk, $\tilde{\nu}_{max}$, cm^{-1}): 3199 (br, v, NH+OH), 1745 (s, v, C=O), 1516 (s, δ_{ip}, CNH), 1439 (m, δ, C-$H_{methyl\ group}$), 1107 (s, v, C-O_{ester}), 1026 (m,v_a, SCS), 843 (s, v_a, PF_6^-), 755 (s, δ, C=C), 558 (s, δ_{ip} PF_6^-), 437 (w, v_s, S-C-S), 303 (w, $v_{a/s}$, S-Au-S). ^{1}H NMR (400 MHz, DMSO-d_6): δ = 9.33 (1H, NH), 8.90-8.92 (1H, $H^{f'}$), 8.27-8.31 (1H, $H^{d''}$), 8.04-8.06 (1H, $H^{c'}$), 7.67 (1H, $H^{e'}$), 7.32-7.36 (2H, $H^{f''}$+$H^{c''}$), 7.24 (1H, $H^{d'}$), 7.13 (1H, $H^{e''}$), 7.05 (2H, H^{e}), 6.67-6.69 (2H, H^{f}), 4.85 (1H,H^{c}), 4.48 (2H, H^{g}), 3.68-3.73 (3H,H^{a}), 3.17 (1H, H^{d}), 2.96 (1H,H^{d}). ^{13}C NMR (400 MHz, DMSO-d_6): δ = 215.9, 168.2, 156.4, 156.0, 151.8, 143.4, 133.4, 130.7, 130.4, 130.2, 128.8, 128.2, 128.1, 126.9, 125.5, 115.4, 65.0, 60.6, 52.7, 46.1, 37.6.

Synthesis of [Au(Bnpy)(dtc-*L*-Tyr-OEt)](PF$_6$)(Au6)

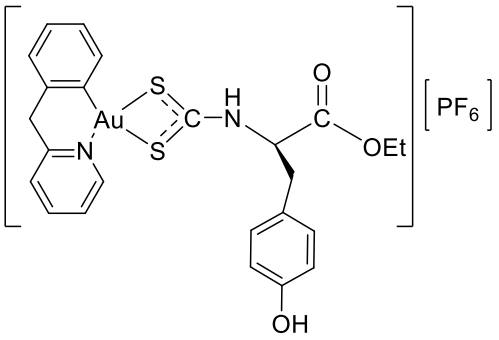

A DMF solution (2 mL) of **Zn6** (36.4 mg, 0.06 mmol) was added dropwise under stirring to a DMF solution (2 mL) of [Au(bpy)Cl_2] (50 mg, 0.12mmol) at room temperature. After 30 minutes KPF_6 (21 mg, 0.12mmol) was added. The mixture was stirred for 17 hours. Upon addition of water (60 mL), the formation of a off-white precipitate was observed, which was then washed with MeOH and dried under vacuum over P_2O_5 (74.4 mg, 95% yield). $C_{24}H_{24}AuF_6N_2O_3PS_2$, MW: 794,52: C, 36.28; H, 3.04; Au, 24.79; F, 14.35; N, 3.53; O, 6.04; P, 3.90; S, 8.07. FT-IR (CsI disk, $\tilde{\nu}_{max}$, cm^{-1}): 3448 (br, v, NH+OH), 1737 (s, v, C=O), 1516 (s, δ_{ip}, CNH), 1446 (m, δ, C-$H_{methyl\ group}$), 1105 (s, v, C-O_{ester}), 1026 (m,v_a, SCS), 845 (s, v_a, PF_6^-), 754 (s, δ, C=C), 558 (s, δ_{ip} PF_6^-), 436 (w, v_s, S-C-S), 303 (w, $v_{a/s}$, S-Au-S).^{1}H NMR (400 MHz, DMSO-d_6): δ = 9.29 (1H, NH), 8.90-8.91 (1H, $H^{f'}$), 8.28(1H, $H^{d'}$), 8.06 (1H, $H^{c'}$), 7.73 (1H, $H^{e'}$), 7.34-7.36 (2H, $H^{f''}$+$H^{c''}$), 7.23 (1H, $H^{d''}$), 7.13 (1H, $H^{e''}$), 7.03 (2H, H^e), 6.66-6.68 (2H, H^f), 4.46 (2H, H^g), 4.09 (3H, H^c + H^b), 3.11 (2H, H^d), 1.15 (3H,H^a).^{13}C NMR (100 MHz, DMSO-d_6): δ = 213.7, 167.7, 156.6, 156.3, 151.8, 143.4, 133.4, 130.9, 130.7, 130.2, 128.7, 128.2, 128.1, 126.9, 125.5, 115.3, 62.1, 61.6, 60.5, 46.1, 37.6, 14.1.

7.7 Chapter 6 – Experimental

Synthesis of [Zn(dtc-Inp-NH_2)$_2$] (Zn7)

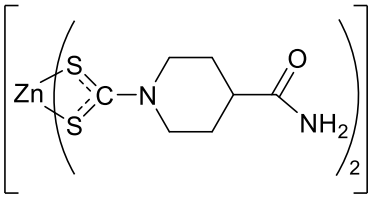

To a methanolic solution (10 mL) of NaOH (310 mg, 7.80 mmol) and isonipecotamide (1 g, 7.80 mmol), CS_2 (470 μL, 7.80 mmol), was added dropwise at 0°C and the mixture was stirred for 3 hours (pH 12 to 8). The mixture was treated further with CS_2 (470 μL, 7.80 mmol), and stored at 4°C overnight. The mixture was then added to an aqueous solution (2 mL) of $[Zn(OAc)_2]\cdot 2H_2O$ (860.0 mg, 3.90 mmol) at room temperature, leading to the sudden precipitation of a white solid. The residue was subsequently washed with water and then dried under vacuum over P_2O_5 (1.77 g, 96% yield). $C_{14}H_{22}N_4O_2S_4Zn$, MW = 471.98: C, 35.63; H, 4.70;N, 11.87. FT-IR (CsI disk, $\tilde{\nu}_{max}$, cm^{-1}):3439/3208 (br, $\nu_{a/s}$, NH_2), 1667 (vs, ν, C=O), 1649 (s, δ_{ip}, CNH), 1492 (s, ν, N-CSS),1007 (m, ν_a, SCS), 531 (m, ν_s, SCS), 391 (w, νa, ZnS_4). ^{1}H NMR (400MHz, DMSO-d_6): δ = 7.36 (2H, NH cis), 6.87 (2H, NH trans), 4.82 (4H, $C^{2',6'}H_{eq}$), 3.26 (4H, $C^{2',6'}H_{ax}$), 2.40 (2H, $C^{4'}H$), 1.80 (4H, $C^{3',5'}H_{eq}$), 1.55 (4H, $C^{3',5'}H_{ax}$). ^{13}C NMR (100 MHz, DMSO-d_6): δ = 202.23, 175.6, 50.7, 40.1, 28.3.

Synthesis of [Zn(dtc-Inp-GlcN2)$_2$] (Zn8):

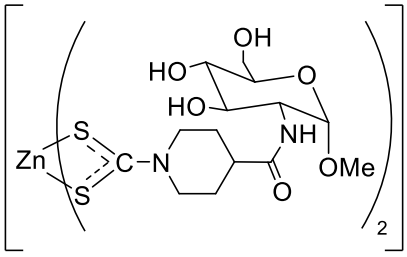

A mixture of GlcN2 (266.1 mg, 1.05 mmol) and DIPEA (76 μL, 0.44 mmol) in anhydrous DMF (2 mL) was added under stirring to a suspension of [Zn(dtc-Inp-OSu)$_2$] (292.8 mg, 0.44 mmol) in anhydrous DMF (2 mL). The mixture was stirred at room temperature under N_2 for 16 hours and then treated with methanol (30 mL), leading to the formation of a white precipitate that was filtered off and discarded. The resulting clear pale-yellow solution was allowed to slowly concentrate under the fume hood at room temperature for two days, leading to the formation of a white solid. The

precipitate was resuspended in methanol (50 mL), filtered, washed with methanol (60 mL), and then dried under vacuum over P_2O_5 (464.6 mg, 35%). $C_{28}H_{46}N_4O_{12}S_4Zn$, MW= 824.31: C, 40.80; H, 5.63; N, 6.80. FT-IR (CsI disk, $\tilde{\nu}_{max}$, cm^{-1}): 3319 (br, ν, OH + NH overlapped), 1645 (s, ν, C=O), 1557 (m, δ_{ip}, CNH), 1494 (s, ν, N-CSS), 1062/1040 (ν_s, ν, C-OH + C^1-O-CH_3 overlapped), 950 (s, ν_a, SCS), 576 (m, ν_s, SCS), 382 (w, ν_a, ZnS_4).^{1}H NMR (400 MHZ, DMSO-d_6): δ = 7.80 (2H, NH), 5.00 (2H,C^4OH), 4.82 (4H, $C^{2',6'}H_{eq}$), 4.73 (2H, C^3OH), 4.56-4.52 (4H, C^1H + C^6OH), 3.67-3.62 (4H, C^2H + C^6H), 3.49-3.42 (4H, C^3H +C^6H'), 3.33-3.24 (6H, C^5H + $C^{2',6'}H_{ax}$), 3.24 (6H, OCH_3), 3.15-3.09 (2H, C^4H),2.55 (2H, $C^{4'}$H), 1.81-1.76 (4H, $C^{3',5'}H_{eq}$), 1.62-1.53 (4H, $C^{3',5'}H_{ax}$).^{13}C NMR (100MHz, DMSO-d_6): δ = 202.2, 173.9, 97.9, 72.8, 70.8, 70.7, 60.9, 54.5, 53.8, 50.8, 40.0, 28.5.

Synthesis of [Zn(dtc-Inp-GlcN3)$_2$] (Zn9):

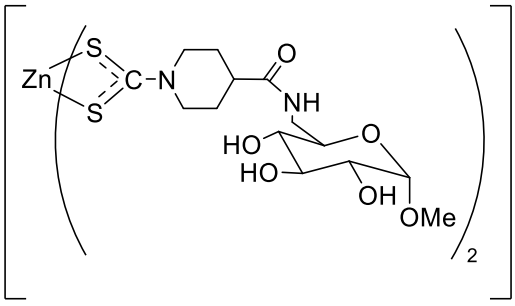

A mixture of GlcN3 (760.0 mg, 3.93 mmol) and DIPEA (1.50 mL, 8.64 mmol) in anhydrous DMF (4 mL) was added under stirring to a suspension of [Zn(dtc-Inp-OSu)$_2$] (1.05 g, 1.57 mmol) in anhydrous DMF (4 mL). The mixture was stirred at room temperature under N_2 for 16 hours and then treated with ethanol (80 mL), leading to the sudden precipitation of a white solid. The precipitate was filtered, washed with methanol (45 mL), and then dried under vacuum over P_2O_5 (980.0 mg, 76% yield). $C_{28}H_{46}N_4O_{12}S_4Zn$, MW =824.31 g mol^{-1}: C, 40.80; H, 5.63; N, 6.80. FT-IR (CsI disk, ṽmax, cm^{-1}): 3392 (br, ν, OH + NH overlapped), 1637 (s, ν, $C{=}O_{amide\ I}$), 1543 (m, δ_{ip}, $CNH_{amide\ II}$), 1494 (s, ν, N-CSS), 1049 (ν_s, ν, C-OH + C^1-O-CH_3 overlapped), 1010 (s, ν_a, SCS), 564 (w, ν_s, SCS), 366 (w, ν_a, ZnS_4). ^{1}H NMR (400 MHz, DMSO-d_6): δ = 7.97 (2H, NH), 4.97 (2H, C^4OH), 4.83 (4H, $C^{2',6'}H_{eq}$), 4.82 (2H, C^3OH), 4.75 (2H, C^2OH), 4.51 (2H, C^1H), 3.55 (2H, C^6H), 3.36 (4H, C^3H +

C^5H), 3.24 (6H, OCH_3), 3.24-3.19 (6H, C^2H + $C^{2',6'}H_{ax}$), 3.01 (2H, C^6H'), 2.90 (2H, C^4H), 2.57-2.53 (2H, $C^{4'}H$), 1.78-1.75 (4H, $C^{3',5'}H_{eq}$), 1.62-1.53 (4H, $C^{3',5'}H_{ax}$). ^{13}C NMR (100 MHz, DMSO-d_6): δ = 202.22, 173.78, 99.64, 72.95, 72.09, 71.97, 70.30, 54.27, 50.74, 40.14, 40.09, 28.42.

Synthesis of [Zn(dtc-Inp-GlcN4)$_2$] (Zn10):

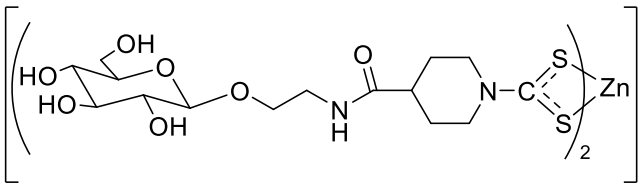

A mixture GlcN4 (91.7 mg, 0.41 mmol) and DIPEA (180 μL, 1.03 mmol) in anhydrous DMF (3 mL) was added under stirring to a suspension of [Zn(dtc-Inp-OSu)$_2$] (133.5 mg, 0.20 mmol) in anhydrous DMF (1 mL). The mixture was stirred at room temperature under N_2 for 16 hours and then treated with diethyl ether (60 mL), leading to the sudden precipitation of a white solid. The precipitate was filtered, washed with ethanol (30 mL), and then dried under vacuum over P_2O_5 (135.3 mg, 77% yield). $C_{30}H_{50}N_4O_{14}S_4Zn$, MW =884.36 g mol^{-1}: C, 40.74; H, 5.60; N, 6.34. FT-IR (CsI disk, $\tilde{\nu}$max, cm^{-1}): 3392 (br, ν, OH + NH overlapped), 1647 (s, ν, C=O), 1556 (m, δ_{ip}, CNH), 1494 (s, ν, N-CSS), 1078/1035 (ν_s, ν, C-OH + C^1-O-CH_2), 1004 (sh, ν_a, SCS), 563 (w, ν_s, SCS), 386 (w, ν_a, ZnS_4). ^1H NMR (400 MHz, DMSO-d_6): δ = 7.89 (2H, NH), 5.01 (2H, C^2OH), 4.98 (2H, C^3OH), 4.85 (2H, C^4OH), 4.83 (4H, $C^{2',6'}H_{eq}$), 4.56 (2H, C^6OH), 4.13 (2H, C^1H), 3.75-3.64 (4H, C^6H + $CH_aH_bCH_2NH$), 3.53-3.47 (2H, C^6H'), 3.42 (2H, $CH_aH_bCH_2NH$), 3.29-3.20 (8H, $C^{2',6'}H_{ax}$ + CH_2NH), 3.17-3.08 (4H, C^3H + C^5H), 3.03 (2H, C^4H), 2.95 (2H, C^2H), 2.45 (2H, $C^{4'}H$), 1.80-1.77 (4H, $C^{3',5'}H_{eq}$), 1.61-1.52 (4H, $C^{3',5'}H_{ax}$). ^{13}C NMR (100 MHz, DMSO-d_6): δ= 202.7, 173.7, 103.2, 76.9, 76.5, 73.5, 70.0, 67.9, 61.1, 50.5, 40.4, 38.7, 28.3.

Synthesis of [Pt(dppe)(dtc-Inp-NH_2)](PF_6) (Pt19):

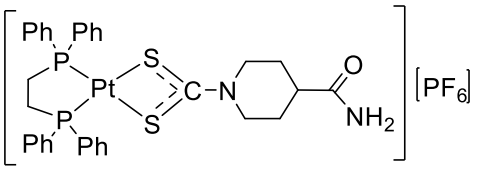

A DMF solution (2 mL) of **Zn7** (33.34 mg, 0.075 mmol) was added dropwise under stirring to a DMF solution (2 mL) of **Pt14** (100 mg, 0.15 mmol) at room temperature. After 30 minutes KPF_6 (27.9 mg, 0.15 mmol) was added. The mixture was stirred for 17 hours. Upon addition of Et_2O (60 mL), the formation of an off-white precipitate was observed, which was then washed with MeOH and dried under vacuum over P_2O_5 (62 mg, 43.2% yield). $C_{33}H_{35}F_6N_2OP_3PtS_2$, MW: 941,77: C, 42.09; H, 3.75; F, 12.10; N, 2.97; O, 1.70; P, 9.87; Pt, 20.71; S, 6.81.FT-IR (CsI disk, $\tilde{\nu}_{max}$, cm^{-1}):3452 (br, ν_{as}, NH_2), 1675 (s, v, C=O), 1557 (w, v, N-CSS), 1433 (w, v, C=C), 1108 (s, ν_a, P-Ph_2), 999 (s, ν_a, SCS), 842 (s, $\tilde{\nu}_3$, PF_6), 708 (s, $\nu_m\nu_{ib}$ P-Ph_2), 559 (br, ν_s SCS), 534 (s, ν_γ, P-Ph + s, ν_4, PF_6), 492 (ν_a, P-Pt-P), 394 (v, S-Pt-S). ^{1}H NMR (400 MHz, DMSO-d_6): δ = 7.80 (8H, ortho-CH), 7.73/7.62 (20H, Ph), 7.45 (4H, para-CH), 7.43 (8H, meta-CH), 7.41 (1H, cis-NH), 6.93 (1H,trans-NH), 4.30 (2H, $C^{2,6}$ H_{eq}), 3.38 (2H, $C^{2,6}H_{ax}$),2.39 (4H, CH_2), 2.32 (2H, CH_2), 1.91 (2H, $C^{3,5}H_{eq}$), 1.57 (2H, $C^{3,5}H_{ax}$). ^{13}C NMR (100 MHz, DMSO-d_6): δ = 175.0, 132.4-132.8, 65.0, 47.0, 35.8, 26.3. ^{31}P NMR (500 MHz, DMSO-d_6): δ = 45.09.

Synthesis of [Pt(dppe)(dtc-Inp-GlcN2)](PF_6) (Pt20):

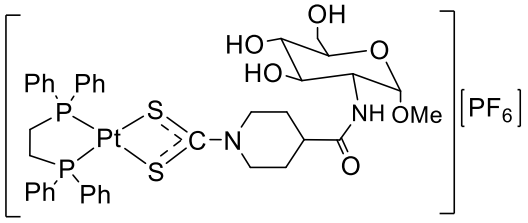

A DMF solution (2 mL) of **Zn8** (37 mg, 0.045mmol) was added dropwise under stirring to a DMF solution (2 mL) of **Pt14** (60 mg, 0.09mmol) at room temperature. After 30 minutes KPF_6 (17mg, 0.09mmol) was added. The mixture was stirred for 17 hours. Upon addition of Et_2O (60 mL), the formation of an off-white precipitate was

observed, which was then washed with MeOH and dried under vacuum over P_2O_5 (40 mg, 78% yield). $C_{40}H_{47}F_6N_2O_6P_3PtS_2$, MW: 1117,94: C, 42.98; H, 4.24; F, 10.20; N, 2.51; O, 8.59; P, 8.31; Pt, 17.45; S, 5.74. FT-IR (CsI disk, $\tilde{\nu}_{max}$, cm^{-1}): 3428 (br, ν, OH + NH overlapped), 1659 (s, ν, C=O), 1536 (m, δ_{ip}, CNH), 1436 (s, ν, N-CSS), 1050 (ν_s, ν, C-OH + C^1-O-CH_3 overlapped), 999 (s, ν_a, SCS), 842 (s, $\tilde{\nu}_3$, PF_6),560 (w, ν_s SCS), 532 (s, ν_γ, P-Ph + s, ν_4, PF_6), 492 (ν_a, P-Pt-P), 393 (v, S-Pt-S).^{1}H NMR (400 MHz, DMSO-d_6): δ = 7.88 (1H, NH), 7.73/7.62 (20H, Ph), 5.04 (1H, C^4OH), 4.79 (1H, C^3OH), 4.54(2H, C^1H + C^6OH), 4.33 (2H, $C^{2',6'}H_{eq}$), 3.63 (2H,C^2H+ C^6H), 3.46 (2H, C^3H+C^6H'), 3.30 (3H, C^5H + $C^{2',6'}H_{ax}$), 3.22 (C^5H), 3.11 (C^4H), 2.89 (4H, P-CH_2),2.67 (2H, $C^{4'}$H), 1.88 (2H, $C^{3',5'}H_{eq}$), 1.59 (2H, $C^{3',5'}H_{ax}$). ^{13}C NMR (100 MHz, DMSO-d_6): δ = 200.6, 173.3, 133.3-129.5, 97.8, 72.8, 70.7, 70.5, 60.8, 54.4, 53.9, 47.0, 40.3, 26.8, 26.4. ^{31}P NMR (500 MHz, DMSO-d_6): δ = 45.11.

Synthesis of [Pt(dppe)(dtc-Inp-GlcN3)](PF$_6$) (Pt21):

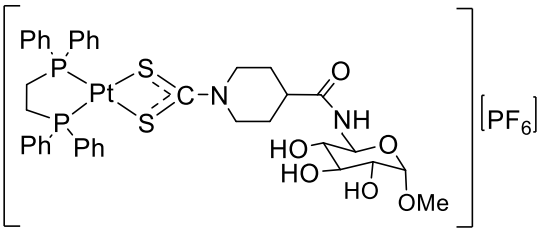

A DMF solution (2 mL) of **Zn9** (37 mg, 0.045mmol) was added dropwise under stirring to a DMF solution (2 mL) of **Pt14** (60 mg, 0.09mmol) at room temperature. After 30 minutes KPF_6 (17mg, 0.09mmol) was added. The mixture was stirred for 17 hours. Upon addition of Et_2O (60 mL), the formation of an off-white precipitate was observed, which was then washed with MeOH and dried under vacuum over P_2O_5 (50 mg, 98% yield). $C_{40}H_{47}F_6N_2O_6P_3PtS_2$, MW: 1117,94: C, 42.98; H, 4.24; F, 10.20; N, 2.51; O, 8.59; P, 8.31; Pt, 17.45; S, 5.74. FT-IR (CsI disk, $\tilde{\nu}_{max}$, cm^{-1}): 3434 (br, ν, OH + NH overlapped), 1661 (s, ν, C=O), 1535 (m, δ_{ip}, CNH), 1436 (s, ν, N-CSS), 1056 (ν_s, ν, C-OH + C^1-O-CH_3 overlapped), 946 (s, ν_a, SCS), 841 (s, $\tilde{\nu}_3$, PF_6),560 (w, ν_s SCS), 532 (s, ν_γ, P-Ph + s, ν_4, PF_6), 491 (ν_a, P-Pt-P), 391 (v, S-Pt-S).^{1}H NMR (400 MHz, DMSO-d_6): δ = 8.02 (1H, NH), 7.73/7.62 (20H, Ph), 5.01 (1H, C^4OH), 4.86 (1H, C^3OH), 4.79 (1H, C^2OH), 4.50(1H, C^1H), 4.32 (2H, $C^{2',6'}H_{eq}$), 3.56 (1H, C^6H), 3.35(2H, C^3H+C^5H), 3.22 (3H, OCH_3), 3.17 (C^2H), 2.99 (1H, C^6H'), 2.92 (6H, P-CH_2

+ $C^{2',6'}H_{ax}$), 2.82 (s, 1H, $C^{4}H$), 2.66 (2H, $C^{4'}H$), 1.85 (2H, $C^{3',5'}H_{eq}$), 1.59 (2H, $C^{3',5'}H_{ax}$). ^{13}C NMR (100 MHz, DMSO-d_6): δ = 200.7, 173.2, 132.8-129.5, 99.7, 73.0, 72.1, 71.9, 70.3, 54.3, 50.2, 40.4, 28.1, 28.1. ^{31}P-NMR (500 MHz, DMSO-d_6): δ = 45.11.

Synthesis of [Pt(dppe)(dtc-Inp-GlcN4)](PF$_6$) (Pt22):

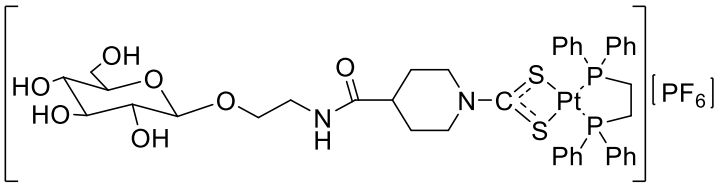

A DMF solution (2 mL) of **Zn10** (40 mg, 0.45mmol) was added dropwise under stirring to a DMF solution (2 mL) of **Pt14** (60 mg, 0.09mmol) at room temperature. After 30 minutes KPF_6 (17mg, 0.09mmol) was added. The mixture was stirred for 17 hours. Upon addition of Et_2O (60 mL), the formation of an off-white precipitate was observed, which was then washed with MeOH and dried under vacuum over P_2O_5 (30 mg, 58% yield). $C_{41}H_{49}F_6N_2O_7P_3PtS_2$, MW: 1147,97: C, 42.90; H, 4.30; F, 9.93; N, 2.44; O, 9.76; P, 8.09; Pt, 16.99; S, 5.59. FT-IR (CsI disk, ῡmax, cm-1): 3436 (br, ν, OH + NH overlapped), 1660 (s, ν, C=O), 1537 (m, δ_{ip}, CNH), 1436 (s, ν, N-CSS), 1036 (ν_s, ν, C-OH + C^1-O-CH_2), 999 (sh, ν_a, SCS), 560 (w, ν_s, SCS),532 (s, ν_γ, P-Ph + s, ν_4, PF_6), 492 (ν_a, P-Pt-P), 389 (v, S-Pt-S). ^1H NMR (400 MHz, DMSO-d_6): δ = 8.05 (1H, NH), 7.73/7.62 (20H, Ph), 5.06-5.00 (3H, C^2OH + C^3OH + C^4OH), 4.61 (1H, C^6OH), 4.31 (2H, $C^{2',6'}H_{eq}$), 4.12 (1H, C^1H), 3.69 (2H, C^6H + $CH_aH_bCH_2NH$), 3.51 (1H, C^6H'), 3.42 (1H, $CH_aH_bCH_2NH$), 3.23 (4H, $C^{2',6'}H_{ax}$ + CH_2NH), 2.95 (2H, C^2H+ C^4H), 2.89 (4H, P-CH_2), 2.63(1H, $C^{4'}H$), 1.91 (2H, $C^{3',5'}H_{eq}$), 1.58 (2H, $C^{3',5'}H_{ax}$). ^{13}C NMR (100 MHz, DMSO-d_6): δ = 202.7, 173.1, 132.7-129.5, 103.2, 76.9, 76.5, 73.4, 70.0, 67.9, 61.0, 47.0, 40.4, 26.8, 26.4. ^{31}P NMR (500 MHz, DMSO-d_6): δ = 45.09.